DESIGN AND SYNTHESIS OF ORGANIC SENSITIZERS FOR DYE SOLAR CELLS: MOLECULAR STRUCTURE VS DEVICE PERFORMANCE

Miquel Angels Planells Dillundé

ISBN: 978-84-693-8861-7
Dipòsit Legal: T.1946-2010

UNIVERSITAT ROVIRA I VIRGILI
DESIGN AND SYNTHESIS OF ORGANIC SENSITIZERS FOR DYE SOLAR CELLS: MOLECULAR STRUCTURE VS DEVICE PERFORMANCE
Miquel Angels Planells Dillundé
ISBN:978-84-693-8861-7/DL:T.1946-2010

Doctoral Thesis

Design and Synthesis of Organic Sensitizers for Dye Solar Cells: Molecular Structure vs Device Performance

Miquel Planells Dillundé

Supervised by Prof. Emilio Palomares

ICIQ - URV

Tarragona - July 2010

ICIQ
Institut Català d'Investigació Química

UNIVERSITAT ROVIRA I VIRGILI

UNIVERSITAT ROVIRA I VIRGILI
DESIGN AND SYNTHESIS OF ORGANIC SENSITIZERS FOR DYE SOLAR CELLS: MOLECULAR STRUCTURE VS DEVICE PERFORMANCE
Miquel Angels Planells Dillundé
ISBN:978-84-693-8861-7/DL:T.1946-2010

UNIVERSITAT ROVIRA I VIRGILI
DESIGN AND SYNTHESIS OF ORGANIC SENSITIZERS FOR DYE SOLAR CELLS: MOLECULAR STRUCTURE VS DEVICE PERFORMANCE
Miquel Angels Planells Dillundé
ISBN:978-84-693-8861-7/DL:T.1946-2010

Emilio Palomares Gil, Group Leader of the Institute of Chemical Research of Catalonia (ICIQ) in Tarragona, and Research Professor of the Catalan Institution for Research and Advanced Studies (ICREA) in Barcelona

CERTIFY:

That the present thesis, entitled “Design and synthesis of organic sensitizers for dye solar cells: Molecular structure *vs* device performance” presented by **Miquel Planells Dillundé** for the award of the degree of Doctor, has been carried out under my supervision at ICIQ and that he fulfills the requirements to obtain a “European Doctorate Mention”.

Tarragona, July 2010

Prof. Dr. Emilio Palomares Gil

ICIQ
Institut Català d'Investigació Química

UNIVERSITAT ROVIRA I VIRGILI

UNIVERSITAT ROVIRA I VIRGILI
DESIGN AND SYNTHESIS OF ORGANIC SENSITIZERS FOR DYE SOLAR CELLS: MOLECULAR STRUCTURE VS DEVICE PERFORMANCE
Miquel Angels Planells Dillundé
ISBN:978-84-693-8861-7/DL:T.1946-2010

UNIVERSITAT ROVIRA I VIRGILI
DESIGN AND SYNTHESIS OF ORGANIC SENSITIZERS FOR DYE SOLAR CELLS: MOLECULAR STRUCTURE VS DEVICE PERFORMANCE
Miquel Angels Planells Dillundé
ISBN:978-84-693-8861-7/DL:T.1946-2010

Abstract

Nowadays, the vast majority of the worlds energy supply is obtained from fossil fuels. However, due to their limited availability and their undesired environmental impact, they cannot continue to be the main energy source in the future. Therefore, obtaining clean alternative energies is essential if we want to maintain our current lifestyle and economic growth. One of the renewable technologies that has been studied extensively is solar energy, although it has up to now not been able to compete successfully with the lower cost of fossil fuels. However, novel solar cell technologies, such as the Dye Sensitized Solar Cell (DSSC), have been developed in order to reduce the solar cell cost, and thus, it could be a possible solution to the current world energy issues.

This kind of solar cell is based on a photoactive unit, a dye, anchored to a nanostructured metal-oxide semiconductor, usually TiO_2, surrounded by a redox electrolyte media and sandwiched between two contact electrodes. When light shines over the device, an electron is promoted from the ground to the excited state of the dye and subsequently injected into the semiconductor. Then, the electron is transported through the semiconductor to the back contact where it passes through an external load generating electrical power. At the same time, the oxidized dye is regenerated by the electrolyte and it, in turn, is regenerated at the counter electrode.

DSSCs have been developed and commercialized using ruthenium polypyridyl complexes as the photosensitizer. However, ruthenium is a non abundant element, and therefore, its utilization in DSSC in large scale is not possible. To overcome this issue, novel organic dyes based on a carbonated structure (CHN) have been developed, although currently no organic dye has been able to match the efficiency of ruthenium photosensitizers in DSSC devices.

The present thesis focuses on the synthesis of organic chromophores as well as their use in optoelectronic devices. In DSSC devices, each component (semiconductor, sensitizer and electrolyte) plays an important role in determining final device efficiency, in a large part due to the charge transfer processes that take place at the TiO_2/dye/electrolyte interface. To understand and establish a relationship between the molecular structure of the dye and the device performance it is crucial to study these charge transfer processes in great detail.

ISBN:978-84-693-8861-7/DL:T.1946-2010

Abstract

In Chapter 3, the use of two porphyrin photosensitizers in DSSC is described. This class of sensitizer is well-known due to its primary role in photosynthesis. Furthermore, they posses unique optical and electrochemical properties. Thus, two unsymmetrical porphyrins were synthesized, with the only difference in structure between them being the presence or absence of alkyl chains at the *meso* phenyl positions. Subsequently, these porphyrins were used in DSSC and the effect of such alkyl chains was studied. The results differ considerably for these dyes when the distribution of the dye on the TiO_2 surface is varied, which can be achieved by variation of the sensitization time. Following short sensitization times (< 15 minutes) when the dyes form a monolayer on the TiO_2 surface, the alkyl chains help to form a compact layer which acts as a blocking layer able to keep away the electrolyte from the nanoparticle surface. In this case the recombination reaction between the photoinjected electrons and the oxidized electrolyte (e^-_{TiO2}/electrolyte$^+$) decreases and as a result higher voltage was obtained. Following long sensitization times (> 4 hours) when the dye forms a multilayer on the TiO_2 surface, it is found that the alkyl chains do not change the e^-_{TiO2}/electrolyte$^+$ recombination reaction kinetics, but they were able to break the possible porphyrin aggregates formed on the nanoparticle surface, due to the multilayer configuration. Therefore, better injection was then obtained, which ensures a higher photocurrent.

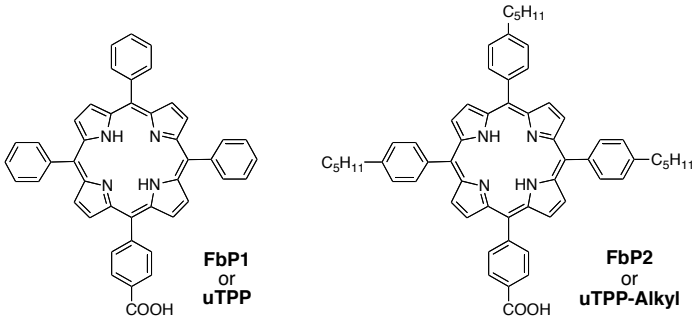

Figure A1 - Chemical structure of porphyrins used in Chapter 3

In Chapter 4, three perylene dyes were studied as photosensitizers for DSSC. In the first study, the effect of dye sensitization time on the final device efficiency as well as the interfacial charge transfer kinetics is discussed. In the second study, the supramolecular interaction between the lithium cation and a crown ether attached to the perylene structure is described. It is well-known that small cations can penetrate into the TiO_2 structure and can shift the conduction band. Thus, the use of lithium

receptors can help to control this shift by controlling the amount of lithium on the nanoparticle surface through supramolecular interactions.

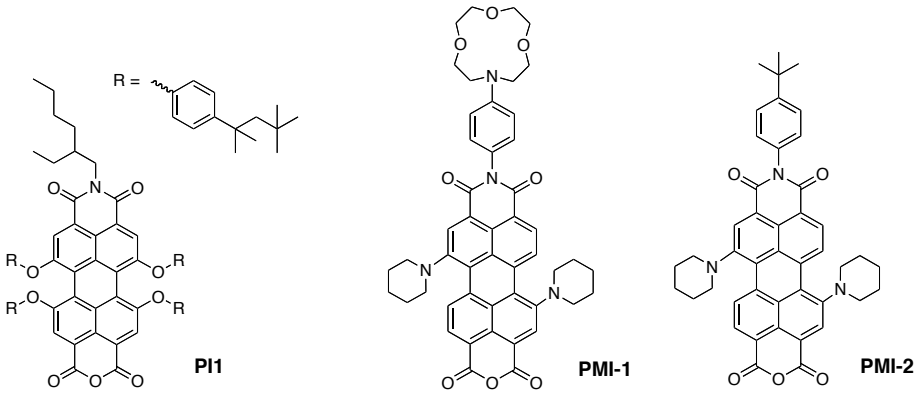

Figure A2 - Chemical structure of perylene dyes used in Chapter 4.

In Chapter 5, the synthesis of two novel organic sensitizers based on a donor π acceptor structure is discussed. The main difference between these dyes relates to the π system, where one dye has an additional electron-donor unit (an *ethandiol* moiety). The addition of this group shifts slightly the absorbance spectrum to the infrared region, which is a requirement of efficient chromophores. Surprisingly, the device final efficiency obtained was lower, due to a reduction in both photocurrent and voltage. Charge transfer reaction kinetics were monitored and the lower photocurrent was assigned to worse dye regeneration by the redox electrolyte. In addition, according to some studies electron-rich atoms, such as oxygen and sulfur, can attract the oxidized electrolyte species. In this study, this also appears to be responsible for the lower voltage obtained for the dye containing the additional *ethandiol* moiety, which is supported by the faster recombination e^-_{TiO2}/electrolyte$^+$ reaction. Therefore, this study demonstrated that a red-shift in absorption is not always indicative of higher efficiency and one should take care about the chemical modifications made to dye structure.

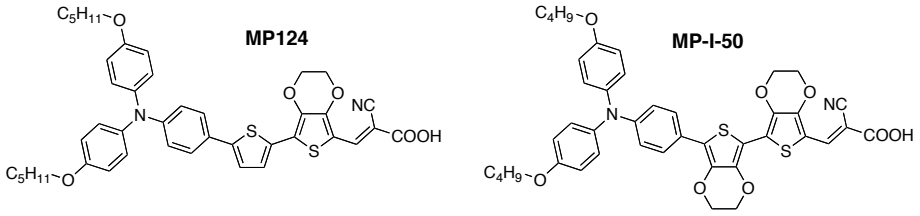

Figure A3 - Chemical structure of push pull organic dyes used in Chapter 5.

ISBN:978-84-693-8861-7/DL:T.1946-2010

Abstract

In Chapter 6 the synthesis of a zinc bisporphyrin and a bipyridyl free base porphyrin is described. These porphyrins were designed and synthesized in order to construct a self assembled supramolecular architecture on the TiO_2 surface through metal mediated interactions. The free base porphyrin consists of two pyridyl ligands at the *meso* position, which form an angle of 90º with the porphyrin ring. On the other hand, the zinc bisporphyrin consisted of two zinc porphyrins, linked by a pyridine bridge with an anchoring group, and forming an angle of 90º between each zinc porphyrin. These two molecules are complementary and they are able to form a self assembly. Thus, by anchoring the zinc bisporphyrin to the TiO_2 nanoparticles and subsequently forming the self assembly, we are able to obtain a higher number of photoactive units per nanoparticle area. The supramolecular effect was firstly observed in plain TiO_2 films, where the quantitative formation of the self assembly was established. Subsequently, this approach was applied to a complete device and the final efficiency obtained for the self assembly was two times higher than the efficiency with the control zinc bisporphyrin. The higher efficiency obtained for the trisporphyrin self assembly was due to an increase in both photocurrent and voltage. The higher photocurrent was assigned to the increased electron injection due to the presence of the additional chromophore. On the other hand, the higher voltage was assigned to a reduction of e^-_{TiO2}/electrolyte$^+$ recombination reaction. Therefore, it has been demonstrated that the use of supramolecular chemistry to the photovoltaic field could be an effective approach for the next generation devices.

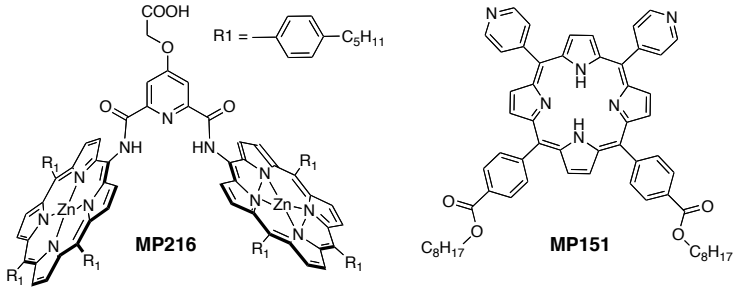

Figure A4 - Chemical structure of porphyrins used for the supramolecular assembly in Chapter 6.

In summary, in the present thesis the design, synthesis and application of novel organic chromophores in Dye Sensitized Solar Cells is described. Moreover, a relationship between the dye molecular structure and the interfacial charge transfer kinetics present at the TiO_2/dye/electrolyte interface, which ultimately control device efficiency, has been established.

ISBN:978-84-693-8861-7/DL:T.1946-2010

Resum

La preocupació per a l'obtenció d'una font d'energia renovable va començar a atraure l'atenció de la comunitat científica quan va quedar palès que no es podria sostenir el nivell de vida actual ni tampoc cap creixement econòmic amb els carburants fòssils disponibles. Per tant, es van desenvolupar diferents tecnologies aprofitant les energies no finites, com per exemple la solar. Diferents tipus de cel·les solars ja han estat comercialitzades, moltes d'elles basades principalment en silici, però degut al seu alt cost de fabricació no han pogut encara competir amb els combustibles fòssils. Així doncs, noves tecnologies solars amb un cost de producció més reduït, com són les cel·les solars sensibilitzades amb colorant (DSSC o *Grätzel cells*, en anglès), són considerades com una possible solució a la problemàtica energètica present avui en dia.

Les DSSC són cel·les foto-electroquímiques formades per un colorant ancorat a un semiconductor nanoestructurat (normalment TiO_2) i en presència d'un electròlit. Quan la llum incideix sobre el dispositiu, l'absorció d'un fotó per part del colorant promou el salt d'un electró des del seu estat fonamental cap a l'estat excitat. Llavors, l'electró es transporta a través de les nanopartícules de TiO_2 cap a l'elèctrode de treball. Un cop allà, l'electró és capaç d'entrar al circuit generant energia elèctrica. Al mateix temps, el colorant oxidat és regenerat per l'electròlit, i aquest és regenerat seguidament al contra-elèctrode.

Aquestes cel·les solars han estat desenvolupades i posteriorment comercialitzades a partir de colorants basats en ruteni. Aquest element és molt poc abundant a l'escorça terrestre, per això el seu ús a gran escala és pràcticament inviable. Per tant, nous colorants orgànics basats en estructures carbonades (CHN) han estat àmpliament investigats per el seu ús en DSSC els darrers anys, ja que són una alternativa més viable econòmicament que els colorants basats en ruteni.

La present tesi està focalitzada tant en la síntesi de molècules orgàniques òpticament actives així com en la seva aplicació i caracterització en dispositius fotovoltaics. En aquests dispositius, cada component té un efecte clau en la eficiència final de la cel·la, degut als processos de transferència electrònica que tenen lloc la interfície TiO_2/colorant/electròlit. Aquests processos varen ser estudiats en gran detall per poder definir uns paràmetres amb els quals la eficiència del dispositiu es pugui relacionar amb l'estructura molecular del colorant.

El capítol 3 tracta de l'ús de porfirines, molècules àmpliament conegudes degut al seu rol principal en la fotosíntesi, com a colorants per a DSSC. Es van dissenyar i sintetitzar dues porfirines que difereixen en la seva estructura molecular per la presència o absència de cadenes alquíliques lineals de 5 àtoms de carboni. Seguidament es va estudiar l'efecte que tenien les cadenes alquíliques en els dispositius fotovoltaics. Es va observar que l'efecte de les cadenes alquíliques era ben diferent si es té en compte com estava distribuït el colorant a la superfície del TiO_2: monocapa o multicapa. En el primer cas, les cadenes alquíliques impedien que l'electròlit s'acostés a la superfície del diòxid de titani, obtenint així una cinètica de recombinació entre l'electró injectat al TiO_2 i l'electròlit oxidat (e^-_{TiO2}/electròlit$^+$) més lenta, fet que va incrementar el voltatge obtingut. En el segon cas, les cadenes no alteraven la cinètica de recombinació esmentada anteriorment, sinó que evitaven la formació d'agregats (espècies que desactiven l'estat excitat de la molècula). Per tant, en el segon cas es va obtenir una una millor injecció i, conseqüentment, un millor foto-corrent.

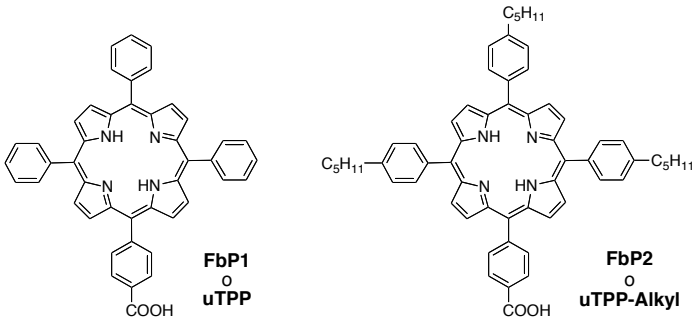

Figura A1 - Estructura química de les porfirines utilitzades en el capítol 3.

Al capítol 4 es varen estudiar perilens com a colorants per DSSC. En un primer estudi es va observar com el temps de sensibilització és un paràmetre que cal controlar, ja que diferents temps donaven diferents cinètiques de recombinació, i com a resultat diferents eficiències. En un segon estudi es va estudiar la interacció supramolecular entre un èter corona situat a un extrem de un perilè amb el catió liti present a l'electròlit. Els cations de menor radi, com el liti, es poden intercalar a l'estructura porosa del diòxid de titani, fent baixar així la seva banda de conducció. El fet de tenir un èter corona al colorant permet disminuir la presencia de liti a la superfície de les nanoparticules, fent pujar la banda de conducció del TiO_2 i millorant-ne el voltatge.

ISBN:978-84-693-8861-7/DL:T.1946-2010

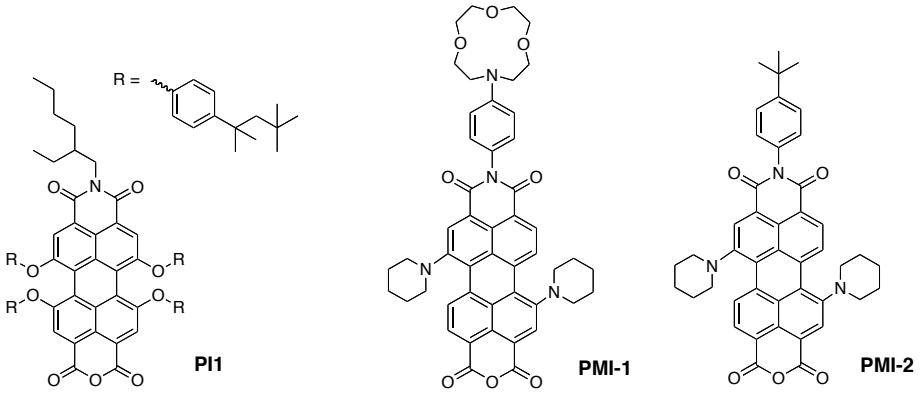

Figura A2 - Estructura química dels perilens utilitzats en el capítol 4.

Al capítol 5, dos colorants orgànics formats per una part donadora, un sistema π i una part acceptora varen ser sintetitzats. La principal diferència entre ells recau al sistema π, on un colorant té un grup electro-donador addicional, format per un diol. Amb l'addició d'aquest grup, es pretenia desplaçar l'espectre d'absorció de la molècula cap a l'infraroig. Aquest efecte es va aconseguir, però l'eficiència final del dispositius fotovoltaics era sorprenentment més baixa tenint en compte la modificació feta, ja que es va observar una disminució tant en la foto-corrent com en el voltatge. Un cop estudiats tots els processos cinètics que tenen lloc a la interfase TiO_2/colorant/electròlit, es va assignar aquesta disminució de corrent a una cinètica de regeneració més lenta per el colorant amb més grups electro-donadors. A més a més, està descrit que grups rics en oxigen i/o sofre poden atraure l'espècie oxidada de l'electròlit, cosa que explicaria la disminució del voltatge observada. La cinètica de recombinació e^-_{TiO2}/electròlit$^+$ més ràpida pel colorant amb més grups electro-donadors va recolzar aquesta hipòtesi. Per tant, s'ha de tenir cura a l'hora de dissenyar un colorant per tal d'absorbir cap a l'infraroig, ja que no sempre una banda d'absorció cap el vermell significa una millor eficiència.

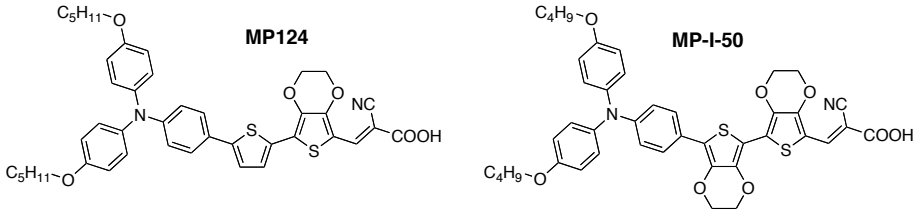

Figura A3 - Estructura química dels colorants D - π - A utilitzats en el capítol 5.

Al capítol 6, es varen sintetitzar una bisporfirina de zinc i una porfirina amb dos lligands piridil que formen un angle de 90 graus. Aquest disseny va ser ideat per tal d'aconseguir una interacció ditòpica zinc - piridina, formant així una trisporfirina cíclica com a ensemblatge supramolecular. Així doncs, ancorant a la bisporfirina a les nanopartícules i posteriorment formant el complex supramolecular es pot aconseguir augmentar el nombre d'unitats foto-actives sense necessitat de tenir un grup d'ancoratge. Aquesta és una estratègia molt poc utilitzada en el camp de la fotovoltaica i que podria donar molt bons resultats. L'efecte supramolecular es va estudiar primer en pel·lícules fines de TiO_2, on es va establir que la formació d'aquest ensemblatge era quantitatiu. Seguidament es va aplicar aquesta estratègia a dispositius fotovoltaics, on l'eficiència obtinguda per l'ensemblatge molecular es va veure duplicada si ho comparem amb una bisporfirina de zinc a soles o complexada per una unitat no foto-activa. Aquest augment es va assignar tant a una injecció d'electrons extra deguda a la unitat cromòfora addicional així com a una disminució de la cinètica de recombinació e^-_{TiO2}/electròlit$^+$. Per tant, la utilització de la química supramolecular aplicada a la fotovoltaica i a les DSSC en particular pot ser una estratègia molt vàlida per futures generacions de dispositius solars.

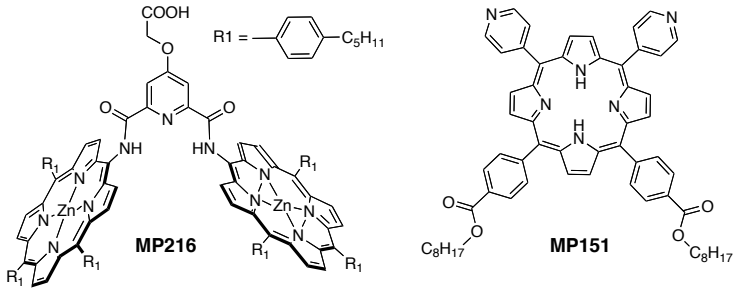

Figura A4 - Estructura química de les porfirines utilitzades per l'ensemblatge supramolecular al capítol 6.

En definitiva, en aquesta tesi s'han dissenyat i sintetitzat nous colorants orgànics, els quals s'han aplicat a les DSSC. Finalment, s'han establert unes relacions entre l'estructura molecular del colorant i les cinètiques que tenen lloc a la interfase TiO_2/ colorant/electròlit, així com amb l'eficiència final dels dispositius.

UNIVERSITAT ROVIRA I VIRGILI
DESIGN AND SYNTHESIS OF ORGANIC SENSITIZERS FOR DYE SOLAR CELLS: MOLECULAR STRUCTURE VS DEVICE PERFORMANCE
Miquel Angels Planells Dillundé
ISBN:978-84-693-8861-7/DL:T.1946-2010

Acknowledgements

This thesis work has not been easy. A Ph.D. is a long journey where some things turn out to be not as good as wished. However, due to the support of several people around me, I have been able to finish this important step in my life.

Therefore, I would like to express my sincere gratitude to:

Emilio Palomares, my supervisor, for accepting and encouraging me during an exciting but rarely easy PhD. These four years of guidance have been very instructive for me.

Pau Ballester for his excellent discussions and guidance of organic and supramolecular chemistry. Even though we often held different points of view in scientific matters, it is always good to share opinions.

The Spanish Ministry of Science (FPU fellowship reference AP2006-828) and the ICIQ foundation for their financial support.

John and Emilio, for their dedication regarding thesis comments and corrections, even in vacation time. Toni, Anna and Javi, your proof-readings have been also valuable.

Laia and Amparo for the awesome solar cells they made.

Javi and Toni for the exciting discussions and for setting up the amazing spectroscopic and electrochemical systems.

All of the members of the Palomares research group who helped in various stages of my Ph.D.: Eugenia, Anna, Josep, Toni, John, Margherita, Laia, Amparo, Iván, James, Aurelien, Lydia, Eva and Bea. I had a great time working with you guys.

Prof. Harry Anderson, for his excellent organic chemistry suggestions, as well as his awesome research group: Karl, Mel, Giussepe, Steve, Johannes, Marie, Louisa, Hazel and Kosuke. I had a great time in Oxford making never-ending porphyrins!

Prof. Seth Marder, for his scientific ideas and discussions, as well as his amazing research group: Sergio, Jess, Jon, Carlos, Annabelle, Helen, Richard, Qing, Yadong, Steve, O'Neil. It was a pleasure to share my time working and enjoying life with you guys in Atlanta!

Dr. Núria López for calculations and interesting ideas.

All ICIQ scientific staff.

Last, but not least, to my family and friends who support me these 4 years in Tarragona. In addition, I would like to thank a very special person and probably the main reason why I have gotten this far. Thanks a lot Anna.

UNIVERSITAT ROVIRA I VIRGILI
DESIGN AND SYNTHESIS OF ORGANIC SENSITIZERS FOR DYE SOLAR CELLS: MOLECULAR STRUCTURE VS DEVICE PERFORMANCE
Miquel Angels Planells Dillundé
ISBN:978-84-693-8861-7/DL:T.1946-2010

Table of Contents

UNIVERSITAT ROVIRA I VIRGILI
DESIGN AND SYNTHESIS OF ORGANIC SENSITIZERS FOR DYE SOLAR CELLS: MOLECULAR STRUCTURE VS DEVICE PERFORMANCE
Miquel Angels Planells Dillundé
ISBN:978-84-693-8861-7/DL:T.1946-2010

UNIVERSITAT ROVIRA I VIRGILI
DESIGN AND SYNTHESIS OF ORGANIC SENSITIZERS FOR DYE SOLAR CELLS: MOLECULAR STRUCTURE VS DEVICE PERFORMANCE
Miquel Angels Planells Dillundé
ISBN:978-84-693-8861-7/DL:T.1946-2010

1. Introduction

1.1. Solar Energy Conversion

1.1.1. Harvesting the sun's energy

"*In any given hour, more energy from sunlight strikes the earth than the entire planet consumes in a year, but solar cells currently contribute less than 0.1 percent of electricity supply*" - David Mitzi, IBM Researcher.

Economic growth, as well as the quality of human life, strongly depends on the availability of energy resources. The total energy consumption in the world in 2008 was $4.8 \cdot 10^{20}$ Joules (15 TW).[1] Up to now, the main energy source has been provided by fossil fuels (from 80 to 90%), such as coal, oil or gas. Fossil fuel based technology is still now dominating the energy market primarily due to their low-cost. However, these supplies are non-renewable, highly polluting and their availability is not infinite. Furthermore, forecasts predict an increase in human energy consumption in the next 50 years as a consequence of population increases and economic development. Therefore, an alternative energy source must be sought.

The amount of sunlight which strikes the earth annually is equivalent to $3 \cdot 10^{24}$ Joules of energy, which is roughly 6000 times higher than global energy consumption. Thus, this environmentally friendly and readily available energy source is receiving significant attention from both governments and industry. Up to now, solar energy has contributed only a small fraction to global energy needs, mainly due to the high cost of production of solar panels. Therefore, solar energy must be captured, converted and stored in a highly efficient manner and at low-cost in order to truly compete with fossil fuels as a source of energy.[2]

1.1.2. Brief history of photovoltaic devices

The first photovoltaic (PV) effect was observed by Becquerél in 1839, who reported a current flow between two silver electrodes in an electrolyte media upon light exposure.[3] This effect was described later in more detail, when Adams and Day noticed that the performance of selenium wires, used in telecommunications, was dependent on sunlight intensity. They demonstrated that sunlight applied to a solid material could generate electricity.[4] Despite efforts to develop solar cells with

selenium wires, only 0.5% efficiency was obtained, which was not high enough for the large scale up of solar modules.

Later in 1953, researchers at Bell Laboratories discovered that silicon material, upon sunlight exposure, gives a current 5 times greater than that observed for selenium wires. After device optimization, silicon solar cells were able to generate power supplies of up to 6%,[4] allowing for their commercialization.

This technology was applied principally to power spacecraft orbiting the earth. Researchers in the USA rapidly developed high performance solar cells, which became a key component in helping the USA to win the space race.

1.1.3. Inorganic solar cells: the p-n junction

Inorganic solar cells are still the most efficient PV technology today and have found many consumer, military and space applications.[4, 5] They are based on a p-n junction of inorganic materials, such as doped silicon, connected to electrodes with different work functions.

A p-n junction is based on the assembly of two semiconductor materials with different compositions: **1**) an n-type material, where the majority carriers are electrons and **2**) a p-type material, where the majority carriers are holes. The contact area of p- and n- type materials is denoted as the p-n junction interface. When n- and p-type materials come into contact, electrons move from the n-type side to the p-type side by diffusion. The result is a build up of positive charge along the n-type side of the interface and build up of negative charge along the p-type side (Figure 1.1). The flow of electrons and holes at the interface creates an electric field, which extends to a region called the depletion layer.

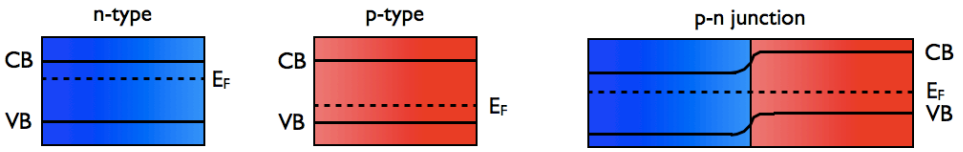

Figure 1.1 - Schematic representation of p- and n-type semiconductors and their assembly in a p-n junction. The fermi level is indicated as E_F whereas the conduction and valence bands are denoted as CB and VB, respectively.

In a semiconductor material, the bandgap is defined as the energy difference between the valence and the conduction bands and is an inherent property of the

material. When the bandgap matches the solar irradiance spectrum, the semiconductor material can absorb the light, which results in free charge carriers. Electrons and holes generated diffuse toward their respective electrodes generating electricity.

Silicon doped material for solar cells have been extensively investigated for a long time and, therefore, are the most used. The highest efficient silicon PV device is based on doped monocrystalline silicon (*c*-Si), which produces an efficiency of 25% (commercially available solar cells produced by SunPower reach 22%).[6] However, such devices require extremely pure materials and laborious encapsulation techniques, thus the cost per generated watt is relatively high.[7] Cheaper alternatives have been developed using both polycrystalline silicon (*p*-Si) and amorphous silicon (*a*-Si) as the semiconductor material, which produce an efficiency of 20% and 13%, respectively.[8, 9] These lower efficiencies compared to *c*-Si are due to defects in the crystalline structure of the *p*-Si morphology as well as the inherent disorder in the material for *a*-Si which accelerates electron and hole recombination and makes charge transport difficult. Furthermore, the bandgap of amorphous silicon, 1.7 eV, is higher than mono- and poly-crystalline, 1.1 eV, which results in a lack of infrared absorption.[9]

An alternative to doped silicon materials are the elements from group III and V of the periodic table, such us gallium arsenide (GaAs).[10] Just like in doped silicon cells, they are based on a p-n junction structure, connected to their respective electrodes. These PV devices show better thermal and radiative stability compared to silicon devices as well as lower bandgaps (e.g. 1.42 eV for GaAs), which match better the solar spectrum. The thermal stability of GaAs PV devices allows them to work under light concentrators, which consist of are a series of refractive lenses that focus the light arriving from the sun onto a small surface area.[11] The use of concentrators, which can achieve intensities of up to 1000 suns, allows the possibility of making cells with lower surface area, resulting in less material needed for fabrication. Moreover, these PV devices should be able to work under extreme conditions of light and temperatures.

In addition, GaAs cells can be improved by the multijunction approach, which involves the addition of various p-n junction layers with different bandgaps, in order to cover the full solar spectrum. In Figure 1.2, a schematic representation of this PV device is shown.

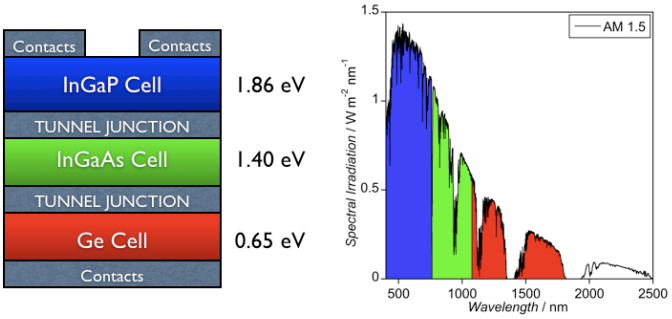

Figure 1.2 - Schematic representation of a multijunction solar cell (*left*). The presence of different bandgaps in the PV device are able to capture most of the solar irradiation spectrum (*right*).

1.1.4. Organic solar cells

Organic semiconductors, either based on small molecules (porphyrins, phthalocyanines, etc.) or polymers, are a new class of π conjugated materials which present very interesting optoelectronic properties for use in light emitting diodes (LEDs),[12, 13] field effect transistors (FETs),[14, 15] and solar cells applications.[16, 17] In recent years, organic photovoltaics (OPVs) have attracted widespread interest in both academia and industry because, the materials used are promising in terms of low cost, flexibility and ease of processing.[18, 19] Efficiencies (5 - 7%) are lower than other solar cell architectures but have been growing steadily over the last few years. OPVs are generally based on two materials, an electron donor (hole transporting material) and an electron acceptor (electron transporting material), which are sandwiched between electrodes of different work function.

When OPVs are exposed to light, excitons (tightly bound electron-hole pairs) are generated mainly in the donor material, although few excitons are also generated in the acceptor material (Figure 1.3a). The exciton dissociation takes place at the donor - acceptor interface. The difference between the electron affinities (or ionization potentials) of the two materials creates an energy offset which enable the exciton splitting to take place (Figure 1.3b). Finally, the charge carriers generated at the interface are transported through the materials to their respective working electrodes (Figure 1.3c).

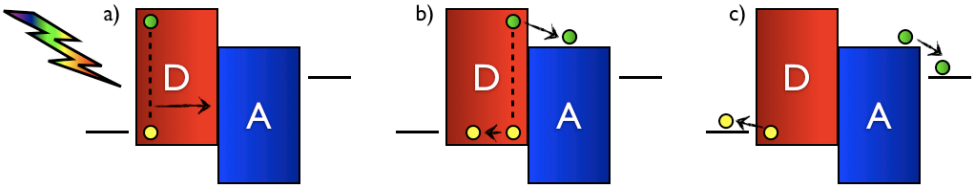

Figure 1.3 - Schematic representation of the processes occurring in OPVs under light illumination.

Efficient exciton transfer and dissociation is crucial for molecular based OPVs, however, the short exciton lifetime (from 100 ps to 1ns) may prevent its effective splitting.[20] Exciton dissociation can be improved by the appropriate selection of the electron donor and acceptor materials as well as an optimization of the thickness of the organic layers. For example, Tang reported 1% efficient OPV solar cells when a bilayer of phthalocyanine/perylene derivatives was employed.[21] The efficiency of such bilayer is limited by the exciton diffusion length, which is approximately 10 nm for organic semiconductor materials.[20] Ideally, the bilayer should only be as thick as the exciton diffusion length, however, this thickness would not be high enough to obtain efficient light harvesting.

In order to solve this problem, bulk heterojunction solar cells have been developed.[22, 23] These cells are based on interpenetrating networks of electron donor and acceptor materials. This approach enhances the donor - acceptor interface area compared to bilayer OPVs, by decreasing the distance between both materials due to the presence of domains. Thus, the domain length is close enough to the exciton diffusion length and thicker devices of 100 nm can be achieved overcoming the issue in bilayers devices.

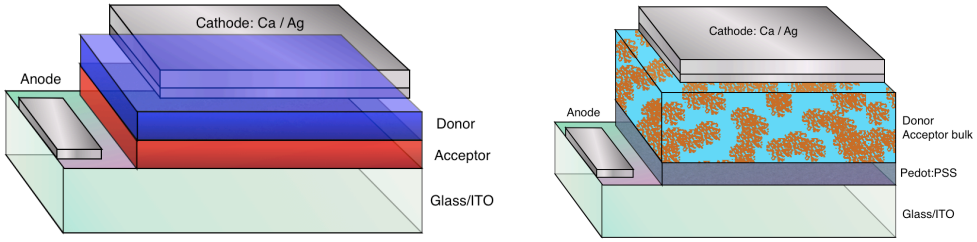

Figure 1.4 - Schematic representation of bilayer (*left*) and bulk heterojunction (*right*) OPVs.

OPVs can be classified depending on the nature of the material used, which can be either small molecules or polymers. Both materials use conjugated π systems as the photoactive core. Small molecule devices are usually fabricated by sublimation of successive layers of electron and hole transporting materials under vacuum. In

contrast, polymer OPVs are usually prepared by solution processing, making them suitable for an easy and cheap way of manufacturing.[24] Several molecules have been designed, synthesized and used by several research groups. Some of the most common ones are shown in the Figures 1.5 and 1.6.

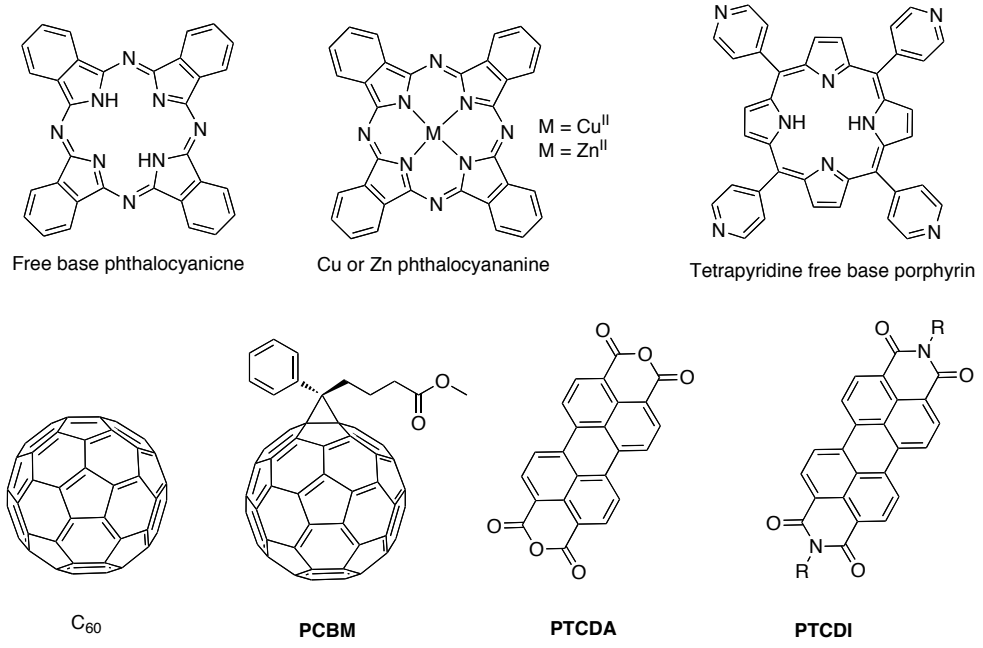

Figure 1.5 - Chemical structures of small molecules used in OPVs. Porphyrins and phthalocyanines are used as donors while fullerene and perylene derivatives are used as acceptors.

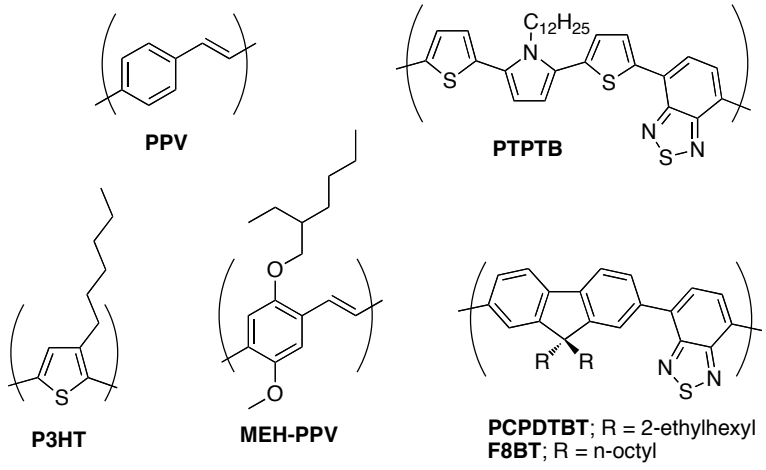

Figure 1.6 - Chemical structures of polymers for OPVs. The polymers are used as donor moieties.

1.1.5. Photoelectrochemical cells

Photoelectrochemical cells are solar cells based on a semiconductor photoanode and a metal cathode immersed in an electrolyte. Some photoelectrochemical cells simply convert light into electrical energy, while others use light to produce hydrogen or reduce CO_2.[25]

An interesting class of photoelectrochemical cells are dye sensitized solar cells (DSSC). This kind of PV device is based on a photosensitizer attached to a wide bandgap semiconductor material. The role of the photosensitizer is to harvest the light, while the charge transport takes place in the semiconductor. The semiconductor material is supported onto conductive glass, which is connected to a counter electrode through an external circuit. An electrolyte which contains a redox pair is placed between both electrodes. An schematic representation is shown in Figure 1.7.

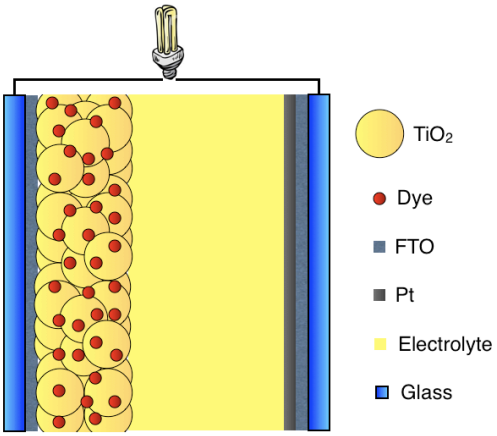

Figure 1.7 - DSSC configuration.

Interest in DSSCs can be traced back to the 1970's when a crystalline semiconductor was used as a support for photosensitizers.[26, 27] However, low efficiencies were obtained due to the small surface area available for dye anchoring resulting in only a small fraction of the incident radiation being harvested. The breakthrough for the DSSC came in 1991, when Grätzel and O'Regan, developed a nanostructured mesoporous semiconductor material.[28] With the semiconductor material in a nanocrystalline form the surface area is increased by up to 1000 times, allowing for higher concentrations of dye to be anchored onto the electrode surface resulting in more efficient harvesting of incident radiation.

A detailed description of the operating principles of the dye sensitized solar cell materials used is explained in section 1.2 and 1.3 of this chapter.

1.1.6. Summary and outlook

Several photovoltaic devices have been reviewed in the previous sections. Silicon PV devices have been commercialized for a relatively long time, therefore, they have been the most optimized for commercial purposes. However, the requirements of using highly pure materials and accurate encapsulating and processing techniques increases the cost of silicon based cells, restricting these photovoltaic devices to certain niche applications. On the other hand, the production cost can be reduced significantly by using other silicon materials, such as *a*-Si and *p*-Si, but at the cost of lower cell efficiencies.

Up to now, multijunction GaAs solar cells are the most efficient PV devices, although, their extremely high production costs restricts their use to space missions.

Emerging PV technologies, such as OPVs and DSSCs, are extremely promising although their efficiencies still need to be improved before large scale commercialization can begin. The distinguishing characteristic of these cells is that charge carriers are generated and simultaneously separated across an interface; the TiO_2/dye and donor/acceptor interface for DSSC and OPVs respectively. In contrast, photogeneration of free electron-hole pairs occurs throughout the bulk semiconductor in conventional inorganic cells, and carrier separation upon their arrival at the junction is a subsequent process. This apparently minor mechanistic distinction results in fundamental differences in photovoltaic behavior.

In particular, DSSC are less sensitive to impurities compared to inorganic PV. This allows an easier cell fabrication methodologies, such as inexpensive and scalable non vacuum and low temperature processing. These cells can also be made on lightweight and flexible or rigid substrates and can be incorporated into portable devices. Moreover, many different materials can be used in DSSCs making it possible to tune their photovoltaic properties. As an example, the photosensitizer dictates the color of the cell, which makes this technology architecturally interesting for their incorporation into homes and buildings thereby performing an aesthetic as well as practical function.

As shown in Figure 1.8, several efforts in developing new generation solar cells as well as improving efficiencies of older PV technologies have been performed over the last decades.

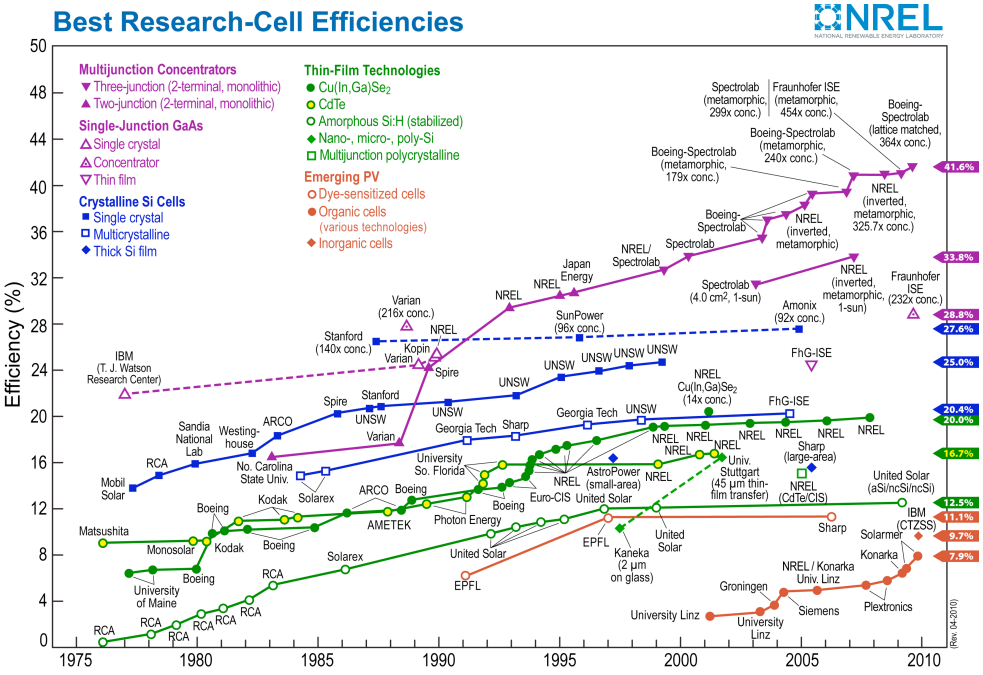

Figure 1.8 - Progress on solar cells. Copyright NREL.

1.1.7. Photovoltaic Performance

Solar cell performance is evaluated by measuring the current, voltage, maximum power, and overall efficiency in converting light into electrical energy.

The power conversion efficiency (η) of a PV device is used is usually given with reference to a specific light irradiation intensity (e.g. AM 1.5). The η plot (or "I-V curve"), involves the measurement of cell photocurrent densities ($I \cdot cm^{-2}$ or J) at a constant light level exposure, while a voltage (V) is applied to the cell.

The standard I-V curve typically passes through two significant points: **1**) the short-circuit current (J_{sc}), which is the current produced when the positive and negative electrodes of the cell are short-circuited, and the voltage is zero and **2**) the open-circuit voltage (V_{oc}), which is the voltage across the positive and negative electrodes under open-circuit conditions, and the current is zero.

ISBN:978-84-693-8861-7/DL:T.1946-2010

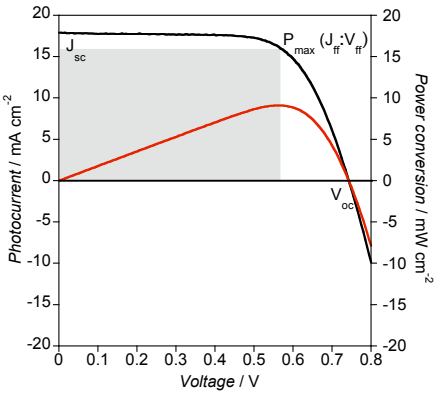

Figure 1.9 - I-V curve of a PV device (*black line*) and its power conversion (*red line*). The gray area indicates the maximum power generated by the cell.

Power is defined as the product of voltage times current. The maximum power (P_{max}) represents the maximum efficiency of the solar device in converting sunlight into electricity.

The fill factor (FF) measures the "squareness" of the I-V curve and describes the degree to which the voltage at the maximum power point (V_{ff}) matches V_{oc} and that the current at the maximum power point (J_{ff}) matches J_{sc} (Equation 1) The higher the fill factor the "squarer" the I-V curve as well as higher the efficiency.

$$FF = \frac{J_{ff} \cdot V_{ff}}{J_{sc} \cdot V_{oc}} \qquad (1)$$

Thus, the power conversion efficiency of a solar cell is the percentage of the solar energy shining on a PV device that is converted into electrical energy. η (%) is determined by the photocurrent density at short circuit (J_{sc} / mA·cm^{-2}), the voltage at open circuit (V_{oc} / V), the fill factor (FF / %) and the power of the incident light (P_{light} / mW·cm^{-2}), as shown in Equation 2:[29]

$$\eta = \frac{P_{max}}{P_{light}} = \frac{J_{sc} \cdot V_{oc} \cdot FF}{P_{light}} \qquad (2)$$

Solar radiation intensity is defined in terms of air mass (AM). The radiation flux outside the Earth's atmosphere is defined as AM 0. The spectrum of sunlight changes when it arrives at the Earth's surface due to light scattering and filtering from the different molecules present in the atmosphere. Thus, solar radiation at the surface of the Earth is defined as AM 1.5 (incident sunlight angle of 41.8º), and is

usually assigned as the reference light intensity (P_{light} = 100 mW·cm^{-2})[30] when measuring the efficiency of solar cells.

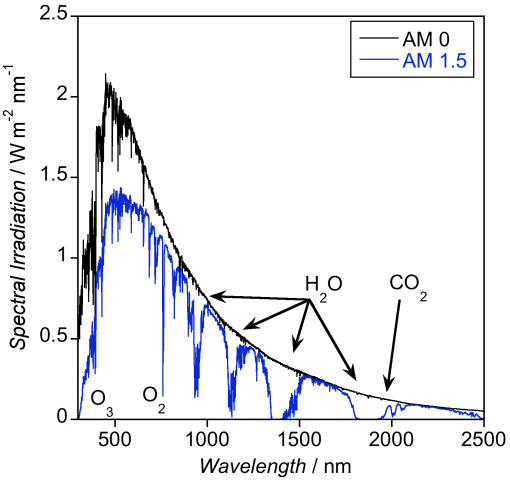

Figure 1.10 - Solar irradiation spectrum at AM 0 (*black line*) and AM 1.5 (*blue line*). The species responsible for the lack of absorption at the Earth's surface are indicated.

The incident photon-to-current conversion efficiency (IPCE), also known as external quantum efficiency (EQE), is the ratio between the number of electrons generated by the solar cell and collected at the external circuit and the number of photons of a given wavelength shining on the solar cell. IPCE is calculated by the number of electrons flowing through the external circuit, $J_{sc}(\lambda)$ / mA·cm^{-2}, divided by the number of incident photons, $P_{light}(\lambda)$ / mW·cm^{-2}, at the measured wavelength, λ / nm, multipled by the conversion factor 1240 as shown in Equation 3. Usually, the IPCE spectrum can be correlated to the absorbance spectrum of the dye.

$$IPCE(\lambda) = \frac{1240 \cdot J_{sc}(\lambda)}{\lambda \cdot P_{light}(\lambda)} \qquad (3)$$

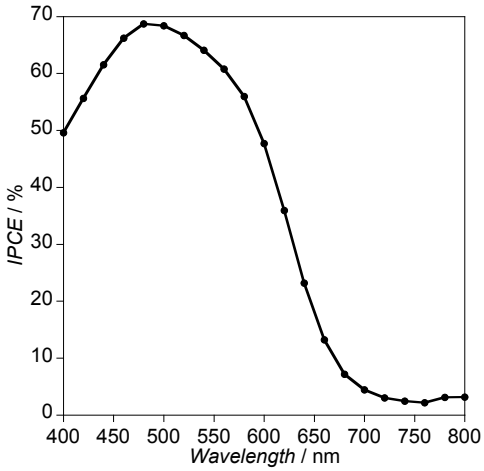

Figure 1.11 - IPCE spectrum of a PV device.

The efficiency of solar cells, as well as IPCE, is affected by a variety of factors, because much of the energy from sunlight is lost before it can be converted into electricity. These factors can be:

- *Wavelength of light*: When light strikes the surface of a solar cell, some photons are reflected and do not enter the cell. In addition, some photons that are able to pass through the material only have enough energy to generate heat.
- *Bandgap*: It is defined as the minimum amount of energy required to generate excitons and it depends on the material in question. Furthermore, the primary reason why PV cells are not 100% efficient is because they cannot respond to the entire spectrum of sunlight. Photons with energy lower than the material's bandgap are not absorbed whereas photons with higher energy can lose a part of its energy through non-radiative relaxation.
- *Recombination*: Electrons and holes generated after light exposure may eventually recombine before they make it into the electrical circuit and contribute to the current of the cell.
- *Resistance*: The natural resistance to electron flow in a cell due to the material properties can effect cell efficiency.
- *Temperature*: Solar cells work best at low temperatures, as determined by their material properties. All cell materials lose efficiency as the operating temperature rises because of increases in recombination pathways.
- *Reflection*: A cell's efficiency can be increased by minimizing the amount of light reflected away from the cell's surface.

1.2. Dye Sensitized Solar Cells (DSSC)

Dye sensitized solar cells, DSSCs, are multi-component devices for the conversion of light into electricity. Their efficiency depends critically on the individual properties of each of the materials used, which play specific roles in the processes involved in converting sunlight into electricity.

1.2.1. Principles of operation

A DSSC is based on a photo active working electrode and a counter electrode contacted by a liquid redox electrolyte (Figure 1.12 - *left*). The working electrode consists in a nanostructured metal oxide semiconductor film, usually TiO_2, attached to a conductive glass substrate. A light absorbing layer, or photosensitizer, is anchored onto the TiO_2 surface. The counter electrode consists of a platinized conductive substrate and the redox system is usually a liquid electrolyte with iodide/ triiodide (I^-/I_3^-) redox couple.

The working principle involves several key processes, such as light absorption, electron injection, transport and collection (Figure 1.12 - *right*). After light irradiation, an electron is promoted from the photosensitizer ground state to the excited state. These excited dyes inject electrons into the semiconductor conduction band. The charge separation processes which occur at the TiO_2-dye interface results in an electron in the semiconductor conduction band and a hole on the dye sensitizer. Following this, electrons will be transported through the nanoparticle network and they finally reach the back contact of the working electrode. The charge collected is extracted and work is performed in the external circuit. The reduction of oxidized dye by the electrolyte and the subsequent reduction of oxidized electrolyte at counter electrode completes the circuit.

ISBN:978-84-693-8861-7/DL:T.1946-2010

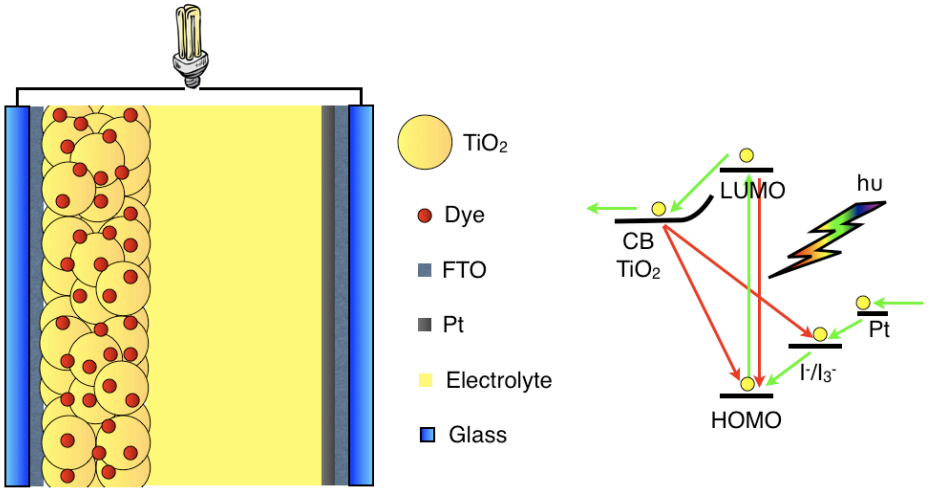

Figure 1.12 - Schematic representation (*left*) and energy level diagram (*right*) of processes occurring in DSSC. Green and red lines represent desired and undesired processes, respectively.

1.2.2. Working electrode

The working electrode is based on a nanocrystalline semiconductor material immobilized onto a conductive substrate. As explained in Chapter 1.1.5, the use of these nanocrystalline materials was a breakthrough for DSSC performance.[25, 28] The large surface area obtained made it possible to increase the number of dye molecules attached to the semiconductor surface, and as consequence, result in much improved light absorption of the electrode.

Common semiconductors used in DSSC are the large bandgap metal oxides, with bandgaps from 3.0 to 3.2 eV. where only UV light energy can be absorbed. In order to enhance the absorption to the visible region, photo active molecules are anchored onto the surface. The most extensively used semiconductor material is TiO_2, although other n-type semiconductors such as Nb_2O_5,[31] ZnO,[32] or SnO_2[33] have also been tested. On the other hand, NiO has been used as p-type semiconductor material.[34] However, TiO_2 has been shown to display the most promising efficiencies in DSSC and in addition is a non-toxic, readily available and non-expensive material.[28]

The electrode consists of interconnected arrays of nanoparticles. They form a porous network electrode (~ 50% porosity) with nanoparticle diameters ranging from 15 to 30 nm with film thickness of between 8 - 12 µm.[35] Furthermore, a 4 µm thick film of larger diameter TiO_2 particles (300 - 400 nm) is often deposited on top of the

15 - 30 nm TiO_2 film which forms the "scatter layer", reflecting light which has passed through unabsorbed back into the film where it can be absorbed by the dye sensitizer molecules.

The nanoparticles are obtained by preliminary deposition of a colloidal dispersion of TiO_2 paste onto a conductive substrate using either doctor blade or screen printing techniques.[36, 37] Subsequently, sintering at 450 - 500 ºC results in a nanostructured mesoporous TiO_2 electrode, which can be soaked in a dye solution for a period of time to obtain a photo active working electrode.

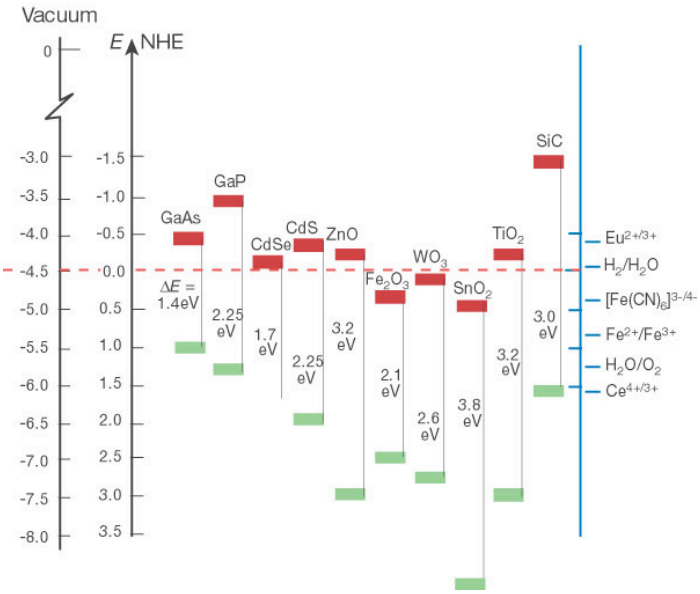

Figure 1.13 - Bandgap positions of several semiconductors. Figure extracted from Nature.[25]

Rutile, anatase and brookite are the three morphological forms of TiO_2. Rutile is the most thermodynamic stable form while anatase is stable only at low temperatures, less than 600 ºC (brookite form is difficult to obtain).[35] The reduced density of anatase compared to rutile leads to remarkable differences in its physical properties, such as bandgap. The lower bandgap of rutile means it can absorb close to the UV region, from 350 to 400 nm. Therefore, upon light irradiation in this region, electron-hole pairs can be generated in the semiconductor and the photosensitizer attached can be oxidized, leading to solar cell instability and degradation. However, the higher bandgap of anatase avoids most of the near UV light absorption, thus, reducing solar cell degradation. Furthermore, anatase has better electron mobility

compared to rutile and for these reasons it is the morphological form chosen for DSSC applications.

The TiO_2 nanoparticles can be characterized by common surface characterization techniques: **1**) X-ray powder diffraction allows us to elucidate the morphological form, **2**) TEM sheds light on the nanoparticle diameter, **3**) SEM indicates the nanoparticle distribution and homogeneity on the film, **4**) AFM shows the roughness of the film, **5**) profilometer determines film thickness and **6**) BET analysis elucidates the surface area and film porosity.

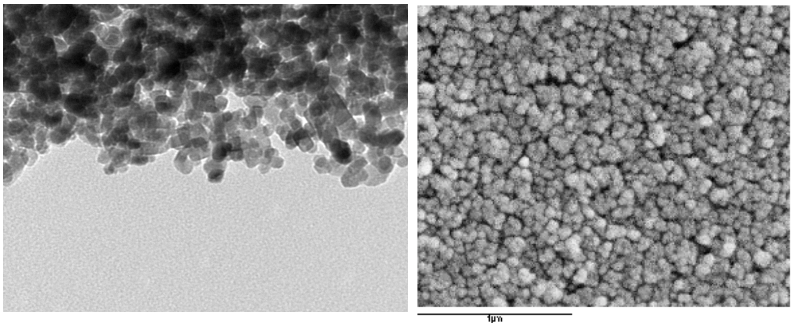

Figure 1.14 - TEM (*left*) and SEM (*right*) images of nanostructured TiO_2.

1.2.3. Photosensitizer

The photosensitizer is responsible for capturing the light in DSSC. The photophysical and electrochemical properties of dyes can vary greatly, however, efficient dyes generally have the following properties:

1. The absorbance profile of the photosensitizer should match as close as possible that of the solar spectrum.

2. The HOMO of the dye should be located as far as possible from the surface of TiO_2 nanoparticles. Furthermore, the HOMO energy level should be lower than that of the redox potential of the redox electrolyte.

3. The LUMO of the dye should be placed on the anchoring group or as close to the surface of the TiO_2 nanoparticle as possible for efficient electron injection into the semiconductor electrode. In addition, the LUMO energy level should be higher with respect to the TiO_2 conduction band potential.

4. The photosensitizer should be luminescent.

5. The dye should not aggregate on the metal oxide surface.

6. The photosensitizer should have chemical, thermal and electrochemical stability during exposure to solar radiation and in the electrolyte media.

The anchoring group is a key point in the photosensitizer. Several anchoring groups can be used, such as alkoxysilyl[38] or phosphoric acid,[39] however, the most common is the carboxylic acid group.[36, 40] All of these groups react spontaneously with the hydroxyl groups on the TiO_2 surface leading to the formation a stable linkage.

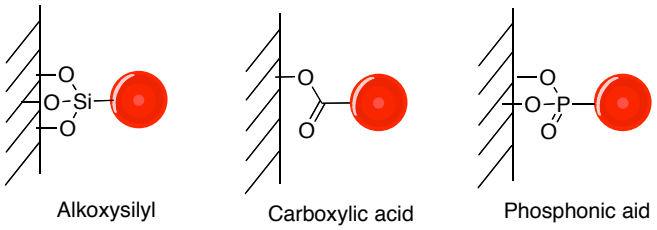

Figure 1.15 - Covalent binding modes of anchoring molecules to TiO_2. Red spot represents a dye.

Co-sensitization with co-adsorbents is an approach which gives excellent results because not only does it control the photosensitizer distribution on the TiO_2 surface, but also it can retard undesired recombination reactions.[41] Chenodeoxycholic acid, denoted as **CDCA**, is one of the most common co-adsorbents used due to: **1**) The insertion of this bulky molecule between the photosensitizers on the TiO_2 surface can break the dye aggregation, which is a big problem when organic dyes are used, and **2**) it can reduce the back electron transfer reaction between the redox electrolyte and electrons in the TiO_2 nanoparticles, decreasing this recombination process.

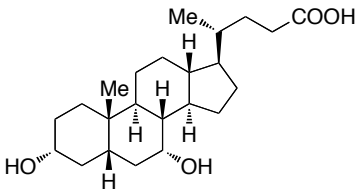

Figure 1.16 - Chemical structure of **CDCA**.

A detailed explanation, as well as illustrative examples of photosensitizers used in DSSC, can be found on Chapter 1.4 of this thesis.

1.2.4. Electrolyte

The electrolyte in a DSSC is a redox media whose function is to regenerate the oxidized dye, and it can be present both in the liquid and solid-state. Electrolyte components, such as the redox couple, solvent, additives, cations, etc. have been optimized over the last two decades, nevertheless, some aspects are essential for any electrolyte:

1. The redox pair should regenerate the oxidized dye efficiently.

2. The electrolyte must be able to permit fast diffusion of charge carriers, higher conductivity, and create an effective contact between the counter and working electrodes.

3. They should have long-term chemical, thermal and electrochemical stability.

4. They should be non-corrosive with DSSC components.

5. Their absorption should not overlap with the photosensitizer absorption spectra.

The I^-/I_3^- redox couple has been demonstrated up to now as the most efficient,[42] however, it can seriously corrode the glass and/or TiO_2 resulting in poor long term stability.[43, 44] Several redox couples, such as Br^-/Br_2,[45] SCN^-/SCN_2,[46] Co^{II}/Co^{III},[47] have been used, however, with disappointing results. Nevertheless, a recent improvement on non-iodine electrolytes, based on sulfur and disulfur bridges (Figure 1.17), results in a moderate DSSC efficiency of 6.4%.[48]

In liquid electrolytes, the redox pair is dissolved in organic solvents, thus, their physical characteristics, such as dipole moment, viscosity, etc. affect DSSC performance. The most common solvents have high dielectric constants, such as acetonitrile (ACN) and *N*-methylpyrrolidine (NMP), and solvent mixtures, such as ACN/valeronitrile. Ionic liquids, which are salts in liquid state, have been used as DSSC electrolyte components (Figure 1.17). They posses chemical and thermal stabilities, high conduction and negligible vapor pressure at room temperature. In addition, they can be a source of iodine and a solvent itself, which is attractive from long term stability and outdoor applications. Despite the higher viscosity of ionic liquids, which limits the I^-/I_3^- diffusion, the best efficiencies are attained by mixing different ratios of ionic liquids and organic solvents.[42]

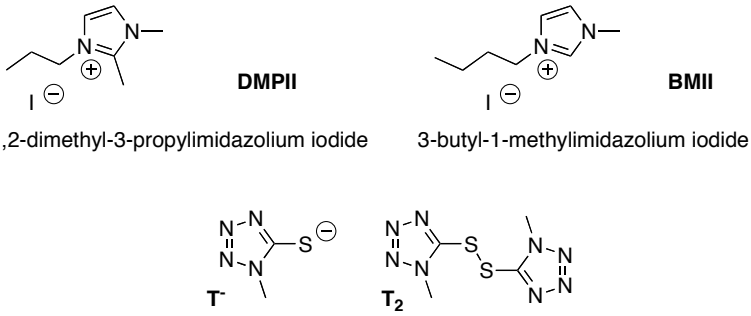

1,2-dimethyl-3-propylimidazolium iodide 3-butyl-1-methylimidazolium iodide

Figure 1.17 - Most common imidazolium iodide salts used as ionic liquids (*top*) and the new redox couple for DSSC (*bottom*).

Cations also play an important role in influencing DSSC performance. Small cations, such as Li^+ or Mg^{2+}, can deeply penetrate and intercalate into the mesoporous TiO_2 nanoparticles, shifting downwards the TiO_2 conduction band.[49] This effect can enhance the driving force of electron injection from the excited state, improving the photocurrent. However the lower conduction band obtained can also accelerate the recombination of photo-injected electrons with oxidized electrolyte, decreasing the cell voltage.[50] However, bigger cations such as TBA^+, cannot penetrate into the TiO_2 surface and any shift in the conduction band is minor.[49]

Additives are another important component. The most commonly used is 4-*tert*-butylpyridine (TBP), which is basic and can shift upwards the conduction band edge. This effect provides an enhancement of the open circuit voltage but at the same time this shift can also decrease the injection driving force, reducing the cell photocurrent. [50] A schematic representation of additive and cation effects over the TiO_2 conduction band is depicted in Figure 1.18.

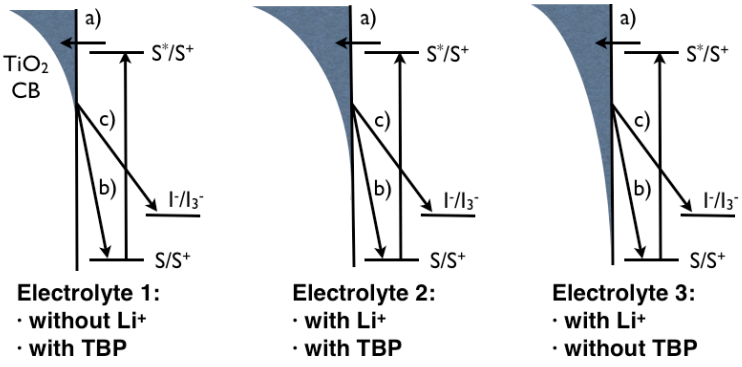

Figure 1.18 - Electrolyte cations and additives effect on the TiO_2 conduction band. Schematic representation of *a*) electron injection, *b*) and *c*) charge recombination reactions.

In spite of the high efficiencies obtained using liquid electrolytes, problems associated with them, such as high volatility, leakage, photodegradation, dye desorption or platinum counterelectrode corrosion by I^-/I_3^- couple have been considered significant drawbacks for long term stability solar cells, limiting their use in commercial devices.

Solid-state electrolytes have therefore been developed in order to avoid the drawbacks associated with liquid electrolytes. The most important solid state electrolyte are hole transport materials (HTMs).[51] The difference is that holes reach the counter electrode by hopping through the material rather than by diffusion. Hopping is a slower process, therefore, the hole resulting from dye regeneration remains for a longer time close to the TiO_2 surface, leading to a higher e^-_{TiO2}/electrolyte$^+$ recombination current for HTMs than liquid electrolytes. Initial HTMs used were inorganic materials, mainly copper derivatives, such as CuI, CuBr and CuSCN.[52, 53] They can form a hole-transporting layer which exhibit good conductivity, but their stability is non satisfactory. The use of organic and polymeric materials, were investigated and in 1998 Bach *et al.*[54] reported an organic HTM denoted as spiro-**OMeTAD** (Figure 1.19). This material is currently the most efficient HTM employed in solid-state DSSC with efficiencies over 5% recorded.[55]

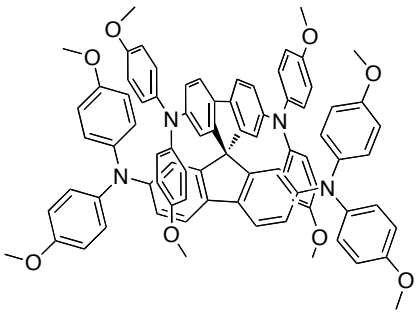

Figure 1.19 - Chemical structure of *2,2',7,7'*-tetrakis(N,N-di-*p*-methoxyphenilamine)-*9,9'*-spirobifluorene (spiro-**OMeTAD**).

1.2.5. Counter electrode

The counter electrode catalyzes the reduction of I_3^- to I^- for liquid electrolytes or in other words collects the holes from HTMs. At present, the platinum coated counter electrode is used due to the high efficiency obtained.[56] However, the use of this precious metal, which is expensive, is not suitable for large scale production of

DSSC. Therefore, several authors have developed new counter electrode alternatives, such as carbon[57] and CoS.[58] Presently, however, neither of these materials can achieve the efficiencies obtained with platinum.

1.3. Requirements for an Efficient DSSC

In order to convert sunlight into electrical energy, solar cells must generate a flow of electrons through the external circuit. Therefore, a potential difference between working and counter electrodes is needed, since it will provide the necessary driving force for the electrical flow.

Furthermore, as briefly explained in section 1.2.1, the efficiency of the DSSC depends on the optimization of each of the interfacial electron transfer processes. These processes must be favored not only thermodynamically, by placing the photosensitizer HOMO and LUMO energy levels correctly, but also kinetically, since they compete with recombination reactions which ultimately determines device performance. The control and understanding of these charge transfer processes is crucial for the continued optimization of DSSC.

1.3.1. Fermi level of TiO_2 conduction band

This overall cell voltage V_{oc} is determined by the difference between the Fermi level of TiO_2 (E_F) conduction band and the electrolyte redox potential. It is worth pointing out that E_F level varies with the electron concentration in the TiO_2 nanoparticles. Thus, at dark conditions, no difference is observed between the Fermi level and the electrolyte potential whereas under light exposure, the Fermi level is shifted upwards, generating the sufficient driving force for electrical flow (Figure 1.20).

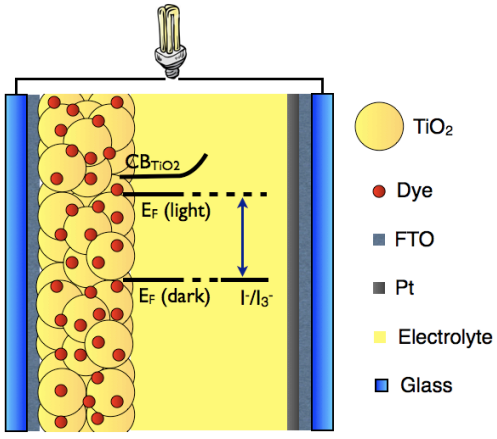

Figure 1.20 - Schematic representation of TiO_2 Fermi level at dark conditions and under illumination.

1.3.2. Light absorption and electron injection

Light absorption is an extremely fast process, which takes place at 10^{-15} s, and promotes an electron from the dye ground state to the excited state (Figure 1.21 - *process 1*). When a photosensitizer is not anchored to metal semiconductor oxide film, either in solution conditions or anchored to an insulator, decay to the ground state (Figure 1.21 - *process 2*) can take place through luminescence (timescale from 10^{-9} to 10^{-6} s) or a non-radiative decay (timescale 10^{-12} s) pathway. However, when the photosensitizer is attached to a metal semiconductor, excited electrons can be injected into its conduction band (Figure 1.21 - *process 3*). This process occurs on timescales ranging from 10^{-13} to 10^{-10} s.[59, 60] Therefore, highly luminescent photosensitizers must be sought in order to avoid non-radiative decay that could compete with electron injection process.

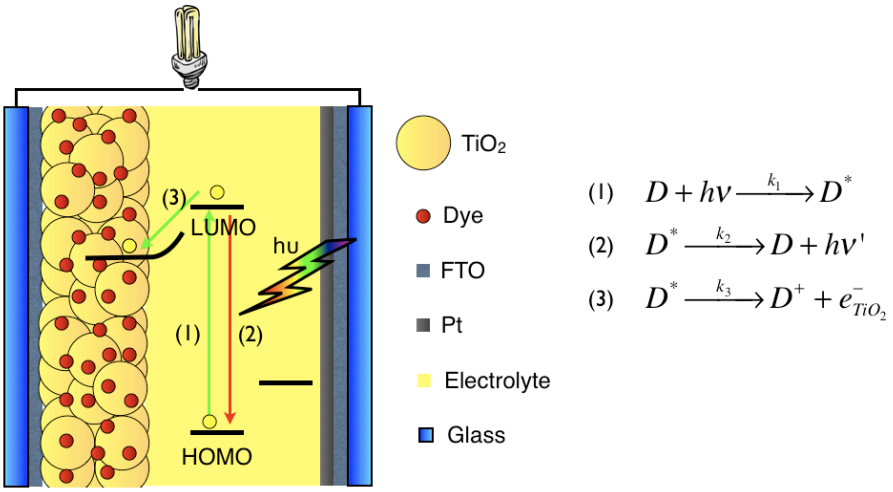

Figure 1.21 - Schematic diagram of light absorption, electron injection and their kinetic competition processes.

The electron injection rate constant (k_3) can be evaluated by monitoring the formation of the photosensitizer cation species (D^+), which appears after electron injection, by subpicosecond *transient absorption spectroscopy* (TAS).[50, 59] An alternative to evaluate the electron injection is measuring the luminescence decays by *time correlated single photon counting* (TC-SPC) apparatus, which are fully commercial and the experiments are easy to perform compared to subpicosecond TAS. However, TC-SPC can only be used as an estimation of electron injection yield because injection is too fast to be monitored.[61]

In order to ensure efficient electron injection, the dye must fulfill some requirements: **1**) The LUMO of the molecule should be placed as close as possible to the semiconductor film surface, and preferably on the anchoring group, in order to obtain effective coupling between the semiconductor *d* orbitals with the LUMO of the molecule. **2**) The LUMO energy level should be placed higher in energy respect to the conduction band of metal semiconductor oxide film. This energy difference is defined as the injection driving force. **3**) The molecule should be highly luminescent whose lifetime is not fast enough to compete with electron injection.

1.3.3. Electron transport, recombination and regeneration

In order to generate electrical energy, photo-injected electrons in the semiconductor conduction band should be transported to the back contact (Figure 1.22 - *process 4*). However, quantitative collection of charge carriers can be achieved only if the thickness of the film is smaller than the electron diffusion length. An optimized thickness for DSSC is usually around 10 - 12 μm.[29, 35]

Undesired charge recombination reactions of photo-injected electrons with the oxidized dye (Figure 1.22 - *process 5*) have been shown to occur with lifetimes ranging from 10^{-5} to 10^{-1} s. However, efficient regeneration of the dye cation by the redox electrolyte (lifetime from 10^{-9} to 10^{-6} s) generally impedes this recombination reaction (Figure 1.22 - *process 7*). The kinetics of both oxidized dye recombination (k_5) and dye regeneration (k_7) can be evaluated by monitoring the decay of the dye cation (D^+) by TAS.[62] Fully operational DSSCs are used to evaluate the dye regeneration while the measurement of e^-_{TiO2}/dye^+ recombination can be performed on dye sensitized electrodes alone.

In order to ensure slow recombination, as well as efficient charge transport, the dye should be regenerated efficiently. It can be accomplished by placing the HOMO of the molecule far from the surface of the semiconductor, which cause a better charge separation. Moreover, the HOMO energy level should be placed lower in energy respect to the redox electrolyte potential. This energy difference defined as the regeneration driving force.

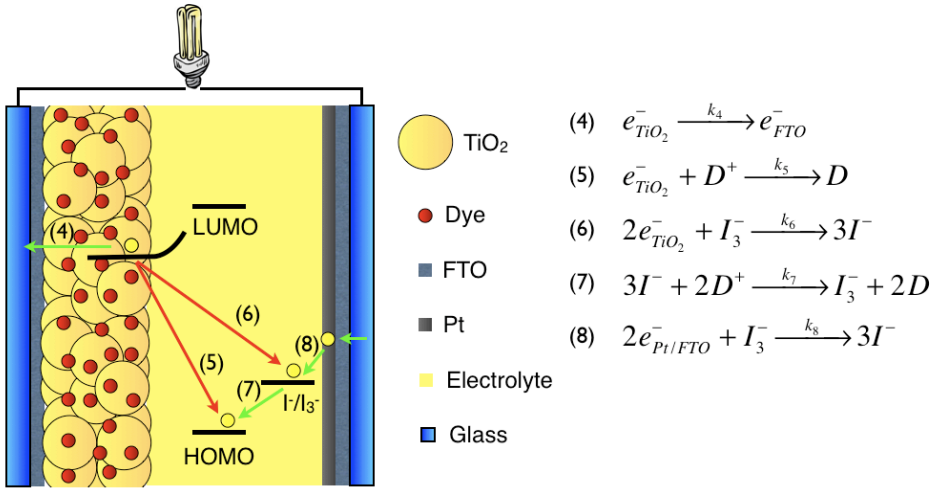

Figure 1.22 - Schematic representation of electron transfer, recombination and regeneration charge transfer processes occurring at the TiO_2/dye/electrolyte interface.

After dye regeneration, the oxidized electrolyte is generated which is now located close to the surface of semiconductor. Therefore, recombination between the photo-injected electrons and the oxidized electrolyte (lifetime from 10^{-3} to 10^{-1} s) can take place (Figure 1.22 - *process 6*). Despite its longer lifetime, this recombination recombination reaction is the principle loss reaction limiting cell voltage, and must be therefore be better understood and controlled.

An accurate way to evaluate this recombination is by using *transient photovoltage decay* (TPV) measurements. The technique involves monitoring cell voltage under light irradiation at open circuit while a light bias pulse is applied.[53, 63, 64] The decay obtained can be assigned to charge recombination between the photo-injected electrons and the oxidized electrolyte. It is worth pointing out that other techniques, such as impedance spectroscopy, can also be used in order to evaluate this recombination.[65, 66] However, the advantage of TPV is that it is a much simpler technique in which the cell is measured under illumination close to cell operating conditions.

In order to ensure slow e^-_{TiO2}/electrolyte$^+$ recombination the oxidized electrolyte should be located as far as possible from semiconductor surface. One strategy consists of the physical separation of the nanoparticle surface from the electrolyte. This can be accomplished through the modification of the dye molecular structure by adding hydrophobic barriers, such as adding bulky groups (e.g. *tert*-butyl).[67-70]

Moreover, additives and co-adsorbents can also be used to retard e^-_{TiO2}/electrolyte$^+$ recombination reaction.

Finally, the reduction of oxidized electrolyte takes place at the counter electrode, which is catalyzed on the platinum coated counter electrode (Figure 1.22 - *process 8*).

Detailed experimental procedures of TAS and TPV are explained in Chapter 2.3 of this thesis.

UNIVERSITAT ROVIRA I VIRGILI
DESIGN AND SYNTHESIS OF ORGANIC SENSITIZERS FOR DYE SOLAR CELLS: MOLECULAR STRUCTURE VS DEVICE PERFORMANCE
Miquel Angels Planells Dillundé
ISBN:978-84-693-8861-7/DL:T.1946-2010

1.4. Dyes used in DSSC

1.4.1. Ruthenium polypyridyl dyes

Ruthenium polypyridyl complexes have been extensively used due to their wide absorption range from the visible to the near-infrared as well as for their thermal and chemical stability. Most of the ruthenium complexes used in DSSC consist of a Ru^{II} atom coordinated by polypyridyl ligands and thiocyanate moieties in an octahedral geometry. These complexes exhibit moderate absorption coefficients ($\varepsilon < 18000\ cm^{-1}\ M^{-1}$) due to the *metal to ligand charge transfer* (MLCT) transition. MLCT transitions cover approximately the whole visible region and it is due to the promotion of one electron from the molecular orbital t_{2g}, distributed mainly on Ru^{II} center and thiocyanate moieties, to an empty π* molecular orbital mainly located on the bipyridyl ligand.[71] Carboxylic acids are often used as anchoring groups and are attached to the bipyridyl moiety, therefore, the excited electron can effectively be channeled to the semiconductor conduction band. The presence of a heavy atom, such as Ru^{II}, can lead to intersystem crossing of the excited electron to the long lived triplet state, which ensures efficient electron injection (Figure 1.23).

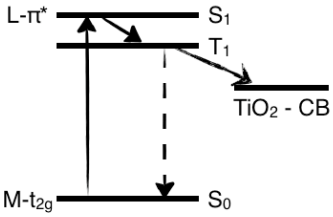

Figure 1.23 - Electronic transitions in ruthenium bipyridyl complexes.

The most commonly used and efficient Ru-sensitizers are tristhiocyanato-4,4',4''-tricarboxy-2,2':6,2''-terpyridine ruthenium(II) (**black dye**),[72] cis-dithiocyanobis(4-4'-dicarboxy-2,2'-bipyridine) ruthenium(II), (**N3**),[36] and its tetrabutylammonium salt, (**N719**) (Figure 1.24).[73] Moreover, the addition of long alkyl chains to the bipyridyl moiety such as for **Z907** can increase the solubility in organic solvents, reduce the presence of water on the TiO_2 surface and retard e^-_{TiO2}/electrolyte$^+$ recombination.[74]

In recent years, the molecular engineering of bipyridyl ligands has generated several new series of Ru based photosensitizers (Figure 1.24). The principal

approach is the addition of π conjugated systems, such as thiophene and its derivatives, to the bipyridyl backbone. As an example, the bipyridyl ligand is substituted with 2-hexylthiophene, (**C101**),[42] 2-(pentylthio)thiophene, 2-hexylthieno[3,2-*b*]thiophene, (**C104**),[75, 76] and 2-hexylselenophene, (**C105**).[77] These modifications were carried out in order to increase and broaden absorption as well as to shift the absorption spectra towards the infrared region.

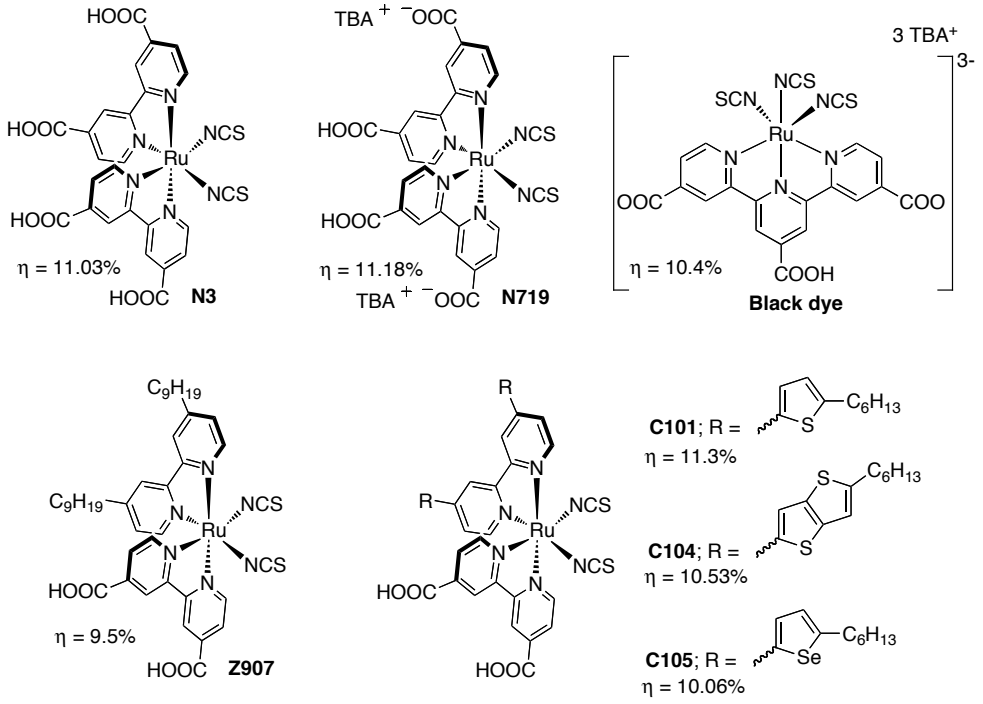

Figure 1.24 - Most efficient ruthenium complexes used in DSSC.

Recently, considerable attention has been focused on replacing the ruthenium complexes by metal-free organic dyes. This is because these dyes do not require any costly or toxic heavy metal component. Moreover, organic dyes could reduce production costs and achieve thinner devices, due to their higher absorption coefficients. It may result in an improved cell voltage as thinner devices will result in less recombination losses.[78, 79] Organic photosensitizers can also incorporate a wide selection of light absorbing groups, making their absorption and electrochemical properties extremely easy to tune.

1.4.2. Porphyrin dyes

Porphyrins are fully conjugated aromatic macrocycles characterized by the presence of four modified pyrrole subunits interconnected at their *a* carbon atoms via methine bridges. Since they are highly-conjugated systems and, they display interesting optical properties suitable for a wide range of molecular electronics, such as non linear optics,[80] photodynamic therapy,[81] molecular wires[82] and organic photovoltaics.[83] Furthermore, porphyrins have been established for long time as good candidates for DSSC due to their primary role in photosynthesis.[84, 85]

Typical porphyrin absorption spectra consist of an intense Soret band centered at 400 - 450 nm ($\varepsilon \sim 420000\ cm^{-1}\ M^{-1}$) and a series of moderately absorbing Q bands at 500 - 650 nm ($\varepsilon \sim 15000\ cm^{-1}\ M^{-1}$).[86] These bands appear from the π - π^* transition and can be explained in terms of a linear combination of transitions from slightly split HOMO and HOMO-1 to degenerated pair of LUMO and LUMO+1 (Figure 1.25). It is worth pointing out that the incorporation of metal ions (usually *d* elements) in the core can induce a shift of the HOMO and LUMO positions, which is reflected in the absorbance spectra.

Radiative deactivation of the singlet excited state can be observed at 500 - 700 nm with a high quantum yield. As observed in absorption spectra, luminescence spectra and luminescence lifetimes may vary by the insertion of Zn^{II}, Cu^{II} or Sn^{IV} atoms into the core, or even disappear with Ni^{II} or Al^{III} atoms due to the non-radiative decay pathway. Moreover, the addition of heavy atoms, such as Pt^{II} and Pd^{II}, can induce intersystem crossing from a singlet to a triplet excited state, leading to phosphorescence emission decay.[86]

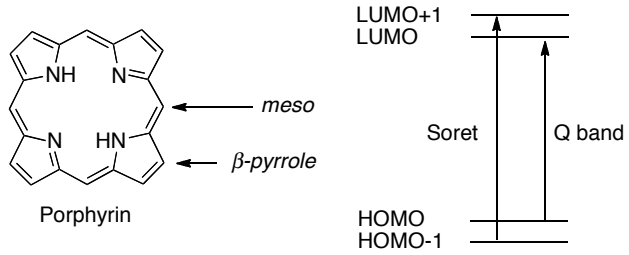

Figure 1.25 - Chemical structure of a porphyrin ring (*left*) and its electronic transitions (*right*).

Although several porphyrins have been applied for the photosensitization of TiO_2 electrodes, the most commonly used are the free base and zinc porphyrins. Initial studies were performed with a benzoic acid as the anchoring group attached at the

ISBN:978-84-693-8861-7/DL:T.1946-2010

meso position (Figure 1.26) and moderate efficiencies of 3 - 4% were obtained.[87-89] One reason for such disappointing efficiencies is because the porphyrin's Soret band does not overlap near the maximum of solar irradiance spectrum. Moreover, the 4 phenyl groups attached at the *meso* position acted as nodes (a potential barrier which breaks the conjugation) due to the perpendicularity between the aryl groups and the porphyrin core. Consequently, the LUMO of the molecule did not interact strongly with the TiO_2 nanoparticles. On the other hand, porphyrin aggregation induced by highly favorable π - π stacking resulted in low electron injection yields due to deactivation of excited state.

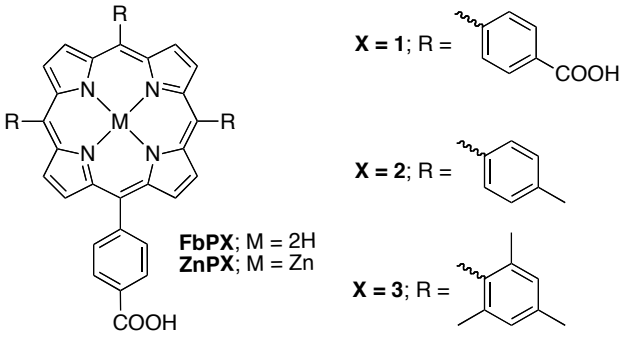

Figure 1.26 - Examples of porphyrins with *meso* substituted carboxyphenyl groups.

Better performances were obtained when the anchoring groups were placed at the *β*-pyrrole position (Figure 1.27).[90-92] This suggested that the position of the anchoring group, connected either on *meso* or *β*-pyrrole position, is particularly important for the development of high efficient solar cells utilizing this class of photosensitizer.

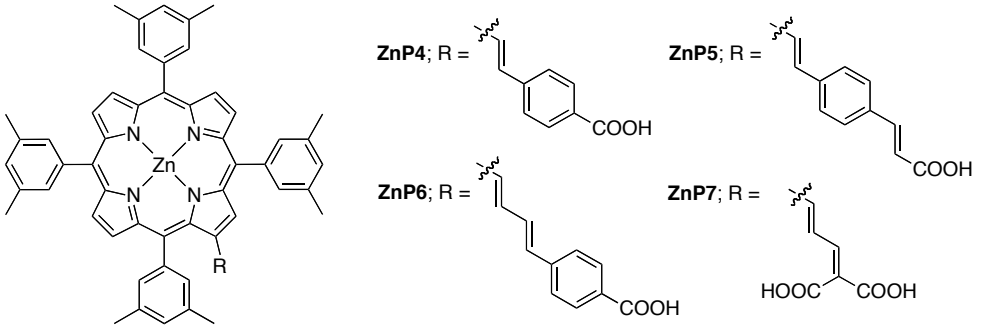

Figure 1.27 - Examples of porphyrins with *β*-pyrrole acid substitution.

In this case, the aromatic plane and *β*-pyrrole substituted porphyrins are fully conjugated with the anchoring group leading to better electronic coupling between the LUMO and TiO_2 which in turn leads to better photovoltaic performance than the *meso* substituted porphyrins.[93]

One of the recent advances in porphyrin molecular engineering also concerns the the breakage of the symmetry of these aromatic systems. In this case a substituent attached at the *meso* position was fused to the *β*-pyrrole position. The elongation of the π system causes a loss of symmetry which results in splitting of π and π* energy levels. Thereby, the HOMO - LUMO gap is reduced, and broadened and red-shifted absorption bands are obtained.[94] As an example shown in Figure 1.28, a naphtyl carboxylic group attached at the zinc porphyrin *meso* position (**ZnP8**) was compared with its respective naphtyl fused porphyrin (**ZnP9**). The oxidative coupling of the naphtyl group at the porphyrin *β* position induces an elongation of the π system.[95, 96] The device efficiency with the fused porphyrin increases by up to 50% with respect to the non fused porphyrin.

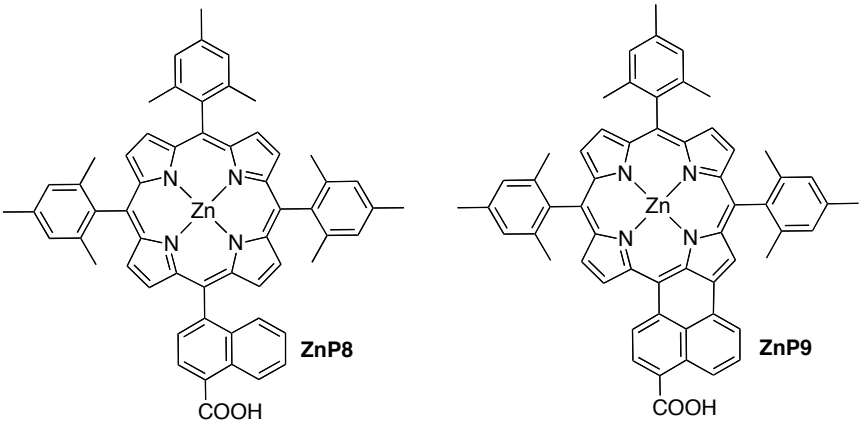

Figure 1.28 - Chemical structure of unfused (**ZnP8**) and fused (**ZnP9**) zinc porphyrins.

More recently, a novel molecular engineered push-pull porphyrin was synthesized (Figure 1.29).[97] **ZnP10** consists in a diarylamine unit linked directly to the *meso* position of the porphyrin ring and, more importantly, a triple bond was used to link the anchor moiety and the porphyrin core.[98] This approach not only extended the conjugation of the porphyrin leading to broader and red-shifted bands, but also enhanced the effective coupling between the molecular LUMO and the TiO_2 nanoparticles. As a result, DSSC made from **ZnP10** show up to 10% efficiency.[99]

ISBN:978-84-693-8861-7/DL:T.1946-2010

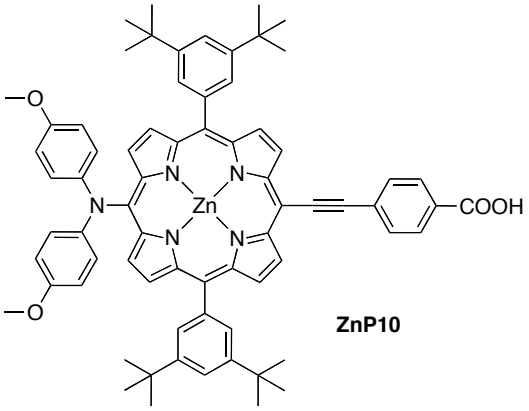

ZnP10

Figure 1.29 - Highly efficient push-pull zinc porphyrin (**ZnP10**).

1.4.3. Perylenes dyes

Perylenes are polycyclic aromatic hydrocarbons consisting of two naphthalene molecules connected by a carbon-carbon bond at the 1 and 8 positions. All of the carbon atoms are sp^2 hybridized, with a strong π delocalization in the core. This provides interesting optical properties for a wide range of optoelectronic applications, such as OLEDs,[100] biological fluorescence probes[101] and solar cells.[102] In addition, perylenes are chemically, thermally and photophysically stable which makes them good potential candidates for DSSC applications.[103, 104]

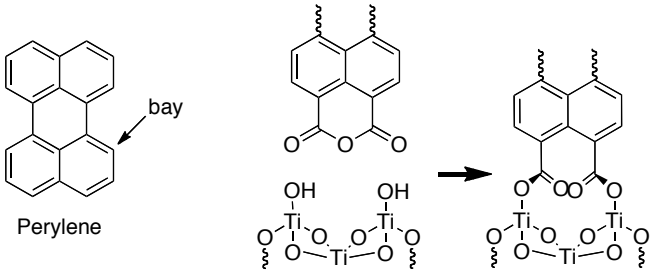

Figure 1.30 - Chemical structure of perylene (*left*) and its anchoring mode through an anhydride group (*right*).

Despite these properties, low efficiency values (η < 2%) were obtained compared with other organic dyes.[105] The main reason for this was due to their poor electron donating ability making electron injection from the excited state to the TiO_2 conduction band unfavorable. In order to improve the electron donating ability, molecular engineering of perylenes was carried out by attaching an appropriate

selection of strong electron donating moieties.[106-109] As a result, higher driving force for the electron injection was obtained as well as red-shifted absorption bands. Figure 1.31 shows some examples of perylene derivatives with different moieties attached at the *bay* position. The electron injection force of these perylenes on TiO_2 and, thereby, cell efficiency increased following **Pery1** < **Pery2** < **Pery3**.

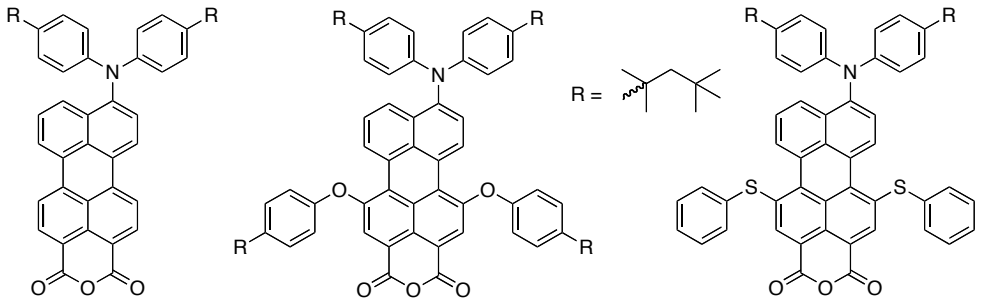

Figure 1.31 - Chemical structures of perylene dyes and their modification at the *bay* position.

The binding group also played an important role in DSSC performance. For example, Imahori *et al.*[107] developed a series of perylenes with two different anchoring groups: an anhydride, **Pery4**, and a 4-carboxybenzoimide moiety, **Pery5** (Figure 1.32). The resulting photovoltaic performances were 100 times higher for the former perylene compared to the latter. This huge difference was rationalized in terms of effective coupling between π conjugated perylene core and TiO_2 nanoparticles (Figure 1.30 - *right*). In this sense, the π conjugated system in **Pery4** was attached directly to the TiO_2 nanoparticles whereas in **Pery5** the imide group acted as node, reducing the electronic coupling between the perylene core and the TiO_2 nanoparticles.[108]

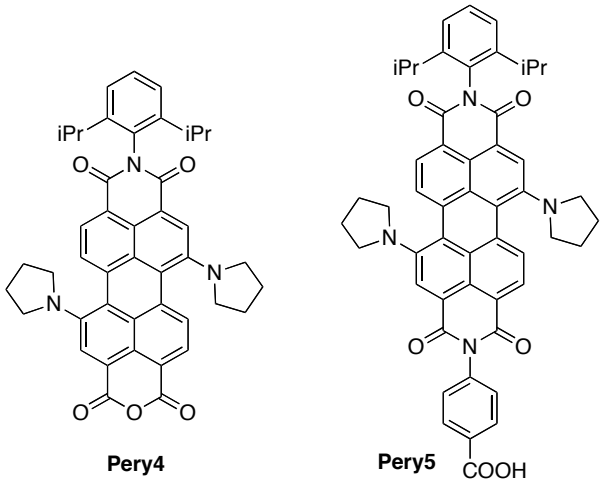

Figure 1.32 - Perylenes with anhydride (**Pery4**) and 4-carboxybenzoimide (**Pery5**) as anchoring groups.

1.4.4. Donor - acceptor π conjugated neutral dyes

Donor - acceptor π conjugated dyes, also known as push-pull dyes, consist of electron-donating and electron-withdrawing groups linked covalently through a π conjugated spacer, as shown in Figure 1.33.

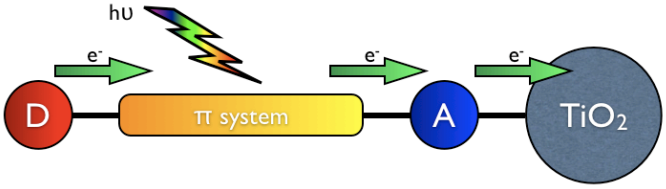

Figure 1.33 - Structure of D - π - A dye and its electron transfer processes.

The photophysical properties of D - π - A dyes are associated with an intramolecular charge transfer from the donor to the acceptor moiety. This transition provides the dye with a high molar extinction coefficient and singlet fluorescence. Computational studies localize the HOMO of the dye mainly on the electron donating and π system moieties, while the LUMO is localized at the acceptor part, which contains the anchoring group. This configuration ensures better charge separation and efficient electron injection from the excited state of the dye into the TiO_2 conduction band. Moreover, the dye cation formed after electron injection, is located

on the donor moiety which is placed far from the TiO_2 surface minimizing charge recombination between dye cations and injected electrons in the TiO_2.

The expansion of the π conjugated structure, by adding either electron donating or withdrawing groups, can induce a shift of both HOMO and LUMO energy levels, resulting in a change of photophysical properties. Due to the fact that they are easy to tune, D - π - A are considered the most promising class of organic dyes for DSSC.[110] Figure 1.34 shows some examples of functional D - π - A photosensitizers. In this section, the particular description of donor, π system and acceptor parts has been reviewed below as separate entities.

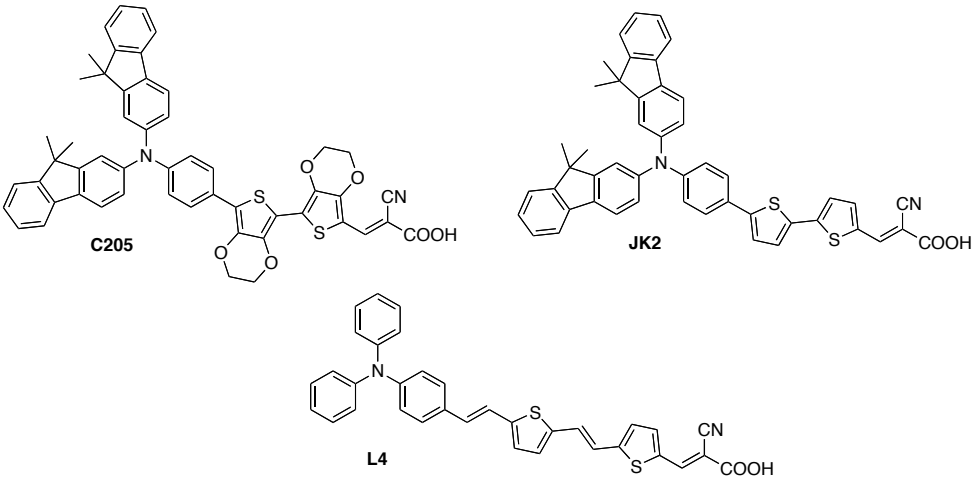

Figure 1.34 - Chemical structures of donor acceptor π conjugated dyes **C205**,[111] **L4**[112] and **JK2**[113] used in DSSC.

Donor groups in D - π - A systems have been extensively studied. Dialkyl amines were used initially with efficiencies of up to 6% obtained. However, molecular engineering of substituted coumarin dyes,[114-116] developed by Hara and coworkers, pushed efficiencies up to 8.2%. Carbazole derivative donor units were also used for dyes synthesized for application in DSSC due to their commercial availability and simple synthesis. The solar cell performance of 7.7% was obtained.[69, 117]

Sun *et al.*[118, 119] developed a new series of dyes using tetrahydroquinoline as the donor moiety and thiophene derivatives as the spacer. This structure allowed a bathochromic shift in which red-shifted absorption bands were obtained due to their strong coupling, but the measured efficiency remained moderate at 6.4%.[120] Another donor moiety extensively used was difluorenephenylamine, which prevented dye aggregation due to its bulky structure and at the same time it ensured excellent

photo-resistance avoiding dye degradation. Efficiencies using this unit ranged from 5.0 to 8.6%.[111, 113, 121] Phenothiazine was also used as the donor unit in sensitizers, with efficiencies of 6.4% obtained.[122]

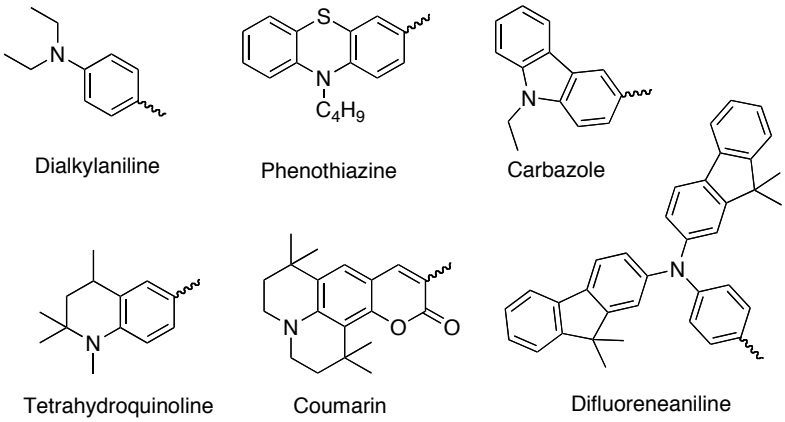

Figure 1.35 - Common donor moieties used in DSSC.

Although several donor moieties have been used, triphenylamine derivatives have received great attention. Sensitizers incorporating triphenylamines generally involve facile synthetic routes by Ullmann coupling, making them readily available and requiring non expensive starting materials.[123] Moreover, structural modifications could be performed easily, such as adding alkyl chains or electron donating groups. Preliminary dyes were designed as simple triphenylamine groups attached to cyanoacetic acids, and surprisingly promising efficiencies from 5.0 to 7.0% were obtained.[124-126] In order to improve the device performance, molecular engineering of triphenylamine sensitizers was carried out by adding methyl[127] or methoxy[40, 126] groups in *para* position (Figure 1.36). However, better solar cell performance was obtained when long alkyl chains were attached to the triphenylamine at *para* position. [128-130]

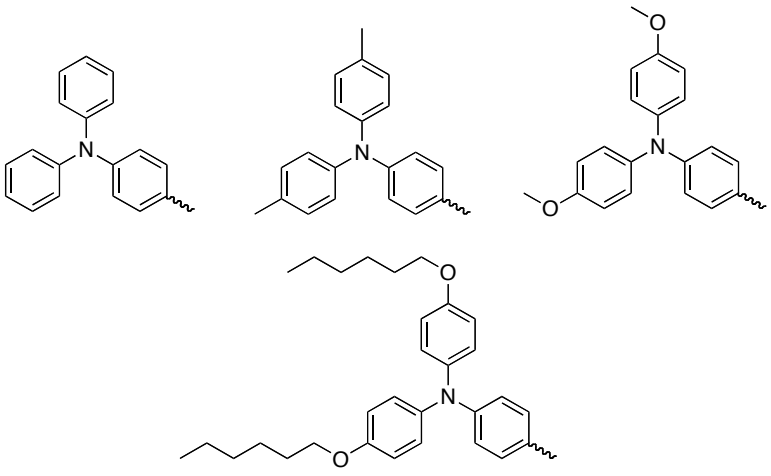

Figure 1.36 - Donor moieties based on triphenylamine building blocks.

Highly π conjugated systems have also attracted considerable attention as spacers in push-pull organic dyes. Initial attempts used oligoenes or phenyl groups, with respectable efficiencies of 6.0% obtained (Figure 1.37).[131, 132] The extension of the methine group, forming dimers, trimers, etc. induced a bathochromic shift in the absorption spectrum due to the extension of the π conjugated system. However, the increased dye instability due to the isomerization of the double bond (cis/trans) and the aggregation issues caused by π - π stacking limited the use of oligoenes in DSSC.

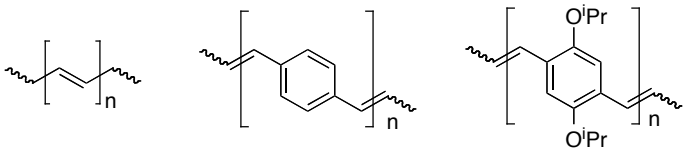

Figure 1.37 - Oligoene and phenyl derivatives π conjugated systems.

Currently, π conjugated oligothiophenes are employed as spacers due to their well-known high polarizability, spectroscopically and electrochemically tunable properties as well as their high chemical stability.[117, 119, 131, 132] Early π conjugated spacers used were thiophenes linked either directly or through double bonds to the donor moiety (Figure 1.38).[124] To induce a bathochromic shift as well as to increase absorption, the number of thiophene units in the spacer was increased. By controlling the length of the thiophene chain, higher efficiencies can be obtained (up to 2 - 3 units).[111, 113] However, for longer dyes, π - π stacking aggregation and solubility becomes a serious issue, resulting in a reduction in cell performance.[117]

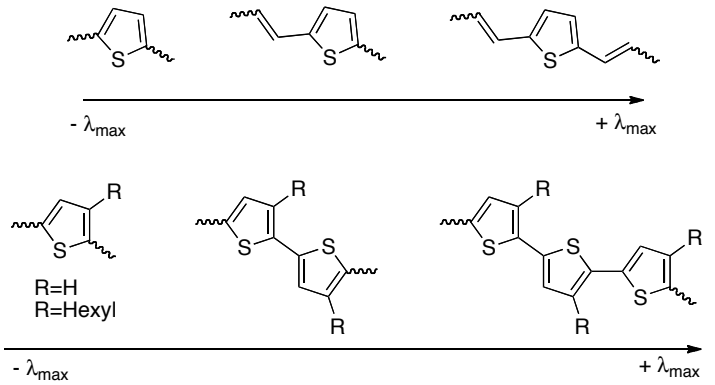

Figure 1.38 - Effect of thiophene systems on the maximum absorption wavelength following the addition of conjugated double bonds (*top*) or merging with adjacent thiophene units (*bottom*).

Molecular engineering of thiophene containing D - π - A sensitizers was employed in order to overcome the stability and solubility issues. Modifications were made either by adding electron-donating groups to the π conjugated thiophene core, obtaining ethylenedioxythiophene (EDOT),[111] or by fusing thiophene units, obtaining thienothiophene[121, 126] and dithienothiophene (Figure 1.39).[133] In addition, the use of selenophene instead of thiophene was also tested.[134] Efficiencies up to 9 - 10% were obtained utilizing these approaches.

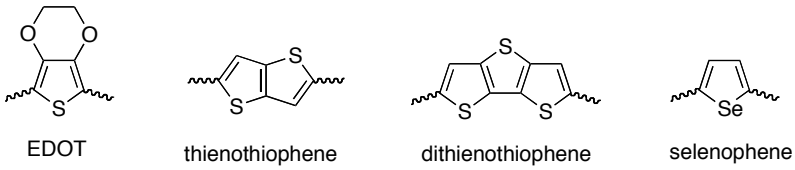

Figure 1.39 - Chemical structures of modified thiophenes as π conjugated building blocks.

The acceptor group in push-pull organic dyes has not been studied to a great degree, compared with the the donor and the π conjugated spacer groups. The most common unit used is cyanoacetic acid because it has a strong electron withdrawing ability necessary for good electron injection. Moreover, the synthesis by Knoevenagel condensation is extremely facile. Alternative acceptors based on rhodanine-3-acetic acid were also tested, however, results indicate unsatisfactory electron injection due to the low lying molecular LUMO.[135, 136]

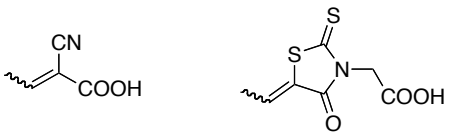

Figure 1.40 - Chemical structures of acceptor moieties cyanoacrylic acid (*left*) and rhodanine-3-acetic acid (*right*).

The huge amount of available donor and π conjugated system moieties generates an incredible range of possible combinations, thus, a vast library of potential push-pull organic dyes can be synthesized and tested for DSSC applications.[110] To date, the most efficient D - π - A dye contains a triphenylamine as donor, an EDOT moiety covalently linked to dithienosilole as π conjugated system and a cyanoacrylic acid as acceptor (Figure 1.41). This photosensitizer prompts an efficiency of 10.3%.[129]

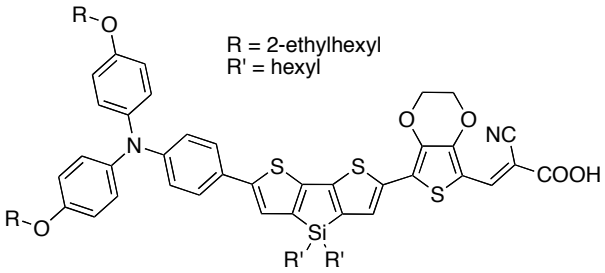

Figure 1.41 - Chemical structure of the highest efficient donor - acceptor π conjugated dye.

1.4.5. Other neutral organic dyes

Phthalocyanines are macrocyclic compounds, related to porphyrins, which exhibit an intense absorption at near UV region, 300 nm (Soret band), and at 700 nm (Q band). It is worth noting that the lack of absorption in the visible region is perhaps useful for their use as “photovoltaic windows”. Furthermore, phthalocyanines are attractive dyes for DSSC applications due to their electrochemical, photochemical and thermal stabilities.[137] However, low efficiencies were reported for zinc base phthalocyanines ($\eta < 1\%$) in the early years, **ZnPc1**, apparently due to dye aggregation, lack of directionally of the excited state and poor coupling between TiO_2 conduction band and the LUMO.[138]

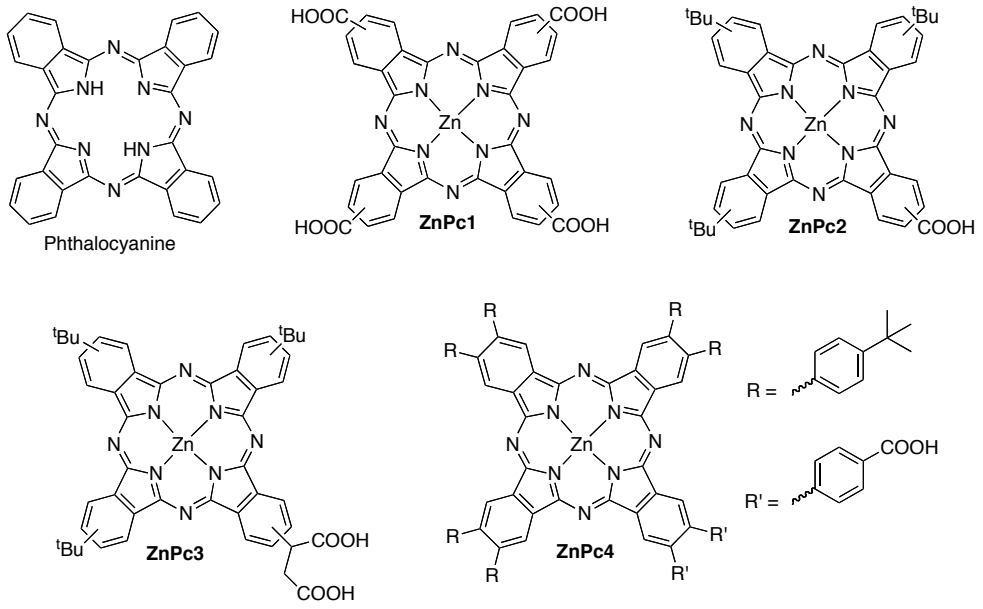

Figure 1.42 - Chemical structures of phthalocyanines for DSSC applications.

In order to overcome the drawbacks mentioned above, unsymmetrical phthalocyanines containing three *tert*-butyl groups and a carboxylic acid moiety, **ZnPc2** and **ZnPc3** were synthesized. Actually, this structure could be related to a push-pull dye. These new phthalocyanines improved the electron injection by effective coupling LUMO - TiO_2 nanoparticles. In addition, bulky groups increased the solubility in common organic solvents and avoided dye aggregation. Using this approach, the solar cell performance was increased up to 3%.[139, 140] Imahori and co-workers synthesized **ZnPc4** with six bulky substituents in order to further reduce aggregation. However, solar cell performance remained low (η = 0.54%) due to small driving force for electron injection.[67]

On the other hand, highly bulky phthalocyanine **ZnPc5** dye developed by Mori *et al.*[141] was able to achieve up to 4.6% efficiency, the highest one using phthalocyanines up to now. (Figure 1.43).

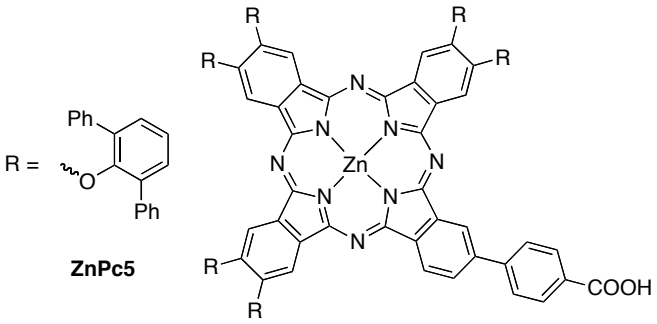

Figure 1.43 - Chemical structure of the highest efficient phthalocyanine dye **ZnPc5**.

Xanthene dyes, such as rhodamine derivatives, are macrocyclic molecules which were employed for DSSC because they are commercially available at low cost (Figure 1.44). However, the solar cell performance based on xanthenes is not ideal due to their poor stability and narrow bands. The best solar cells for **Eosin Y** and **Mercurochrome** gave efficiencies of 1.3% and 1.4%, respectively.[142, 143]

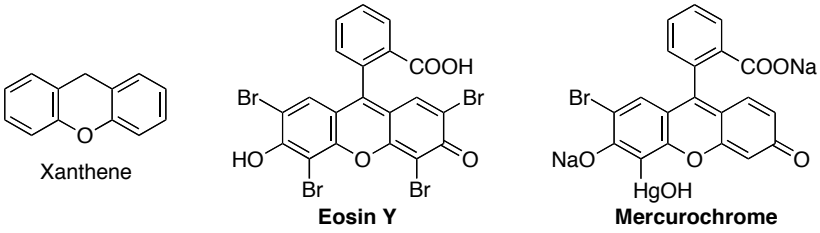

Figure 1.44 - Chemical structures of xanthene derivatives.

1.4.6. Ionic organic dyes

Ionic dyes are promising dyes for DSSC applications because they posses near infrared (NIR) tunable absorption spectra with a high extinction coefficients.

Cyanine dyes consist of two cyclic aromatic nitrogen containing units connected through a methine chain (Figure 1.45). These dyes are anchored onto the TiO_2 nanoparticles by attaching carboxylic acids to the peripheral aryl groups, such as **Cy1**. Efficiencies up to 2% were obtained.[144, 145] The use of unsymmetrical cyanine dye, **Cy2**, provided an unidirectional flow of excited state electron density resulting in efficient electron injection kinetics and excellent charge separation yield. In this case, the efficiency rose to almost 3%.[144] Currently, the most efficient solar cells based on cyanine dyes have been developed by Tian and co-workers,using **Cy3**, inspired by the push-pull structure, resulting in an efficiency of 7.6%.[146]

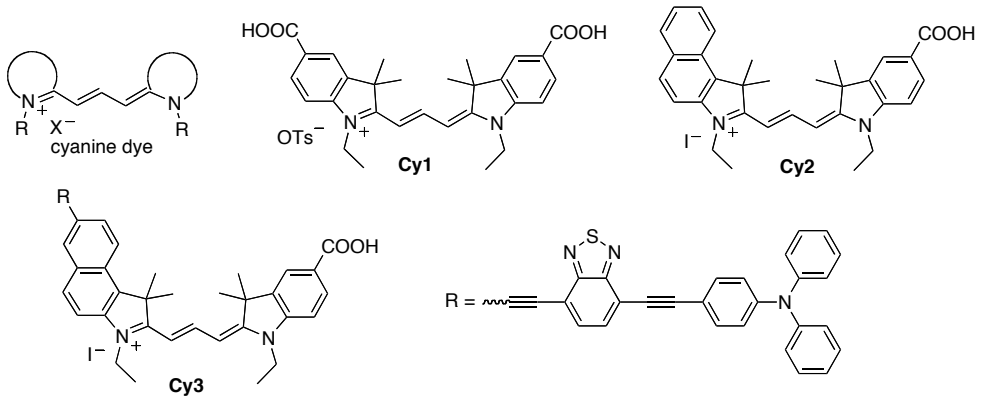

Figure 1.45 - Chemical structures of cyanine dyes.

Squaraine dyes, which contain a squaric acid ring, have been considered a promising alternative for NIR absorption solar cells (Figure 1.46). The presence of a four member ring affords photostability by impeding cis/trans isomerization of the adjacent double bond(s) and also shifts the absorption to the red. The symmetrical squaraine **Sq1**, with the COOH anchoring group covalently linked to the *N* position, was compared with unsymmetrical squaraine **Sq2**. Efficiencies of 1.0% and 2.1% were obtained for **Sq1** and **Sq2**, respectively.[147] In fact, the latter squaraine showed a broader and blue-shifted absorption spectrum compared to **Sq1**, which resulted in higher IPCE and photocurrent values. Again, the push-pull strategy followed for **Sq2** contributed to an unidirectional flow of excited state electron density and ultimately improved charge separation (as indicated by the improved photocurrent). This effect was also observed when squaraines **Sq3** and **Sq4** were compared. However, the attachment of the anchoring group to a benzopyrrole moiety allowed an effective coupling between the dye LUMO with TiO_2 conduction band, thus, efficient electron injection was observed. Enhanced efficiencies of 3.9% and 4.5% were obtained for squaraine **Sq3** and **Sq4**, respectively.[148, 149]

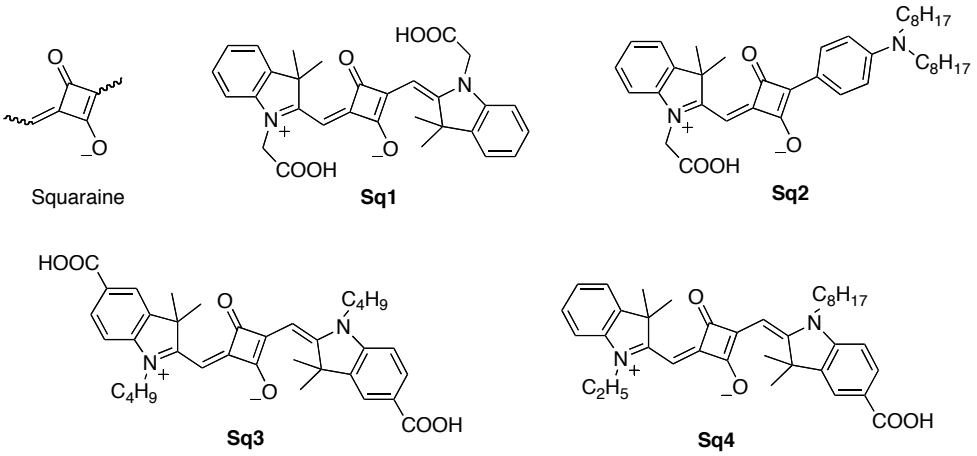

Figure 1.46 - Chemical structures of squaraine dyes.

UNIVERSITAT ROVIRA I VIRGILI
DESIGN AND SYNTHESIS OF ORGANIC SENSITIZERS FOR DYE SOLAR CELLS: MOLECULAR STRUCTURE VS DEVICE PERFORMANCE
Miquel Angels Planells Dillundé
ISBN:978-84-693-8861-7/DL:T.1946-2010

1.5. The Aim of this Thesis

This PhD thesis involves the design, synthesis and characterization of novel organic chromophores and the investigation of their electron transfer processes occurring at the TiO_2/dye/electrolyte interface. Moreover, the overall efficiencies of complete DSSC devices are elucidated. Ultimately, however, the aim of this thesis is to greater understand the underlying requirements for efficient dyes in DSSC.

The principle role of the dye is to harvest as much light as possible in order to generate efficient photocurrents. Moreover, the dye plays a crucial role in determining the interfacial charge transfer kinetics, which determine device efficiency. Modifications to dye structure and their effect on recombination and regeneration reactions are discussed. The core of this thesis is to establish a relationship between the photosensitizer structure, the interfacial charge transfer reactions and the device performance, which is essential for developing new of organic dyes.

1.6. References

[1] BP, in *Statistical Review of World Energy*, **2009**.

[2] N. S. Lewis, *Science* **2007**, *315*, 798.

[3] E. Becquerél, *C. R. Acad. Sci.* **1839**, *9*, 561.

[4] J. Perlin, *Opt. Sci. Eng.* **2005**, *99*, 3.

[5] P. A. Iles, *Prog. Photovolt. Res. Appl.* **2000**, *8*, 39.

[6] M. A. Green, K. Emery, Y. Hishikawa, W. Warta, *Prog. Photovolt. Res. Appl.* **2010**, *18*, 346.

[7] M. A. Green, *Phys. E* **2002**, *14*, 65.

[8] J. Zhao, A. Wang, M. A. Green, F. Ferrazza, *Appl. Phys. Lett.* **1998**, *73*, 1991.

[9] S. Guha, J. Yang, A. Banerjee, *Prog. Photovolt. Res. Appl.* **2000**, *8*, 141.

[10] H. Cotal, C. Fetzer, J. Boisvert, G. Kinsey, R. King, P. Hebert, H. Yoon, N. Karam, *Energy Environ. Sci.* **2009**, *2*, 174.

[11] R. D. McConnell, M. Symko-Davies, *Multijunction Photovoltaic Technologies for High Performance Concentrators (Presentation)*, **2006**.

[12] A. Kraft, A. C. Grimsdale, A. B. Holmes, *Angew. Chem., Int. Ed.* **1998**, *37*, 402.

[13] C.-T. Chen, *Chem. Mater.* **2004**, *16*, 4389.

[14] C. D. Dimitrakopoulos, P. R. L. Malenfant, *Adv. Mater.* **2002**, *14*, 99.

[15] C. R. Newman, C. D. Frisbie, D. A. da Silva Filho, J.-L. Bredas, P. C. Ewbank, K. R. Mann, *Chem. Mater.* **2004**, *16*, 4436.

[16] C. J. Brabec, N. S. Sariciftci, J. C. Hummelen, *Adv. Funct. Mater.* **2001**, *11*, 15.

[17] K. M. Coakley, M. D. McGehee, *Chem. Mater.* **2004**, *16*, 4533.

[18] J. Y. Kim, K. Lee, N. E. Coates, D. Moses, T.-Q. Nguyen, M. Dante, A. J. Heeger, *Science* **2007**, *317*, 222.

[19] J. Peet, J. Y. Kim, N. E. Coates, W. L. Ma, D. Moses, A. J. Heeger, G. C. Bazan, *Nat. Mater.* **2007**, *6*, 497.

[20] J.-L. Bredas, J. E. Norton, J. Cornil, V. Coropceanu, *Acc. Chem. Res.* **2009**, *42*, 1691.

[21] C. W. Tang, *Appl. Phys. Lett.* **1986**, *48*, 183.

[22] G. Yu, J. Gao, J. C. Hummelen, F. Wudl, A. J. Heeger, *Science* **1995**, *270*, 1789.

[23] P. Peumans, S. Uchida, S. R. Forrest, *Nature* **2003**, *425*, 158.

[24] B. Ma, C. H. Woo, Y. Miyamoto, J. M. J. Fréchet, *Chem. Mater.* **2009**, *21*, 1413.

[25] M. Gratzel, *Nature* **2001**, *414*, 338.

[26] H. Gerischer, F. Willig, *Top. Curr. Chem.* **1976**, *61*, 31.

[27] H. Tsubomura, M. Matsumura, Y. Nomura, T. Amamiya, *Nature* **1976**, *261*, 402.

[28] B. O'Regan, M. Gratzel, *Nature* **1991**, *353*, 737.

[29] M. Gratzel, *Inorg. Chem.* **2005**, *44*, 6841.

[30] M. K. Nazeeruddin, M. Grätzel, *Compr. Coord. Chem. II* **2004**, *9*, 719.

[31] F. Lenzmann, J. Krueger, S. Burnside, K. Brooks, M. Gratzel, D. Gal, S. Ruhle, D. Cahen, *J. Phys. Chem. B* **2001**, *105*, 6347.

[32] M. Quintana, T. Edvinsson, A. Hagfeldt, G. Boschloo, *J. Phys. Chem. C* **2006**, *111*, 1035.

[33] A. N. M. Green, E. Palomares, S. A. Haque, J. M. Kroon, J. R. Durrant, *J. Phys. Chem. B* **2005**, *109*, 12525.

[34] P. Qin, H. Zhu, T. Edvinsson, G. Boschloo, A. Hagfeldt, L. Sun, *J. Am. Chem. Soc.* **2008**, *130*, 8570.

[35] K. Kalyanasundaram, M. Gratzel, *Coord. Chem. Rev.* **1998**, *177*, 347.

[36] M. K. Nazeeruddin, A. Kay, I. Rodicio, R. Humphry-Baker, E. Mueller, P. Liska, N. Vlachopoulos, M. Gratzel, *J. Am. Chem. Soc.* **1993**, *115*, 6382.

[37] P. Wang, S. M. Zakeeruddin, P. Comte, R. Charvet, R. Humphry-Baker, M. Gratzel, *J. Phys. Chem. B* **2003**, *107*, 14336.

[38] A. K. M. Fung, B. K. W. Chiu, M. H. W. Lam, *Water Res.* **2003**, *37*, 1939.

[39] A. Zaban, S. Ferrere, B. A. Gregg, *J. Phys. Chem. B* **1998**, *102*, 452.

[40] D. P. Hagberg, J.-H. Yum, H. Lee, F. De Angelis, T. Marinado, K. M. Karlsson, R. Humphry-Baker, L. Sun, A. Hagfeldt, M. Gratzel, M. K. Nazeeruddin, *J. Am. Chem. Soc.* **2008**, *130*, 6259.

[41] N. R. Neale, N. Kopidakis, J. van de Lagemaat, M. Gratzel, A. J. Frank, *J. Phys. Chem. B* **2005**, *109*, 23183.

[42] F. Gao, Y. Wang, D. Shi, J. Zhang, M. Wang, X. Jing, R. Humphry-Baker, P. Wang, S. M. Zakeeruddin, M. Gratzel, *J. Am. Chem. Soc.* **2008**, *130*, 10720.

[43] J. Wu, Z. Lan, S. Hao, P. Li, J. Lin, M. Huang, L. Fang, Y. Huang, *Pure Appl. Chem.* **2008**, *80*, 2241.

[44] M. Toivola, F. Ahlskog, P. Lund, *Sol. Energy Mater. Sol. Cells* **2006**, *90*, 2881.

[45] S. Ferrere, A. Zaban, B. A. Gregg, *J. Phys. Chem. B* **1997**, *101*, 4490.

[46] G. Oskam, B. V. Bergeron, G. J. Meyer, P. C. Searson, *J. Phys. Chem. B* **2001**, *105*, 6867.

[47] H. Nusbaumer, J.-E. Moser, S. M. Zakeeruddin, M. K. Nazeeruddin, M. Gratzel, *J. Phys. Chem. B* **2001**, *105*, 10461.

[48] M. Wang, N. Chamberland, L. Breau, J.-E. Moser, R. Humphry-Baker, B. Marsan, S. M. Zakeeruddin, M. Grätzel, *Nat. Chem.* **2010**, *2*, 385.

[49] S. Nakade, T. Kanzaki, W. Kubo, T. Kitamura, Y. Wada, S. Yanagida, *J. Phys. Chem. B* **2005**, *109*, 3480.

[50] S. A. Haque, E. Palomares, B. M. Cho, A. N. M. Green, N. Hirata, D. R. Klug, J. R. Durrant, *J. Am. Chem. Soc.* **2005**, *127*, 3456.

[51] S. Yanagida, Y. Yu, K. Manseki, *Acc. Chem. Res.* **2009**, *42*, 1827.

[52] B. O'Regan, D. T. Schwartz, *Chem. Mater.* **1995**, *7*, 1349.

[53] B. C. O'Regan, F. Lenzmann, *J. Phys. Chem. B* **2004**, *108*, 4342.

[54] U. Bach, D. Lupo, P. Comte, J. E. Moser, F. Weissortel, J. Salbeck, H. Spreitzer, M. Gratzel, *Nature* **1998**, *395*, 583.

[55] H. J. Snaith, R. Humphry-Baker, P. Chen, I. Cesar, S. M. Zakeeruddin, M. Gratzel, *Nanotechnology* **2008**, *19*, 424003.

[56] T. N. Murakami, M. Gratzel, *Inorg. Chim. Acta* **2008**, *361*, 572.

[57] A. Kay, M. Gratzel, *Sol. Energy Mater. Sol. Cells* **1996**, *44*, 99.

[58] M. Wang, A. M. Anghel, B. Marsan, N.-L. Cevey Ha, N. Pootrakulchote, S. M. Zakeeruddin, M. Gratzel, *J. Am. Chem. Soc.* **2009**, *131*, 15976.

[59] Y. Tachibana, J. E. Moser, M. Gratzel, D. R. Klug, J. R. Durrant, *J. Phys. Chem.* **1996**, *100*, 20056.

[60] Y. Tachibana, S. A. Haque, I. P. Mercer, J. R. Durrant, D. R. Klug, *J. Phys. Chem. B* **2000**, *104*, 1198.

[61] S. E. Koops, J. R. Durrant, *Inorg. Chim. Acta* **2008**, *361*, 663.

[62] S. A. Haque, Y. Tachibana, D. R. Klug, J. R. Durrant, *J. Phys. Chem. B* **1998**, *102*, 1745.

[63] B. C. O'Regan, J. R. Durrant, P. M. Sommeling, N. J. Bakker, *J. Phys. Chem. C* **2007**, *111*, 14001.

[64] B. C. O'Regan, S. Scully, A. C. Mayer, E. Palomares, J. Durrant, *J. Phys. Chem. B* **2005**, *109*, 4616.

[65] J. Bisquert, V. S. Vikhrenko, *J. Phys. Chem. B* **2004**, *108*, 2313.

[66] M. Wang, P. Chen, R. Humphry-Baker, S. M. Zakeeruddin, M. Gratzel, *ChemPhysChem* **2009**, *10*, 290.

[67] S. Eu, T. Katoh, T. Umeyama, Y. Matano, H. Imahori, *Dalton Trans.* **2008**, 5476.

[68] K. Sayama, K. Hara, H. Sugihara, H. Arakawa, N. Mori, M. Satsuki, S. Suga, S. Tsukagoshi, Y. Abe, *Chem. Commun.* **2000**, 1173.

[69] N. Koumura, Z.-S. Wang, S. Mori, M. Miyashita, E. Suzuki, K. Hara, *J. Am. Chem. Soc.* **2006**, *128*, 14256.

[70] J. E. Kroeze, N. Hirata, S. Koops, M. K. Nazeeruddin, L. Schmidt-Mende, M. Gratzel, J. R. Durrant, *J. Am. Chem. Soc.* **2006**, *128*, 16376.

[71] V. Balzani, A. Juris, M. Venturi, S. Campagna, S. Serroni, *Chem. Rev.* **1996**, *96*, 759.

[72] M. K. Nazeeruddin, P. Pechy, T. Renouard, S. M. Zakeeruddin, R. Humphry-Baker, P. Comte, P. Liska, L. Cevey, E. Costa, V. Shklover, L. Spiccia, G. B. Deacon, C. A. Bignozzi, M. Gratzel, *J. Am. Chem. Soc.* **2001**, *123*, 1613.

[73] M. K. Nazeeruddin, F. De Angelis, S. Fantacci, A. Selloni, G. Viscardi, P. Liska, S. Ito, B. Takeru, M. Grätzel, *J. Am. Chem. Soc.* **2005**, *127*, 16835.

[74] M. K. Nazeeruddin, S. M. Zakeeruddin, J. J. Lagref, P. Liska, P. Comte, C. Barolo, G. Viscardi, K. Schenk, M. Gratzel, *Coord. Chem. Rev.* **2004**, *248*, 1317.

[75] F. Gao, Y. Wang, J. Zhang, D. Shi, M. Wang, R. Humphry-Baker, P. Wang, S. M. Zakeeruddin, M. Gratzel, *Chem. Commun.* **2008**, 2635.

[76] M. Wang, S.-J. Moon, M. Xu, K. Chittibabu, P. Wang, N.-L. Cevey-Ha, R. Humphry-Baker, S. M. Zakeeruddin, M. Grätzel, *Small* **2010**, *6*, 319.

[77] F. Gao, Y. Cheng, Q. Yu, S. Liu, D. Shi, Y. Li, P. Wang, *Inorg. Chem.* **2009**, *48*, 2664.

[78] N. Robertson, *Angew. Chem., Int. Ed.* **2006**, *45*, 2338.

[79] J. M. Kroon, N. J. Bakker, H. J. P. Smit, P. Liska, K. R. Thampi, P. Wang, S. M. Zakeeruddin, M. Gratzel, A. Hinsch, S. Hore, U. Wuerfel, R. Sastrawan, J. R. Durrant, E. Palomares, H. Pettersson, T. Gruszecki, J. Walter, K. Skupien, G. E. Tulloch, *Prog. Photovolt. Res. Appl.* **2007**, *15*, 1.

[80] S. Webster, S. A. Odom, L. A. Padilha, O. V. Przhonska, D. Peceli, H. Hu, G. Nootz, A. D. Kachkovski, J. Matichak, S. Barlow, H. L. Anderson, S. R. Marder, D. J. Hagan, E. W. Van Stryland, *J. Phys. Chem. B* **2009**, *113*, 14854.

[81] M. Balaz, H. A. Collins, E. Dahlstedt, H. L. Anderson, *Org. Biomol. Chem.*, *7*, 874.

[82] M. U. Winters, E. Dahlstedt, H. E. Blades, C. J. Wilson, M. J. Frampton, H. L. Anderson, B. Albinsson, *J. Am. Chem. Soc.* **2007**, *129*, 4291.

[83] T. Hasobe, Y. Kashiwagi, M. A. Absalom, J. Sly, K. Hosomizu, M. J. Crossley, H. Imahori, P. V. Kamat, S. Fukuzumi, *Adv. Mater.* **2004**, *16*, 975.

[84] D. Gust, T. A. Moore, A. L. Moore, *Acc. Chem. Res.* **2009**, *42*, 1890.

[85] M.-S. Choi, T. Yamazaki, I. Yamazaki, T. Aida, *Angew. Chem., Int. Ed.* **2004**, *43*, 150.

[86] M. Gouterman, *Porphyrins* **1978**, *3*, 1.

[87] H. Imahori, S. Hayashi, T. Umeyama, S. Eu, A. Oguro, S. Kang, Y. Matano, T. Shishido, S. Ngamsinlapasathian, S. Yoshikawa, *Langmuir* **2006**, *22*, 11405.

[88] M. Gervaldo, F. Fungo, E. N. Durantini, J. J. Silber, L. Sereno, L. Otero, *J. Phys. Chem. B* **2005**, *109*, 20953.

[89] S. Cherian, C. C. Wamser, *J. Phys. Chem. B* **2000**, *104*, 3624.

[90] J. K. Park, H. R. Lee, J. Chen, H. Shinokubo, A. Osuka, D. Kim, *J. Phys. Chem. C* **2008**, *112*, 16691.

[91] A. J. Mozer, P. Wagner, D. L. Officer, G. G. Wallace, W. M. Campbell, M. Miyashita, K. Sunahara, S. Mori, *Chem. Commun.* **2008**, 4741.

[92] W. M. Campbell, K. W. Jolley, P. Wagner, K. Wagner, P. J. Walsh, K. C. Gordon, L. Schmidt-Mende, M. K. Nazeeruddin, Q. Wang, M. Gratzel, D. L. Officer, *J. Phys. Chem. C* **2007**, *111*, 11760.

[93] Q. Wang, W. M. Campbell, E. E. Bonfantani, K. W. Jolley, D. L. Officer, P. J. Walsh, K. Gordon, R. Humphry-Baker, M. K. Nazeeruddin, M. Gratzel, *J. Phys. Chem. B* **2005**, *109*, 15397.

[94] N. K. S. Davis, M. Pawlicki, H. L. Anderson, *Org. Lett.* **2008**, *10*, 3945.

[95] M. Tanaka, S. Hayashi, S. Eu, T. Umeyama, Y. Matano, H. Imahori, *Chem. Commun.* **2007**
, 2069.

[96] S. Hayashi, M. Tanaka, H. Hayashi, S. Eu, T. Umeyama, Y. Matano, Y. Araki, H. Imahori, *J. Phys. Chem. C* **2008**, *112*, 15576.

[97] C.-W. Lee, H.-P. Lu, C.-M. Lan, Y.-L. Huang, Y.-R. Liang, W.-N. Yen, Y.-C. Liu, Y.-S. Lin, E. W.-G. Diau, C.-Y. Yeh, *Chem.--Eur. J.* **2009**, *15*, 1403.

[98] H. L. Anderson, *Chem. Commun.* **1999**, 2323.

[99] M. Gratzel, *Abstracts of Papers, 239th ACS National Meeting, San Francisco, CA (US)* **2010**.

[100] P. Ranke, I. Bleyl, J. Simmerer, D. Haarer, A. Bacher, H. W. Schmidt, *Appl. Phys. Lett.* **1997**, *71*, 1332.

[101] N. Klonis, H. Wang, N. H. Quazi, J. L. Casey, G. M. Neumann, D. R. Hewish, A. B. Hughes, L. W. Deady, L. Tilley, *J. Fluo.* **2001**, *11*, 1.

[102] W. S. Shin, H. H. Jeong, M. K. Kim, S. H. Jin, M. R. Kim, J. K. Lee, J. W. Lee, Y. S. Gal, *J. Mater. Chem.* **2006**, *16*, 384.

[103] C. Ego, D. Marsitzky, S. Becker, J. Y. Zhang, A. C. Grimsdale, K. Mullen, J. D. MacKenzie, C. Silva, R. H. Friend, *J. Am. Chem. Soc.* **2003**, *125*, 437.

[104] S. Alibert-Fouet, S. Dardel, H. Bock, M. Oukachmih, S. Archambeau, I. Seguy, P. Jolinat, P. Destruel, *ChemPhysChem* **2003**, *4*, 983.

[105] S. Ferrere, B. A. Gregg, *New J. Chem.* **2002**, *26*, 1155.

[106] C. Li, J.-H. Yum, S.-J. Moon, A. Herrmann, F. Eickemeyer, N. G. Pschirer, P. Erk, J. Schoeneboom, K. Muellen, M. Gratzel, M. K. Nazeeruddin, *ChemSusChem* **2008**, *1*, 615.

[107] Y. Shibano, T. Umeyama, Y. Matano, H. Imahori, *Org. Lett.* **2007**, *9*, 1971.

[108] T. Edvinsson, C. Li, N. Pschirer, J. Schoeneboom, F. Eickemeyer, R. Sens, G. Boschloo, A. Herrmann, K. Muellen, A. Hagfeldt, *J. Phys. Chem. C* **2007**, *111*, 15137.

[109] Y. Jin, J. Hua, W. Wu, X. Ma, F. Meng, *Synth. Met.* **2008**, *158*, 64.

[110] A. Mishra, M. K. R. Fischer, P. Bauerle, *Angew. Chem., Int. Ed.* **2009**, *48*, 2474.

[111] M. Xu, S. Wenger, H. Bala, D. Shi, R. Li, Y. Zhou, S. M. Zakeeruddin, M. Gratzel, P. Wang, *J. Phys. Chem. C* **2009**, *113*, 2966.

[112] D. P. Hagberg, T. Marinado, K. M. Karlsson, K. Nonomura, P. Qin, G. Boschloo, T. Brinck, A. Hagfeldt, L. Sun, *J. Org. Chem.* **2007**, *72*, 9550.

[113] S. Kim, J. K. Lee, S. O. Kang, J. Ko, J. H. Yum, S. Fantacci, F. De Angelis, D. Di Censo, M. K. Nazeeruddin, M. Gratzel, *J. Am. Chem. Soc.* **2006**, *128*, 16701.

[114] K. Hara, M. Kurashige, Y. Dan-oh, C. Kasada, A. Shinpo, S. Suga, K. Sayama, H. Arakawa, *New J. Chem.* **2003**, *27*, 783.

[115] Z.-S. Wang, Y. Cui, Y. Dan-oh, C. Kasada, A. Shinpo, K. Hara, *J. Phys. Chem. C* **2007**, *111*, 7224.

[116] Z.-S. Wang, Y. Cui, Y. Dan-oh, C. Kasada, A. Shinpo, K. Hara, *J. Phys. Chem. C* **2008**, *112*, 17011.

[117] Z.-S. Wang, N. Koumura, Y. Cui, M. Takahashi, H. Sekiguchi, A. Mori, T. Kubo, A. Furube, K. Hara, *Chem. Mater.* **2008**, *20*, 3993.

[118] R. Chen, X. Yang, H. Tian, L. Sun, *J. Photochem. Photobiol., A* **2007**, *189*, 295.

[119] R. Chen, X. Yang, H. Tian, X. Wang, A. Hagfeldt, L. Sun, *Chem. Mater.* **2007**, *19*, 4007.

[120] H. Tian, X. Yang, J. Cong, R. Chen, C. Teng, J. Liu, Y. Hao, L. Wang, L. Sun, *Dyes Pigm.* **2010**, *84*, 62.

[121] M. Wang, M. Xu, D. Shi, R. Li, F. Gao, G. Zhang, Z. Yi, R. Humphry-Baker, P. Wang, S. M. Zakeeruddin, M. Gratzel, *Adv. Mater.* **2008**, *20*, 4460.

[122] H. Tian, X. Yang, R. Chen, Y. Pan, L. Li, A. Hagfeldt, L. Sun, *Chem. Commun.* **2007**, 3741.

[123] A. A. Kelkar, N. M. Patil, R. V. Chaudhari, *Tetrahedron Lett.* **2002**, *43*, 7143.

[124] D. P. Hagberg, T. Marinado, K. M. Karlsson, K. Nonomura, P. Qin, G. Boschloo, T. Brinck, A. Hagfeldt, L. Sun, *J. Org. Chem.* **2007**, *72*, 9550.

[125] W.-H. Liu, I.-C. Wu, C.-H. Lai, C.-H. Lai, P.-T. Chou, Y.-T. Li, C.-L. Chen, Y.-Y. Hsu, Y. Chi, *Chem. Commun.* **2008**, 5152.

[126] M. Xu, R. Li, N. Pootrakulchote, D. Shi, J. Guo, Z. Yi, S. M. Zakeeruddin, M. Gratzel, P. Wang, *J. Phys. Chem. C* **2008**, *112*, 19770.

[127] G. Li, K.-J. Jiang, Y.-F. Li, S.-L. Li, L.-M. Yang, *J. Phys. Chem. C* **2008**, *112*, 11591.

[128] J.-H. Yum, D. P. Hagberg, S.-J. Moon, K. M. Karlsson, T. Marinado, L. Sun, A. Hagfeldt, M. K. Nazeeruddin, M. Gratzel, *Angew. Chem., Int. Ed.* **2009**, *48*, 1576.

[129] W. Zeng, Y. Cao, Y. Bai, Y. Wang, Y. Shi, M. Zhang, F. Wang, C. Pan, P. Wang, *Chem. Mater.* **2010**, *22*, 1915.

[130] G. Zhang, H. Bala, Y. Cheng, D. Shi, X. Lv, Q. Yu, P. Wang, *Chem. Commun.* **2009**, 2198.

[131] K. Hara, T. Sato, R. Katoh, A. Furube, T. Yoshihara, M. Murai, M. Kurashige, S. Ito, A. Shinpo, S. Suga, H. Arakawa, *Adv. Funct. Mater.* **2005**, *15*, 246.

[132] K. Hara, M. Kurashige, S. Ito, A. Shinpo, S. Suga, K. Sayama, H. Arakawa, *Chem. Commun.* **2003**, 252.

[133] H. Qin, S. Wenger, M. Xu, F. Gao, X. Jing, P. Wang, S. M. Zakeeruddin, M. Gratzel, *J. Am. Chem. Soc.* **2008**, *130*, 9202.

[134] R. Li, X. Lv, D. Shi, D. Zhou, Y. Cheng, G. Zhang, P. Wang, *J. Phys. Chem. C* **2009**, *113*, 7469.

[135] T. Marinado, D. P. Hagberg, M. Hedlund, T. Edvinsson, E. M. J. Johansson, G. Boschloo, H. Rensmo, T. Brinck, L. Sun, A. Hagfeldt, *Phys. Chem. Chem. Phys.* **2009**, *11*, 133.

[136] M. Liang, W. Xu, F. Cai, P. Chen, B. Peng, J. Chen, Z. Li, *J. Phys. Chem. C* **2007**, *111*, 4465.

[137] G. de la Torre, C. G. Claessens, T. Torres, *Chem. Commun.* **2007**, 2000.

[138] J. He, A. Hagfeldt, S.-E. Lindquist, H. Grennberg, F. Korodi, L. Sun, B. Akermark, *Langmuir* **2001**, *17*, 2743.

[139] P. Y. Reddy, L. Giribabu, C. Lyness, H. J. Snaith, C. Vijaykumar, M. Chandrasekharam, M. Lakshmikantam, J.-H. Yum, K. Kalyanasundaram, M. Gratzel, M. K. Nazeeruddin, *Angew. Chem., Int. Ed.* **2007**, *46*, 373.

[140] J.-J. Cid, M. Garcia-Iglesias, J.-H. Yum, A. Forneli, J. Albero, E. Martinez-Ferrero, P. Vazquez, M. Gratzel, M. K. Nazeeruddin, E. Palomares, T. Torres, *Chem.--Eur. J.* **2009**, *15*, 5130.

[141] S. Mori, M. Nagata, Y. Nakahata, K. Yasuta, R. Goto, M. Kimura, M. Taya, *J. Am. Chem. Soc.* **2010**, *132*, 4054.

[142] K. Hara, T. Horiguchi, T. Kinoshita, K. Sayama, H. Sugihara, H. Arakawa, *Sol. Energy Mater. Sol. Cells* **2000**, *64*, 115.

[143] K. Sayama, M. Sugino, H. Sugihara, Y. Abe, H. Arakawa, *Chem. Lett.* **1998**, 753.

[144] M. Guo, P. Diao, Y.-J. Ren, F. Meng, H. Tian, S.-M. Cai, *Sol. Energy Mater. Sol. Cells* **2005**, *88*, 23.

[145] K. Sayama, S. Tsukagoshi, T. Mori, K. Hara, Y. Ohga, A. Shinpou, Y. Abe, S. Suga, H. Arakawa, *Sol. Energy Mater. Sol. Cells* **2003**, *80*, 47.

[146] X. Ma, J. Hua, W. Wu, Y. Jin, F. Meng, W. Zhan, H. Tian, *Tetrahedron* **2008**, *64*, 345.

[147] S. Alex, U. Santhosh, S. Das, *J. Photochem. Photobiol., A* **2005**, *172*, 63.

[148] Y. Chen, Z. Zeng, C. Li, W. Wang, X. Wang, B. Zhang, *New J. Chem.* **2005**, *29*, 773.

[149] J.-H. Yum, P. Walter, S. Huber, D. Rentsch, T. Geiger, F. Nuesch, F. De Angelis, M. Grätzel, M. K. Nazeeruddin, *J. Am. Chem. Soc.* **2007**, *129*, 10320.

UNIVERSITAT ROVIRA I VIRGILI
DESIGN AND SYNTHESIS OF ORGANIC SENSITIZERS FOR DYE SOLAR CELLS: MOLECULAR STRUCTURE VS DEVICE PERFORMANCE
Miquel Angels Planells Dillundé
ISBN:978-84-693-8861-7/DL:T.1946-2010

2. Experimental Techniques

UNIVERSITAT ROVIRA I VIRGILI
DESIGN AND SYNTHESIS OF ORGANIC SENSITIZERS FOR DYE SOLAR CELLS: MOLECULAR STRUCTURE VS DEVICE PERFORMANCE
Miquel Angels Planells Dillundé
ISBN:978-84-693-8861-7/DL:T.1946-2010

2.1. Organic Synthesis

2.1.1. General reagents and solvents

All reagents were purchased from either Sigma-Aldrich or Alfa Aeasar and they were used as received without further purification unless otherwise stated. Liquid and oils with relatively low boiling points were distilled prior to use. Common solvents were purchased from SdS and chlorinated solvents were kept under K_2CO_3 and filtered prior to use. For moisture sensitive reactions, anhydrous solvents which contained less than 0.005% of H_2O were purchased from Fluka.

2.1.2. General instrumentation

^1H and ^{13}C NMR spectra were recorded on a Bruker Avance 400 (400 MHz for ^1H and 100 MHz for ^{13}C). The deuterated solvents used are indicated; chemical shifts, δ, are given in ppm, referenced to the solvent residual signal (^1H, ^{13}C). Coupling constants, *J*, are given in Hz.

High Resolution Mass Spectra (HR-MS) were recorded on a Waters LCT Premier liquid chromatograph coupled time-of-flight mass spectrometer (HPLC/MS-TOF), using electrospray ionization (ESI) as ionization mode. Matrix assisted laser desorption ionization (MALDI) were recored on a BRUKER Autoflex time-of-flight mass spectrometer.

Elemental analyses (EA) were recorded on a LECO 932 CHNS elemental analyzer, and they were carried out by both Atlantic Microlabs and Santiago de Compostela University.

Fourier transform infrared (FT-IR) spectra were recored on a Bruker spectrometer model Alpha with an ATR accessory. Spectral range was from 4000 to 400 cm^{-1}.

The electrochemical data were obtained employing a conventional three-electrode cell connected to a CH Instruments© 660c potentiostat-galvanostat. The working electrode consisted of either platinum or carbon while the auxiliary electrode was platinum. The reference electrode was either SCE or Ag/AgCl. The solvents used were purged under argon prior the use. Cyclic (CV) and square wave (SWV) voltammetries were carried out in the presence of 0.1 M TBA·PF_6 supporting electrolyte, using ferrocene as an internal reference.

2.2. Dye Sensitized Solar Cell Preparation

2.2.1. Nanoparticle preparation

Al_2O_3 was prepared using a commercial water based solution of Al_2O_3 nanoparticles with a uniform diameter of 20 nm (Alfa-Aesar).

Highly transparent TiO_2 anatase nanoparticles were prepared by Josep Albero, Antonio Sanchez an d Amparo Forneli as previously reported.[1] Titanium isopropoxide (40 mL, 0.13 mol) was added to glacial acetic acid (9.12 g) under stirring. The resulting solution was cooled in an ice-bath and 240 mL of 0.1 M HNO_3 were added under vigorous stirring. The mixture was heated at 80 ºC for 8 h. Then it was allowed to cool to room temperature and filtered through a 0.45 mm PTFE filter. The filtrate was diluted to 5% weight of TiO_2 by the addition of water. The solution was then placed into a high pressure autoclave at 220 ºC for 12 h. After centrifugation, the aqueous phase was decanted and the solid residue was rinsed with ethanol twice. The aggregates were broken up using an ultrasonic bath and the solvent was removed. The nanoparticles were dissolved in a solution of terpineol containing 5% of ethylcellulose and the paste was homogenized by ball milling.

For high efficient cells, 20 and 400 nm diameter TiO_2 nanoparticles were purchased from Dyesol© and Solaronix©, respectively.

2.2.2. Device assembly

Two kind of cells were used in this thesis, depending on the measurement in question. On the one hand, highly transparent thin film devices with large active area (1 cm^2) were used mainly for TAS experiments. These devices were made using 4 to 9 µm thick TiO_2 (homemade paste) films and sensitized with the organic dyes until the absorbance reach 0.5 a.u. at the maximum absorption wavelength.

On the other hand, for optimized cell efficiencies, smaller active area (0.16 cm^2) devices were made using thick films consisting of a layer of 4 to 10 µm of 20 nm TiO_2 nanoparticles (Dyesol© paste) and an additional layer of 4 µm of 400 nm TiO_2 particles (scatter layer). Prior to the deposition of the TiO_2 paste the conducting glass substrates were immersed in a solution of $TiCl_4$ (40 mM) for 30 minutes and then dried. The TiO_2 nanoparticle paste was deposited onto a conducting glass substrate

(Hartford Glass inc. with 15 Ω per square resistance) using either doctor blade or screen printing technique. The TiO_2 electrodes were gradually heated under an airflow at 325 ºC for 5 min, 375 ºC for 5 min, 450 ºC for 15 min and 500 ºC for 15 min. The heated TiO_2 electrodes were then immersed in a solution of $TiCl_4$ (40 mM) at 70 ºC for 30 min and then washed with ethanol. The electrodes were heated at 500 ºC for 30 min and cooled prior dye adsorption.

The counter electrode was made by spreading a 10 mM solution of H_2PtCl_6 in ethanol onto a conducting glass substrate followed by heating at 390 ºC for 15 minutes. The counter electrode contains a small hole to allow the introduction of the liquid electrolyte into the cell using vacuum following the assembly of the counter and working electrodes.

For the high efficient cells, the solvent and concentration of dye solution as well as the immersion time were varied until the conditions necessary for the highest efficiencies were achieved. The sensitized electrodes were washed with the solvent used in the sensitization process and dried under air. Finally, the working and counter electrodes were sandwiched together using a thin thermoplastic (Surlyn) frame that melts at 100 ºC. The liquid electrolyte used consisted of the redox couple iodine - iodide with the presence of different additives, such as ionic liquids, *tert*-butylpyridine and guanidinium thiocyanate, at different concentrations in a mixture of acetonitrile/ valeronitrile. The concentration of each electrolyte component will be detailed in the experimental section of each chapter.

2.3. Photophysical Characterization Techniques

2.3.1. General techniques

Electronic absorption spectra in solution were recorded using 1 cm path length quartz cells in a Shimadzu© UV spectrophotometer 1700 with optical range from 190 to 1100 nm. UV-Visible spectra of dye sensitized films of TiO_2 or Al_2O_3, were also recorded in this spectrophotometer. Fluorescence and excitation spectra in solution were also recorded using 1 cm path length quartz cuvettes in an Aminco-Bowman© series 2 luminescence spectrophotometer. Furthermore, for film measurements, a holder with an angle of 16º with respect to the excitation source was used.

Time correlated single photon counting (TC-SPC) was used in order to measure fluorescence lifetimes using a LifeSpec-ps apparatus from Edinburgh Instruments©, with wavelength response from 200 to 850 nm and lifetime range from 300 picoseconds to 10 microseconds. Several pulsed diode lasers at 405, 505 or 635 nm were used as excitation sources, depending on the sample. The lifetime decay was fitted using the software provided by Edinburgh Instruments©. Appropriate filters were placed in front of the detector channel in order to block undesired laser reflections.

2.3.2. Transient absorbance spectroscopy

Transient absorbance spectroscopy (TAS) allows one to look at transient species present in physical and chemical reactions that only have a short lifetime. It was originally developed by Lord Porter around 1950, for which he was awarded the Nobel Prize for Chemistry in 1967.[2] This technique can be described as an elaborate spectrometer that is able to observe the spectrum of short lived species and their decay kinetics.[3-5]

The technique involves the irradiation of a sample with a short intense pulse of light, known as the excitation pulse, and observing the consequent change in the samples optical density. The optical density is determined by monitoring the transmission of a second and less intense beam of light that passes through the sample, known as the “probe”. This technique provides information about the kinetic decay over a wide timescale (from μs to s) of the transient species at single excitation and probe wavelength. In addition, probe wavelength can be changed over

a broad range (from 400 to 1000 nm) by the use of monochromators giving the absorption spectrum of the transient at a chosen time delay.

The excitation source used was a PTI GL-3300 Nitrogen Laser, which produced pulses at a wavelength of 337 nm with an energy of 1.45 mJ. The pulse was provided by a TG330 function generator from Thurlby Thandar Instruments© at 1 Hz repetition rate. A PTI GL-301 Dye laser head was used in conjunction with the nitrogen laser to provide a variable source of excitation wavelength, from 360 to 750 nm, as shown in Figure 2.1.

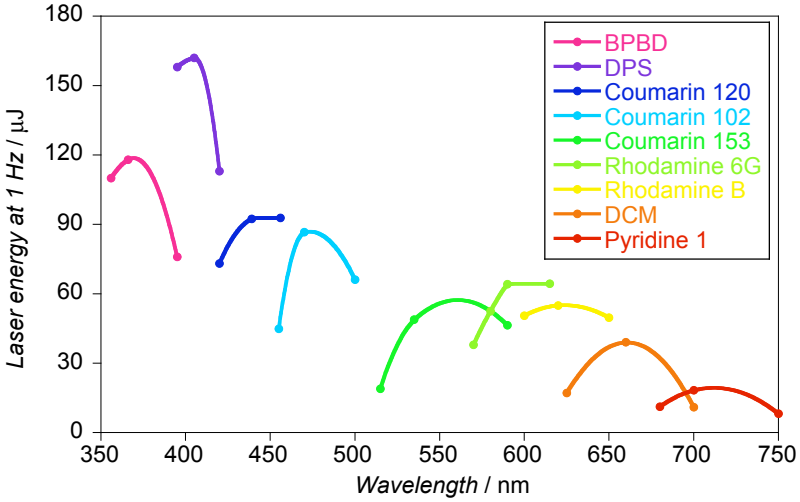

Figure 2.1 - Laser dyes and their energy output measured at the tip of the optical light guide.

A PTI 150 W tungsten lamp was used as the probe light source. The monitoring wavelength from the lamp was selected by using monochromator one (M1). A second monochromator (M2) was used after the sample to reduce the noise from laser light scattering. The optical detector is based on a silicon photodiode, which converts the optical signal into an electrical signal. That signal was amplified and filtered by a electronic system provided by Costronics©. Finally, the signal acquisition was carried out by a TDS 2022 oscilloscope from Tektronix©. The data collected was treated using TakeWave software, converting the electrical signal to units of optical density (*ΔO.D.*) as shown in the Equation 1:

$$\Delta O.D.(t) = -\log\left[\frac{I_{probe}}{I_{ref}}\right] \approx \frac{1}{\ln(10)}\frac{I_{probe} - I_{ref}}{I_{ref}} \approx \alpha \cdot \left[\frac{\Delta V(t)}{V_0}\right] \qquad (1)$$

where $\Delta V(t)$ is the transient signal size which is proportional to the light intensity, V_0 is the DC voltage level, which is proportional to the intensity of the probe and α is the amplification factor constant, which was set to 0.00174 and depends on the apparatus used.

The apparatus set up is shown in Figure 2.2. The sample, which can be either a sensitized TiO_2 film or a highly transparent complete cell, was placed between the monochromators. The laser pulse, at which the excitation wavelength was chosen to be as close to the maximum sample absorption as possible, was applied pointing the sample at 45º respect the probe light direction. The pulse frequency was set as 1 Hz.

The absorption spectra of transient species, such as dye cations, can be identified by changing the probe wavelength and recording the signal intensity at a particular time delay, such as 100 μs.[3] Once the transient absorption spectrum has been measured, the transient kinetic decay was recorded at its maximum.

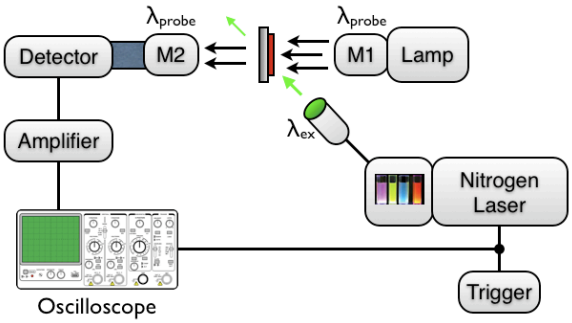

Figure 2.2 - Schematic representation of a transient absorption spectroscopy system.

The kinetic data of the transient can be fitted to a stretched exponential function, as shown in Equation 2:

$$\Delta O.D.(t) = A_0 + A_1 e^{-(t/\tau)^{\beta}} \qquad (2)$$

where A_0 (a.u.) is the baseline, A_1 (a.u.) is the signal amplitude, τ (s) is the lifetime of the transient and β (a.u.) is the empirical stretched factor whose value is between 0 and 1. An example of a transient decay is shown in Figure 2.3.

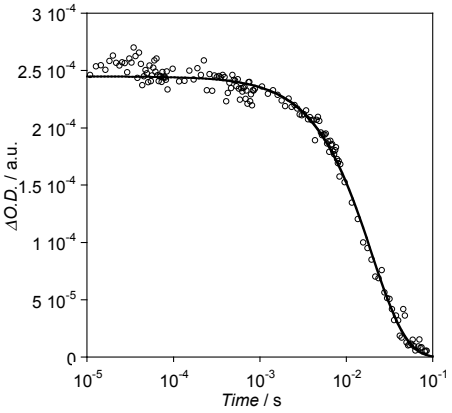

Figure 2.3 - Example of transient absorption experimental kinetic data (empty circles) and its fitting to Equation 2 (straight line).

2.3.3. Charge extraction

Charge extraction (CE) is an experimental technique developed by several researchers which allows one to obtain the accumulated charge in the TiO_2 film under cell operation conditions.[6, 7] Therefore, not only the conduction band edge shift can be obtained, but also the elucidation of the charge density in the film. A schematic representation of the device apparatus is shown in Figure 2.4.

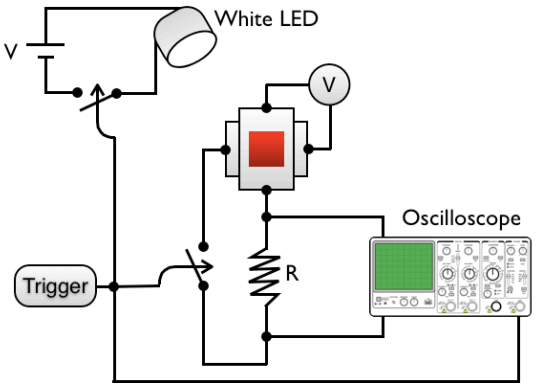

Figure 2.4 - Schematic representation of the charge extraction system.

The illumination system consists of 6 white light LED's from Luxeon Lumileds, which are focussed onto the the cell and connected to a DC power supply. A function generator TGP110, *Trigger*, from Thurlby Thandar Instruments© was used in order to

generate a pulsed voltage. The drop in voltage between the resistance *R* of 6.8 Ω was measured using an oscilloscope TDS 2022 from Tektronix©.

All charge extraction measurements were performed in the dark and care was taken to eliminate stray light falling on the sample. The cell, which is initially short circuited, was connected as shown in Figure 2.4. Then, the processes of **1**) switching the cell regime to open circuit and **2**) cell illumination by the white LED at 1 sun were synchronized by the pulse generator (*trigger*). Once light is applied, the dye injects electrons into the TiO_2, however, they cannot flow through an external circuit due to the open circuit conditions. Therefore, charges are accumulated in the film until it reaches a steady state set by the light intensity. The pulse length needed for reaching this steady state was set to 4 seconds. Finally, after the pulse, the circuit was closed and the light was switched off simultaneously, allowing all of the electrons accumulated in the traps of the film to flow through the external circuit. The drop in voltage versus time between the resistance *R* was recorded and treated as explained below. The process was repeated several times decreasing the LED light intensity, allowing for different voltages and different charge accumulations within the cell.

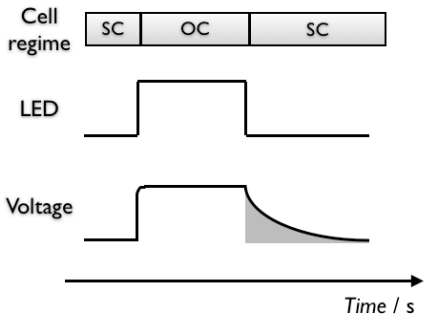

Figure 2.5 - Short circuit (SC) and open circuit (OC) sequences showing the relationship between the illumination by white LEDs and the voltage measured in the charge extraction technique. The integrated area (*gray*) is proportional to the accumulated charge (Equation 3).

The accumulated charge *Q* (C) is defined as:

$$Q = \frac{1}{R}\int_{t=0}^{t=t} V(t)\,dt \qquad (3)$$

where *R* (Ω) is the resistance showed in Figure 2.4 and *V*(t) (V) is the voltage measured at each time. However, the accumulated charge is not an intrinsic value, since it depends on the amount of TiO_2 nanoparticles. Therefore, electron density (e^- cm^{-3}) is used to define the charge accumulated in the film, and it is expressed as:

$$e^-_{density} = Q \cdot \frac{1}{C_e} \cdot \frac{1000}{d \cdot A \cdot (1-p)} \quad (4)$$

where C_e (C) is the electronic charge, d (μm) and A (cm²) are the thickness and area of the film, respectively, and p is the porosity of TiO_2 which was set as 0.6.[8]

The graphical representation between the electron density and the voltage applied to the cell can give the onset of the conduction band of TiO_2 (Figure 2.6). The data can be fitted to the single exponential function, as shown in Equation 5:

$$e^-_{density}(V) = A_0 + A_1 \cdot e^{V/m_c} \quad (5)$$

where A_0 and A_1 are constants and m_c (V) is the characteristic energy which describes the curvature distribution.[8]

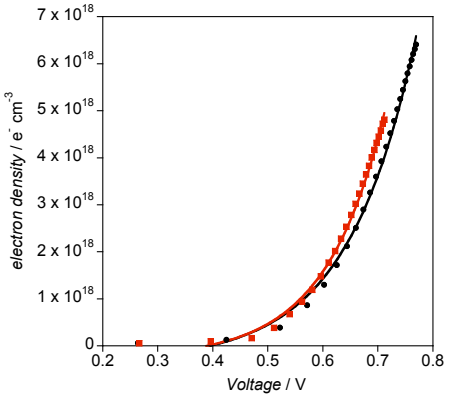

Figure 2.6 - Example of charge extraction data where electron density is plotted *vs* voltage induced by the light applied.

2.3.4. Transient photovoltage

Transient photovoltage (TPV) technique was developed by O'Regan *et al.*[8, 9] in order to evaluate the recombination between the electrons in the TiO_2 conduction band and the oxidized electrolyte. The measurement consists of the application of small perturbations of light to the cell at open circuit regime, which is maintained at a constant steady state voltage by background illumination using white LEDs. These small perturbations induce extra injected electrons in the conduction band and these electrons eventually recombine with oxidized electrolyte due to the open circuit conditions. By varying the background voltage (by increasing/decreasing the

background illumination) the small voltage perturbations allows one to monitor the recombination of injected electrons with oxidized electrolyte over several voltages.

A schematic representation of the TPV system is shown in Figure 2.7. The illumination system consists of 6 white LEDs and 4 red LEDs from Luxeon®. Green LEDs can also be used, depending on the absorption spectrum of the sample. The LEDs are connected to power supplies and focused onto the working electrode side of the solar cell. A function generator TGP110, *Trigger*, from Thurlby Thandar Instruments© was used to generate a pulse. The voltage data was acquired using an oscilloscope TDS 2022 from Tektronix©.

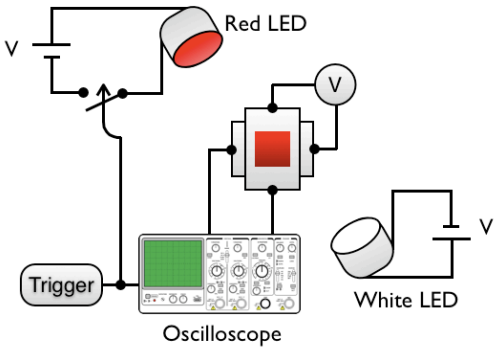

Figure 2.7 - Schematic representation of transient photovoltage system.

The measurement consists of the illumination of the solar cell at 1 sun using the white LEDs. The maximum voltage applied is usually the V_{oc}. of the cell under measurement, identified previously from its I-V curve. A short pulse of light, usually lasting 100 µs using the red LEDs is generated by the *trigger*. The pulse injects electrons into the TiO_2 film increasing the cell voltage usually by only 10 mV in order to ensure that the TiO_2 conduction band level is kept more or less in the steady state before and after the application of the red LED pulse.[8] Therefore, the extra electrons injected on the TiO_2 at open circuit regime can only escape through recombination with the oxidized electrolyte. The drop in voltage over time is recorded using the oscilloscope and repeated several times by decreasing the white light intensity, obtaining different decays at different cell voltages.

The data obtained from TPV can be fitted to a single exponential decay of the following form:

$$V(t) = V_0 + V_1 \cdot e^{-(t/\tau)} \qquad (6)$$

where V_0 (V) is the voltage at open circuit, V_1 (V) is the voltage amplitude generated by the pulse and τ (s) is the recombination lifetime.

However, comparing lifetimes obtained from TPV measurements at different cell voltages is not a good method to compare recombination in different devices. Solar cells contain different components, such as dyes, electrolyte additives, etc. which can influence recombination by shifting the conduction band. Therefore, a more meaningful way to compare electron recombination in different samples is to compare kinetics at similar electron densities. These electron densities are calculated by the charge extraction method as discussed in the previous section.

The lifetime τ (s) *vs* electron density is usually plotted in logarithmic scale and the data can be fitted to a power law function, as shown in Equation 7:

$$\tau = 10^{A} \cdot \left(e^{-}_{density}\right)^{k} \qquad (7)$$

where *A* and *k* are constants. An example of transient photovoltage data is shown in Figure 2.8 below.

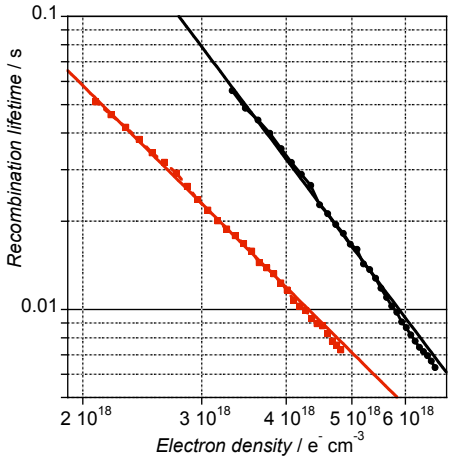

Figure 2.8 - Example of transient photovoltage data fitted with Equation 7.

2.4. Device Performance Techniques

2.4.1. Power conversion efficiency (η)

The photovoltaic measurements were carried out with a 150 W solar simulator from ABET© Technologies with the appropriate set of filters for the correct simulation of the 1.5 AM G solar spectrum. The incident light power was measured at 100 mW cm^{-2} with a calibrated Silicon photodiode, in which the spectral sensitivity was close to the devices under test. The applied potential and cell current were measured with a Keithley model 2400 digital source meter. The current to voltage (I-V) curve was measured automatically with home-built Labview© software.

2.4.2. Incident photon-to-current conversion efficiency (IPCE)

IPCE measurements were carried out with a home made system set up, consisting of a 150 W Oriel Xenon lamp as light source, a motorized monochromator which changes the measured wavelength and a Keithley 2400 digital source meter for acquiring the current generated. An integrating sphere was employed in order to provide homogeneous monochromatic light distribution over the whole active area of the devices. In addition, photocurrent and irradiated light intensity were measured simultaneously.

2.5. References

[1] E. Palomares, J. N. Clifford, S. A. Haque, T. Lutz, J. R. Durrant, *J. Am. Chem. Soc.* **2003**, *125*, 475.

[2] G. Porter, *Proc. R. Soc. A* **1950**, *200*, 284.

[3] Y. Tachibana, J. E. Moser, M. Gratzel, D. R. Klug, J. R. Durrant, *J. Phys. Chem.* **1996**, *100*, 20056.

[4] S. A. Haque, Y. Tachibana, R. L. Willis, J. E. Moser, M. Gratzel, D. R. Klug, J. R. Durrant, *J. Phys. Chem. B* **2000**, *104*, 538.

[5] S. A. Haque, Y. Tachibana, D. R. Klug, J. R. Durrant, *J. Phys. Chem. B* **1998**, *102*, 1745.

[6] N. W. Duffy, L. M. Peter, R. M. G. Rajapakse, K. G. U. Wijayantha, *Electrochem. Commun.* **2000**, *2*, 658.

[7] N. W. Duffy, L. M. Peter, R. M. G. Rajapakse, K. G. U. Wijayantha, *J. Phys. Chem. B* **2000**, *104*, 8916.

[8] B. C. O'Regan, S. Scully, A. C. Mayer, E. Palomares, J. Durrant, *J. Phys. Chem. B* **2005**, *109*, 4616.

[9] B. C. O'Regan, K. Bakker, J. Kroeze, H. Smit, P. Sommeling, J. R. Durrant, *J. Phys. Chem. B* **2006**, *110*, 17155.

UNIVERSITAT ROVIRA I VIRGILI
DESIGN AND SYNTHESIS OF ORGANIC SENSITIZERS FOR DYE SOLAR CELLS: MOLECULAR STRUCTURE VS DEVICE PERFORMANCE
Miquel Angels Planells Dillundé
ISBN:978-84-693-8861-7/DL:T.1946-2010

UNIVERSITAT ROVIRA I VIRGILI
DESIGN AND SYNTHESIS OF ORGANIC SENSITIZERS FOR DYE SOLAR CELLS: MOLECULAR STRUCTURE VS DEVICE PERFORMANCE
Miquel Angels Planells Dillundé
ISBN:978-84-693-8861-7/DL:T.1946-2010

3. Porphyrins as Sensitizers for DSSC

TOC Figure

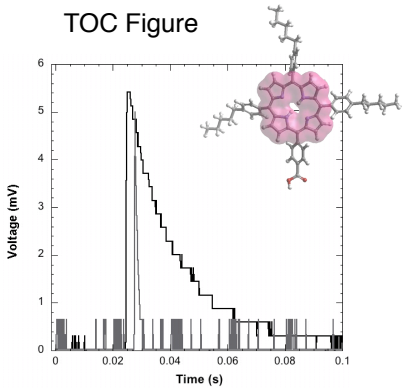

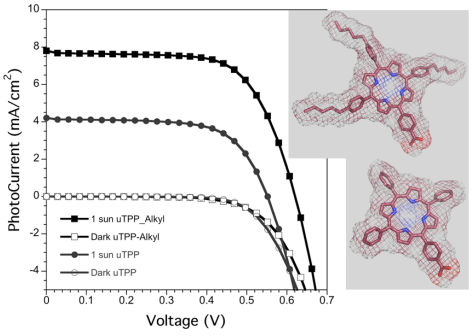

J. Mat. Chem. **2008**, *18*, 1652.

Appl. Phys. Lett. **2008**, *92*, 153506/1.

UNIVERSITAT ROVIRA I VIRGILI
DESIGN AND SYNTHESIS OF ORGANIC SENSITIZERS FOR DYE SOLAR CELLS: MOLECULAR STRUCTURE VS DEVICE PERFORMANCE
Miquel Angels Planells Dillundé
ISBN:978-84-693-8861-7/DL:T.1946-2010

3.1. General Introduction

Porphyrins are highly conjugated macrocycles which exhibit interesting optical properties. Moreover, they are excellent candidates for a wide range of optoelectronic applications. The photophysical properties and device performance of various porphyrin dyes have been reviewed extensively in Chapter 1.4.

Porphyrins can be substituted either at the *meso* or *β*-pyrrole positions and may be conjugated with the porphyrin core, modifying the porphyrins photochemical and redox properties.[1-3] However, phenyl group substituents attached at the *meso* position are positioned perpendicular with respect to the porphyrin core due to sterical hindrance, and as a consequence, no conjugation is attained between ring and substituent. As a result, it is possible to modify chemically the phenyl groups with negligible effect on the porphyrin photophysical properties.

The approach of attaching alkyl chains to sensitizer dyes has been used by several authors[4-8] as a strategy to: **1**) minimize dye aggregation **2**) act as an effective hydrophobic barrier against water, minimizing dye desorption from the TiO_2 film and thereby improving the cell stability and **3**) retard the recombination reaction between e^-_{TiO2} and electrolyte$^+$. However, the length of the alkyl chain is an important detail to control. Longer alkyl chains can affect dye packing, resulting in fewer molecules anchored onto the TiO_2 semiconductor, whereas shorter alkyl chains are not effective enough to fulfill the functions 1-3 outlined above.

In this chapter, the synthesis of two different unsymmetrical free base porphyrins is described. Their structures differ by the presence and absence of alkyl chains on the *meso* phenyl substituents. As already mentioned, modification at this position does not affect the porphyrin photophysical or electrochemical properties. Therefore, any differences observed in device efficiency as well as charge transfer kinetics on nanocrystalline TiO_2 in DSSC devices using these sensitizers can be attributed directly to the effect of the alkyl chains. Such insight into sensitizer structure: device function relationships are key to improving device efficiency in DSSC

The synthesis of these macrocycles was carried out under Lindsey conditions,[9] which is a modification of Alder-Longo methodology.[10] For unsymmetrical one-pot porphyrin synthesis, two different aldehydes and a pyrrole were used with catalytic amounts of a Lewis acid (Figure 3.1). The starting materials reached an equilibrium with the formation of a four membered porphyrogen macrocycle, which is then converted irreversibly into a porphyrin by the addition of an oxidizing reagent.

However, this reaction produces a large number of side products, such as polypyrrole, cyclic and acyclic oligomers as well as a statistical mixture of 6 porphyrin derivatives. Due to this fact, the purification processes were difficult and tedious and overall yields do not exceed 10% in most cases.[11, 12]

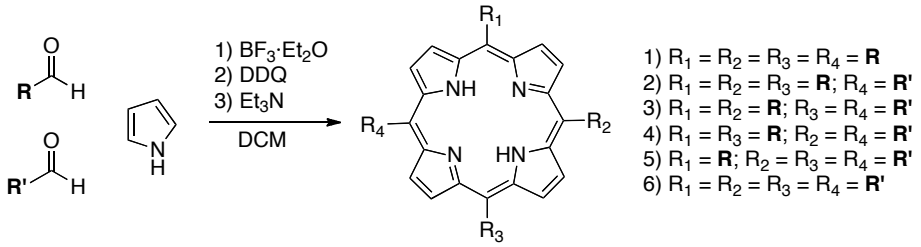

Figure 3.1 - One pot synthesis of unsymmetrical *meso*-tetraphenyl porphyrin (TPP) using the Lindsey method. The reaction gave a statistical mixture of six porphyrins. **R** and **R'** are different phenyl derivative substituents.

3.2. *Paper I*: The Role of *para*-Alkyl Substituents on *meso*-Phenyl Porphyrin Sensitised TiO_2 Solar Cells: Control of e^-_{TiO2}/ electrolyte$^+$ recombination reaction

Amparo Forneli,[a] Miquel Planells,[a] Maria Angeles Sarmentero,[a] Eugenia Martínez-Ferrero,[a] Brian C. O'Regan,[b] Pablo Ballester,[a,c,*] and Emilio Palomares[a,c,*]

[a] Institute of Chemical Research of Catalonia (ICIQ), Avda. Països Catalans,16, Tarragona, Spain. Fax: 34 977 920 224; Tel: 34 977 920 241; Corresponding Author E-mail: epalomares@iciq.es

[b] Centre for Electronic Materials and Devices. Dept. Chemistry. Imperial College of London. SW7 2AZ. London, U.K.

[c] Catalan Institution for Research and Advanced Studies (ICREA), Spain.

Abstract: We aim to investigate the effect of adding hydrophobic alkyl chains substituents to unsymmetrical free base tetra-phenyl porphyrins used for the preparation of dye sensitised solar cells (DSSC). We have used two different unsymmetrical *meso*-tetraphenyl substituted free base porphyrins attending to two objectives: (a) to observe how the substitution of three *para* positions of the *meso*-phenyl groups with hydrophobic alkyl chains influences the formation of molecular aggregates onto the semiconductor nanoparticles and (b) to deduce the influence that the substitution exerts over the e^-_{TiO2}/electrolyte$^+$ recombination reaction in operating devices. To achieve these goals we have focussed on the study of the electron transfer processes that take place at the different interfaces of the photovoltaic device using electrochemistry, steady-state and time resolved spectroscopic techniques.

3.2.1. Introduction

Since the seminal paper of O'Regan and Grätzel,[13] about the use of mesoporous semiconductor metal oxides sensitised with a monolayer of photo-active molecules to convert solar irradiation into electrical power, there has been an intensive effort towards the synthesis of efficient dyes that could push the efficiency above 10%. In fact, this has already been achieved by several groups using ruthenium dyes,[14-16]

where the optical and electrochemical properties have been designed to achieve optimal electron injection into the semiconductor, slow back-electron transfer kinetics and efficient regeneration of the light-induced oxidized molecule by the solution electrolyte.

The electron transfer (ET) reactions taking place at the different interfaces of the dye sensitized solar cell device have an extraordinary resemblance to the ET reactions that occur at the photosynthetic reaction centre (PSC) of several bacteria and plants.[17-19] In fact, an extensive number of scientists have synthesized dyads and triads based on porphyrins, or even more complex structures such as dendrimers, to mimic, in solution, the ET processes at the PSC.[20-22] Only recently, the use of such biological dyes, *i.e.* Zn-porphyrins, in molecular photovoltaic devices have given impressive light-to-energy efficiencies when irradiated at 1 sun[23-27] (100 mW cm^{-2}) although free-base porphyrins have only reached efficiencies higher than 5% but at much lower light intensities (1.5 mW cm^{-2}).[28-30] Several authors have assigned the low performance of porphyrin based devices to the dye desorption process and to the formation of molecular aggregates onto the surface of the nanoparticles.[28, 31] To avoid or limit the aggregation inconvenience we have decided to explore the use of alkyl chain substituents in the porphyrin structure. Other authors, using ruthenium bis-thiocyanate polypyridyl dyes, have already used such a strategy in order to increase not only the device efficiency but also the stability of the photovoltaic cells under illumination.[4, 32] However, there is still some controversy about the effect of the hydrophobic alkyl chains on the control of the electron recombination dynamics between the photo-injected electrons at the semiconductor metal oxide and the electrolyte.[6] In principle, porphyrins, due to their tendency to form aggregates, are ideal candidates to study whether the presence of hydrophobic alkyl chain substituents in their molecular structure not only inhibits or reduces the formation of molecular aggregates, but also creates a compact hydrophobic layer at the nanoparticle surface that may increase the distance with the I^-/I_3^- redox electrolyte and, therefore, slow the back electron transfer reaction. Hence, we decided to use such “biological like” dyes for our study.

As molecular sensitizers we synthesised the unsymmetrical porphyrins illustrated in Fig. 1.

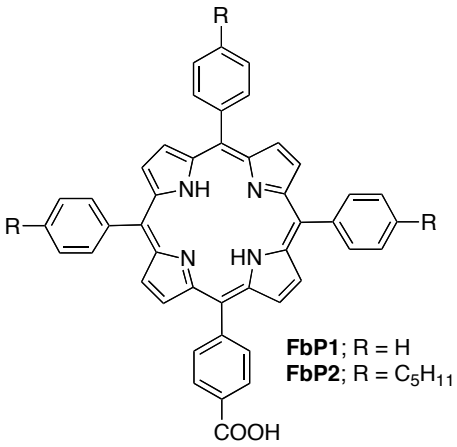

Fig. 1 Molecular structure of **FbP1** and **FbP2**.

3.2.2. Experimental

Materials and reagents

All reagents were purchased from Aldrich© and the solvents from SDS©. All were used as received without further purification, except pyrrole that was distilled under vacuum prior to use.

Synthesis of porphyrins

The methodology for the synthesis of unsymmetrical free base porphyrins has been described by Lindsey *et al.*[9] **Scheme 1** illustrates the synthetic steps for the preparation of **FbP1** and **FbP2**.

Synthesis of 4-pentylbenzaldehyde

25 mL of pentylbencene (0.145 mol) and 20.4 g of hexamethylenetetramine (0.145 mol) were added in a round bottom flask to 250 mL of TFA (trifluoroacetic acid). The mixture was heated to 100 ºC for 12 hours. Then, TFA was removed under vacuum and 250 mL of ice-water were added to the concentrate. Under stirring, sodium carbonate was added to the solution until a pH value ~8 was achieved. Diethyl ether was added and the organic layer was separated and washed with water. The organic layer was dried over sodium sulphate, filtered and concentrated under vacuum. Finally, the product was purified by distillation of the residue under diminished pressure (130 ºC, 1 mbar). The compound was isolated as a colorless liquid in 39 % yield.

^{1}H NMR (400 MHz, $CDCl_3$) δ_H: 9.96 (1H, s); 7.79 (2H, d, J = 8.0 Hz); 7.32 (2H, d, J = 8.0 Hz); 2.67 (2H, t, J = 8.0 Hz); 1.64 (2H, m); 1.33 (2H, m); 1.32 (2H, m); 0.89 (3H, t, J = 6.8 Hz).

^{13}C NMR (100 MHz, $CDCl_3$) δ_C: 191.93; 150.45; 134.43; 129.86; 129.07; 36.17; 31.42; 30.75; 22.48; 13.97.

Synthesis of 5-(4-carboxyphenyl)-10,15,20-trisphenylporphyrin (FbP1) and 5-(4-carboxyphenyl)-10,15,20-tris(4-pentylphenyl)porphyrin (FbP2)

1 g of methyl 5-formylbenzoate (6.1 mmol), the appropriate aldehyde (either 0.95 mL of benzaldehyde (9.1 mmol) or 1.45 gr of 4-pentylbenzaldehyde (9.1 mmol) and 0.95 mL of freshly distilled pyrrole (15.2 mmol) were added to a solution consisting of 530 mL of dichlorometane and 4 mL of ethanol. The resulting solution was stirred under argon for 10 minutes. The reaction mixture was protected from light and 0.69 mL of boron trifluoride dietherate (6.1 mmol) was added. The solution was stirred for 60 minutes. Subsequently, 3.11 gr of 2,3-dicyano-5,6-dichloroparabenzoquinone (15.2 mmol) were added and the reaction was stirred for another 90 minutes. After, the reaction was quenched by the addition of 3 mL triethylamine. The solvent was removed under vacuum and the crude was purified by column chromatography on silica gel using a 1:1 solvent mixture hexane:dichloromethane. The mono-carboxymethylporphyrins were isolated as purple solids in 10% (**FbP1-COOMe**) and 7.5 % (**FbP2-COOMe**) yield. Finally, the ester functional group was hydrolyzed to the carboxylic acid anchoring group. In brief, 90 mg of mono-carboxymethylporphyrin **FbP1-COOMe** (0.14 mmol) or **FbP2-COOMe** (0.1 mmol) were added to a mixture of 8 mL of THF (tetrahydrofuran) and 2 mL of 2M aqueous KOH. The reaction was stirred for 14 hours at 90 ºC. After, the THF was removed under vacuum and 80 mL of water were added to the resulting concentrate. The pH of the solution was adjusted to pH 4.0-5.0 using a solution of HCl 2M, followed by the addition of 100 mL of chloroform. The organic layer was separated, washed with water, dried over sodium sulphate and filtered. The organic solvent was removed under vacuum, given the pure free base monocarboxylic acid porphyrins as purple solids with 95% yield in both cases. The porphyrins were dried overnight before being used in the construction of the devices.

FbP1: ^{1}H NMR (400 MHz; $CHCl_3$) δ_H: 8.77 (8H, m); 8.37 (2H, d, J = 7.9 Hz); 8.23 (2H, d, J = 7.9 Hz); 8.14 (6H, m); 7.70 (9H, m); -2.89 (2H, br s).

ESI/MS (m/z): $[M+H]^+$ = 659.2442 (calc. M for $C_{45}H_{30}N_4O_2$ = 658.2369).

FT-IR (cm^{-1}): 2952, 2922(w), 2852(w), 1684, 1606, 1556, 1422, 1288, 797, 722, 700.

FbP2: ^1H NMR (400 MHz, $CDCl_3$) δ_H: 8.92 (2H, d, *J* = 4.8 Hz); 8.89 (4H, s); 8.80 (2H, d, *J* = 4.8 Hz); 8.51 (2H, d, *J* = 8.0 Hz); 8.36 (2H, d, *J* = 8.0 Hz); 8.13 (6H, d, *J* = 8.0 Hz); 7.59 (6H, d, *J* = 8.0 Hz); 2.98 (6H, t, *J* = 8.0 Hz); 1.95 (6H, m); 1.56 (12H, m); 1.08 (9H, t, *J* = 6.8 Hz); -2.73 (2H, br s).

MALDI/MS (m/z): $[M-H]^-$ = 867.4623 (calc. M for $C_{60}H_{60}N_4O_2$ = 868.4716).

FT-IR (cm^{-1}): 2953, 2922(s), 2852(s), 1688, 1606, 1420, 1278, 1178(s), 965(s), 797, 729.

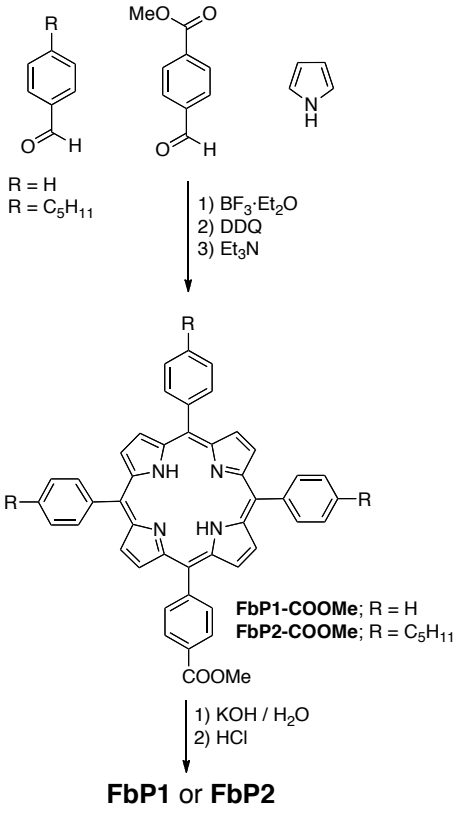

Scheme 1 Synthetic route of **FbP1** and **FbP2**.

Titanium nanoparticles synthesis

TiO_2 anatase nanoparticles were prepared as previously reported by Palomares *et al.*[33] Titanium isopropoxide (40 mL, 0.13 mol) was added to glacial acetic acid (9.12 g) under stirring. The resulting solution was cooled in an ice-bath and 240 mL of 0.1M HNO_3 were added under vigorous stirring. The mixture was heated at 80 ºC for 8 h.

Then it was allowed to cool at room temperature and then filtered through 0.45 µm filter. The filtrate was diluted to 5% weight of TiO_2 by the addition of water. Then solution was placed into a high-pressure autoclave at 220 ºC for 12h. After centrifugation, the aqueous phase was decanted and the solid residue was rinsed with ethanol twice. The aggregates were broken using an ultrasonic bath and the solvent was removed. The nanoparticles were dissolved in a solution of terpineol containing 5% of ethylcellulose and the paste was homogenized by ball milling. The TiO_2 nanoparticles crystallinity was characterized by X-ray powder analysis confirming the presence of a 95% of anatase and 5% of brookite TiO_2 phase.

Alumina nanoparticles synthesis.

The Al_2O_3 was prepared using commercial water based solution of Al_2O_3 nanoparticles with uniform diameter of 20 nm (Alfa-Aesar).

Spectroscopical characterization techniques

The UV-Visible spectra were recorded using a Shimadzu© UV-1700 spectrophotometer. When the absorption spectrum was registered for dye sensitized films we used the same film without dye to measure the instrument blank and ensure that the light scatter effects have been minimized. For the steady-state fluorescence emission spectra we used an Aminco-Bowman© Series 2 fluorimeter with the adequate support for solid samples.

Time correlated single photon counting (TCSPC) experiments were carried out with LifeSpec-red picosecond fluorescence lifetime spectrophotometer from Edinburgh Instruments© equipped with lasers as excitation sources. The instrument response was always shorter than 300 ps measured at full width half maximum (FWHM).

The transient absorbance experiments were recorded using a home-built system as reported before.[33]

^1H and ^{13}C NMR spectra were recorded with Bruker Avance 400 Ultrashield NMR spectrometer, equipped with BBI probe for proton spectra and BBO probe for carbon spectra.

FT-IR spectra were recorded using a FT-IR ThermoNicolet 5700 spectrometer with solid-state samples.

MS spectra were recorded with a Waters LCT Premier, which operates with a Bruker Autoflex instrument. The ionization technique was matrix assisted laser desorption/ionization (MALDI) and the mass was measured by time of flight (TOF) method.

Materials characterization

The mesoporous nanocrystalline titanium dioxide films were characterized by scanning probe microscopy techniques. Scanning electron microscopy (SEM) images were obtained using a JEOL JSM 6400 microscope. Before the measurements, the samples were covered with a thin layer of gold to increase the conductivity for superior image quality. Molecular Imaging Pico SPMII apparatus was used to obtain atomic force microscopy (AFM) images. Transmission electron microscopy (TEM) measures were done with a JEOL 1011 microscope. The surface analysis was carried out with an Autosorb 1-MP Quantachrome apparatus and the X-ray power diffraction measurements were acquired with a Bruker Siemens Smart CCD diffractometer.

Electrochemical and device characterization

The photoelectrochemical measurement were carried out with a ORIEL 150 W xenon light source equipped with the correct set of filters to achieve the solar spectrum 1.5 AM G. The light intensity was adjusted to 100 mW/cm^2, the equivalent of 1 sun, using a calibrated Si photodiode. The applied potential and cell current were measured with Keithley model 2600 digital source meter. The current to voltage (I - V curve) was measured automatically with a home-built Labview© software. The charge extraction and photovoltage decay was carried out with a system set-up as previously reported by O'Regan *et al.*[34] using a CHI Instruments model 600B potentiostat-galvanostat which was used for the cyclic voltammetry experiments too.

Device preparation

Nanocrystalline TiO_2 (19 nm particle size) was deposited onto a FTO conducting glass substrate (Hafordt glass© TEC 15 Ω/cm^2 resistance) by the commonly known as doctor blade technique. The resulting thickness was 4 μm and the device active area was 1 cm^2. The resulting electrodes were gradually heated under airflow at 325 ºC for 5 min., 375 ºC for 5 min., 450 ºC for 15 min. and 500 ºC for 15 min. The heated electrodes were soaked into $TiCl_4$ aqueous solution 0.04 M at 70 ºC for 15 min. and then washed with ethanol. Electrodes were heated again at 500 ºC for 30 min. and cooled before dye adsorption. The platinized counter electrode was made applying a drop of $5{\cdot}10^{-3}$ M of H_2PtCl_6 in 2-propanol dry solution and spreading onto the conducting glass substrate (FTO). The coated glass was heated under airflow at 390 ºC for 15 min.

A solution ($5{\cdot}10^{-4}$ M) of **FbP1** or **FbP2** in THF were prepared and the film was immersed in the solution at room temperature until desired absorbance values were

reached. The sensitized electrodes were assembled by sandwiching the working and the counter electrode using a thin thermoplastic (Surlyn©) frame that melts at 100 ºC.

The liquid electrolyte was elaborated using 0.6 M of 1-propyl-2,3-dimethylimidazolium iodide (DMPII), 0.025 M of lithium iodide (LiI), 0.04M of iodine (I_2) in a mixture of acetonitrile and valeronitrile (85:15). This electrolyte is quoted as **AF4**.

The cells were filled with the electrolyte through a hole previously made in the back of platinized counter electrode. Then, the hole was sealed with a thermoplastic polymer and a cover slide glass. Finally, a drop of silver conductive paint was spread at the electrode contacts to increase the conductivity.

3.2.3. Results and Discussion

UV-Visible measurements

The visible spectra of **FbP2** in solution and on a TiO_2 film are illustrated in Fig. 2. For the **FbP2** dye, we found that after 2 min of sensitisation, a 4 µm thick mesoporous sensitised film shows an “optimised” (less aggregated) visible spectrum with a sharp Soret band (λ_{Soret} = 415 nm). The broadening observed between the solid state and solution measurements, as reported before, is mainly due to the adsorption of the molecules onto the mesoporous film and not to the formation of typical aggregates.[35, 36]

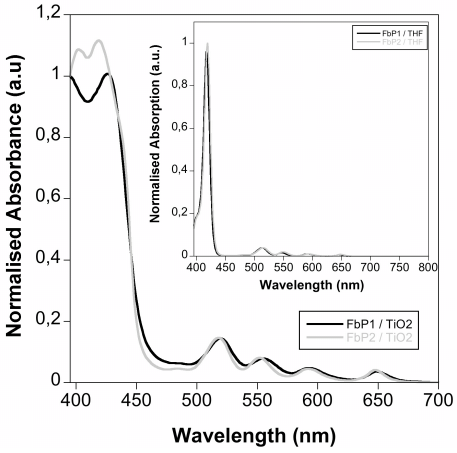

Fig 2 UV-Visible spectra of **FbP1** (black) and **FbP2** (grey) onto a transparent 4 µm thick mesoporous TiO_2 film and in THF solution (inset).

UNIVERSITAT ROVIRA I VIRGILI
DESIGN AND SYNTHESIS OF ORGANIC SENSITIZERS FOR DYE SOLAR CELLS: MOLECULAR STRUCTURE VS DEVICE PERFORMANCE
Miquel Angels Planells Dillundé
ISBN:978-84-693-8861-7/DL:T.1946-2010

In order to compare the adsorption kinetics of both porphyrins, we monitored the change in absorbance at λ = 520 nm of two identical 4 μm thick TiO_2 films until the absorbance reached a plateau. Fig. 3 shows the adsorption kinetics comparison for the films after immersion on a $5 \cdot 10^{-4}$ M solution of each dye.

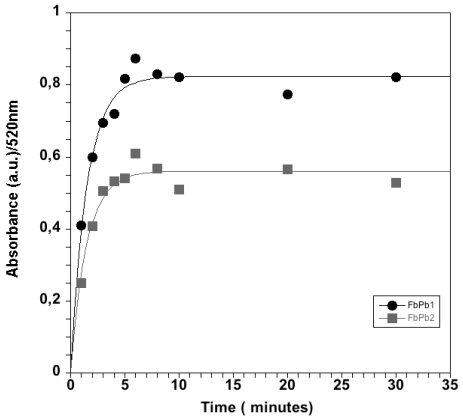

Fig. 3 Absorbance kinetics for **FbP1** (dots) and **FbP2** (squares) onto a transparent 4 μm thick mesoporous TiO_2 film at room temperature.

As can be seen in Fig. 3, both films reached different maximum absorbance at 520 nm under the same conditions. In the case of **FbP1** (ε_{520} = 17250 M^{-1} cm^{-1}) the film reached a maximum absorbance of 0.8 units while for **FbP2** (with the same ε_{520}) the maximum absorbance was 0.6 units. This can be understood in terms of porphyrin spatial distribution[28] if we take into account that the presence of alkyl chains in **FbP2** implies that the dye occupies a higher surface are at the nanoparticle and also avoids the adsorption of other molecules nearby, preventing the formation of aggregates. Moreover, we also found that the presence of the alkyl chains does not have a large influence over the dye adsorption kinetics. The rate constant for adsorption was studied fitting the experimental adsorption data following the pseudo-first order Lagergren's equation[37] (eqn (1))

$$A(t) = A_{\max}\left(1 - e^{-K_{ads} \cdot t}\right) \qquad (1)$$

where A_{max} represents the absorbance maxima and K_{ads} is the rate constant of dye adsorption. For both **FbP1** and **FbP2** K_{ads} was found to be 0.65 min^{-1}. Taking into account these data and the calculated surface area of the TiO_2 films, 99.4 m^2 g^{-1}, we have also estimated the porphyrin density in the films: 2.1 **FbP1** nm^2 $molecule^{-1}$ and 2.8 **FbP2** nm^2 $molecule^{-1}$.

Hence, we can assume that the presence of alkyl groups on the molecule affects the formation of porphyrin aggregates under controlled dye adsorption conditions but does not have a significant influence over the dye adsorption kinetics.

Dye solar cell characterization

We focused our attention on the device performance of **FbP2** using for comparison purposes **FbP1**. We have already demonstrated that the presence of pentyl groups on the porphyrin ring does not really have an influence over the dye adsorption kinetics. However, as can be seen in Fig. 4 the cell characteristics are different.

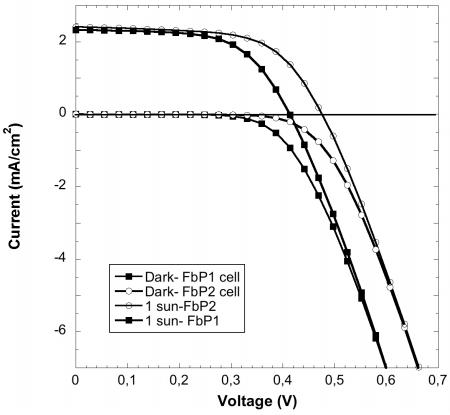

Fig. 4 Current vs Voltage characteristics for 4 μm transparent thick DSSC devices. The cell active area was 1 cm^2 and the electrolyte **AF4**.

In both devices the dye adsorption was controlled to achieve the same film absorbance (0.6 a.u. at λ = 520 nm), which explains the similar photocurrent in both devices despite the presence of alkyl groups in **FbP2**, but more interesting is the fact that the voltage increased too. In spite of this result we decided to study further the different charge transfer processes taking place at the device which have been previously identified in the literature as: (i) electron injection from the dye excited state into the semiconductor conduction band, (ii) electron recombination between the photo-injected electrons and the oxidised dye (e^-_{TiO2}/dye^+), (iii) dye regeneration by the redox active electrolyte (dye^+/electrolyte) and (iv) electron recombination between the photo-injected electrons and the electrolyte (e^-_{TiO2}/$electrolyte^+$).

Time correlated single photon counting measurements

The measurement of the excited-state emission lifetime decay of the sensitised films is a straightforward measurement to estimate the electron injection yield of a

dye adsorbed onto a semiconductor.[38] As a control sample, a mesoporous wide band-gap metal oxide such as Al_2O_3 is used to prevent electron injection from the excited state since the conduction band of the metal oxide is above the LUMO of the molecule. As an example, Fig. 5 shows the emission lifetime measurements for **FbP1** adsorbed onto nanocrystalline mesoporous films of Al_2O_3 and TiO_2. Both films were sensitized to achieve identical optical absorption (0.6 a.u. at λ = 520 nm). Under the same measurement conditions (the acquisition time was 900 s) **FbP1** and **FbP2** show almost comparable kinetics. In fact, we would like to note that both on Al_2O_3 transparent mesoporous films or in tetrahydrofuran solvent the kinetics were fitted to identical monoexponential decay.

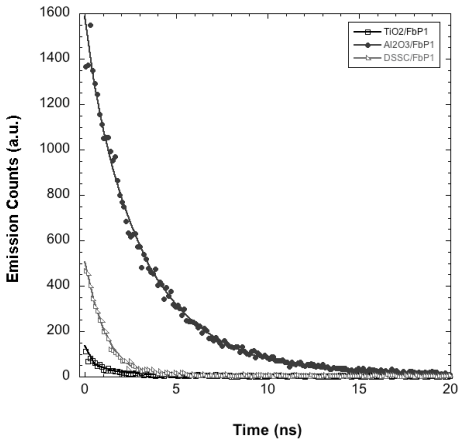

Fig 5 Time correlated single photon counting measurements for **FbP1** on Al_2O_3 (circles), TiO_2(squares) and a 4 μm thick DSSC with **AF4** electrolyte (triangles). The λ_{ex} was 635 nm and the λ_{em} was 720 nm. Acquisition time was 900 s. The curve fits were obtained using eqn (2).

Further analysis of the emission dynamics reveals that the decays can be also fitted using an extension of the Kohlrausch-Williams-Watts (KWW) function (eqn (2)). As an example **FbP1** sensitised films can be fitted with a monoexponential time of τ = 2.95 ns for Al_2O_3 and a τ = 0.67 ns for TiO_2 while **FbP2** results in τ = 3.12 ns for Al_2O_3 and τ = 1.10 ns for TiO_2.

$$y(t) = A \cdot e^{-\left(t/\tau\right)^{\alpha}} \qquad (2)$$

Recent work of Koops and Durrant,[39] using DSSC sensitised with ruthenium polypyridyl complexes, proposes that the fitting to the KWW function is consistent with the presence of inhomogeneous broadening of the energetics of electron injection. Moreover, in the case of DSSC sensitised with either **FbP1** or **FbP2** the

initial decay amplitude is considerably higher when compared to the TiO_2 sensitised films which is indicative that, in complete devices with redox active electrolyte, the electron injection is much slower in good agreement with the case of ruthenium bis-thiocyanate polypyridyl complexes studied elsewhere.[40] Following the methodology described Koops and Durrant, we estimated that the injection half-time for **FbP1** and **FbP2** occurs in less than 100 ps.

Laser transient absorption spectroscopy (L-TAS)

We utilized L-TAS as a technique that allows us to carry out the measurements of the electron recombination dynamics for 4 μm TiO_2 films sensitized with either **FbP1** or **FbP2** in the presence or absence of redox active I^-/I_3^- electrolyte. The signal decay after the laser pulse is assigned to charge recombination of the dye cation with the electrons in the trap/conduction band states of the TiO_2 semiconductor as reported before (Fig. 6).[41]

As expected, all recombination decay dynamics can be fitted to eqn (2) as a consequence of their dependence on the electron trapping/detrapping process at the nanocrystalline TiO_2 particles with $\alpha = 0.42$ for both **FbP1** and **FbP2**. The estimated recombination half time for both porphyrins was in the range of 100 - 150 ms. From these data it seems difficult to assign the slight differences in electron recombination dynamics between the dyes and the TiO_2 to the presence of the alkyl chains. In spite of this, we decided to study the electron recombination dynamics in the presence of the redox active electrolyte.

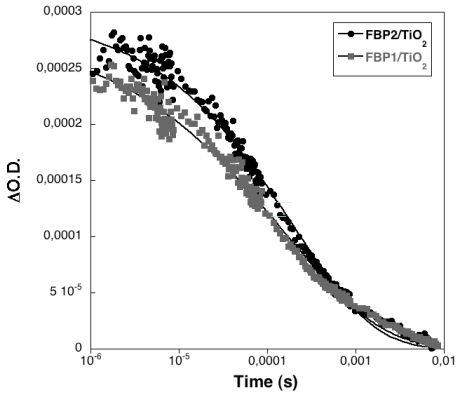

Fig. 6 Electron recombination dynamics for a 4 μm thick dye sensitized mesoporous TiO_2 film. The sensitized film optical absorbance at the laser excitation wavelength (λ_{ex} = 525 nm) was 0.3 a.u for each film. The probe wavelength for the measurement was fixed at λ_{probe} = 715 nm.

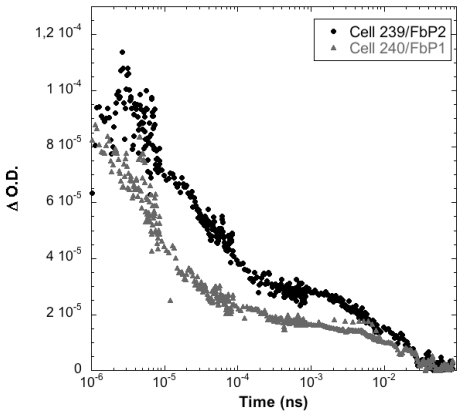

Fig. 7 The electron recombination dynamics for two 4 μm thick DSSC. The sensitized film optical absorbance at the laser excitation wavelength (λ_{ex} = 525 nm) was 0.3 a.u. The probe wavelength for the measurements was λ_{probe} = 715 nm.

As illustrated in Fig. 7, in the presence of a redox active electrolyte the electron recombination kinetics become biphasic. Previous work[42] demonstrated that the second phase observed in the presence of electrolyte arises from slower formation of by-products as a result of the regeneration of the dye ground state by subsequent electron transfer from the I^-/I_3^- electrolyte after the electron injection from the dye into the semiconductor conduction band. The fastest component of the optical transient is assigned to the dye cation, which is rapidly regenerated by the electrolyte, and therefore, its lifetime becomes shorter as can be confirmed when compared with the kinetics in Fig. 6, where the signal reaches a plateau at ΔO.D. of $2 \cdot 10^{-4}$ units while in Fig. 7 the decay has almost disappeared at times shorter than 1 ms. Attending to the results detailed above, we can conclude that in both devices the electron regeneration dynamics compete efficiently with the TiO_2/dye^+ electron recombination process under the cell operating conditions and the presence of hydrophobic pentyl groups on the porphyrin ring does not affect significantly the kinetic competition between the TiO_2/dye^+ recombination dynamics and the dye^+/I^- regeneration reaction.

Transient photovoltage measurements

Recently, several authors have employed transient photovoltage measurements, also known as V_{oc} decays, to evaluate the electron recombination dynamics between the photo-injected electrons at the TiO_2 and the oxidised electrolyte.[43, 44] For DSSC employing liquid redox electrolytes, such dynamics generally occur on the millisecond time scale and, therefore, no longer compete with the regeneration reaction studied above. On the other hand, it is worth noting that V_{oc} decays are

measurements strongly dependent on the accumulated charge at the semiconductor (charge density), and hence to obtain a fair comparison of the e^-_{TiO2}/electrolyte$^+$ recombination dynamics between different devices the charge density on both cells must be equal. As illustrated in Fig. 8, in our case, this condition is achieved when the cell voltage is 415 mV.

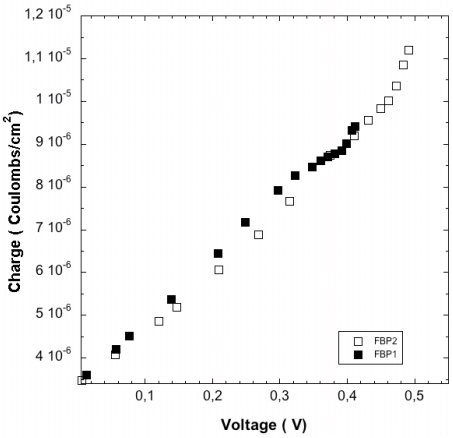

Fig. 8 Charge density as a function of V_{oc} for 4 µm DSSC sensitized with **FbP1** and **FbP2**. The electrolyte was **AF4**. Measurements performed at 1 sun.

As can be seen in Fig. 8 for DSSCs sensitised with both **FbP1** and **FbP2** the experimental points emerge along the same curve. Note, as indicated on the figure, that the cells have different V_{oc} when illuminated at 1 sun as expected from the results illustrated before (Fig. 4). The differences in voltage may be due to: (a) a shift on the TiO_2 conduction band with respect to the electrolyte potential or (b) differences in the e^-_{TiO2}/electrolyte$^+$ recombination reaction. The former hypothesis can be discarded because a change in the TiO_2 conduction band position also implies a shift in the cell charge density as demonstrated previously by other authors.[42] In our case, the hydrophobic pentyl group on **FbP2** does not shift the curve, thus, the differences in voltage must be due to the increase in the e^-_{TiO2}/electrolyte$^+$ recombination reaction in **FbP1**.

UNIVERSITAT ROVIRA I VIRGILI
DESIGN AND SYNTHESIS OF ORGANIC SENSITIZERS FOR DYE SOLAR CELLS: MOLECULAR STRUCTURE VS DEVICE PERFORMANCE
Miquel Angels Planells Dillundé
ISBN:978-84-693-8861-7/DL:T.1946-2010

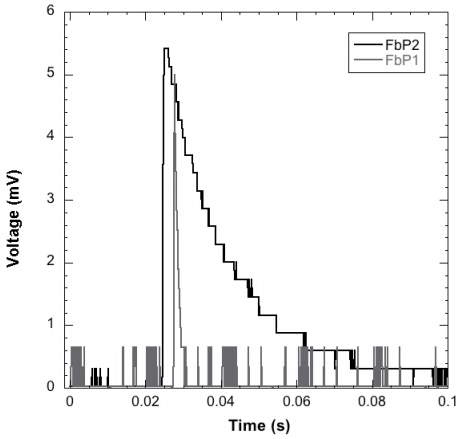

Fig. 9 Photovoltage transients for two 4 µm DSSC sensitized with **FbP1** and **FbP2**. The electrolyte was **AF4**.

Fig. 9 shows the V_{oc} decay for both devices measured at the same charge density (V_{oc} = 415 mV). It is noticeable that the presence of the pentyl groups on the free-base tetra-phenyl porphyrin (**FbP2**) results in slower recombination dynamics between the photo-injected electrons at the TiO_2 and the **AF4** electrolyte. We would like to mention that although the measurements were performed on sensitised films with the same absorbance (0.6 a.u. at λ = 520 nm) and, thus, we could expect that the lack of complete coverage would also play an important role in the accelerated recombination dynamics, experiments performed using complete full-monolayer coverage, according to Fig. 3, showed identical performance.

3.2.4. Conclusions

It can be concluded from our studies that the presence of hydrophobic alkyl chains on the molecular structures of porphyrins decreases the recombination between the photo-injected electrons at the TiO_2 nanoparticles and the electrolyte. However, their presence does not have a severe influence on the adsorption kinetics, and it suggests that they have little influence over the electron recombination between the photo-injected electrons at the TiO_2 nanoparticles and the oxidized porphyrin. This is in good agreement with the “distance-dependence” electron recombination theory,[45] if we consider that the highest occupied molecular orbital (HOMO) in the porphyrins is delocalized on the aromatic ring, which implies that the distance between the HOMO of the oxidised porphyrin and the surface of the TiO^2 nanoparticles must be identical.[46] Moreover, both porphyrin dyes showed almost identical decays for

electron recombination and electron regeneration dynamics in the presence of an active redox couple. This implies that the presence of the alkyl chain does not affect the regeneration reaction, which is key for the efficient performance of the devices. The yields of regeneration products are similar with and without the presence of hydrophobic alkyl chains, and the regeneration occurs before the e^-_{TiO2}/dye^+ recombination takes place. However, the analysis of the photovoltage transients revealed that, in fact, the effect of the hydrophobic alkyl chains on the free base porphyrin is to slow the electron recombination dynamics between the photo-injected electrons at the semiconductor and the oxidised electrolyte. The control of this wasteful reaction is key for improving the performance of the DSSC and requires careful attention.

In summary, we have demonstrated using free base porphyrins that the e^-_{TiO2}/$electrolyte^+$ recombination can be tuned by molecular engineering of the dyes and its consequences at the molecular level have important implications for the device efficiency.

3.2.5. Acknowledgements

EMF and MP thanks the Spanish MEC for the Juan de la Cierva Fellowship and the Ph.D. grant respectively. EP and AF also thank the MEC for the CONSOLIDER-HOPE 0007-2007 project and OrgaPVNet FP6 EU project. PB and MAS thank Dirección General de Investigación, Ministerio de Ciencia y Tecnología (CTQ2005-08989C01-C02/BQU and CSD2006-0003), Generalitat de Catalunya DURSI (2005SGR00108) and ICIQ Foundation for financial support.

3.3. *Paper II*: The Effect of Molecular Aggregates over the Interfacial Charge Transfer Processes on Dye Sensitized Solar Cells

Miquel Planells,[a] Amparo Forneli,[a] Eugenia Martínez-Ferrero,[a] Antonio Sánchex-Díaz,[a] Maria Angeles Sarmentero,[a] Pablo Ballester,[a,b]* Emilio Palomares,[a,b]* and Brian C. O'Regan[c]

[a] Institute of Chemical Research of Catalonia (ICIQ), Avda. Països Catalans,16, Tarragona, Spain. Fax: 34 977 920 224; Tel: 34 977 920 241; Corresponding Author E-mail: epalomares@iciq.es; pballester@iciq.es

[b] Catalan Institution for Research and Advanced Studies (ICREA), Spain.

[c] Centre for Electronic Materials and Devices. Dept. Chemistry. Imperial College of London. SW7 2AZ. London, U.K.

Abstract: The electron transfer reaction between the photoinjected electrons in the nanocrystalline TiO_2 mesoporous sensitized films and the oxidized electrolyte in dye sensitized solar cells (DSSC) plays a major role on the device efficiency. In this communication we show that, although the presence of molecular aggregates on the free base porphyrin DSSC limits the device photocurrent response under illumination, they form an effective hydrophobic barrier against the oxidized electrolyte impeding fast back-electron transfer kinetics. Therefore, their drawback can be overcome by designing dyes with peripheral moieties that prevent the formation of the aggregates and are able to achieve efficiencies as high as 3.2% under full sun.

3.3.1. Introduction

Tetraphenyl free base porphyrins have attracted much attention during the last years as a possible alternative to the use of ruthenium(II) complexes as sensitizers in dye sensitized solar cells (DSSC). Those dyes have excellent light harvesting properties due to their excellent molecular extinction coefficient which, in some cases, is ten times greater than the most used ruthenium dye, namely N719 [cis-bis(isothiocyanato) bis (2,2'-bipyridyl-4,4'-dicarboxylato)-ruthenium(II) bis-tetrabutylammonium. However, most of the time, despite the fact that they show better light absorption properties, these devices have not reached the same light-to-

energy conversion efficiency as those fabricated utilizing ruthenium polypyridyl complexes as sensitizers.[2, 28, 29]

Several authors have assigned the moderate performance of DSSC based on porphyrins to the formation of molecular aggregates onto the semiconductor nanoparticle surface and have designed several strategies to minimize the effect of the molecular aggregates over the performance of the photovoltaic devices. Some of the strategies have been (1) the film cosensitization using deoxycholic acid (Cheno) and (2) the synthesis of dyes with long alkyl chains.[29, 30] We have recently demonstrated that, for unsymmetrical tetraphenyl free base porphyrin, the presence of hydrophobic alkyl chains retards the electron recombination between the photoinjected electrons and the oxidized liquid electrolyte when we compared between devices made using an identical porphyrin without the alkyl chains and avoiding the formation of molecular aggregates.[47] In this communication, we aim to study and compare devices made using the same unsymmetrical tetraphenyl free base porphyrins with and without alkyl chains (**uTPP-alkyl** and **uTPP**, respectively) when the dye adsorption is controlled, not with the aim of comparing identical dye coverage as before, but to achieve optimum device performance. We have previously examined the dyes adsorption kinetics and demonstrated the formation of molecular aggregates after sensitization times longer than 5 min for **uTPP** devices. Nonetheless, the optimum devices were obtained after 8 h of sensitization. This experimental result was unexpected since most of the scientific literature on DSSC using organic dyes refer to the formation of molecular aggregates as a major issue to prevent in order to achieve high efficient light-to-energy conversion devices.[5, 48] Thus, in this letter, we intend to understand the molecular aggregates/device efficiency relationship over the charge transfer processes taking place at the different interfaces of the DSSC (see Scheme 1). Details about synthetic procedure can be found in *Ref.*[47]

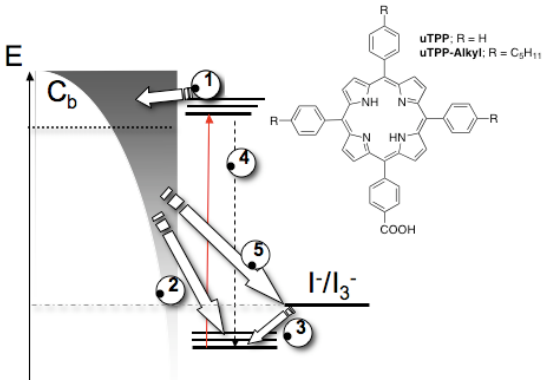

Scheme 1 Charge transfer processes taking place at the interfaces of the DSSC. The inset shows the molecular structures of the porphyrins employed in this work.

3.3.2. Results and Discussion

Figure 1 shows the photocurrent versus voltage characteristics for both cells (I-V curves). As can be seen, devices made using **uTPP-alkyl** have higher performance when irradiated at 1 sun (100 mW / cm^2 under 1.5 AM solar spectrum). The efficiencies are 3.2 % and 1.5 % for **uTPP-alkyl** and **uTPP** devices, respectively. The major differences between devices are in terms of photocurrent. In fact, the incident photon to current efficiency (IPCE) spectra clearly supports the I-V curves being the **uTPP-alkyl** based DSSC the device with greatest light-to-electron conversion (Fig. 2).

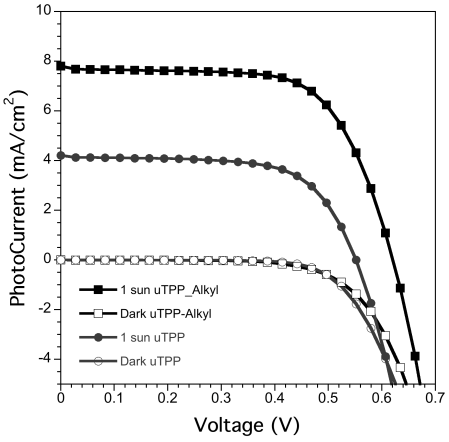

Fig. 1 Photocurrent vs. Voltage curves for DSSC sensitized with **uTPP-Alkyl** and **uTPP** porphyrins during 8 hours. The cell area was 0.152 cm^2.

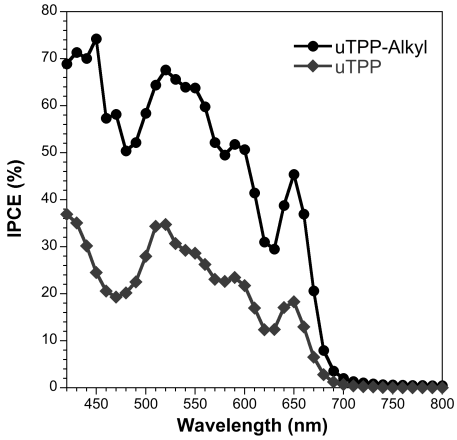

Fig. 2 IPCE spectra for DSSC sensitized with **uTPP-Alkyl** and **uTPP** porphyrins.

Moreover, both dyes show identical emission luminescence spectra upon excitation at the Q bands (λ_{ex} = 520 nm) with two maxima at λ_{em} = 655 and 720 nm and identical red-ox chemistry too, being the oxidation potential of 1.005 V versus standard calomel electrode (SCE). From these data, we have calculated the lowest unoccupied molecular orbital energy as reported before which, as expected was alike for both dyes, -1.21 V versus SCE. Hence, the formal differences on device efficiency must be due to either the presence of aggregates on the device sensitized using **uTPP** dye, which impedes efficient electron injection (*process 1* in Scheme 1), or the recombination process between the photo-injected electrons and the oxidized liquid electrolyte (*process 5* in Scheme 1). In an effort to understand the details, analogously, as we reported in a previous work,[47] we have measured the electron recombination dynamics between the electrons at the semiconductor and the oxidized electrolyte (Fig. 3).

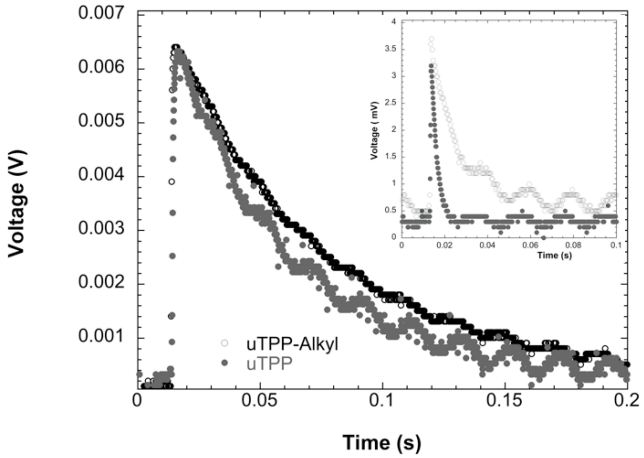

Fig. 3 Photovoltage transients for DSSC devices sensitized with **uTPP-Alkyl** and **uTPP** porphyrins for 8 hours. The inset shows the photovoltage transients for devices sensitized for 5 minutes. The cell area was 1 cm^2.

Surprisingly, we observed that, when sensitized for 8 h, both decay kinetics show almost identical dynamics. We have previously observed that for devices where the presence of molecular aggregates was negligible, the presence of alkyl chains plays a major role in controlling the kinetics of charge transfer between electrons at the TiO_2 and the oxidized electrolyte (Fig. 3, inset) while other electron transfer reactions are not influenced by the presence of the hydrophobic groups on the porphyrin. In order to ensure that this is still the case for 8 h sensitization, we carried out photo-induced electron recombination measurements between the electrons at the TiO_2 and the oxidized dye (*process 2* in Scheme 1) on complete devices using laser transient absorption spectroscopy. Typical decays were observed as we illustrated in Fig. 4.

As can be seen, the decay dynamics are identical for both devices independent of the sensitization time and, hence, of the presence of molecular aggregates, in good agreement with our previous data.[47] Thus, the experimental results with devices sensitized for 8 h implicate that the charge recombination kinetics between the electrons at the TiO_2 and the oxidized dye are independent of the formation of molecular aggregates at the semiconductor film, which has not been reported before.

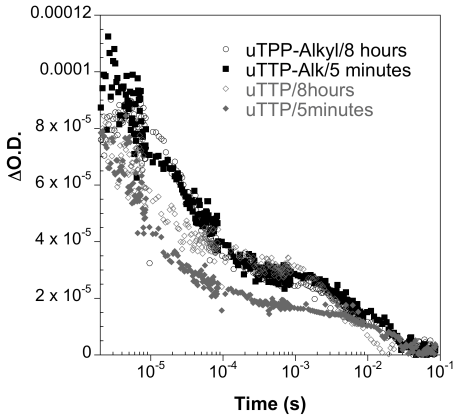

Fig. 4 Laser transient absorption kinetics for devices made using **uTPP-Alkyl** and **uTPP** porphyrins with different sensitization time. The cell area was 1 cm^2.

Of utmost importance is the fact that, in our case, the presence of molecular aggregates does affect, indeed, the electron recombination dynamics between the photoinjected electrons and the oxidized liquid electrolyte (*process 5* in Scheme 1). This is evidenced by comparing the main figure and the inset in Fig. 3. This experimental observation has not been previously observed and implicates that the presence of molecular aggregates, or an overloading of adsorbed dyes onto the film surface, prevents the wasteful electron recombination reaction with the oxidized electrolyte. Moreover, the experimental results confirm that the enhancement of the efficiency, on dye senzitized solar cells using porphyrins bearing alkyl chains, is also due to the lesser formation of molecular aggregates after long dye-sensitization periods and, hence, to the better charge injection, which indeed has been widely reported before.[5, 48]

3.3.3. Conclusion

In conclusion, we have shown that the electron transfer kinetics between the photoinjected electrons and the oxidized dye are independent of dye loading in clear contrast with the electron recombination kinetics with the oxidized electrolyte where the dye loading slows the recombination dynamics. These results have important implications on the design of innovative organic dyes where the molecular aggregates-device function relationship is still an object of intense research.

3.3.4. Acknowledgements

Financial support from the Spanish MEC is gratefully acknowledged (Consolider-Hope 0007-2007 project). MP and EMF also thanks the MEC for the Ph.D. grant and Juan de la Cierva fellowship, respectively. BO and EP also thanks the EU-FP6 OrgaPVNet project for funding. PB and MAS are grateful to the Dirección General de Investigación, Ministerio de Ciencia y Tecnología (CTQ2005-08989/BQU), Generalitat de Catalunya DURSI (2005SGR00108) and ICIQ Foundation for financial support.

3.4. References

[1] A. K. Burrell, D. L. Officer, P. G. Plieger, D. C. W. Reid, *Chem. Rev.* **2001**, *101*, 2751.

[2] W. M. Campbell, A. K. Burrell, D. L. Officer, K. W. Jolley, *Coord. Chem. Rev.* **2004**, *248*, 1363.

[3] H. L. Anderson, *Chem. Commun.* **1999**, 2323.

[4] J. E. Kroeze, N. Hirata, S. Koops, M. K. Nazeeruddin, L. Schmidt-Mende, M. Gratzel, J. R. Durrant, *J. Am. Chem. Soc.* **2006**, *128*, 16376.

[5] N. Koumura, Z.-S. Wang, S. Mori, M. Miyashita, E. Suzuki, K. Hara, *J. Am. Chem. Soc.* **2006**, *128*, 14256.

[6] S. N. Mori, W. Kubo, T. Kanzaki, N. Masaki, Y. Wada, S. Yanagida, *J. Phys. Chem. C* **2007**, *111*, 3522.

[7] M. Miyashita, K. Sunahara, T. Nishikawa, Y. Uemura, N. Koumura, K. Hara, A. Mori, T. Abe, E. Suzuki, S. Mori, *J. Am. Chem. Soc.* **2008**, *130*, 17874.

[8] M. K. Nazeeruddin, S. M. Zakeeruddin, J. J. Lagref, P. Liska, P. Comte, C. Barolo, G. Viscardi, K. Schenk, M. Gratzel, *Coord. Chem. Rev.* **2004**, *248*, 1317.

[9] J. S. Lindsey, I. C. Schreiman, H. C. Hsu, P. C. Kearney, A. M. Marguerettaz, *J. Org. Chem.* **1987**, *52*, 827.

[10] A. D. Adler, F. R. Longo, J. D. Finarelli, J. Goldmacher, J. Assour, L. Korsakoff, *J. Org. Chem.* **1967**, *32*, 476.

[11] T. Gianferrara, D. Giust, I. Bratsos, E. Alessio, *Tetrahedron* **2007**, *63*, 5006.

[12] M. Sirish, V. A. Chertkov, H.-J. Schneider, *Chem.--Eur. J.* **2002**, *8*, 1181.

[13] B. O'Regan, M. Gratzel, *Nature* **1991**, *353*, 737.

[14] M. Gratzel, *Inorg. Chem.* **2005**, *44*, 6841.

[15] L. Han, N. Koide, Y. Chiba, A. Islam, R. Komiya, N. Fuke, A. Fukui, R. Yamanaka, *Appl. Phys. Lett.* **2005**, *86*, 213501.

[16] N. Robertson, *Angew. Chem., Int. Ed.* **2006**, *45*, 2338.

[17] J. R. Durrant, S. A. Haque, E. Palomares, *Chem. Commun.* **2006**, 3279.

[18] D. Gust, T. A. Moore, A. L. Moore, *Acc. Chem. Res.* **2001**, *34*, 40.

[19] H. Imahori, Y. Mori, Y. Matano, *J. Photochem. Photobiol., C* **2003**, *4*, 51.

[20] M.-S. Choi, T. Yamazaki, I. Yamazaki, T. Aida, *Angew. Chem., Int. Ed.* **2004**, *43*, 150.

[21] S. J. Lee, J. T. Hupp, *Coord. Chem. Rev.* **2006**, *250*, 1710.

[22] R. F. Kelley, R. H. Goldsmith, M. R. Wasielewski, *J. Am. Chem. Soc.* **2007**, *129*, 6384.

[23] W. M. Campbell, K. W. Jolley, P. Wagner, K. Wagner, P. J. Walsh, K. C. Gordon, L. Schmidt-Mende, M. K. Nazeeruddin, Q. Wang, M. Gratzel, D. L. Officer, *J. Phys. Chem. C* **2007**, *111*, 11760.

[24] S. Eu, S. Hayashi, T. Umeyama, A. Oguro, M. Kawasaki, N. Kadota, Y. Matano, H. Imahori, *J. Phys. Chem. C* **2007**, *111*, 3528.

[25] J. Rochford, D. Chu, A. Hagfeldt, E. Galoppini, *J. Am. Chem. Soc.* **2007**, *129*, 4655.

[26] J. R. Stromberg, A. Marton, H. L. Kee, C. Kirmaier, J. R. Diers, C. Muthiah, M. Taniguchi, J. S. Lindsey, D. F. Bocian, G. J. Meyer, D. Holten, *J. Phys. Chem. C* **2007**, *111*, 15464.

[27] M. Tanaka, S. Hayashi, S. Eu, T. Umeyama, Y. Matano, H. Imahori, *Chem. Commun.* **2007**, 2069.

[28] S. Cherian, C. C. Wamser, *J. Phys. Chem. B* **2000**, *104*, 3624.

[29] F. Odobel, E. Blart, M. Lagree, M. Villieras, H. Boujtita, N. E. Murr, S. Caramori, C. A. Bignozzi, *J. Mater. Chem.* **2003**, *13*, 502.

[30] J. Jasieniak, M. Johnston, E. R. Waclawik, *J. Phys. Chem. B* **2004**, *108*, 12962.

[31] A. Kay, M. Graetzel, *J. Phys. Chem.* **1993**, *97*, 6272.

[32] L. Schmidt-Mende, J. E. Kroeze, J. R. Durrant, M. K. Nazeeruddin, M. Gratzel, *Nano Lett.* **2005**, *5*, 1315.

[33] E. Palomares, J. N. Clifford, S. A. Haque, T. Lutz, J. R. Durrant, *J. Am. Chem. Soc.* **2003**, *125*, 475.

[34] B. C. O'Regan, S. Scully, A. C. Mayer, E. Palomares, J. Durrant, *J. Phys. Chem. B* **2005**, *109*, 4616.

[35] T. Ma, K. Inoue, H. Noma, K. Yao, E. Abe, *J. Photochem. Photobiol., A* **2002**, *152*, 207.

[36] M. Gervaldo, F. Fungo, E. N. Durantini, J. J. Silber, L. Sereno, L. Otero, *J. Phys. Chem. B* **2005**, *109*, 20953.

[37] G. Annadurai, M. Chellapandian, M. R. V. Krishnan, *Environ. Monit. Assess.* **1999**, *59*, 111.

[38] Y. Tachibana, I. V. Rubtsov, I. Montanari, K. Yoshihara, D. R. Klug, J. R. Durrant, *J. Photochem. Photobiol., A* **2001**, *142*, 215.

[39] S. E. Koops, J. R. Durrant, *Inorg. Chim. Acta* **2008**, *361*, 663.

[40] S. A. Haque, E. Palomares, B. M. Cho, A. N. M. Green, N. Hirata, D. R. Klug, J. R. Durrant, *J. Am. Chem. Soc.* **2005**, *127*, 3456.

[41] Y. Tachibana, S. A. Haque, I. P. Mercer, J. R. Durrant, D. R. Klug, *J. Phys. Chem. B* **2000**, *104*, 1198.

[42] I. Montanari, J. Nelson, J. R. Durrant, *J. Phys. Chem. B* **2002**, *106*, 12203.

[43] B. C. O'Regan, J. R. Durrant, *J. Phys. Chem. B* **2006**, *110*, 8544.

[44] A. Zaban, M. Greenshtein, J. Bisquert, *ChemPhysChem* **2003**, *4*, 859.

[45] J. N. Clifford, E. Palomares, M. K. Nazeeruddin, M. Gratzel, J. Nelson, X. Li, N. J. Long, J. R. Durrant, *J. Am. Chem. Soc.* **2004**, *126*, 5225.

[46] O. Cramariuc, T. I. Hukka, T. T. Rantala, *Chem. Phys.* **2004**, *305*, 13.

[47] A. Forneli, M. Planells, M. A. Sarmentero, E. Martinez-Ferrero, B. C. O'Regan, P. Ballester, E. Palomares, *J. Mater. Chem.* **2008**, *18*, 1652.

[48] S. Alex, U. Santhosh, S. Das, *J. Photochem. Photobiol., A* **2005**, *172*, 63.

UNIVERSITAT ROVIRA I VIRGILI
DESIGN AND SYNTHESIS OF ORGANIC SENSITIZERS FOR DYE SOLAR CELLS: MOLECULAR STRUCTURE VS DEVICE PERFORMANCE
Miquel Angels Planells Dillundé
ISBN:978-84-693-8861-7/DL:T.1946-2010

UNIVERSITAT ROVIRA I VIRGILI
DESIGN AND SYNTHESIS OF ORGANIC SENSITIZERS FOR DYE SOLAR CELLS: MOLECULAR STRUCTURE VS DEVICE PERFORMANCE
Miquel Angels Planells Dillundé
ISBN:978-84-693-8861-7/DL:T.1946-2010

4. Perylenes as Sensitizers for DSSC

TOC Figure

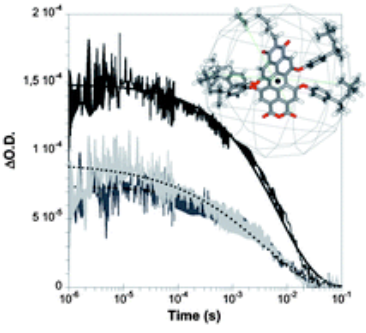

J. Mat. Chem. **2008**, *18*, 802.

TOC Figure

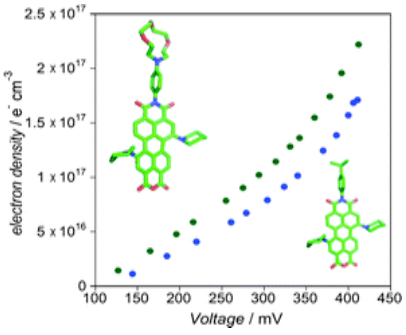

J. Mat. Chem. **2009**, *19*, 5818.

4.1. General Introduction

Perylenes are highly conjugated π systems and also excellent electron acceptors. Therefore, basing DSSC devices on these dyes is problematic due to their low lying LUMO energy level, which results in poor electron injection into the conduction band of the TiO_2.[1] To overcome this drawback, molecular engineering of perylenes is necessary in order to shift their LUMO energy level upwards. This is possible by the attachment of electron donating groups to these structures.[2] The main perylene photophysical properties as well as their utilization as sensitizers in DSSC has already been reviewed extensively in Chapter 1.4 of this thesis.

A common problem associated with highly π conjugated planar molecules such as perylenes is aggregation. Such molecules have a high tendency to pack together by π - π stacking, which can result in deactivation of dye excited states, with a subsequent negative impact upon electron-injection and therefore photocurrent. Modification of the sensitizer structure by the addition of bulky substituent groups is one way to minimize aggregation. In addition, the immersion time of TiO_2 film in the dye solution as well as the solvent used can be important parameters affecting aggregation, and therefore must be controlled.

In this chapter, the performance of novel perylene dye sensitizers in DSSC devices is investigated. The sensitization conditions and dye loading on nanocrystalline TiO_2 of perylenes containing bulky groups attached at the *bay* positions is discussed, as well as the interfacial charge transfer kinetics in DSSC devices. In addition, perylenes containing a crown ether substituent capable of forming supramolecular interactions with Li^+ cations present in the electrolyte are investigated. Small cations, such as Li^+ and H^+, can interact strongly with the TiO_2 surface shifting down the conduction band.[3] This shift can increase the electron-injection driving force and photocurrent while at the same time the recombination reactions can speed up, decreasing the voltage. Sensitizers capable of complexing with cations such as Li^+, keeping them far from the TiO_2 surface are expected to improve DSSC voltage.

It should be pointed out that this work was done as a collaboration with researchers from *Miguel Hernández University* (Elche, Spain). They carried out the perylene synthesis as well as NMR titrations.

4.2. *Paper III*: Interfacial Photo-induced Charge Transfer Reactions in Perylene Imide Dye Sensitised Solar Cells

Miquel Planells,[a] F. Javier Céspedes-Guirao,[b] Amparo Forneli,[a] Ángela Sastre-Santos,[b,*] Fernando Fernández-Lázaro,[b,*] and Emilio Palomares[a,c,*]

[a] Institute of Chemical Research of Catalonia (ICIQ), Avda. Països Catalans,16, Tarragona, Spain. Fax: 34 977 920 224; Tel: 34 977 920 241;Corresponding Author E-mail: epalomares@iciq.es

[b] División de Química Orgánica. Instituto de Bioingenieria, Universidad Miguel Hernández. Edificio Vinalopó, Avda. Universidad s/n. Elche, Spain.

[c] Catalan Institution for Research and Advanced Studies (ICREA). Spain.

Abstract: The interfacial electron transfer reactions of a perylene imide based dye sensitised solar cell (DSSC) with an efficiency of 3.15% under standard conditions have been characterised. The observed interfacial charge transfer dynamics under different sensitisation conditions have been correlated with the device efficiency.

4.2.1. Introduction

Molecular materials are of great interest in the field of dye sensitised solar cells (DSSC).[4-8] Moreover, if these materials present molecular extinction coefficients (ε) above 35000 M^{-1} cm^{-1} at the lowest energy absorption band, they can be used as sensitizers in mesoporous films with thicknesses below 10 µm and still achieve high photocurrents. Since the breakthrough by O'Regan and Gratzel,[9] the use of ruthenium complexes as sensitizers in DSSC has predominated. However, for most of those ruthenium complexes ε is generally below 30000 M^{-1} cm^{-1} and thicker films must be used with direct implications for device efficiency losses, mainly due to fill factor and cell voltage.[10] On the other hand, there has been recent interest in metal-free dyes which could lead to similar efficiencies when compared with the DSSC paradigm molecule, the so-called **N719** (chemical name: cis-bis(isothiocyanato)bis(2,2'-bipyridyl-4,4'-dicarboxylate)-ruthenium(II) bis-tetrabutylammonium) and, therefore, several groups have explored the use of organic dyes as proficient light collector moieties in DSSC.[11-15]

Organic dyes present many advantages for photovoltaic applications. As already mentioned above, most organic dyes show higher molecular extinction coefficients in the visible range (400 - 700 nm) than the ruthenium complexes allowing the use of thinner films and, hence, less mesoporous TiO_2 material is needed. Moreover, the lack of precious metal on the sensitizer molecular structure will also lower the production cost of the devices. Finally, the organic molecules can be modified at will to tune the photo-physical and electrochemical properties. However, the use of organic dyes presents other particular problems which limit, at present, the efficiency of the DSSC: (a) the dyes tend to form molecular aggregates on the semiconductor nanoparticle surfaces preventing efficient electron injection, (b) the devices show moderate voltages, when compared to ruthenium complexes, and (c) the stability of those devices decreases without a UV protective filter. Moreover, unlike the ruthenium complexes used for making efficient devices, the interfacial charge transfer reactions have not been studied in detail. For example, the effect of those aggregates on the device features (photocurrent, voltage, electron recombination processes, dye regeneration by the electrolyte, etc.) is still not well understood.

The use of perylenes as sensitizers is a particular case in organic dye based DSSC.[1, 16-19] Recently, several groups have reported important improvements in the efficiencies of perylene based DSSC using steric hindering groups in the *bay* positions that decrease the formation of molecular aggregates and, therefore, improve the device photocurrent.[20-22]

The aim of this paper is to study the interfacial charge transfer reactions of a perylene monoimide dye that bears bulky groups (Fig. 1) in order to modulate the degree of aggregation on the surface of the TiO_2 nanocrystalline particles. Our group among others has demonstrated that these alkyl moieties play a key role in the control of the charge transfer dynamics at the DSSC.[23-25] In this work, we will focus particularly on three interfacial electron recombination processes: (1) the photo-injection of electrons into the semiconductor conduction band, (2) the recombination reaction between those photo-injected electrons and the oxidised dye (e^--TiO_2/Dye^+) and (3) with the oxidised electrolyte (e^--TiO_2/$electrolyte^+$). The control and knowledge of these reactions are paramount for the achievement of efficient devices and, moreover, to shed light on the design of new perylene dyes with enhanced performance in DSSC.

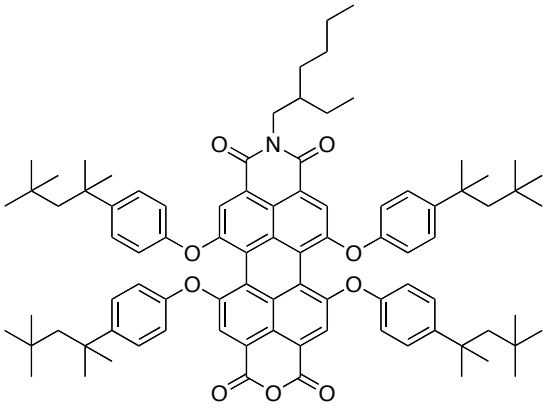

Fig. 1 Molecular structure of perylene monoimide **PI1**.

4.2.2. Experimental

All reagents were purchased from commercial suppliers and used without further purification unless otherwise noted. Commercial TLC plates (silica gel 60 F254, SDS) were used to monitor the progress of the reaction, with spots observed under UV light at 254 and 365 nm. Column chromatography was performed with silica gel 60A (particle size 40-63 μm, SDS).

NMR spectra were taken using a 300 MHz Bruker Avance 300 or a Bruker AC-300. Ultraviolet visible (UV-Vis) absorption measurements were taken on a ThermoSpectronic Helios γ spectrophotometer. Infrared measurements were taken with a Fourier Transform (FT-IR) ThermoNicolet model IR 200 Spectrometer in transmission method with KBr. Mass spectra were obtained from a Bruker Reflex III matrix-assisted laser desorption/ionization time of flight (MALDI-TOF) spectrometer using dithranol as a matrix. Elemental analyses were performed on a Thermo Finnigan Flash 1112 CHN elemental analyzator.

Synthesis of 1,6,7,12-Tetrakis-[4'(1'',1'',3'',3''-tetramethylbutyl)phenoxy] perylene-3,4:9,10-tetracarboxylic dianhydride (**3**): A suspension of 2 g (1.4 mmol) of N-N´-dioctylperylenebisimide **2**, 300 mL of 2-propanol, 30 mL of water and 60 g of KOH was refluxed with vigorous stirring under argon for 36 h. During the course of the reaction the color changed from red of the diimide to bright green of the tetracarboxylate anion. After being cooled to 0 ºC, the saponification was interrupted by adding 600 mL of 2 N HCl. The obtained brown precipitate was filtered off and repeatedly washed with water, treated with 300 mL of glacial acetic acid and 300 mL

of 2 N HCl, and stirred 24 h at room temperature. The red precipitate was filtered off and repeatedly washed with water. Purification by chromatography (SiO_2, CH_2Cl_2 / petroleum ether 8:2) gave 1.27 g (75%) of **3** as a red powder. Mp (ºC): 250; $\lambda_{max}(CHCl_3)$/nm (log ε): 293 (4.40), 452 (4.18), 543 (4.30), 585 (4.51); υ_{max}(KBr)/cm^{-1}: 2956, 2903, 1774 (C=O anhydride), 1745 (C=O anhydride), 1590, 1503, 1395, 1365, 1338, 1289, 1215, 1172, 1102, 1015, 995; δ_H(300 MHz; $CDCl_3$; Me_4Si): 8.10 (s, 4H, H-2.4,8,11), 7.32 (d, *J* = 8.6 Hz, 8H, Ph-H-3), 6.88 (d, *J* = 8.6 Hz, 8H, Ph-H-2), 1.74 (s, 8H, -CH2-), 1.38 (s, 24H, -CH3), 0.78 (s, 36H, *tert*-butyl); δ_C(75 MHz; $CDCl_3$; Me_4Si): 159.75, 156.77, 151.94, 147.49, 133.27, 128.02, 121.17, 120.81, 120.72, 119.77, 118.61, 57.11, 38.42, 32.43, 31.84, 31.51; MS: MALDI-TOF (Dithranol): m/z: 1209 $[M]^+$, 1210 $[M+1]^+$; $C_{80}H_{88}O_{10}$: Calcd: C, 79.44; H, 7.33. Found: C, 79.35; H, 7.42.

***N*-(2'-Ethylhexyl)-1,6,7,12-tetrakis-[4'(1'',1'',3'',3''-tetramethylbutyl)phenoxy]perylene-3,4-dicarboxyanhydride-9,10-dicarboximide** (**PI1**): 1 g (0.83 mmol) of dianhydride **3** and 660 mg (9.7 mmol) of imidazole were refluxed in 250 mL of chloroform for 0.5 h. Then, 110 mg (0.83 mmol) of 2-ethylhexylamine in 10 mL of $CHCl_3$ were added, followed by 5 drops of trifluoroacetic acid, and the mixture was refluxed for 3 days. After cooling to room temperature, the reaction mixture was poured into 100 mL of acetic acid, stirred for 0.5 h and washed 3 times with water, and dried with anhydrous K_2CO_3. Purification by chromatography (SiO_2, CH_2Cl_2 / petroleum ether 8:2) gave 515 mg (50%) of **PI1** as a red powder. Mp (ºC): 300; $\lambda_{max}(CHCl_3)$/nm (log ε): 268 (4.09), 450 (4.30), 543 (4.47), 584 (4.67); υ_{max}(KBr)/cm^{-1}: 2956, 1774 (C=O anhydride), 1744 (C=O anhydride), 1703 (C=O imide), 1665 (C=O imide), 1590, 1503, 1408, 1365, 1339, 1289, 1215, 1173, 1099, 1014, 977; δ_H(500 MHz; $CDCl_3$; Me_4Si): 8.17 (s, 2H, H-2,5), 8.07 (s, 2H, H-8,11), 7.29 (d, *J* = 8.8 Hz, 8H, Ph-H-3), 6.89 (d, *J* = 8,8 Hz, 4H, Ph-H-2), 6.83 (d, *J* = 8,8 Hz, 4H, Ph-H-2´), 4.03 (m, 2H, -CH2-N), 1.85 (m, 1H, -CH-), 1.74 (s, 4H, -CH2-), 1.73 (s, 4H, -CH2-), 1.37 (s, 24H, -CH3), 1.34-1.23 (m, 8H, -CH2-), 0.88 (t, 3J = 7.1 Hz, 3H, -CH3), 0.85 (t, *J* = 7.1 Hz, 3H, -CH3), 0.79 (s, 18H, *tert*-butyl), 0.77 (s, 18H, *tert*-butyl); δ_C(75 MHz; $CDCl_3$; Me_4Si): 163.62, 159.97, 156.80, 156.22, 152.30, 152.19, 147.17, 146.99, 133.13, 132.83, 127.91, 127.79, 123.10, 121.56, 121.39, 120.85, 119.78, 119.64, 119.32, 119.22, 119.09, 117.94, 57.14, 57.06, 44.37, 38.39, 37.99, 32.44, 31.89, 31.83, 31.52, 30.73, 30.19, 29.69, 28.70, 24.05, 23.03, 14.09, 10.62; MS: MALDI-TOF (Dithranol) m/z 1320 $[M]^+$, 1321 $[M+1]^+$; $C_{88}H_{105}NO_9$: Calcd: C, 80.02; H, 8.01; N, 1.06. Found: C, 79.77; H, 8.25; N, 1.08.

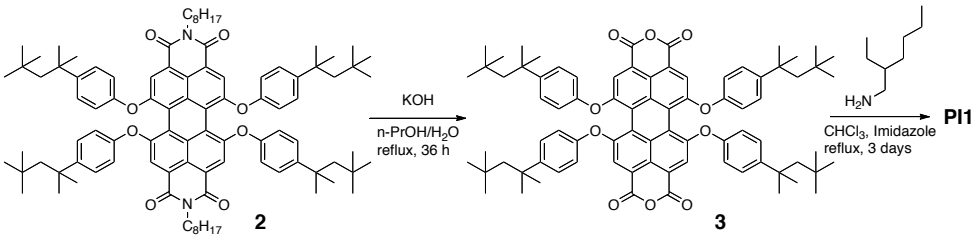

Scheme 1 Synthesis of perylene monoimide **PI1**.

UV-Visible and fluorescence emission spectroscopy

The UV-Visible spectrum was recorded using a Shimadzu double beam UV-1700 spectrophotometer. When the absorption spectrum was recorded for **PI-1** sensitized films, the same film without dye was used to measure the instrument blank and ensure, doing so, that the light scattering effects are minimized. For the steady-state fluorescence emission spectra an Aminco-Bowman Series 2 fluorimeter with the adequate support for liquid and solid samples was used.

Time correlated single photon counting (TCSPC)

Fluorescence emission lifetime for **PI-1**, either in solution or adsorbed onto mesoporous metal oxide films, were recorded with a LifeSpec picosecond fluorescence lifetime spectrophotometer from Edinburgh Instruments© equipped with lasers as excitation sources. The instrument response was always shorter than 350 ps measured at the full width at half maximum (FWHM). The decay lifetime was fitted using the software provided by Edinburgh Instruments©.

Laser Transient Absorption Spectroscopy (L-TAS)

The e^{-}_{TiO2}/Dye^{+} recombination measurements were carried out with a system consisting in a PTI nitrogen dye laser with tunable excitation wavelength. The sample is positioned between two monochromators and a 150W tungsten lamp is used as light probe. A Costronics© silicon detector connected to a Tektronic© oscilloscope TDS 2022 and to an electronic filter box is used to monitor the change in absorbance after the laser pulse excitation.

Electrochemical and device characterization

The electrochemical measurements were carried out using a CHI Instruments model 600B potentiostat-galvanostat. The samples were purged with nitrogen prior measurements.

The photoelectrochemical data was recorded using a ABET 150W xenon light source equipped with the correct filter to achieve the solar spectrum AM 1.5 G. The

light intensity was adjusted to 100 mW cm^{-2}, the equivalent of 1 sun, using a calibrated Si photodiode. The applied potential and cell current were registered with a Keithley model 2600 digital source meter. The current to voltage (I-V curve) was measured automatically with a home-built Labview software.

The charge extraction and photovoltage decay were carried out with a system set-up as previously reported by O'Regan *et al.*[26]

Device preparation

The TiO_2 paste (20 nm particle size) was screen-printed onto a fluorine doped tin oxide (FTO) coated glass substrate (Nippon sheet glass 10 Ω cm^{-2} resistance). The resulting thickness was 8 µm plus 4 µm of a light-scatter TiO_2 film composed by TiO_2 particles (size 300 nm). The device active area was 0.196 cm^2. Prior to the deposition of the TiO_2 paste the conducting glass substrates were immersed in a solution of $TiCl_4$ (40mM). The TiO_2 electrodes were gradually heated under airflow at 325 ºC for 5 minutes, 375 ºC for 5 minutes, 450 ºC for 15 minutes and 500 ºC for 15 minutes. The heated TiO_2 electrodes were soaked into $TiCl_4$ aqueous solution 40 mM at 70 ºC for 15 minutes and then washed with ethanol. The electrodes were heated again at 500 ºC for 30 minutes and cooled before dye adsorption. The platinized counter electrode was made applying a drop of 5 mM of H_2PtCl_6 in dry 2-propanol and spreading onto the conducting glass substrate (FTO). The coated glass was heated under airflow at 390 ºC for 15 minutes.

A solution (0.15 mM) of **PI-1** in cyclohexane was prepared and the film was immersed in the solution at room temperature at different times. The sensitized electrodes were assembled by sandwiching the working and the counter electrode using a thin thermoplastic (Surlyn) frame that melts at 100 ºC.

The liquid electrolyte was elaborated using 0.6 M of 1-buthyl-3-methylimidazolium iodide (BMII), 0.1 M of lithium iodide (LiI), 0.05M of iodide (I_2) and 0.1 mM of *tert*-butyl pyridine (TBP) in a mixture of acetonitrile and valeronitrile (85:15). This electrolyte is denoted as **AF25**. The cells were filled with the electrolyte through a hole previously made in the back of a platinized counter electrode. Then, the hole was sealed with a thermoplastic polymer and a cover slide glass. Finally, the electrodes were metallized with CERASOLZER© to increase the conductivity.

4.2.3. Results and Discussion

Synthesis

N-(2-Ethylhexyl)perylene carboximide carboxyanhydride **PI1** was synthesized and isolated for the first time following a standard synthesis procedure for the synthesis of monoimide monoanhydride perylene derivatives[27] (Scheme 1). Hydrolysis of the quite soluble diimide derivative *N,N'*-dioctylperylenebisimide **2** using KOH gave rise to the known tetracarboxylic anhydride **3**[28] in very good yield. Finally, alkylated monoimide **PI1** was obtained in 50% yield after treating the bisanhydride **3** with 2-ethylhexylamine.

UV-visible measurements

The **PI1** visible spectra in dichloromethane (DCM) and adsorbed onto TiO_2 (**PI1**/TiO_2) are illustrated in Fig. 2.

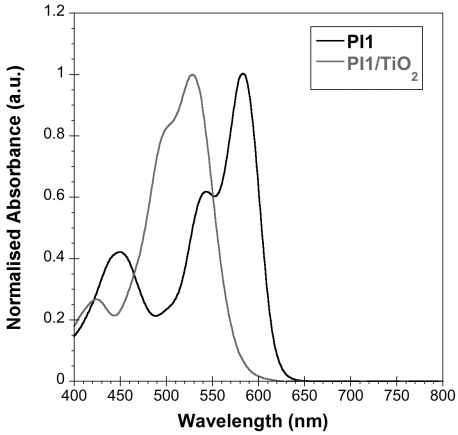

Fig. 2 UV-Visible spectra for **PI1** in DCM ($5 \cdot 10^{-5}$ M) and when adsorbed onto mesoporous 4 μm thick TiO_2 film.

As can be seen a hypsochromic shift occurs upon binding to the mesoporous TiO_2 film. The shift has been previously assigned to the ring opening of the perylene anhydride group to form two carboxylates, which act as functional anchoring groups to the film.[22]

The luminescence emission properties of **PI1** in solution were also measured (Fig. 3). Upon excitation at the maximum of the absorption band (λ_{ex} = 580 nm) a typical band corresponding to the fluorescence of the perylene can be observed (λ_{em} = 620 nm). The intersection of the excitation and emission spectra allowed us to estimate the 0 - 0 energy for **PI1**, which has been calculated to be close to 2 eV.

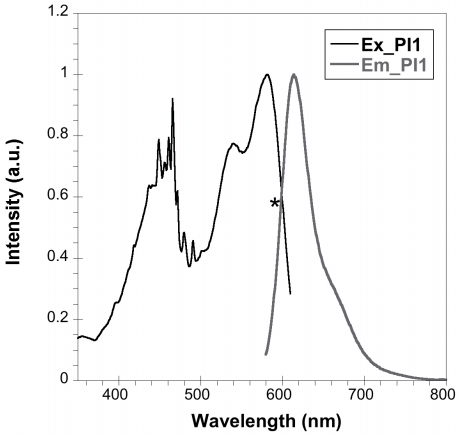

Fig. 3 Fluorescence emission and excitation spectra of **PI1** in DCM ($5 \cdot 10^{-5}$ M). The mark (*) shows the energy of the 0-0 transition.

Moreover, the fluorescence emission properties of **PI1** were studied when the dye was adsorbed on a mesoporous film of Al_2O_3 (**PI1**/Al_2O_3) and compared to those of a **PI1**/TiO_2 film (Fig. 4). As has already been shown,[29] the decrease of the fluorescence emission quantum yield of the sensitizer when anchored on TiO_2 can be related to efficient photo-induced electron transfer, upon light excitation, from the lowest unoccupied molecular orbital (LUMO) of the dye to the TiO_2 semiconductor conduction band (CB).

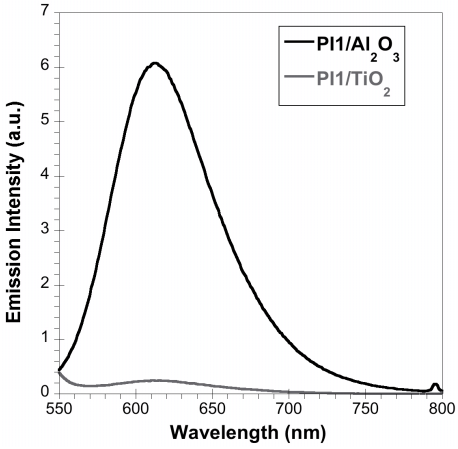

Fig. 4 Fluorescence emission of **PI1** when adsorbed onto 4 μm thick films of Al_2O_3 and TiO_2 measured under the same conditions. The excitation wavelength was λ_{ex} = 525 nm.

Furthermore, the fluorescence emission kinetics were also measured for both samples (Fig. 5). Interestingly, the emission lifetime of **PI1**/Al_2O_3 when excited at 405

nm is much shorter (τ = 3.35 ns) than that of **PI1** dissolved in DCM (τ = 7.7 ns), which could be due to the increase of the non-radiative pathway in the deactivation of the excited **PI1** when adsorbed onto a solid support. Yet, both emission decays can be fitted to a single monoexponential with a χ^2 of 0.96. In the case of the **PI1**/TiO_2, the emission decay is faster than in the Al_2O_3 analogue (1.5 ns) due to the efficient electron transfer from the dye to the TiO_2 conduction band. Furthermore, like in the emission steady-state experiment (Fig. 4), we can establish a comparison between **PI1**/Al_2O_3 and PI1/TiO_2 and estimate the photo-induced electron injection yield of **PI1** into the TiO_2 conduction band. For the Al_2O_3 sample the **PI1** sensitizer cannot inject electrons since the conduction band of the metal oxide is higher in energy than the LUMO of the molecule. Thus, the amplitude of the decay signal was considered as a blank, *i.e.* there is no electron injection whatsoever. On the other hand, for the TiO_2 sensitised film most of the electrons are injected and, therefore, the decay amplitude is drastically reduced (Fig. 5).

Keeping the acquisition time constant, it was estimated that the photo-induced electron injection into the TiO_2 occurs almost in unit yield and, therefore, more than 90% of the electrons are injected faster than our instrument response (350 ps).

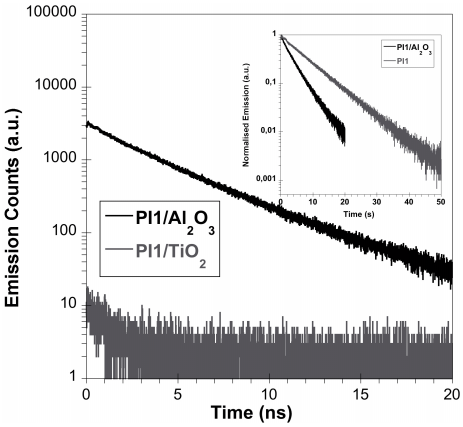

Fig. 5 Emission decay dynamics for the sensitized 4 μm thick films monitored at λ_{em} = 620 nm under the same conditions (acquisition time: 30 minutes). The inset shows the comparison between the dye in DCM solution ($5 \cdot 10^{-5}$ M) and adsorbed onto Al_2O_3 monitored at λ_{em}=620 nm.

Once the luminescence properties of **PI1** were established, we focussed on the electron recombination dynamics. These recombination dynamics are assigned to the regeneration of the ground state of the **PI1** cation by the photo-injected electrons into the TiO_2 (e^--TiO_2/dye^+).[30]

Two approaches were examined with 3 different TiO_2 films sensitised at different times. The maximum absorbance for the 3 samples was 0.30 (15 minutes), 0.50 (4 hours) and 0.75 (14 hours) measured at λ_{abs} = 535 nm. First, we excited the samples with the same laser power intensity (60 mJ) at identical **PI1**/TiO_2 absorbance (Fig. 6).

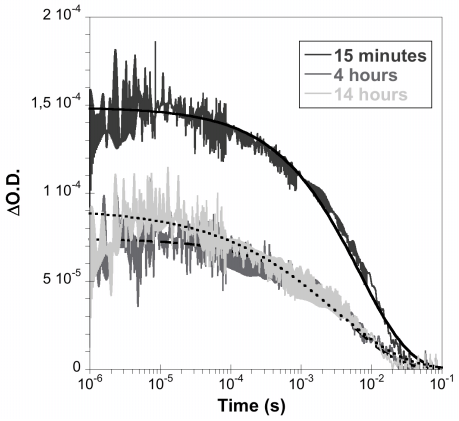

Fig. 6 Recombination decay dynamics for a 4 μm thick film with an optical density of 0.15 at 560 nm. The excitation wavelength was λ_{ex} = 560 nm and the probe wavelength was λ_{pr} = 830 nm. The fits correspond to the stretched exponential equation.

As can be seen in Fig. 6, the film sensitised for 15 minutes shows the highest signal amplitude, as well as the slowest decay dynamics, while the films sensitised for 4 and 14 hours show almost the same decay dynamics. All decays can be fitted to a stretched exponential $f(t) = A \cdot \exp[-(t/\tau)^{\alpha}]$ and the most relevant parameters from this fitting are listed in Table 1.

Table 1 Parameters obtained as a result of the fitting to a stretched exponential function of the decays illustrated in Fig. 6.

Sensitization time	Signal Amplitude (ΔO.D.)	τ / s	α
15 minutes	$1.5 \cdot 10^{-4}$	0.0068	0.61
4 hours	$7.4 \cdot 10^{-5}$	0.0046	0.60
14 hours	$9.1 \cdot 10^{-5}$	0.0030	0.43

In all cases, the excited spectra of **PI1**/TiO_2 show a maximum at 830 nm, which was assigned to the spectrum of the **PI1** cation (Fig. 7).

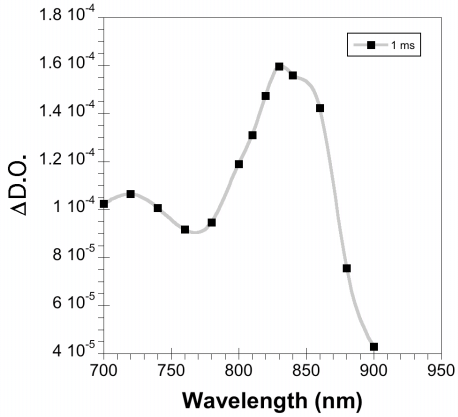

Fig. 7 Excited spectrum of a 4 μm thick film sensitized with **PI1**. The film absorbance was 0.3 a.u. at λ_{abs} = 535 nm. The excitation wavelength was 535 nm.

Secondly, we excited the samples at the maximum of the absorbance. As illustrated in Fig. 8, the decay kinetics are less monoexponential (α = 0.5 for the samples sensitised for 15 minutes and 4 hours and α = 0.3 for the sample sensitised for 14 hours). Moreover, for the sample sensitised for 14 hours the recombination life-time is much shorter (1 ms). Thus, apparently, longer sensitisation times, and therefore more dye adsorbed onto the nanocrystalline TiO_2 particles, accelerate the e^-_{TiO2}/**PI1**$^+$ recombination reaction.

Taking into account these results, we carried out the preparation of **PI1** devices controlling the sensitisation time with the aim to find out whether there is a relationship between the device efficiency and the charge transfer processes observed in Fig. 6 and 8. The measured device characteristics are listed in Table 2.

Table 2 **PI1** device[a] parameters at 100 mW/cm^2

Sensitisation time	Photocurrent / mA cm^{-2}	Voltage / V	Fill Factor	Efficiency / %
1 hour	4.08	0.50	71.47	1.46
4 hours	8.80	0.52	63.10	2.89
5 hours	9.20	0.52	62.87	3.15
14 hours	8.62	0.52	62.20	2.79

[a] The cell area was 0.196 cm^2 with a cell thickness of 8 + 4 μm and the efficiency was measured using a mask of 0.2 cm^2. The electrolyte composition was: 0.6 M BMII, 0.05 M I_2, 0.1 M LiI and 0.1 M TBP in 85:15 (v/v) valeronitrile/acetonitrile.

UNIVERSITAT ROVIRA I VIRGILI
DESIGN AND SYNTHESIS OF ORGANIC SENSITIZERS FOR DYE SOLAR CELLS: MOLECULAR STRUCTURE VS DEVICE PERFORMANCE
Miquel Angels Planells Dillundé
ISBN:978-84-693-8861-7/DL:T.1946-2010

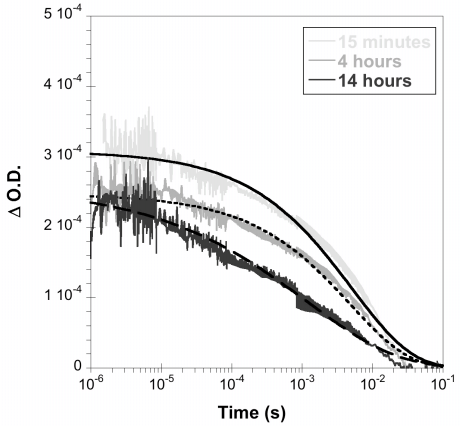

Fig. 8 Recombination decay dynamics for the 3 different 4 μm thick sensitized TiO_2 films. The excitation wavelength was λ_{ex} = 535 nm and the probe wavelength was λ_{probe} = 830 nm. The fits correspond to the stretched exponential equation.

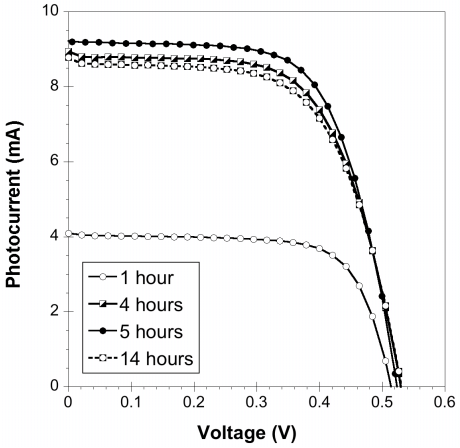

Fig. 9 IV curves for 4 different devices with an area of 0.196 cm^2 when illuminated at 100 mW/cm^2.

The highest efficiency was obtained after five hours of sensitisation. Fig. 9 shows the photocurrent vs. voltage curves under simulated 1.5 AM Global sun spectra at 100 mW/cm^2 for all devices. As can be observed, after 5 hours a decrease in efficiency occurs. The lower efficiency is due mainly to the decrease in photocurrent, which is in good agreement with the smaller amplitude on the decay kinetics in Fig. 8. However, the film sensitised for 1 hour showed less photocurrent while on the TAS experiments the film sensitised for less time achieved higher electron injection yield and slow electron recombination kinetics (e^-_{TiO2}/Dye^+). This experimental evidence can be explained if we take into account that the presence of a smaller amount of dye covering the surface of TiO_2 in the device could enhance the recombination

between the photo-injected electrons at the TiO_2 and the oxidised electrolyte (e^--TiO_2/electrolyte$^+$) due to the presence of uncovered TiO_2 surface. In fact, the measured V_{oc} decays confirm that the e^--TiO_2/electrolyte$^+$ recombination reactions are faster for the device with the film sensitised for 1 hour (Fig. 10).

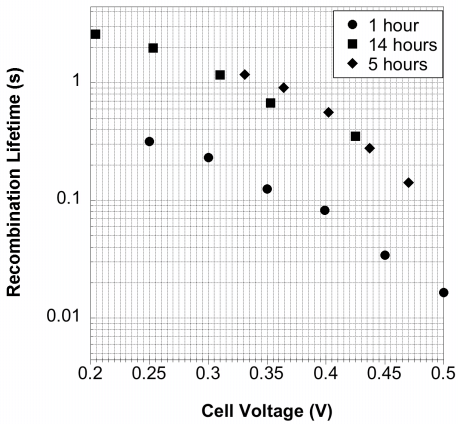

Fig. 10 Recombination lifetime for the devices sensitized during different time.

4.2.4. Conclusions

In conclusion, we have demonstrated that the perylene imide-sensitised TiO_2 films show different e^--TiO_2/Dye$^+$ recombination dynamics depending on the dye loading. These differences have been observed when exciting either at the same absorption or at the maximum absorption wavelength of each sample. When we observed the efficiencies for each sensitised film, we already can foresee that, in this case, the presence of a higher concentration of dye on the nanocrystalline TiO_2 particles surface does not affect the cell voltage. However, the generated photocurrent decreases after 5 hours of sensitization in good agreement with the decay kinetics measured in Fig. 6 and 8. Moreover, the film sensitised for 1 hour shows less photocurrent and also less voltage and we have demonstrated that, in this case, the recombination between the photo-injected electrons and the oxidised electrolyte is playing a role in reducing the overall device efficiency. Thus, we can state that the presence of a high concentration of this perylene on the surface of the TiO_2 nanoparticles neither quenches the electron injection dramatically nor reduces the cell voltage, in contrast with what has been usually observed in the case of other organic dyes.[31-33]

We would like to remark that the efficiency observed for the film sensitised for 5 hours is a high value among perylene imide-sensitised dye solar cells in the line of similar work reported previously by other groups. [16-19, 21, 22, 34]

4.2.5. Acknowledgements

The authors thank the Spanish Ministerio de Ciencia e Innovación for the CONSOLIDER-HOPE 0007-2007 project. MP, AF and EP also thank the Ministerio for the CTQ2007-60746/BQU project and the PhD fellowship. ASS and FF are grateful for financial support through grants MAT2005-07369-C03-02 and CTQ2007-67888/BQU. F.J.C.-G. thanks the MEC for a FPU fellowship.

4.3. *Paper IV*: Supramolecular Interaction in Dye Sensitised Solar Cells

Miquel Planells,[a] F. Javier Céspedes-Guirao,[b] Luis Gonçalves,[c] Ángela Sastre-Santos,[b,*] Fernando Fernández-Lázaro,[b,*] and Emilio Palomares[a,*]

[a] Institute of Chemical Research of Catalonia (ICIQ), Avda. Països Catalans,16, Tarragona, Spain. Fax: 34 977 920 224; Tel: 34 977 920 241;Corresponding Author E-mail: epalomares@iciq.es

[b] División de Química Orgánica. Instituto de Bioingenieria, Universidad Miguel Hernández. Edificio Vinalopó, Avda. Universidad s/n. Elche, Spain.

[c] LEPAE-Departamento de Engenharia Quimica, Facultade de Engenharia, Universidade do Porto. R. Dr. Roberto Frias, Porto, Portugal.

Abstract: A new Li^+-coordinating perylene monoimide dye has been synthesised. The dye was used as a sensitiser in dye-sensitised solar cells (DSCs), and the effect of Li^+ coordination on the device performance was analyzed using various spectroscopic techniques.

4.3.1. Introduction

Dye-sensitised solar cells (DSCs) based on nanocrystalline semiconductors have been the subject of intense investigation due to their potential low cost, easy processing and high performance, with light-to-energy conversion efficiencies reaching 11.3%.[35] To date, devices made using ruthenium polypyridyl complexes have had a predominant role. However, in recent years, there has been much effort in replacing the ruthenium complexes with organic metal-free sensitisers due to economic and practical reasons, such as lower device production cost and the possibility of obtaining thinner devices with improved voltage.[7, 10] We, with other research groups, have focussed on perylene imides as good sensitisers for DSCs due to their outstanding chemical, thermal and photophysical stabilities. Moreover, several groups, including our own, have reported DSCs with light-to-energy conversion efficiencies ranging from 4 to 6% under standard conditions (100 mW/cm^2 1.5 AM G solar spectrum).[21, 36] The reason that such cell efficiencies have been obtained is that these perylene imides have been rationally designed to achieve not only a low degree of molecular aggregation at the semiconductor surface, but also

directionality of the excited state to improve the injection of electrons into the TiO_2 conduction band.

Here, we aim to move one step further and present a new perylene imide sensitiser, which contains a complexing unit capable of binding selectively lithium ions (Fig. 1). The interest arises from the high affinity of 12-crown-4 ether towards Li^+ ions.[37-39] Previous studies have revealed that lithium ions can intercalate or get strongly adsorbed onto the TiO_2 surface, inducing a shift of the semiconductor conduction band.[40-42] The nanoscopic effect of Li^+ at the nanoparticle surface has a macroscopic consequence, which is the improvement of the DSC current. However, the shift at the TiO_2 conduction band edge also induces a loss in voltage. Thus, the device efficiency, which is determined by eqn (1), is barely affected despite the increase in current.

$$\eta = J_{sc} \cdot V_{oc} \cdot FF \qquad (1)$$

Based on preliminary studies by Haque *et al.*[43] and later by Schmidt-Mende and co-workers,[44] it seems that the supramolecular control of the lithium ions contained either in the liquid or the solid electrolyte is the key to device improvement. However, in the former case the ion-coordinating moieties were situated in the hole-transporting organic material utilized as electrolyte, while in the latter case they were placed at the bipyridine ligand of the ruthenium sensitiser. However, in both cases they used polyethylene glycol chains as the lithium ion coordinating ligand, which may have much lower binding affinity for lithium ions than the macrocyclic crown ether.[3, 45]

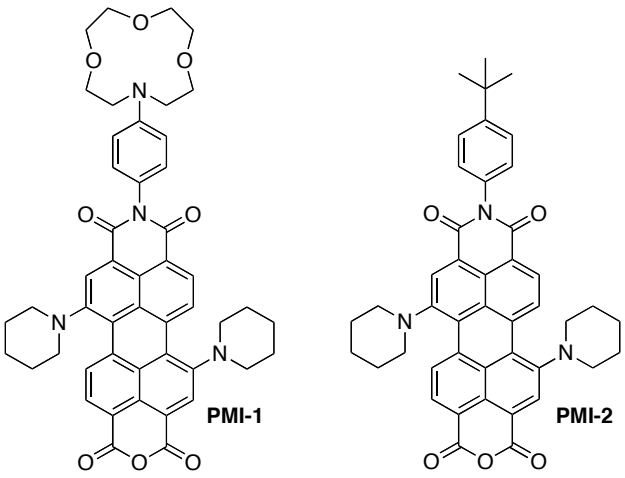

Fig. 1 Molecular structures of perylene imide dyes.

Hence, it will be of particular interest to study how this affects the supramolecular interaction in the performance of the DSCs. Fig. 1 illustrates the molecular structure for both perylene imide sensitisers used in this work.

4.3.2. Results and Discussion

Synthesis

Perylenediimides are aromatic, planar compounds that display a strong tendency to aggregate in solution. In addition, unsubstituted perylenes are insoluble in organic solvents, and so functionalization is a necessity. 1,7-dipiperidinylperylenes were selected, since two piperidines are expected to ensure high solubility, reduce aggregation in solution, and provide electron-donating features. Some groups[21, 46, 47] have reported strongly electron-donating perylenetetracarboxylic acid derivatives with amine substituents at their perylene core (*bay*-positions). This strategy opens the possibility to change the poor electron-donating ability of the perylene imides, which makes the efficient injection of electrons from the excited perylene imide to the conduction band (CB) of the TiO_2 electrode difficult.[21] The saponification of the perylene diimide **3**[48, 49] in *i*-PrOH/H_2O with excess KOH (Scheme 1) afforded 1,7-dipiperidinylperylene dianhydride **4**[50] in 92% yield. Alkylated monoanhydride monoimides **PMI-1** and **PMI-2** were then obtained by treating the dianhydride **4** with *N'*-(4-aminophenyl)aza-12-crown-4 (**5**) and 4-*tert*-butylaniline respectively.

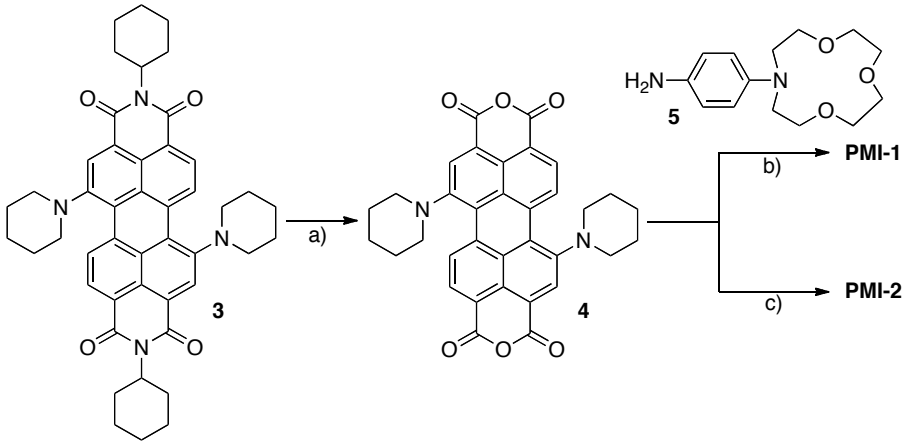

Scheme 1 Synthetic route to perylene **PMI-1** and **PMI-2**: (a) KOH, *i*-PrOH/H_2O (15:1), reflux. 3 h, 92%; (b) *N'*-(4-aminophenyl)aza-12-crown-4 (**5**), imidazole, $CHCl_3$, TFA, 3d, reflux, 55%; (c) 4-*tert*-butylaniline, imidazole, $CHCl_3$, TFA, 4 days, reflux, 30%.

UV-Visible measurements

The UV-visible spectra of **PMI-1** measured in acetonitrile (ACN) and adsorbed onto metal oxide films (either TiO_2 or Al_2O_3) are illustrated in Fig. 2.

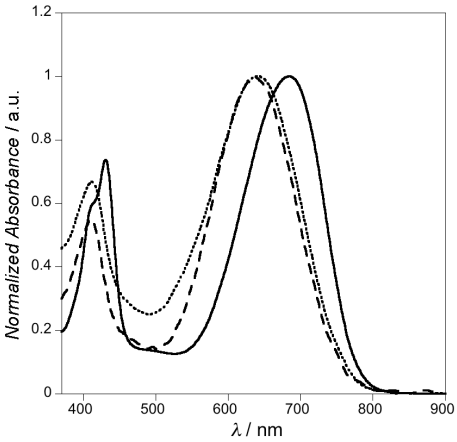

Fig. 2 Normalized UV-Visible spectra of **PMI-1** in ACN (solid line) and onto Al_2O_3 (dashed line) and TiO_2 (dotted line).

The maximum absorption band of **PMI-1** in solution (λ_{abs} = 680 nm) is hypsochromically shifted 40 nm when **PMI-1** is anchored to either Al_2O_3 or TiO_2 (λ_{abs} = 640 nm). This shift has been previously assigned to the ring opening of the anhydride group on perylene to form two carboxylates, providing anchor sites with the metal oxide surface.[22]

We used UV-visible spectroscopy to monitor whether the addition of lithium ions to a solution of **PMI-1** produced a change in the ground-state spectrum of the latter. As expected, the presence of lithium ions did not induced changes in the UV-visible spectrum of **PMI-1** and, hence, the formation of a charge transfer complex in the ground state can be discarded. This result is a consequence of the fact that both the HOMO and LUMO orbitals of the perylenebisimides exhibit nodes at the imide nitrogens.[51]

In fact, in terms of film adsorption and UV-Visible absorption properties, both **PMI-1** and **PMI-2** show identical features. Thus, in order to prove the interaction of lithium ions with the coordinating moiety in **PMI-1** we carried out ^{1}H-NMR experiments and mass spectrometry analysis as detailed below.

^{1}H-NMR complexation and mass spectrometry studies

To demonstrate the complexation of lithium salt into the aza-12-crown-4 of **PMI-1** we performed various ^{1}H-NMR experiments with different mixtures of solvents, and

different lithium salts. Firstly, we tried to use CD_3CN, but **PMI-1** was not soluble enough to reach 0.5 mM concentration. After that, we tried with CD_3COCD_3, but the **PMI-1**-lithium complex precipitated immediately after mixing solutions of **PMI-1** and lithium perchlorate. Finally, ^{1}H-NMR titration experiments were carried out either in $CDCl_3/CD_3CN$ 1:2 or in $CDCl_3/CD_3COCD_3$ 4.5:1 at 25ºC in order to evaluate the coordination of **PMI-1** with lithium perchlorate and lithium triflouromethanesulfonate, respectively.

The addition of increasing amounts of lithium perchlorate to a solution of **PMI-1** resulted in a downfield shift of the protons H-4, H-3 and H-2, and a upfield shift of proton H-1 of the aza-crown moiety (Fig. 3). The addition of 8 equiv. of lithium perchlorate allowed the observation of four well-resolved triplets in the ^{1}H-NMR.

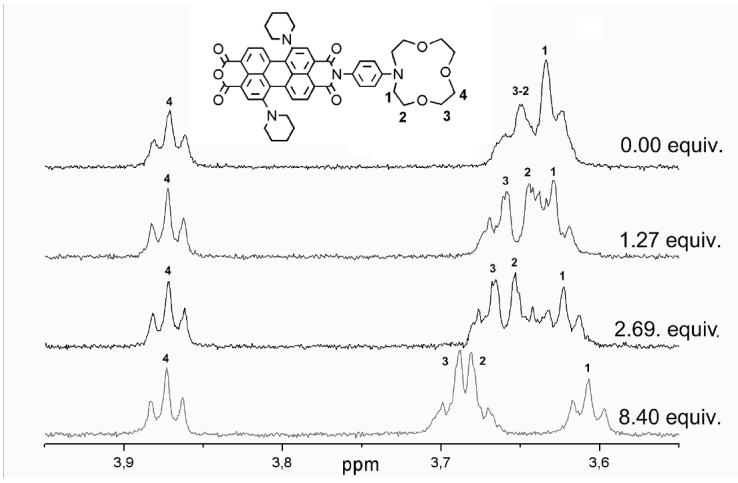

Fig. 3 Partial ^{1}H-NMR spectra ($CDCl_3/CD_3CN$ 1:2, 500 MHz, 25 ºC) showing the shift of the protons of the azacrown moiety upon the addition of lithium perchlorate to a solution of **PMI-1**.

The downfield shift of the H-3 proton in the aza-12-crown-4 moiety was used to evaluate the stoichiometry of the complex and to determine its binding constant (Fig. 4). The Job plot[52] obtained exhibited a maximum at a mole ratio of 0.5, consistent with a 1:1 interaction (Fig. 4, inset). The changes in the chemical shift of H-3 were plotted as a function of increasing concentration of lithium perchlorate, these data being subjected to a nonlinear least-squares curve-fitting analysis.[53] The binding constant for the 1:1 complex between **PMI-1** and lithium perchlorate was determined to be 215 ± 13 M^{-1}.

^{1}H NMR titration was also carried out using a more apolar mixture of deuterated solvents ($CDCl_3/CD_3COCD_3$ 4.5:1), and a different lithium salt (lithium trifluoromethanesulfonate), in order to study the effect of the solvent and the lithium

salt in the complexation. The measured binding constant was in the same order of magnitude as that already obtained.

Finally, solid complexes of **PMI-1**-lithium perchlorate were prepared by dissolving one part **PMI-1** and 10 parts lithium perchlorate in $CHCl_3/CH_3CN$ 1:2. The solvent was carefully removed by evaporation, and the residue was dried under low pressure, washed with CH_3CN, and finally dried. The formation of this complex was confirmed by electrospray ionization (ESI) mass spectrometry (m/z = 813 $[M]^+$). Also, high-resolution mass spectrometry (HRMS-ESI) confirmed the existence of the complex (found: 813.3447, calculated for $C_{48}H_{46}LiN_4O_8$: 813.3470).

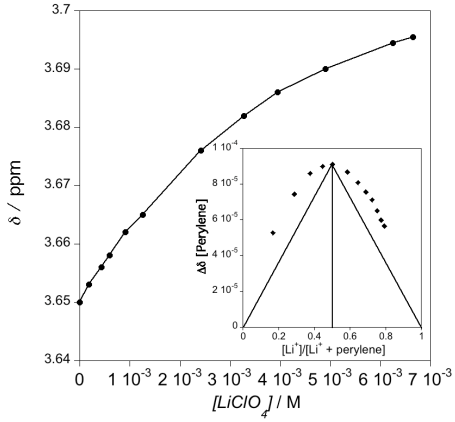

Fig. 4 ^1H NMR titration curve ($CDCl_3/CD_3CN$ 1:2) showing the changes in the chemical shift of the H-3 proton of the aza-12-crown-4 moiety of **PMI-1** upon addition of increasing amounts of $LiClO_4$ ([**PMI-1**] = 0.5 mM). Inset: ^1H NMR Job´s Plot of **PMI-1** *vs* $LiClO_4$ ([**PMI-1**] + [$LiClO_4$] ≈ 6.0 mM).

Characterization of the dye-sensitised solar cell

After demonstrating the interaction of the lithium ions with **PMI-1**, we focused our interest on the device performance of **PMI-1**, using **PMI-2** for comparison purposes. To this end, we prepared two identical devices using **PMI-1** and **PMI-2** as sensitisers. The cells were not optimized individually to obtain the highest efficiency, but rather to be as similar as possible, and for this reason we avoided the use of chemical agents to decrease the formation of aggregates, such as chenodeoxychenoic acid (CDCA). The film was immersed 4 hours in order to achieve an absorbance of 0.7 a.u. at λ_{abs} = 640 nm.

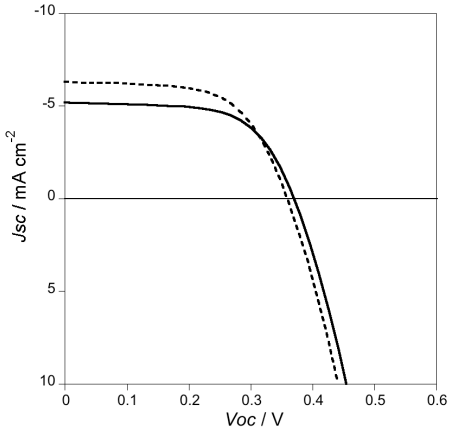

Fig. 5 Current *vs* Voltage (IV curve) of **PMI-1** (straight line) and **PMI-2** (dashed line) DSC device. The cell area was 0.196 cm^2 with 6 + 5 µm of TiO_2 and the electrolyte was **EMP2**.

Fig. 5 shows the device performance for **PMI-1** and **PMI-2**. We observed an increase of the V_{oc} and a decrease of photocurrent when we used the dye with azacrown ether. Hence, we decided to study the influence that the supramolecular interaction between the lithium ions and the perylene sensitiser had over the charge transfer processes that govern the cell efficiency and explain the origin of this behaviour.

Steady-state fluorescence emission and time-correlated single photon counting measurements

The luminescence emission properties of **PMI-1** were studied with the dye anchored on both Al_2O_3 and TiO_2 mesoporous films, the former being used as a control sample. The Al_2O_3 conduction band was above the LUMO of the dye, preventing the electron injection from the dye's excited state into the metal oxide conduction band,[54, 55] and thus the dye's fluorescence emission properties could be studied in solid thin films, avoiding the use of **PMI-1** in solution, which could lead to misleading results.

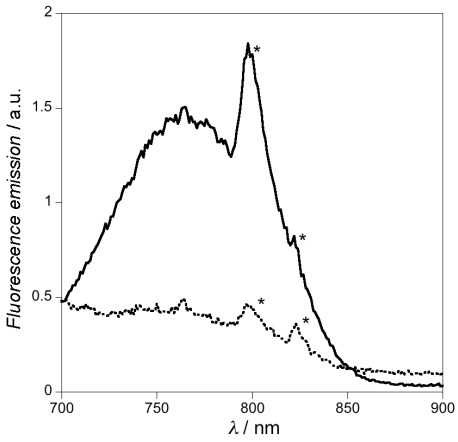

Fig. 6 Fluorescence emission of **PMI-1** exciting at λ_{ex} = 640 nm when it is anchored onto Al_2O_3 (solid line) and TiO_2 (dotted line). The asterisks denotes the optical artifacts due to our set-up system.

As illustrated in Fig. 6, we observed a decrease of the fluorescence emission quantum yield of the sensitiser when anchored onto TiO_2. This change in emission quantum yield is directly related with the efficient photo-injection of electrons, upon light excitation, from the dye's excited state into the TiO_2 conduction band (CB). We would like to point out that both **PMI-1** and **PMI-2** showed identical results.

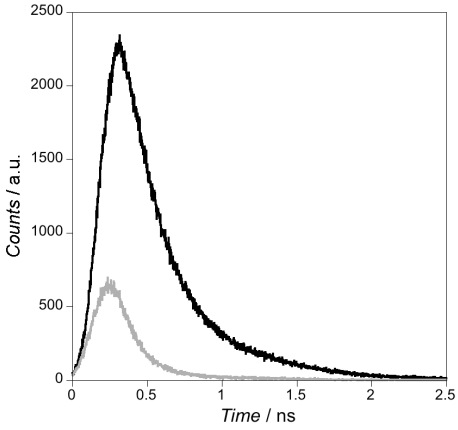

Fig. 7 Emission decay kinetics for **PMI-1** onto Al_2O_3 (black line) and TiO_2 (grey line). The excitation wavelength was 635 nm.

In the case of the fluorescence emission kinetics (Fig. 7), the experiments were carried out with the same measurement conditions (λ_{ex} = 635 nm, λ_{em} = 760 nm and a fixed acquisition time of 900 s). The lifetime for **PMI-1** onto Al_2O_3 was estimated, from the deconvolution fitting equation using the laser instrument response, to be τ_1

= 350 ps. However, the lifetime for the sensitised TiO_2 sample was difficult to differentiate from the laser instrument response, and no fitting could be obtained. The result for the **PMI-1**/TiO_2 sample suggests that for these perylene dyes the photo-induced electron injection occurs faster than in the case of the standard ruthenium polypyridyl complexes used in DSCs. Thus, and according to the results illustrated below, we can assume that the yield for electron injection in **PMI-1**/TiO_2 films is higher than 80%.

Laser transient absorbance spectroscopy

Once the electron injection was studied, we focussed on the electron recombination dynamics in the presence or absence of a redox active electrolyte (I^-/I_3^-). There are several charge transfer reactions that can be studied in detail using this technique. As previously shown,[56] the back-electron transfer between the photo-injected electrons at the TiO_2 and the oxidised dyes is one of the most important reactions to be considered. Hence, adjusting the acquisition time below the recombination lifetime, we were able to record the spectrum of the dye cation, obtaining a maximum dye cation signal at 900 nm (Fig. 8, inset). The signal decay after the laser pulse (λ_{ex} = 620 nm), in the absence of electrolyte, was assigned to charge recombination dynamics of the dye cation with the electrons located at the traps/conduction band of the TiO_2. The decay for **PMI-1**/TiO_2 is depicted in Fig. 8.

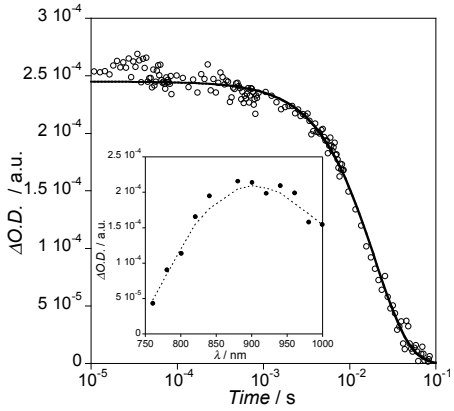

Fig. 8 Electron recombination dynamics for a 5 μm transparent TiO_2 film sensitized with **PMI-1**. The film optical absorbance was 0.6 a.u. at λ_{max} = 640 nm. The laser excitation wavelength was λ_{ex} = 620 nm and the probe wavelength was λ_{pr} = 900 nm. The inset illustrates the radical cation spectrum of **PMI-1**.

As shown before, the decay dynamics for electron recombination in sensitised TiO_2 mesoporous thin films can be fitted using an extension of the Kohlraush-

Williams-Watts (KWW) function (eqn (2)), giving a recombination time of τ = 19 ms with a correction factor β = 1, which implies that the decay dynamics for the back electron transfer in this system are monoexponential.

$$y(t) = A \cdot e^{-\left(t/\tau\right)^{\beta}} \qquad (2)$$

As illustrated in Fig. 9, in the presence of a redox-active electrolyte, the electron recombination becomes biphasic. Previous work[57] demonstrated that the second phase observed in the presence of I^-/I_3^- couple arises from slower formation of by-products as a result of regeneration of the dye's ground state by subsequent electron transfer from the redox-active electrolyte. The faster component of the transient is assigned to the perylene cation, which is quickly regenerated by the electrolyte, and therefore its lifetime was shorter than that in the absence of electrolyte (Fig. 8). This feature is necessary in order to achieve efficient devices. If the regeneration process is not fast enough, then the devices will show low photocurrent yields. The decays were measured with complete cells and the regeneration lifetime was 10 μs for both cells. This is in a good agreement with the result of ruthenium polypyridyl complexes.

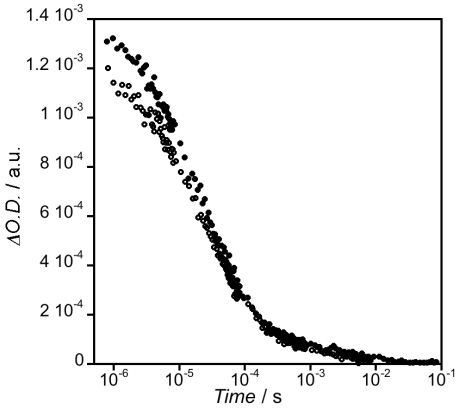

Fig. 9 Laser transient absorbance electron recombination decays measured in complete cells for **PMI-1** (●) and **PMI-2** (○).

Transient photovoltage measurements

Recently, several authors have employed transient photovoltage measurements, also known as V_{oc} decays, to evaluate the electron recombination dynamics between the photo-injected electrons at the TiO_2 and the oxidized electrolyte.[24, 26, 58-62] In order to measure these recombination dynamics, which occur on the millisecond timescale, it is very important to know the accumulated charge in the semiconductor (charge density), since the V_{oc} decays are strongly dependent of this.

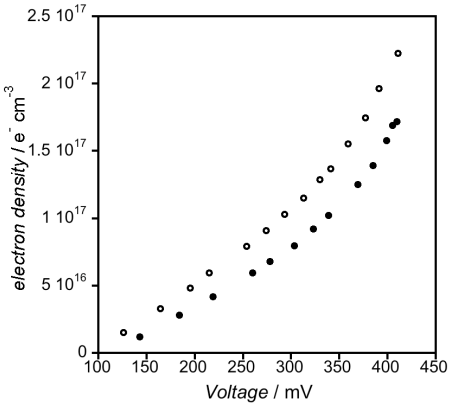

Fig. 10 Charge extraction of **PMI-1** (•) and **PMI-2** (○).

As can be seen in Fig. 10, the experimental data showed a shift of the charge density, which indicates that the CB edge is positioned higher in energy for **PMI-1** than for **PMI-2**. This shift can be assigned to the complexation of Li^+ with the azacrown ether, which may induce the formation of a dipole at the nanoparticle surface.[63, 64] The Li^+ cations cannot be intercalated to the TiO_2 nanoparticles because they are captured in the crown ether of **PMI-1**.

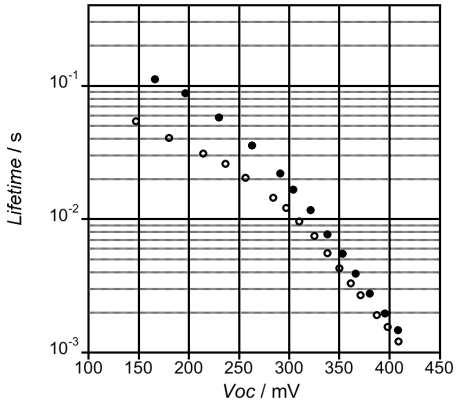

Fig. 11 Recombination decay dynamics for the 6 + 5 µm sensitised TiO_2 cells of **PMI-1** (•) and **PMI-2** (○).

As we can see in Fig. 11, **PMI-1** had a longer electron-electrolyte recombination lifetime than **PMI-2**. This experiment confirms that the presence of Li^+ coordinated to the crown ether shifts the TiO_2 conduction band edge, and, moreover, it slows the recombination dynamics between the photo-injected electrons and the oxidized electrolyte.

4.3.3. Conclusions

In summary, we have designed and synthesised a new perylene dye bearing a moiety capable of binding lithium ions. The sensitiser has affinity for Li^+ ions, the constant for which was calculated from ^{1}H-NMR experiments. Devices made using **PMI-1** gave higher voltages but a lower photocurrent under simulated sunlight. We believe that the increase in voltage is due to a shift in the TiO_2 conduction band edge, as we have illustrated in this paper.

The supramolecular interactions between the additives used in DSCs and the dyes are of utmost importance to understand the changes in the charge-transfer kinetics observed in functional devices. Control of these charge-transfer kinetics in organic sensitisers DSCs will be the key to reaching the same efficiencies as the devices made using ruthenium polypyridyl dyes.

4.3.4. Experimental

Synthesis

All reagents were purchased from commercial suppliers and used without further purification unless otherwise noted. Commercial TLC plates (silica gel 60 F254, SDS) were used to monitor the progress of the reaction, with spots observed under UV light at 254 and 365 nm. Column chromatography was performed with silica gel 60A (particle size 40 - 63 mm, SDS). NMR spectra were taken using a 500 MHz Bruker Avance 500 or a 300 MHz Bruker AC-300. Ultraviolet visible (UV-Vis) absorption measurements were taken on a ThermoSpectronic Helios g spectrophotometer. Infrared measurements were taken with a Fourier Transform (FT-IR) ThermoNicolet model IR 200 Spectrometer in attenuated total reflection (ATR) with a germanium window or in transmission method with KBr. Mass spectra were obtained from a Bruker Reflex III matrix-assisted laser desorption/ionization time of flight (MALDI-TOF) spectrometer using dithranol as a matrix. Mass spectra of **PMI-1**-lithium complex were obtained from a hybrid analyzer QTOF, model QSTAR-Applied Biosystems (ESI). Elemental analyses were performed on a LECO CHNS-932 elemental analyzator.

1,7-dipiperidinylperylene-3,4:9,10-tetracarboxilic dianhydride (**4**): A suspension of 2.1 g (2.91 mmol) of N-N´-dicyclohexyl-1,7-dipiperidinylperylene diimide **3**, 150 mL of 2-propanol, 10 mL of water and 20 g of KOH was vigorously stirred and refluxed under argon for 3 h. During the course of the reaction the color

changed from dark green of the diimide to bright red-purple of the tetracarboxylate anion. After being cooled to room temperature, the saponification was interrupted by adding 700 mL of glacial acetic acid. The obtained green precipitate was filtered off and repeatedly washed with water and methanol. The dark-green precipitate was dried. Purification by chromatography (SiO_2, CH_2Cl_2/acetone 10:0.25) gave 1.5 g (92%) of **4** as a dark green powder.

λ_{max} ($CHCl_3$)/nm (log ε): 289 (4.42), 435 (4.24), 705 (4.37); υ_{max} (KBr)/cm^{-1}: 2934, 1755 (C=O anhydride), 1727 (C=O anhydride), 1598, 1584, 1559, 1510, 1431, 1288, 1249, 1195, 1161, 1029. 1000; δ_H (300 MHz; $CDCl_3$; Me_4Si): 9.50 (d, *J* = 8.3 Hz, 2H, perylene), 8.47 (s, 2H, perylene), 8.42 (d, *J* = 8.3 Hz, 2H, perylene), 3.50 (m, 4H, piperidinyl), 3.00 (m, 4H, piperidinyl), 1.96-1.70 (m, 12H, piperidinyl); δ_C (75 MHz; $CDCl_3$; Me_4Si): 160.62, 159.98, 151.18, 136.75, 130.79, 130.23, 126.74, 125.99, 123.58, 123.28, 123.24, 117.15, 52.92, 25.60, 23.61; MS: MALDI-TOF (Dithranol) m/z: 558 ($[M]^+$), 559 ($[M+1]^+$) Calcd for $C_{34}H_{26}N_2O_6 \cdot 1/2H_20$: C, 71.82; H, 4.79; N, 4.93. Found: C, 72.10; H, 4.72; N, 5.12.

***N*-[4-(aza-12-crown-4-N´-yl)phenyl]-1,7-dipiperidinylperylene-3,4-dicarboxyanhydride-9,10-dicarboximide** (**PMI-1**): 200 mg (0.36 mmol) of dianhydride **4** and 290 mg (4.26 mmol) of imidazole were refluxed in 120 mL of chloroform for 0.5 h. Then, 100 mg (0.36 mmol) of *N*-(4-aminophenyl)aza-12-crown-4 **5** in 10 mL of $CHCl_3$ were added, followed by 300 µL of trifluoroacetic acid, and refluxed for 3 days. After cooling to room temperature, the reaction mixture was poured into 50 mL of acetic acid, stirred for 0.5 h and washed 3 times with water, and dried with anhydrous K_2CO_3. Purification by chromatography (SiO_2, CH_2Cl_2/acetone 20:3) gave 159 mg (55%) of **PMI-1** as a green powder.

λ_{max} ($CHCl_3$)/nm (log ε): 267 (4.62), 435 (4.24), 698 (4.37); υ_{max} (KBr)/cm^{-1}: 2929, 1764 (C=O anhydride), 1730 (C=O anhydride), 1702 (C=O imide), 1664 (C=O imide), 1595, 1583, 1559, 1517, 1405, 1350, 1314, 1278, 1249, 1196, 1134, 1024, 1002; δ_H (300 MHz; $CDCl_3$; Me_4Si): 9.65 (d, *J* = 8.3 Hz, 1H, perylene), 9.54 (d, *J* = 8.3 Hz, 1H, perylene), 8.54 (s, 1H, perylene), 8.47 (d, *J* = 8.3 Hz, 1H, perylene), 8.45 (s, 1H, perylene), 8.42 (d, *J* = 8.3 Hz, 1H, perylene), 7.13 (d, *J* = 9 Hz, 2H, Ph-H-3), 6.87 (d, *J* = 9 Hz, 2H, Ph-H-2), 3.91 (t, *J* = 9.8 Hz, 4H, methylene), 3.73-3.59 (m, 12H, methylene), 3.51 (m, 4H, piperidinyl), 2.97 (m, 4H, piperidinyl), 1.95-1.68 (m, 12H, piperidinyl); δ_C (75 MHz; $CDCl_3$; Me_4Si): 164.16, 163.97, 160.75, 160.18, 151.40, 150.62, 148.65, 137.25, 135.11, 130.52, 130.30, 130.29, 128.82, 128.34, 126.80, 125.63, 124.64, 124.55, 124.35, 123.60, 123.46, 123.37, 122.89, 121.99, 121.96, 118.03, 116.25, 112.61, 71.60, 69.90, 69.61, 52.92, 52.76, 52.72, 25.66, 25.59,

23.70, 23.65; MS: MALDI-TOF (Dithranol) m/z 807 ([M]+); Calcd for $C_{48}H_{26}N_4O_8 \cdot 1/2H_20$: C, 70.57; H, 5.80; N, 6.86. Found: C, 70.52; H, 6.10; N, 6.61.

***N*-(4-*tert*-butylphenyl)-1,7-dipiperidinylperylene-3,4-dicarboxyanhydride-9,10-dicarboximide** (**PMI-2**): 100 mg (0.18 mmol) of dianhydride **4** and 145 mg (2.13 mmol) of imidazole were refluxed in 60 mL of chloroform for 0.5 h. Then, 30 mg (0.18 mmol) of 4-*tert*-butylaniline in 10 mL of $CHCl_3$ were added, followed by 150 µL of trifluoroacetic acid, and refluxed for 4 days. After cooling to room temperature, the reaction mixture was poured into 25 mL of acetic acid, stirred for 1 h and washed 3 times with water, and dried with anhydrous K_2CO_3. Purification by chromatography (SiO_2, CH_2Cl_2) gave 37 mg (30%) of **PMI-2** as a green powder.

λ_{max} ($CHCl_3$)/nm (log ε): 281 (4.37), 435 (4.20), 683 (4.36); υ_{max} (KBr)/cm^{-1}: 2935, 1766 (C=O anhydride), 1731 (C=O anhydride), 1705 (C=O imide), 1668 (C=O imide), 1595, 1583, 1560, 1510, 1405, 1365, 1349, 1315, 1249, 1197, 1003; δ_H (300 MHz; $CDCl_3$; Me_4Si): 9.61 (d, *J* = 8.3 Hz, 1H, perylene), 9.52 (d, *J* = 8.3 Hz, 1H, perylene), 8.53 (s, 1H, perylene), 8.46 (d, *J* = 8.3 Hz, 1H, perylene), 8.43 (s, 1H, perylene), 8.40 (d, *J* = 8.3 Hz, 1H, perylene), 7.58 (d, *J* = 8.6 Hz, 2H, Ph-H-3), 7.26 (d, *J* = 9 Hz, 2H, Ph-H-2), 3.50 (m, 4H, piperidinyl), 2.97 (m, 4H, piperidinyl), 1.95-1.68 (m, 12H, piperidinyl), 1.4 (s, 9H, *tert*-butyl); δ_C (75 MHz; $CDCl_3$; Me_4Si): 163.89, 163.66, 160.77, 160.18, 151.51, 151.39, 150.73, 137.25, 135.36, 132.43, 130.62, 130.39, 130.33, 128.44, 127.88, 126.85, 126.43, 125.73, 124.66, 124.58, 124.39, 123.48, 123.38, 123.00, 122.21, 121.79, 118.17, 116.39, 52.93, 52.81, 34.79, 31.39, 25.67, 25.61, 23.71, 23.66; MS: MALDI-TOF (Dithranol) m/z 690 ([M]+); Calcd for $C_{44}H_{39}N_3O_5 \cdot 1/2H_20$: C, 75.52; H, 5.76; N, 6.00. Found: C, 75.34; H, 5.89; N, 5.88.

Characterization techniques

^{1}H-NMR Experiments. The Job Plot to determine the stoichiometry of the binding between **PMI-1** and lithium perchlorate was carried out using a continuous variation ^{1}H-NMR spectroscopic experiment. An initial volume of 500 µL of a 6 mM $CDCl_3$/CD_3CN 1:2 solution of **PMI-1** was placed in an ^{1}H-NMR tube. 100 µL aliquots of a 6 mM $CDCl_3$/CD_3COCD_3 4.5:1 solution of lithium perchlorate were subsequently added and a spectrum was recorded after each addition.

The NMR titrations of lithium salts with **PMI-1** were performed as follows:

With $CDCl_3$/CD_3CN as solvent: An initial volume of 500 µL of a 0.5 mM $CDCl_3$/CD_3CN 1:2 solution of **PMI-1** was placed in a ^{1}H-NMR tube. Aliquots of a $CDCl_3$/CD_3CN 1:2 solution containing lithium perchlorate (9 mM) and **PMI-1** (0.5 mM) were

subsequently added and a spectrum was recorded after each addition. **PMI-1** was added in order to avoid dilution effects.

With $CDCl_3/CD_3COCD_3$ as solvent: An initial volume of 500 µL of a 1 mM $CDCl_3/CD_3COCD_3$ 4.5:1 solution of **PMI-1** was placed in a ^{1}H-NMR tube. Aliquots of a $CDCl_3/CD_3COCD_3$ 4.5:1 solution containing lithium trifluoromethanesulfonate (12 mM) and **PMI-1** (1 mM) were subsequently added and a spectrum was recorded after each addition. **PMI-1** was added. in order to obviate the need to account for dilution effects during the titrations.

The data were analyzed using standard curve fitting methods[53] and the binding constants were evaluated by nonlinear least-squares regression analysis from the change in chemical shift of the H-3 protons of the aza-12-crown-4 moiety.

UV-Visible and fluorescence emission spectroscopy. The UV-Vis spectrum was recorded using a Shimadzu© double beam UV-1700 spectrophotometer. For the steady-state fluorescence emission spectra an Aminco-Bowman Series 2 fluorimeter with the adequate for liquid or solid support was used.

Time correlated single photon counting (TC-SPC). Fluorescence emission lifetimes, either in solution or in film, were recorded with LifeSpec picosecond fluorescence lifetime spectrophotometer form Edinburgh Instruments© equipped with lasers as excitation sources. The decay lifetime was fitted using the software provided by Edinburgh Instruments©.

Laser transient absorption spectroscopy (L-TAS). The e^-_{TiO2}/Dye^+ recombination measurements were carried out with a system consisting of a PTI nitrogen dye laser with a tunable excitation wavelength. The sample was placed between two monochromators and a 150 W tungsten lamp was used as light probe. A Costronics© silicon detector connected to a Tektronic© oscilloscope TDS 2022 and to an electronic filter box was used to monitor the change in absorbance after the laser pulse excitation.

Device characterization. The photoelectrochemical data were recorded using a ABET 150 W xenon light source equipped with the correct filter in order to achieve the solar spectrum AM 1.5 G. The light intensity was adjusted to 100 mW cm^{-2}. The equivalent of 1 sun, using a calibrated Si photodiode. The applied potential and cell current were registered with a Keithley model 2600 digital source meter. The current to voltage (I-V) curve was measured automatically with a home-built Labview software.

The transient photovoltage or V_{oc} decay were carried out with a system set-up s previously reported by O'Regan *et al*.[65]

Device preparation. The TiO_2 paste (20 nm particle size) was screen-printed onto a fluorine doped tin oxide (FTO) conducting glass substrate by the well-known doctor blade technique. The resulting thickness was 6 µm plus 5 µm of a light-scatter TiO_2 film composed by TiO_2 particles (size 300 nm). The device active area was 0.196 cm^2. Prior to the deposition of the TiO_2 paste the conducting glass substrates were immersed in a solution of $TiCl_4$ (40 mM). The TiO_2 electrodes were gradually heated under airflow at 325 ºC for 5 minutes, 375 ºC for 5 minutes, 450 ºC for 15 minutes and 500 ºC for 15 minutes. The heated TiO_2 electrodes were soaked in $TiCl_4$ aqueous solution 40 mM at 70 ºC for 15 minutes and then washed with ethanol. The electrodes were heated again at 500 ºC for 30 minutes and cooled before dye adsorption. The platinised counter electrode was made applying a drop of 5 mM of H_2PtCl_6 in dry 2-propanol and spreading onto the conducting glass substrate (FTO). The coated glass was heated under airflow at 390 ºC for 30 minutes.

A solution of **PMI-1** and **PMI-2** ($1.5 \cdot 10^{-4}$ M in chlorobenzene) was prepared and the film of TiO_2 was immersed for 4 hours at room temperature. The sensitised electrodes were washed several times with chlorobenzene and dichloromethane and then assembled by sandwiching the working and the counter electrode using a thin thermoplastic (Surlyn) frame that melts at 100 ºC.

The electrolyte was made using 0.5 M of 1-butyl-3-methylimidazolium iodide (BMII), 0.1 M of lithium iodide (LiI), 0.05 M of iodine (I_2) and 0.01 M of 4-*tert*-butylpyridine in a mixture acetonitrile and varelonitrile (85:15). This electrolyte was denoted as **EMP2**.

4.3.5. Acknowledgements

The authors thank the Spanish Ministerio de Ciencia e Innovación for the CONSOLIDER-HOPE 0007-2007 project. MP and EP also thank the Ministerio for the CTQ2007-60746/BQU project and the PhD fellowship. ASS and FF are grateful for financial support throught grants MAT2005-07369-C03-02 abd CTQ2007-67888/ BQU. F.J.C.-G. thanks the MEC for FPU fellowship.

4.4. References

[1] S. Ferrere, A. Zaban, B. A. Gregg, *J. Phys. Chem. B* **1997**, *101*, 4490.

[2] H. Imahori, T. Umeyama, S. Ito, *Acc. Chem. Res.* **2009**, *42*, 1809.

[3] D. Kuang, C. Klein, J. Snaith Henry, E. Moser Jacques, R. Humphry-Baker, P. Comte, M. Zakeeruddin Shaik, M. Gratzel, *Nano Lett.* **2006**, *6*, 769.

[4] E. Coronado, E. Palomares, *J. Mater. Chem.* **2005**, *15*, 3593.

[5] J. Boucle, P. Ravirajan, J. Nelson, *J. Mater. Chem.* **2007**, *17*, 3141.

[6] J. R. Durrant, S. A. Haque, E. Palomares, *Chem. Commun.* **2006**, 3279.

[7] N. Robertson, *Angew. Chem., Int. Ed.* **2006**, *45*, 2338.

[8] S. Gunes, N. S. Sariciftci, *Inorg. Chim. Acta* **2008**, *361*, 581.

[9] B. O'Regan, M. Gratzel, *Nature* **1991**, *353*, 737.

[10] J. M. Kroon, N. J. Bakker, H. J. P. Smit, P. Liska, K. R. Thampi, P. Wang, S. M. Zakeeruddin, M. Gratzel, A. Hinsch, S. Hore, U. Wuerfel, R. Sastrawan, J. R. Durrant, E. Palomares, H. Pettersson, T. Gruszecki, J. Walter, K. Skupien, G. E. Tulloch, *Prog. Photovolt. Res. Appl.* **2007**, *15*, 1.

[11] M. Liang, W. Xu, F. Cai, P. Chen, B. Peng, J. Chen, Z. Li, *J. Phys. Chem. C* **2007**, *111*, 4465.

[12] Z.-S. Wang, Y. Cui, K. Hara, Y. Dan-oh, C. Kasada, A. Shinpo, *Adv. Mater.* **2007**, *19*, 1138.

[13] H. Choi, C. Baik, S. O. Kang, J. Ko, M.-S. Kang, M. K. Nazeeruddin, M. Gratzel, *Angew. Chem., Int. Ed.* **2008**, *47*, 327.

[14] W. H. Howie, F. Claeyssens, H. Miura, L. M. Peter, *J. Am. Chem. Soc.* **2008**, *130*, 1367.

[15] S. Kim, H. Choi, C. Baik, K. Song, S. O. Kang, J. Ko, *Tetrahedron* **2007**, *63*, 11436.

[16] C. Zafer, M. Kus, G. Turkmen, H. Dincalp, S. Demic, B. Kuban, Y. Teoman, S. Icli, *Sol. Energy Mater. Sol. Cells* **2007**, *91*, 427.

[17] C. Zafer, C. Karapire, N. Serdar Sariciftci, S. Icli, *Sol. Energy Mater. Sol. Cells* **2005**, *88*, 11.

[18] C. Karapire, C. Zafer, S. Icli, *Synth. Met.* **2004**, *145*, 51.

[19] S. Ferrere, B. A. Gregg, *New J. Chem.* **2002**, *26*, 1155.

[20] J. Fortage, M. Severac, C. Houarner-Rassin, Y. Pellegrin, E. Blart, F. Odobel, *J. Photochem. Photobiol., A* **2008**, *197*, 156.

[21] Y. Shibano, T. Umeyama, Y. Matano, H. Imahori, *Org. Lett.* **2007**, *9*, 1971.

[22] T. Edvinsson, C. Li, N. Pschirer, J. Schoeneboom, F. Eickemeyer, R. Sens, G. Boschloo, A. Herrmann, K. Muellen, A. Hagfeldt, *J. Phys. Chem. C* **2007**, *111*, 15137.

[23] J. E. Kroeze, N. Hirata, S. Koops, M. K. Nazeeruddin, L. Schmidt-Mende, M. Gratzel, J. R. Durrant, *J. Am. Chem. Soc.* **2006**, *128*, 16376.

[24] M. Planells, A. Forneli, E. Martinez-Ferrero, A. Sanchez-Diaz, M. A. Sarmentero, P. Ballester, E. Palomares, B. C. O'Regan, *Appl. Phys. Lett.* **2008**, *92*, 153506/1.

[25] Z.-S. Wang, N. Koumura, Y. Cui, M. Takahashi, H. Sekiguchi, A. Mori, T. Kubo, A. Furube, K. Hara, *Chem. Mater.* **2008**, *20*, 3993.

[26] B. C. O'Regan, J. R. Durrant, P. M. Sommeling, N. J. Bakker, *J. Phys. Chem. C* **2007**, *111*, 14001.

[27] C.-C. You, F. Wurthner, *Org. Lett.* **2004**, *6*, 2401.

[28] C. Former, S. Becker, A. C. Grimsdale, K. Mullen, *Macromolecules* **2002**, *35*, 1576.

[29] C.-W. Chang, C. K. Chou, I. J. Chang, Y.-P. Lee, E. W.-G. Diau, *J. Phys. Chem. C* **2007**, *111*, 13288.

[30] S. A. Haque, Y. Tachibana, D. R. Klug, J. R. Durrant, *J. Phys. Chem. B* **1998**, *102*, 1745.

[31] S.-L. Li, K.-J. Jiang, K.-F. Shao, L.-M. Yang, *Chem. Commun.* **2006**, 2792.

[32] K. Hara, T. Sato, R. Katoh, A. Furube, T. Yoshihara, M. Murai, M. Kurashige, S. Ito, A. Shinpo, S. Suga, H. Arakawa, *Adv. Funct. Mater.* **2005**, *15*, 246.

[33] Z.-S. Wang, F.-Y. Li, C.-H. Huang, L. Wang, M. Wei, L.-P. Jin, N.-Q. Li, *J. Phys. Chem. B* **2000**, *104*, 9676.

[34] A. Morandeira, J. Fortage, T. Edvinsson, L. Le Pleux, E. Blart, G. Boschloo, A. Hagfeldt, L. Hammarstrom, F. Odobel, *J. Phys. Chem. C* **2008**, *112*, 1721.

[35] D. Shi, N. Pootrakulchote, R. Li, J. Guo, Y. Wang, S. M. Zakeeruddin, M. Gratzel, P. Wang, *J. Phys. Chem. C* **2008**, *112*, 17046.

[36] M. Planells, F. J. Cespedes-Guirao, A. Forneli, A. Sastre-Santos, F. Fernandez-Lazaro, E. Palomares, *J. Mater. Chem.* **2008**, *18*, 5802.

[37] A. F. D. de Namor, J. C. Y. Ng, M. A. L. Tanco, M. Salomon, *J. Phys. Chem.* **1996**, *100*, 14485.

[38] Y. Inoue, T. Hakushi, Y. Liu, L. H. Tong, *J. Org. Chem.* **1993**, *58*, 5411.

[39] U. Olsher, F. Frolow, N. K. Dalley, W. Jiang, Z. Y. Yu, J. M. Knobeloch, R. A. Bartsch, *J. Am. Chem. Soc.* **1991**, *113*, 6570.

[40] C. L. Olson, J. Nelson, M. S. Islam, *J. Phys. Chem. B* **2006**, *110*, 9995.

[41] B. C. O'Regan, K. Bakker, J. Kroeze, H. Smit, P. Sommeling, J. R. Durrant, *J. Phys. Chem. B* **2006**, *110*, 17155.

[42] R. L. Willis, C. Olson, B. O'Regan, T. Lutz, J. Nelson, J. R. Durrant, *J. Phys. Chem. B* **2002**, *106*, 7605.

[43] S. A. Haque, T. Park, C. Xu, S. Koops, N. Schulte, R. J. Potter, A. B. Holmes, J. R. Durrant, *Adv. Funct. Mater.* **2004**, *14*, 435.

[44] H. J. Snaith, S. M. Zakeeruddin, L. Schmidt-Mende, C. Klein, M. Gratzel, *Angew. Chem., Int. Ed.* **2005**, *44*, 6413.

[45] D. Kuang, C. Klein, H. J. Snaith, R. Humphry-Baker, S. M. Zakeeruddin, M. Gratzel, *Inorg. Chim. Acta* **2008**, *361*, 699.

[46] Y. Shibano, T. Umeyama, Y. Matano, N. V. Tkachenko, H. Lemmetyinen, Y. Araki, O. Ito, H. Imahori, *J. Phys. Chem. C* **2007**, *111*, 6133.

[47] A. S. Lukas, Y. Zhao, S. E. Miller, M. R. Wasielewski, *J. Phys. Chem. B* **2002**, *106*, 1299.

[48] L. Fan, Y. Xu, H. Tian, *Tetrahedron Lett.* **2005**, *46*, 4443.

[49] F. Wurthner, V. Stepanenko, Z. Chen, C. R. Saha-Moeller, N. Kocher, D. Stalke, *J. Org. Chem.* **2004**, *69*, 7933.

[50] J. Feng, Y. Zhang, C. Zhao, R. Li, W. Xu, X. Li, J. Jiang, *Chem.--Eur. J.* **2008**, *14*, 7000.

[51] F. Wurthner, *Chem. Commun.* **2004**, 1564.

[52] P. Job, *Ann. Chim. Appl.* **1928**, *9*, 113.

[53] K. A. Connors, *Binding Constants: The Measurements of Molecular Complex Stability*, **1987**.

[54] F. Fabregat-Santiago, J. Garcia-Canadas, E. Palomares, J. N. Clifford, S. A. Haque, J. R. Durrant, G. Garcia-Belmonte, J. Bisquert, *J. Appl. Phys.* **2004**, *96*, 6903.

[55] E. Palomares, J. N. Clifford, S. A. Haque, T. Lutz, J. R. Durrant, *J. Am. Chem. Soc.* **2003**, *125*, 475.

[56] Y. Tachibana, S. A. Haque, I. P. Mercer, J. R. Durrant, D. R. Klug, *J. Phys. Chem. B* **2000**, *104*, 1198.

[57] I. Montanari, J. Nelson, J. R. Durrant, *J. Phys. Chem. B* **2002**, *106*, 12203.

[58] S. Mori, K. Sunahara, Y. Fukai, T. Kanzaki, Y. Wada, S. Yanagida, *J. Phys. Chem. C* **2008**, *112*, 20505.

[59] L. M. Peter, *J. Phys. Chem. C* **2007**, *111*, 6601.

[60] D. Shi, Y. Cao, N. Pootrakulchote, Z. Yi, M. Xu, S. M. Zakeeruddin, M. Gratzel, P. Wang, *J. Phys. Chem. C* **2008**, *112*, 17478.

[61] A. Reynal, A. Forneli, E. Martinez-Ferrero, A. Sanchez-Diaz, A. Vidal-Ferran, B. C. O'Regan, E. Palomares, *J. Am. Chem. Soc.* **2008**, *130*, 13558.

[62] A. Forneli, M. Planells, M. A. Sarmentero, E. Martinez-Ferrero, B. C. O'Regan, P. Ballester, E. Palomares, *J. Mater. Chem.* **2008**, *18*, 1652.

[63] S. Ruhle, M. Greenshtein, S. G. Chen, A. Merson, H. Pizem, C. S. Sukenik, D. Cahen, A. Zaban, *J. Phys. Chem. B* **2005**, *109*, 18907.

[64] F. De Angelis, S. Fantacci, A. Selloni, M. Gratzel, M. K. Nazeeruddin, *Nano Lett.* **2007**, *7*, 3189.

[65] B. C. O'Regan, S. Scully, A. C. Mayer, E. Palomares, J. Durrant, *J. Phys. Chem. B* **2005**, *109*, 4616.

UNIVERSITAT ROVIRA I VIRGILI
DESIGN AND SYNTHESIS OF ORGANIC SENSITIZERS FOR DYE SOLAR CELLS: MOLECULAR STRUCTURE VS DEVICE PERFORMANCE
Miquel Angels Planells Dillundé
ISBN:978-84-693-8861-7/DL:T.1946-2010

5. Donor – Acceptor π Conjugated Sensitizers for DSSC

TOC Figure

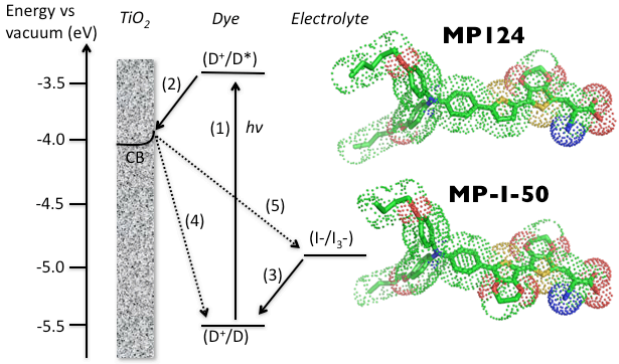

Ready to be submitted to *Chem. Mat.*

UNIVERSITAT ROVIRA I VIRGILI
DESIGN AND SYNTHESIS OF ORGANIC SENSITIZERS FOR DYE SOLAR CELLS: MOLECULAR STRUCTURE VS DEVICE PERFORMANCE
Miquel Angels Planells Dillundé
ISBN:978-84-693-8861-7/DL:T.1946-2010

5.1. General Introduction

Donor - acceptor π conjugated photosensitizers are a class of highly conjugated organic molecules which have received much attention in recent years in the DSSC field. Indeed they are perhaps the most promising organic alternative to the dominance of Ru(II) polypyridyl dyes in DSSC, with efficiencies already breaking the 10% barrier. The main photophysical properties as well as their background as sensitizers for DSSC have been reviewed extensively in Chapter 1.4 of this thesis.

In this chapter, the synthesis of two novel D - π - A photosensitizers, **MP124** and and **MP-I-50**, is described and their interfacial charge transfer processes at the TiO_2/ dye/electrolyte interface in DSSC under operational conditions evaluated.

In these photosensitizers the donor moieties consist of triphenylamines containing long alkyl chains at the *para* positions of two of the phenyl rings. and acceptor moieties consist of cyanoacetic acid. The key difference between the two dyes is the nature of the π bridge connecting the donor and acceptor groups. In **MP124** this bridge consists of a single thiophene and a single 3,4-ethylenedioxythiophene (EDOT) unit whereas in **MP-I-50** it consists of two EDOT units.[1] The addition of an extra EDOT group is chosen to increase the conjugation and therefore obtain a red-shift in absorption.

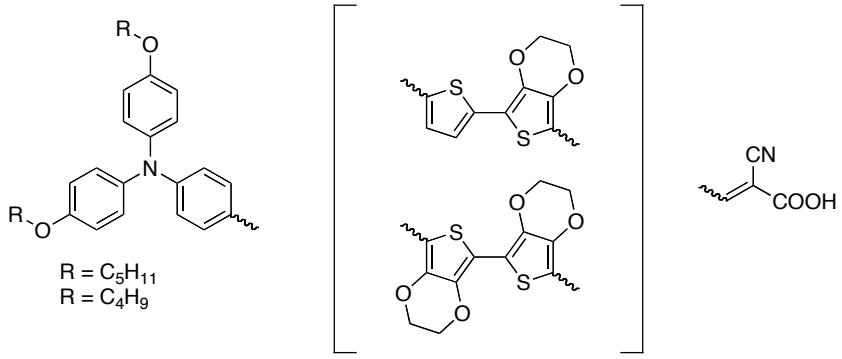

Figure 5.1 - Chemical structure of donor (*left*), π bridge (*center*) and acceptor (*right*) of novel donor - acceptor π conjugated photosensitizers.

The synthesis of these two novel dyes was carried out via different synthetic routes. On the one hand, the synthesis of triphenylamine was attained under either Ullmann conditions[2] or under Pd catalysis.[3] Reactions under Ullmann conditions gave low yields due to the large amount of side products obtained, although the low-

cost of the copper reagents needed made them an interesting synthetic route. On the other hand, the spacer was obtained by the successive coupling of thiophene derivatives. The union of the π conjugated spacer with the triphenylamine was carried out under Suzuki or Stille couplings.[4, 5] Finally, the accepter moiety, cyanoacetic acid or methyl cyanoacetate, was condensed with an aldehyde group under Knoevenagel conditions.

5.2. *Paper V*: Energy Levels, Charge Injection, Charge Recombination and Dye Regeneration Dynamics for Donor - Acceptor π Conjugated Organic Dyes in Mesoscopic TiO_2 Sensitized Solar Cells

Miquel Planells,[a] Laia Pellejà,[a] John N. Clifford,[a] Nuria López,[a] Mariachiara Pastore,[b] Filippo DeAngelis,[b] Seth R. Marder,[c] and Emilio Palomares[a,d,*]

[a] Institute of Chemical Research of Catalonia (ICIQ), Avda. Països Catalans,16, Tarragona, Spain. Fax: 34 977 920 224; Tel: 34 977 920 241;Corresponding Author E-mail: epalomares@iciq.es

[b] Istituto (CNR) di Scienze e Tecnologie Molecolari (ISTM), c/o Dipartimento di Chimica, Università di Perugia, Via Elce di Sotto 8, I-06123 Perugia, Italy.

[c] School of Chemistry and Biochemistry and Center for Organic Photonics and Electronics (COPE), Georgia Institute of Technology (GATECH), Atlanta, GA 30332, U.S.A.

[d] Catalan Institution for Research and Advanced Studies (ICREA). Spain.

Abstract: Two new organic sensitizers, **MP124** and **MP-I-50**, of type D-π-A were synthesized and their electrochemical and spectroscopic properties studied. Efficiencies of DSSC devices utilizing these dyes were also investigated using different sensitization solvents, sensitization times and additives. Under standard AM 1.5G simulated solar radiation, optimized **MP124** devices show an efficiency of 7.45% (V_{oc} = 0.73 V; J_{sc} = 14.44 mA cm^{-2}; FF = 70%) while optimized **MP-I-50** devices show an efficiency of 5.66% (V_{oc} = 0.68 V; J_{sc} = 12.06 mA cm^{-2}; FF = 69%). Transient absorption spectroscopy studies show that regeneration of dye cations by the red-ox electrolyte was more efficient in **MP124** cells owing to its higher HOMO energy leading to greater driving force for the regeneration reaction. Transient photovoltage studies showed that electron lifetimes were longer lived in **MP124** explaining the higher V_{oc} for these cells compared to **MP-I-50** cells. This can be explained not only by the greater tendency of **MP-I-50** to form charge-transfer complexes with I_3^- and/or I_2 species due to the presence of the additional two oxygen atoms in its structure compared to **MP124**, but also by the presence of different molecular packing at the TiO_2 surface. This work highlights the effect that small

changes to the sensitizer structure can have over the interfacial charge transfer reaction and ultimately on device efficiency.

5.2.1. Introduction

Dye sensitized solar cells (DSSC) based on nanocrystalline TiO_2 have received a great deal of attention in the last two decades.[6-8] With cell efficiencies already over 11% they are now justifiably considered as viable for large scale commercial exploitation.[9] Since the demonstration by Grätzel and O'Regan of the first efficient devices,[8] the best DSSC performances have continued to be recorded using Ru(II)polypyriyl dyes. However there are a number of limitations concerning these sensitizers beyond the most obvious that they contain a costly precious metal component. They have relatively low extinction coefficients meaning thicker TiO_2 mesoporous films need to be utilized in order to absorb all of the incident radiation. This requires that devices should be fabricated with TiO_2 film thicknesses over 10 μm compromising cell voltage due to increased recombination losses.[10] Furthermore, barring some exceptions such as **N749** (black dye)[11] and latterly heteroleptic sensitizers such as **C101**[9] which incorporate thiophene units into the ancillary bipyridyl ligand, Ru(II) polypyridyls show relatively poor absorption at wavelengths longer than 700 nm.

Schematically principles of operation are shown in Figure 1. Briefly, the light promotes one electron from the ground state to excited state (1). Then, the electron is injected easily to the TiO_2 conduction band (2) and transported to the working electrode, generation electrical power. The oxidized dye formed after the electron injection is regenerated efficiently by the red-ox electrolyte (3). However, when the electron is placed to the conduction band, undesired recombination reactions can take place either with the oxidized dye (4) or oxidized electrolyte (5). These recombination processes have been probed as limiting factors in the device efficiencies.

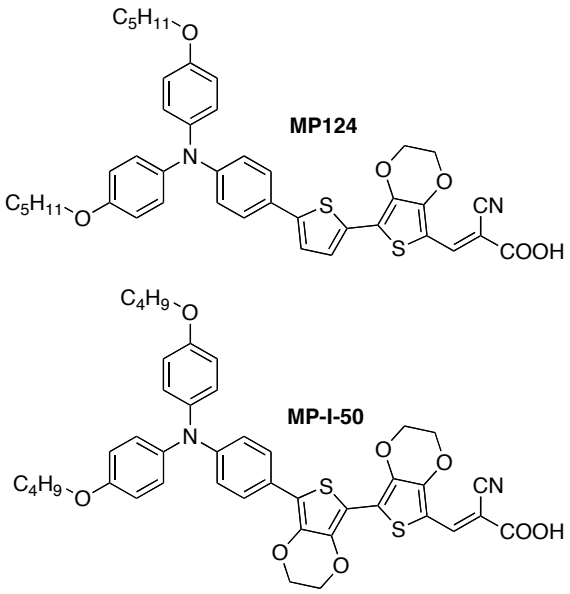

Figure 1. Schematic representation of DSSC processes of (1) absorption, (2) electron injection, (3) dye regeneration, (4) recombination with oxidized dye and (5) recombination with oxidized electrolyte.

Utilization of organic dyes in DSSC can address many of these limitations.[12] They do not contain any metal centre and their red-ox and absorption properties can be readily tuned by facile structural modification. They have very high extinction coefficients meaning that thinner device architectures can be utilized making them perfect for use in solid state DSSC. Nevertheless there are also a number of issues associated with organic dyes including poor stability and a tendency towards aggregation.[13-15] Coumarines,[16, 17] indolines,[18, 19] perylenes,[20-22] cyanines,[23, 24] hemicyanines,[25] porphyrins,[26, 27] squarines[28, 29] and phthalocyanines[30] have all been utilized successfully in DSSC.

More recently, organic sensitizers have achieved efficiencies which closely rival those of Ru(II) polypyridyls in DSSC, with a recent study reporting an efficiency of over 10%.[31] Many of these sensitizers have the same structural motif in common, namely the donor – acceptor π conjugated (D-π-A) motif.[32-37] The most common donors used are arylamines while the acceptor is usually the cyanoacrylate group. The π bridge often consists of one or more thiophene units. Molecular orbital calculations for these sensitizers have shown that the HOMO is located on the arylamine donor unit whereas the LUMO is centered on the cyanoacrylate anchoring group resulting in efficient electron injection into the TiO_2. Stability tests have also found these sensitizers to be extremely promising for use in DSSC.[33, 35, 36]

In this paper we present two new organic sensitizers from the D-π-A family, namely **MP124** and **MP-I-50** (Figure 1). Their structures differ very slightly by the presence of two ethylenedioxythiophenes in the π bridge of **MP-I-50** as opposed to a single ethylenedioxythiophene and thiophene in the case of **MP124**. However, this subtle structural change has a big effect upon efficiency for cell devices based on these sensitizers. Herein we explain the difference in DSSC performance utilizing these sensitizers principally by monitoring the electron transfer processes in complete devices by comparison to theoretical results and we discuss the results with reference to design rules for optimized dye sensitizers for DSSC.[12]

5.2.2. Experimental Section.

Materials and reagents. All reagents were purchased from either Sigma-Aldrich or Alfa Aesar and they were used as received without further purification unless otherwise stated.

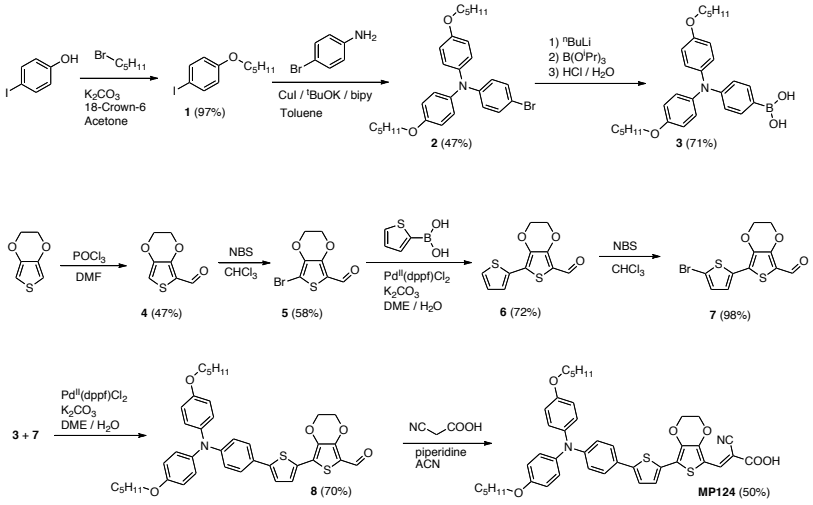

Scheme 1. Synthesis of organic dye **MP124**.

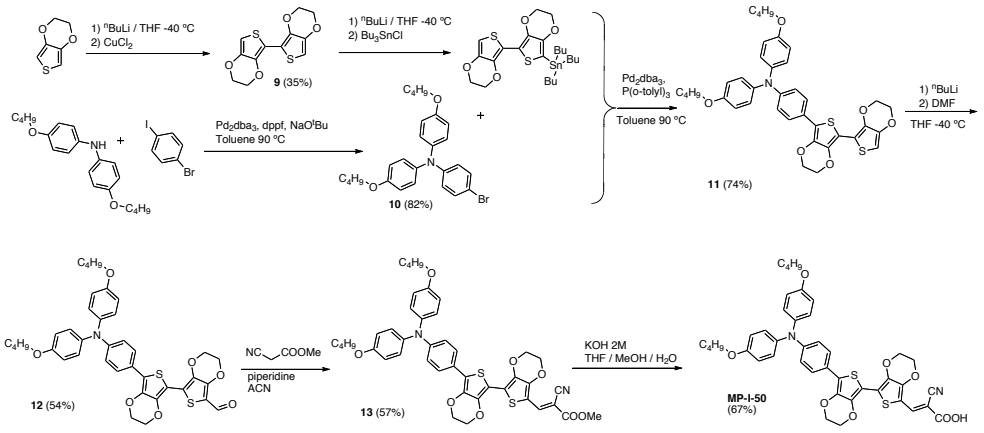

Scheme 2. Synthesis of organic dye **MP-I-50**.

*Synthesis of 4-pentoxy-iodobenzene (**1**).* 4-iodophenol (5 g, 22.7 mmol), potassium carbonate (4.39 g, 31.8 mmol) and 18-crown-6 (1.2 g, 4.5 mmol) were placed in a round bottom flask with 250 mL of acetone (1 mL/mmol). The mixture was stirred and then bromopentane (4 mL, 31.8 mmol) was added. The reaction was stirred under reflux overnight. After cooling at room temperature (r.t.) the crude was filtered off and the solvent removed. The crude was extracted with Et_2O and washed with H_2O. The organic layer was dried over Na_2SO_4 and the solvent removed. The crude was then purified by column chromatography (SiO_2, CH_2Cl_2 / Hexane 1:1) to afford colorless oil as the final product (6.4 g, 97% yield). ^{1}H-NMR (400 MHz, $CDCl_3$) δ_H: 7.54 (d, *J* = 8.8 Hz, 2H); 6.67 (d, *J* = 8.8 Hz, 2H); 3.91 (t, *J* = 6.6 Hz, 2H); 1.77 (m, 2H); 1.39 (m, 4H); 0.93 (t, *J* = 7.1 Hz, 3H). ^{13}C-NMR (100 MHz, $CDCl_3$) δ_C: 159.2; 138.3; 117.4; 82.6; 68.3; 29.1; 28.3; 22.6; 14.2.

*Synthesis of 4-bromo-N,N-bis(4-(pentyloxy)phenyl)aniline (**2**).* 4-bromoaniline (237 mg, 1.3 mmol), ^{t}BuOK (464 mg, 4.1 mmol); CuI (10 mg, 0.05 mmol) and 2,2'-bipyridine (9 mg, 0.05 mmol) were added to a Schlenck flask and dried under high vacuum for 20 minutes. **1** (1 g, 3.4 mmol) was then added to 5 mL of toluene (4 mL/mmol) and the reaction was heated up to 120 ºC. The reaction was stirred at this temperature overnight under argon atmosphere. After cooling to r.t. the crude was filtered over celite eluding with dicholomethane (DCM). Finally, the crude was purified by column chromatography (SiO_2, CH_2Cl_2 / Hexane 1:3) to afford the product as a yellow oil (471 mg, 47%). ^{1}H-NMR (400 MHz, $CDCl_3$) δ_H: 7.22 (d, *J* = 8.9 Hz, 2H); 7.01 (d, *J* = 8.9 Hz, 4H); 6.81 (d, *J* = 9.0 Hz, 2H); 6.78 (d, *J* = 9.0 Hz, 4H); 6. 3.92 (t, *J* = 6.6 Hz, 4H); 1.77 (m, 4H); 1.39 (m, 8H); 0.93 (t, *J* = 7.1 Hz, 6H). ^{13}C-NMR (100

MHz, $CDCl_3$) δ_C: 155.8; 148.2; 140.5; 131.9; 126.8; 122.1; 115.5; 112.3; 68.4; 29.2; 28.4; 22.7; 14.2.

*Synthesis of (4-(bis(4-(pentyloxy)phenyl)amino)phenyl)boronic acid (**3**).* **2** (165 mg, 0.33 mmol) was added to a round bottom flask with 2 mL of dry THF (6 mL/mmol) and was stirred under nitrogen atmosphere at -78 ºC. ^{n}BuLi 1.6M in hexane (300 µL, 0.5 mmol) was added dropwise and the mixture was stirred for 1 hour at -78 ºC. Following this, $B(O^iPr)_3$ was added in a single portion using a syringe and the reaction was stirred again for 1 hour at -78 ºC. The crude was warmed to r.t. and 1 mL of H_2O was added dropwise. Et_2O was added and the mixture was then washed with water. The organic layer was dried over Na_2SO_4 and the solvent removed. Column chromatography (SiO_2, CH_2Cl_2 / EtOAc 1:1) was used to purify the product, which was obtained as a yellow oil (100 mg, 71% yield). The product was used immediately in the next step.

*Synthesis of 2,3-dihydrothieno[3,4-b][1,4]dioxine-5-carbaldehyde (**4**).* Freshly distilled 3,4-ethylenedioxythiophene (7 g, 49 mmol) was placed in a two neck round bottom flask with 75 mL of dimethylformamide (DMF) (1.5 mL/mmol). The mixture was cooled down to -10 ºC and $POCl_3$ (4.6 mL, 50 mmol) was added dropwise for 5 minutes, and stirred for 1 hour at -10 ºC. 200 mL of H_2O then was added and the reaction was stirred overnight at r.t. The cake formed was filtered off and washed with H_2O. Column chromatography (SiO_2, CH_2Cl_2) was used to purify the product, which was obtained as white solid (4 g, 47 %). ^{1}H-NMR (400 MHz, $CDCl_3$) δ_H: 9.91 (s, 1H); 6.79 (s, 1H); 4.36 (m, 2H); 4.27 (m, 2H). ^{13}C-NMR (100 MHz, $CDCl_3$) δ_C: 180.3; 148.6; 142.0; 118.7; 110.9; 65.5; 64.5.

*Synthesis of 7-bromo-2,3-dihydrothieno[3,4-b][1,4]dioxine-5-carbaldehyde (**5**).* **4** (1.2 g, 7 mmol) was added to a round bottom flask with 40 mL of $CHCl_3$ (6 mL/mmol) and was stirred at 0 ºC. N-Bromosuccinimide (NBS) (1.4 g, 7.7 mmol) was then added in one portion and the mixture was stirred overnight at r.t. The crude was washed with a saturated solution of $NaHCO_3$ and H_2O. The organic layer was dried over Na_2SO_4 and the solvent removed. Column chromatography (SiO_2, CH_2Cl_2) was used to purify the product, which was obtained as a brown solid (1 g, 58% yield). ^{1}H-NMR (400 MHz, $CDCl_3$) δ_H: 9.83 (s, 1H); 4.36 (m, 4H). ^{13}C-NMR (100 MHz, $CDCl_3$) δ_C: 179.0; 1404; 1142.0; 118.7; 110.9; 65.5; 64.5.

*Synthesis of 7-(thiophen-2-yl)-2,3-dihydrothieno[3,4-b][1,4]dioxine-5-carbaldehyde (**6**).* **5** (60 mg, 0.24 mmol), 2-thiophene boronic acid (47 mg, 0.36 mmol) and $Pd^{II}(dppf)Cl_2$ (5 mg, 0.007 mmol) were added to a Schlenck flask and dried under

vacuum for 15 minutes. 2.5 mL of degassed solution of dimethoxyethane (10 mL/mmol) was then added and the mixture was degassed again. After stirring at r.t. for 30 minutes, 0.6 mL of degassed aqueous solution of K_2CO_3 1M was added. The reaction was heated up to 90 ºC and stirred for 1.5 hours. After cooling at r.t. the solvent was removed under vacuum. Column chromatography (SiO_2, CH_2Cl_2) was used to purify the product, which was obtained as a yellow solid (42 mg, 68% yield). ^{1}H-NMR (400 MHz, $CDCl_3$) δ_H: 9.91 (s, 1H); 7.44 (dd, *J* = 3.7 Hz, 1.1 Hz, 1H) 7.38 (dd, *J* = 5.2Hz, 1.1 Hz, 1H); 7.08 (dd, *J* = 5.1 Hz, 3.7 Hz, 1H); 4.42 (m, 4H). ^{13}C-NMR (100 MHz, $CDCl_3$) δ_C: 179.6; 148.8; 137.0; 133.6; 127.7; 127.1; 126.1; 123.5; 115.0; 65.5; 65.0.

*Synthesis of 7-(5-bromothiophen-2-yl)-2,3-dihydrothieno[3,4-b][1,4]dioxine-5-carbaldehyde (**7**).* **6** (278 mg, 1.1 mmol) was added to a round bottom flask with 20 mL of $CHCl_3$ (18 mL/mmol). The mixture was stirred at 0 ºC and NBS (215 mg, 1.2 mmol) was added in one portion. The reaction was stirred at r.t. for 3 hours. The crude was washed with a saturated solution of $NaHCO_3$ and H_2O. The organic layer was dried over Na_2SO_4 and the solvent removed. Column chromatography (SiO_2, CH_2Cl_2) was used to purify the product, which was obtained as yellow solid (357 mg, 98% yield). ^{1}H-NMR (400 MHz, $CDCl_3$) δ_H: 9.91 (s, 1H); 7.15 (d, *J* = 4.0 Hz, 1H); 7.02 (d, *J* = 4.0 Hz, 1H); 4.41 (m, 4H). ^{13}C-NMR (100 MHz, $CDCl_3$) δ_C: 179.6; 148.6; 148.1; 137.2; 130.4; 125.7; 122.3; 115.3; 114.6; 65.5; 65.1. MS-ESI (m/z): $[M+H]^+$ calcd for $C_{11}H_8O_3S_2Br$: 330.9098; found: 330.9109. Anal. Calcd for $C_{11}H_7BrO_3S_2$: C, 39.89; H, 2.13; S, 19.36; Found: C, 39.69; H, 2.16; S, 19.42.

*Synthesis of 7-(5-(4-(bis(4-(pentyloxy)phenyl)amino)phenyl)thiophen-2-yl)-2,3-dihydrothieno[3,4-b][1,4]dioxine-5-carbaldehyde (**8**).* **7** (36 mg, 0.11 mmol) and $Pd^{II}(dppf)Cl_2$ (4 mg, 0.005 mmol) were added to a Schlenck flask and dried under vacuum for 15 minutes. 1.2 mL of degassed solution of dimethoxyethane (5 mL/mmol) containing **3** (70 mg, 0.16 mmol) was then added and the mixture was degassed again. After stirring at r.t. for 30 minutes, 0.3 mL of degassed aqueous solution of K_2CO_3 1M was added. The reaction was heated up to 90 ºC and stirred for 2 hours. After cooling at r.t. the solvent was removed under vacuum. Column chromatography (SiO_2, CH_2Cl_2) was used to purify the product, which was obtained as an orange solid (51 mg, 70% yield). ^{1}H-NMR (400 MHz, $CDCl_3$) δ_H: 9.89 (s, 1H); 7.40 (d, *J* = 8.9 Hz, 2H); 7.38 (d, *J* = 3.9 Hz, 1H); 7.13 (d, *J* = 4.0 Hz, 1H); 7.06 (d, *J* = 8.9 Hz, 4H); 6.90 (d, *J* = 8.8 Hz, 2H); 6.83 (d, *J* = 9.0 Hz, 4H); 4.42 (m, 4H); 3.94 (t, *J* = 6.4 Hz, 4H); 1.74 (m, 4H); 1.41 (m, 8H); 0.93 (m, 6H). ^{13}C-NMR (100 MHz, $CDCl_3$) δ_C: 179.4, 155.9, 149.0, 148.8, 146.6, 143.5, 140.3, 136.6, 131.2, 127.3,

127.0, 126.6, 125.5, 122.2, 120.2, 115.5, 114.5, 68.4, 65.5, 65.0, 29.2, 28.4, 22.6, 14.2.

*Synthesis of (E)-3-(7-(5-(4-(bis(4-(pentyloxy)phenyl)amino)phenyl)thiophen-2-yl)-2,3-dihydrothieno[3,4-b][1,4]dioxin-5-yl)-2-cyanoacrylic acid (**MP124**).* **8** (119 mg, 0.18 mmol) and cyanoacetic acid (23 mg, 0.27 mmol) were added to a Schlenck flask with 1 mL of acetonitrile (ACN) (5 mL/mmol). Piperidine (365 µL, 3.7 mmol) was then added and the reaction was stirred at reflux for 3 hours. After cooling at r.t. the solvent was removed and the crude was extracted with $CHCl_3$ and washed with diluted HCl (0.1% v/v) and brine. The organic layer was dried over Na_2SO_4 and the solvent removed. Size exclusion chromatography (Bio-beads S-X1, THF) was used in order to purify the product, which was obtained as a purple solid (67 mg, 50% yield). ^{1}H-NMR (400 MHz, $CDCl_3$) δ_H: 8.39 (s, 1H); 7.46 (d, J = 4.1 Hz, 1H); 7.40 (d, J = 8.8 Hz, 2H); 7.16 (d, J = 4.1 Hz, 1H); 7.06 (d, J = 8.9 Hz, 4H); 6.89 (d, J = 8.6 Hz, 2H); 6.83 (d, J = 9.0 Hz, 4H); 4.44 (m, 4H); 3.94 (t, J = 6.4 Hz, 4H); 1.78 (m, 4H); 1.41 (m, 8H); 0.93 (t, J = 6.8 Hz, 6H). MS-ESI (m/z): $[M-H]^-$ calcd for $C_{42}H_{41}N_2O_6S_2$: 733.2406; found: 733.2396. Anal. Calcd for $C_{42}H_{42}N_2O_6S_2$: C, 68.64; H, 5.76; N, 3.81; S, 8.73 Found: C, 69.54; H, 7.24; N, 3.22; S, 8.29.

*Synthesis of 2,2'-bis(3,4-ethylenedioxythiophene) (**9**).* Freshly distilled 3,4-ethylenedioxythiophene (2 mL, 18.6 mmol) was placed in a two neck round bottom flask with 20 mL of freshly distilled THF (1 mL/mmol) and it was stirred under nitrogen atmosphere at -40 ºC (ACN/dry ice bath). ^{n}BuLi 2.5M in hexane (8 mL, 20 mmol) was added dropwise and the mixture was stirred 1 hour at -40 ºC. Then, $CuCl_2$ anhydrous (2.5 g, 18.6 mmol) was added in one portion and the reaction was allowed to reach r.t. The mixture was stirred overnight. 200 mL of H_2O was added to the crude mixture and green precipitate appeared. The cake was filtered off and washed with 50 mL of H_2O and 100 mL of hexane. The filtered cake was digested with CH_2Cl_2 (3 x 100 mL) and the crude was dried under vacuum and purified by column chromatography (SiO_2, CH_2Cl_2 / Hexane 1:1, then CH_2Cl_2 / Hexane 2:1) to afford the product as a white solid (930 mg, 35% yield). ^{1}H-NMR (300 MHz, $CDCl_3$) δ_H: 6.27 (s, 2H); 4.32 (m, 4H); 4.24 (m, 4H). ^{13}C-NMR (75 MHz, $CDCl_3$) δ_C: 141.4; 137.2; 110.1; 97.7; 65.2; 64.8. MS-EI (m/z): $[M]^+$ calcd for $C_{12}H_{10}O_4S_2$: 282.0021; found: 282.0011.

*Synthesis of 4-bromo-N,N–(bis(4-butoxyphenyl)aniline (**10**).* Pd_2dba_3 (29 mg, 0.032 mmol), diphenylphosphinoferronce (26 mg, 0.048 mmol) and 4-bromoiodobencene (1.3 g, 4.8 mmol) were added to a Schlenck tube and dried under high vacuum for 30 minutes. 8 mL of dry toluene (2.5 mL/mmol) was added to the mixture and was stirred for 15 minutes under nitrogen atmosphere. Bis(4-

butoxyphenhyl)amine (1 g, 3.2 mmol) and NaO^{t}Bu (430 mg, 4.5 mmol) were added and the reaction was heated up to 90 ºC and stirred overnight. After cooling at room temperature, the crude material was washed with water (50 mL) and extracted with diethyl ether (50 mL). The organic layer was dried over $MgSO_4$ and the solvent was removed. Column chromatography (SiO_2, Hexane / CH_2Cl_2 4:1) was used to purify the product, which was obtained as pale brown liquid (1.22 g, 82% yield). ^{1}H-NMR (300 MHz, $CDCl_3$) δ_H: 7.23 (d, *J* = 9.0 Hz, 2H); 7.02 (d, *J* = 8.9 Hz, 4H); 6.81 (m, 6H); 3.94 (t, *J* = 6.5 Hz, 4H); 1.77 (m, 4H); 1.50 (m, 4H); 0.99 (t, *J* = 7.4 Hz, 6H). ^{13}C-NMR (75 MHz, $CDCl_3$) δ_C: 155.8; 148.2; 140.5; 131.9; 126.7; 122.0; 115.5; 112.3; 68.1; 31.6; 19.5; 14.1. MS-EI (m/z): $[M]^+$ calcd for $C_{26}H_{30}NO_2$: 467.1448; found: 467.1460.

*Synthesis of 4-butoxy-N-(4-butoxyphenyl)-N-(4-(2,2',3,3'-tetrahydro-5,5'-bithieno[3,4-b][1,4]dioxin-7-yl)phenyl)aniline (**11**).* **9** (700 mg, 2.5 mmol) was placed in a two neck round bottom flask with 25 mL of freshly distilled THF (10 mL/mmol) and was stirred under nitrogen atmosphere at -40 ºC (ACN/dry ice bath). ^{n}BuLi 2.5M in hexane (1.1 mL, 2.75 mmol) was added dropwise and the mixture was stirred for 1 hour at -40 ºC. Tributyltinchloride (678 µL, 2.5 mmol) was then added dropwise and the mixture was allowed to reach r.t. and stirred overnight. The crude was washed with brine (30 mL) and the organic layer was dried over $MgSO_4$, filtrated and the solvent removed. The formation of the tin compound was checked by ^{1}H-NMR. Pd_2dba_3 (45 mg, 0.05 mmol) and tri(o-tolyl)phosphine (30 mg, 0.1 mmol) were added to a Schlenck tube and dried under high vacuum for 30 minutes. A degassed solution of the tin compound and **10** (1.17 g, 2.5 mmol) in 10 mL of toluene (2 mL/ mmol) was then added via cannula. The mixture was degassed again by pump/freeze technique and stirred overnight under nitrogen atmosphere at 90 ºC. The mixture was poured into a KF aqueous solution and stirred vigorously for 1 hour (white precipitate appears – tin side product). The mixture was filtered off and extracted with DCM (150 mL) and washed twice with KF aqueous solution. The organic layer was dried over $MgSO_4$ and the solvent removed. The crude was purified by column chromatography (SiO_2, $CHCl_3$ / Hexane 3:1) to afford the product as a yellow solid (1.19 g, 74% yield). ^{1}H-NMR (300 MHz, $CDCl_3$) δ_H: 7.52 (d, *J* = 8.7 Hz, 2H); 7.03 (d, *J* = 9.0 Hz, 4H); 6.91 (d, *J* = 8.4 Hz, 2H), 6.81 (d, *J* = 9.0 Hz, 4H); 6.27 (s, 1H); 4.24 (m, 8H); 3.93 (t, *J* = 6.3 Hz, 4H); 1.76 (m, 4H); 1.48 (m, 4H); 0.98 (t, *J* = 7.2 Hz, 6H). ^{13}C-NMR (75 MHz, $CDCl_3$) δ_C: 155.6; 147.4; 141.5; 140.9; 137.0; 136.9; 127.1; 126.8; 126.6; 125.4; 120.9; 115.7; 115.6; 115.4; 97.7; 97.6; 68.1; 65.2; 65.1; 64.9; 64.8; 31.6; 19.5; 14.1. MS-MALDI (m/z):$[M]^+$ = 669.2. Anal. Calcd for $C_{38}H_{39}NO_6S_2$: C, 68.14; H, 5.87; N, 2.09; Found: C, 68.42; H, 5.90; N, 2.19.

*Synthesis of 7'-(4-(bis(4-butoxyphenyl)amino)phenyl)-2,2',3,3'-tetrahydro-5,5'-bithieno[3,4-b][1,4]dioxine-7-carbaldehyde (**12**).* **11** (1 g, 1.5 mmol) was placed in a two neck round bottom flask with 9 mL of freshly distilled THF (6 mL/mmol) and was stirred under nitrogen atmosphere at -40 ºC (ACN/dry ice bath). ^{n}BuLi 2.5M in hexane (0.72 mL, 1.8 mmol) was added dropwise and the mixture was stirred for 1 hour at -40 ºC. DMF (210 µL, 2.7 mmol) was then added dropwise and the reaction was allowed to reach r.t. and stirred for 2 hours. The crude was poured into 1% HCl aqueous solution (150 mL) and the precipitate was filtered off. Size Exclusion column (Bio-beads S-X1 in DCM) was used in order to obtain pure orange solid (454 mg, 44%). ^{1}H-NMR (300 MHz, $CDCl_3$) δ_H: 9.88 (s, 1H); 7.54 (d, J = 8.9 Hz, 2H); 7.05 (d, *J* = 8.9 Hz, 4H); 6.90 (d, *J* = 8.9 Hz, 2H); 6.82 (d, *J* = 9.0 Hz, 4H); 4.41 (m, 8H); 3.94 (t, *J* = 6.5 Hz, 4H); 1.76 (m, 4H); 1.51 (m, 4H); 0.98 (t, *J* = 7.4 Hz, 6H). ^{13}C-NMR (75 MHz, $CDCl_3$) δ_C: 179.6; 155.8; 148.4; 148.3; 148.1; 141.0; 140.5; 136.9; 135.9; 127.1; 126.9; 124.4; 120.3; 115.4; 114.9; 105.9; 85.4; 68.2; 65.5; 65.3; 65.1; 64.8; 31.6; 19.5; 14.1. MS-MALDI (m/z): $[M]^+$ = 697.2. Anal. Calcd for $C_{39}H_{39}NO_7S_2$: C, 67.12; H, 5.63; N, 2.01; Found: C, 67.28; H, 5.53; N, 2.04.

*Synhtesis of (E)-methyl 3-(7'-(4-(bis(4-butoxyphenyl)amino)phenyl)-2,2',3,3'-tetrahydro-5,5'-bithieno[3,4-b][1,4]dioxin-7-yl)-2-cyanoacrylate (**13**).* **12** (101 mg, 0.145 mmol) was added to a Schlenk flask with 6 mL of ACN (40 mL/mmol). Piperidine (150 µL, 1.45 mmol) and methyl cyanoacetate (25 µL, 0.29 mmol) were then added and the mixture was heated up to 75 ºC for 2.5 hours under nitrogen atmosphere. After this, the solvent was removed under vacuum and the crude was purified by column chromatography (SiO_2, $CHCl_3$ up to $CHCl_3$ / 2% AcOEt) followed by size exclusion column (Bio-beads S-X1 in DCM) to afford the product as a purple solid (65 mg, 57 % yield). ^{1}H-NMR (300 MHz, $CDCl_3$) δ_H: 8.34 (s, 1H); 7.54 (d, *J* = 8.9 Hz, 2H); 7.05 (d, *J* = 8.9 Hz, 4H); 6.89 (d, *J* = 8.9 Hz, 2H); 6.82 (d, *J* = 8.9 Hz, 4H); 4.40 (m, 8H); 3.94 (t, *J* = 6.5 Hz, 4H); 3.85 (s, 3H); 1.76 (m, 4H); 1.49 (m, 4H); 0.98 (t, *J* = 7.4 Hz, 6H). ^{13}C-NMR (75 MHz, $CDCl_3$) δ_C: 164.9; 155.9; 151.5; 148.4; 148.3; 141.6; 141.5; 140.4; 137.0; 135.8; 127.2; 127.0; 124.3; 124.0; 121.7; 120.1; 117.8; 115.4; 110.4; 90.2; 68.1; 65.7; 65.6; 65.0; 64.8; 52.9; 31.6; 19.5; 14.1. Anal. Calcd for $C_{43}H_{42}N_2O_8S_2$: C, 66.30; H, 5.43; N, 3.60; Found: C, 66.33; H, 5.36; N, 3.64.

*Synthesis of (E)-3-(7'-(4-(bis(4-butoxyphenyl)amino)phenyl)-2,2',3,3'-tetrahydro-5,5'-bithieno[3,4-b][1,4]dioxin-7-yl)-2-cyanoacrylic acid (**MP-I-50**).* **13** (53 mg, 0.068 mmol) was added to a Schlenk flask with 10 mL of THF, 3 mL of MeOH and 2 mL of KOH 2M aqueous solution. The mixture was stirred overnight at room

temperature. The organic solvent was removed under vacuum and the crude was extracted with DCM (50 mL) and washed with 1% HCl (50 mL) and H_2O (2 x 50 mL). The organic layer was dried over $MgSO_4$ and the solvent removed. The crude was purified by size exclusion column (Bio-beads S-X1 in DCM) to afford the product as a purple solid (35 mg, 67 % yield). ^{1}H-NMR (300 MHz, THF-d_8) δ_H: 10.86 (s, 1H); 8.29 (s, 1H); 7.55 (d, J = 8.4 Hz); 7.02 (br s, 4H); 6.84 (br d, J = 8.2 Hz, 6H); 4.43 (m, 8H); 3.94 (t, J = 6.3 Hz); 1.73 (m, 4H); 1.52 (m, 4H); 0.98 (t, J = 7.4 Hz). MS-ESI (m/z): $[M+Na]^+$ calcd for $C_{42}H_{40}N_2O_8S_2Na$: 787.2124; found: 787.2114. Anal. Calcd for $C_{42}H_{40}N_2O_8S_2$: C, 65.95; H, 5.27; N, 3.66; S, 8.36 Found: C, 65.25; H, 5.77; N, 3.29; S, 8.85.

Characterization techniques. ^{1}H and ^{13}C NMR spectra were recorded on both a Bruker Avance 400 (400 MHz for ^{1}H and 100 MHz for ^{13}C) and a Mercury Varian 300 (300 MHz for ^{1}H and 75 MHz for ^{13}C) spectrometer. The deuterated solvents used are indicated; chemical shifts, δ, are given in ppm, referenced to the solvent residual signal (^{1}H, ^{13}C). Coupling constants, J, are given in Hz. MS spectra were recorded on both Waters LCT Premier and VG Instruments 70-SE, using electron impact (EI), electrospray ionization (ESI) and matrix-assisted laser desorption/ionization (MALDI) modes depending on the sample. Elemental analyses were carried out by Atlantic Microlabs using a LECO 932 CHNS elemental analyzer.

Optical, Electrochemical, and Spectroscopic Measurements. The UV-Visible and fluorescence spectra were recorded using a 1 cm path length quartz cell on a Shimadzu© UV spectrophotometer 1700 and an Aminco-Bowman© series 2 luminescence spectrometer with a temperature controller, respectively. The electrochemical data were obtained employing a conventional three-electrode cell connected to a CH Instruments© 660c potentiostat-galvanostat. For square wave voltammetry, we used platinum working electrode, a Ag/AgCl reference electrode and a platinum wire as the auxiliary electrode. The laser transient absorption spectroscopy (L-TAS) measurements were carried out by the same procedure as Durrant *et al*.[38, 39] employing a PTI nitrogen dye laser as excitation source and a 150 W tungsten lamp is used as light probe. The charge extraction and transient photovoltage (TPV) decay were carried out with a system set-up as previously reported by O'Regan *et al*.[40, 41]

Device preparation. In the present work two different types of devices are utilized depending on the measurements being conducted. Highly transparent thin film devices were utilized for TAS experiments. These devices were made using 9 μm thick films and sensitized with the organic dyes until the absorbance reach 0.5 a.u. at

the maximum absorption wavelength. On the other hand, for optimized cell efficiencies, devices were made using 13 µm thick films consisting of a layer of 9 µm of 20 nm TiO_2 nanoparticles (Dyesol© paste) and a layer of 4 µm of 400 nm TiO_2 particles (scatter layer). Prior to the deposition of the TiO_2 paste the conducting glass substrates were immersed in a solution of $TiCl_4$ (40 mM) for 30 minutes and then dried. The TiO_2 nanoparticle paste was deposited onto a conducting glass substrate (Hartford Glass inc. with 15 Ω cm^{-2} resistance) using the screen printing technique. The TiO_2 electrodes were gradually heated under an airflow at 325 ºC for 5 min, 375 ºC for 5 min, 450 ºC for 15 min and 500 ºC for 15 min. The heated TiO2 electrodes were immersed again in a solution of $TiCl_4$ (40 mM) at 70 ºC for 30 min and then washed with ethanol. The electrodes were heated again at 500 ºC for 30 min and cooled before dye adsorption. For the thin film devices the area was 1 cm^2 while for the optimized thick film DSSC the active area was 0.16 cm^2. The counter electrode was made by spreading a 10 mM solution of H_2PtCl_6 in ethanol onto a conducting glass substrate with a small hole to allow the introduction of the liquid electrolyte using vacuum, followed by heating at 390 ºC for 15 minutes. A batch of solutions of both dyes at concentrations of 300 µM in various solvents was prepared and the film immersed at room temperature for a variety of time periods. The sensitized electrodes were washed with ethanol and dried under air. Finally, the working and counter electrodes were sandwiched together using a thin thermoplastic (Surlyn) frame that melts at 100 ºC. Two different electrolytes were used depending on the characterization technique used. For efficient solar cells the electrolyte **EL1** consisted of 1 M buthyl-methyl imidazolium iodide (BMII), 0.05 M lithium iodide, 0.03 M iodine, 0.1 M guanidinium thiocyanate (GNCS) and 0.5 M *tert*-butylpyridine in a mixture of acetonitrile/valeronitrile (85:15). For thin film cells, the electrolyte **EL2** was used which is the same as **EL1** minus *tert*-butylpyridine.

Device Characterization. The photovoltaic measurements were carried out with a 150W solar simulator from ABET© Technologies with the appropriated set of filters for the correct simulation of the 1.5 AM G solar spectrum. The incident light power was measured at 1000 W/m^2 with a calibrated Silicon photodiode, which the spectral sensitivity was closed to the devices under test. The applied potential and cell current were measured with a Keithley model 2400 digital source meter. The current to voltage (I–V curve) was measured automatically with home-built Labview© software. Incident photon to current conversion efficiency (IPCE) measurements were carried out with a home made set up, consisting in a 150 W Oriel Xenon lamp, a motorized monochromator and a Keithley 2400. An integrating sphere was employed in order to

provide homogeneous monochromatic light distribution over active area of the devices. In addition, photocurrent and irradiated light intensity were measured simultaneously.

Theoretical approach. Calculations on the structure and simulated spectra were performed through Density Functional Theory, DFT, and its extension to the Time-Dependent formulation, TDDFT, as implemented in Gaussian 09 program.[42] The ground state geometry for both protonated and deprotonated versions of the **MP124** and **MP-I-50** dyes were optimized in gas-phase within the B3LYP functional[43] with the 6-31G* basis set.[44] At the optimized ground state geometries we performed TDDFT (MPW1K[45]/6-31G*) excited state calculations in gas phase as well as in various solvents (ethanol, acetonitrile), adopting the non-equilibrium Conductor-like Polarization Model, CPCM.[46]

5.2.3. Results and Discussions

Spectral and Electrochemical properties. The UV-Visible spectra of D-π-A organic dyes with a basic triphenylamine acting as donor and an acidic cyanoacetic acid acting as acceptor are highly dependent upon the degree of protonation.[37] Therefore the work up described in the experimental section and the solvent used for measuring the spectra can lead to a mixture of different protonated, deprotonated, neutral and zwitterionic species (see supporting information S1 and S2). In order to achieve comparable conditions not only in solution, but also on TiO_2 film, basic media were produced by adding small amounts of triethylamine, leading to only fully deprotonated dye species.

The absorption maxima of **MP124** and **MP-I-50** in solution are 460 nm and 480 nm respectively. The 20 nm red-shift for **MP-I-50** compared to **MP124** can be ascribed to the greater electron-donating ability of the two ethylenedioxythiophenes in the π-bridge of this dye. Upon anchoring the sensitizers to the TiO_2 electrode these absorption maxima remain the same indicating that the dyes on the film were mainly on deprotonated form. Furthermore, the broader absorption observed for anchored dye compared to dye in solution due to scatter and/or aggregation ensures efficient light harvesting of TiO_2 electrodes sensitized with these dyes.

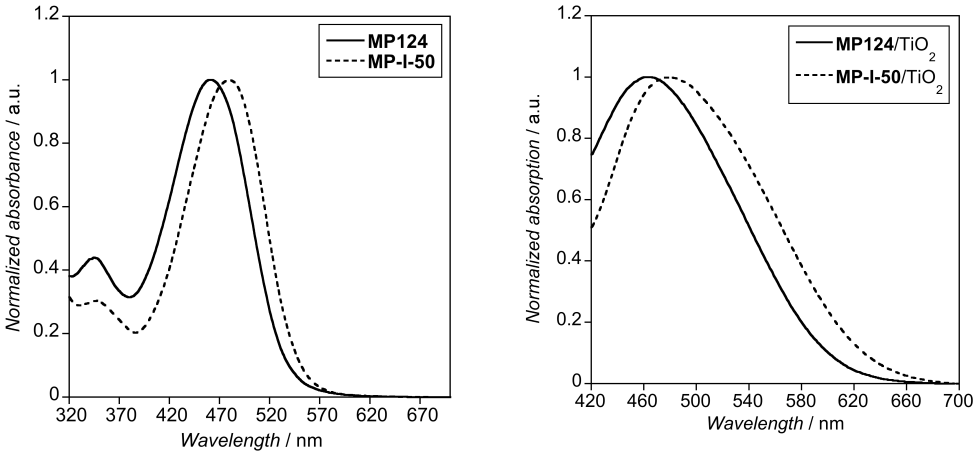

Figure 3. Normalized UV-Visible spectra of **MP124** (solid line) and **MP-I-50** (dash line) in ACN/^{t}BuOH with 2% TEA (*left*) and on nanocrystalline TiO_2 film (*right*).

The oxidation potentials for both dyes were acquired by square wave voltammetry (Figure 4) in DCM. The HOMO level was estimated from the equation E_{HOMO} (*vs* vacuum) = -4.88 – $E_{1/2}$(*vs* Fc/Fc$^+$).[47] The values of -5.08 eV and -5.02 eV vs vacuum for **MP124** and **MP-I-50**, respectively, ensure efficient regeneration by the iodide/tri-iodide red-ox electrolyte (E_{redox} = -4.75 eV) in functioning cells. This agrees with the difference observed in the molecular calculations where a difference of -0.08 (gas-phase) or -0.06 eV (ACN) was determined (Figure 5). The LUMO levels were described as $E_{LUMO} = E_{HOMO} + E_{0\text{-}0}$, where $E_{0\text{-}0}$ is the energy bandgap, estimated from the intersection of excitation and emission spectra. The experimental values of fluorescence and excitation intersection (see supporting information S3) gave an energy bandgap of 2.39 eV and 2.34 eV, leading a LUMO of -2.69 eV and -2.68 eV vs vacuum for **MP124** and **MP-I-50**, respectively. The calculated levels are positioned at about -2.30 eV in ACN, in reasonable agreement with the above data. Thus, the high LUMO energy level position respect the conduction band of TiO_2 (E_{TiO2} = -4.0 eV) show electron injection is energetically possible from the excited state of the each dye.

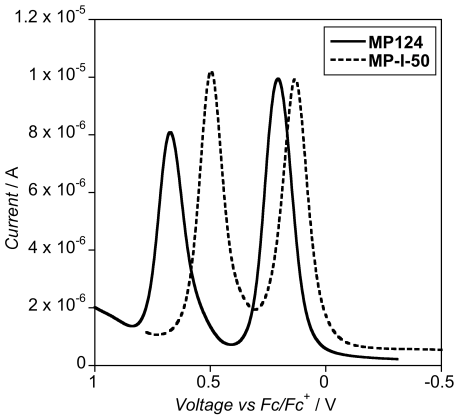

Figure 4. Squarewave voltammetry of **MP124** (solid line) and **MP-I-50** (dashed line) in DCM. Ferrocene was used as the internal reference standard. Experimental conditions: 0.1 M TBA·PF_6, Pt working electrode, Ag/AgCl reference electrode and Pt auxiliary electrode.

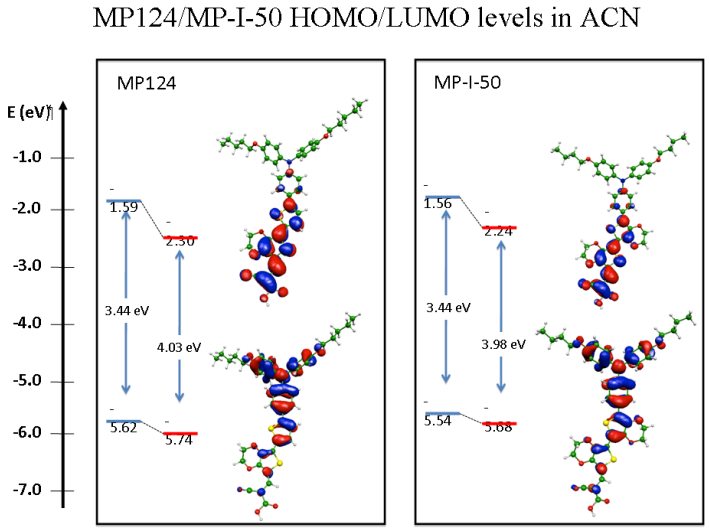

Figure 5. Calculated positions for the HOMO and LUMO levels in gas-phase and ACN for **MP124** and **MP-I-50**.

Photovoltaic Performance. Several conditions, such as dye solvent used, co-adsorbents and immersion time were tested on DSSC performance for both dyes, and only the most efficient results are summarized on Table 1. In addition, we found that if the immersion time exceeds the optimal, the current can drop by up to 50% (results not shown), which suggests that D-π-A type dyes can aggregate easily on the TiO_2 surface quenching dye excited states leading to poor photocurrent generation.

Table 1. Detailed photovoltaic parameters of best MP124 and MP-I-50 DSSC's in various solvents. The TiO2 films were immersed in a 0.3 mM dye solution containing 30 mM chenodeoxycholic acid (CDCA) at r.t. unless otherwise stated.

Dye	Solvent	Time	J_{sc} / mA cm^{-2}	V_{oc} / V	FF / %	η[a] / %
MP124	THF[b]	3 h	10.13	0.67	68	4.66 (5.61)
	ACN/^{t}BuOH 1:1	5 h	14.44	0.73	70	7.45 (9.12)
	Chlorobenzene[c]	6 h	14.63	0.68	68	6.76 (8.04)
MP-I-50	THF	3h	9.75	0.69	70	4.70 (5.60)
	ACN/^{t}BuOH 1:1	3 h	12.06	0.68	69	5.66 (6.57)
	Chlorobenzene	5 h	12.69	0.67	70	5.98 (6.76)

[a] The cells were measured at 1 sun 1.5 AM G with mask (area = 0.16 cm^2). In brackets, efficiencies at 1 sun without mask. [b] Without CDCA. [c] 3 mM CDCA used.

From the values listed in the table above solvent clearly plays a key role in determining DSSC performance. The best solar cell performances for **MP124** were obtained with ACN/^{t}BuOH, while in chlorobenzene and THF the efficiency drops by 10% and 30% respectively. However, there is no clear relationship between solvent used and DSSC performance for **MP-I-50**. We observed that for both dyes the optimized conditions for the best solar cells were almost the same.

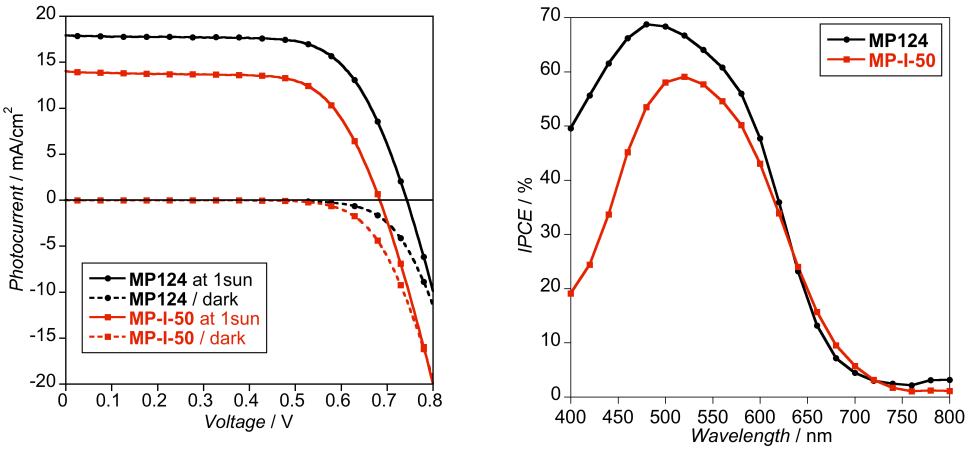

Figure 6. On the left, IV curves of **MP124** (black spheres) and **MP-I-50** (red squares) cells made using ACN/^{t}BuOH as sensitization solvent at 1 sun (solid line) and in the dark (dashed line). On the right, the photocurrent action spectra for the same cells. The cells were measured with mask (area = 0.16 cm^2).

Interfacial Charge Transfer Kinetics. To explain the substantial difference in device efficiency observed in Figure 6, we studied the interfacial charge transfer

processes in **MP124** and **MP-I-50** devices. The yield of electron injection from the excited state of the dye into the conduction band on the TiO_2 can be estimated using steady state fluorescence by comparing emission spectra of dye sensitized TiO_2 and Al_2O_3 films acquired under identical conditions (see supporting information S4). The conduction band of Al_2O_3 is higher than the LUMO of most dyes absorbing in the UV-visible so it acts as an electron injection barrier. Thus, we compared the emission of Al_2O_3 sensitized films, where injection is unlikely; with the TiO_2 dye sensitized films, where electron injection is efficient. It can provide an estimation of the yield of electron injection into the TiO_2 conduction band. In this way, an electron injection yield higher that 72% for both **MP124** and **MP-I-50** was estimated. This identical yield is not so surprising as the estimated LUMO energy levels for both dyes are the same and therefore electron injection is expected to have the same driving force for **MP124** and **MP-I-50** sensitized TiO_2.

Laser transient absorbance spectroscopy (TAS) has been described as a reliable method in order to monitor the charge recombination of electrons onto the TiO_2 with the oxidized dye.[48, 49] The inset of Figure 7 shows the dye cation spectrum at 1 μs after excitation of a 470 nm laser pulse where the maximum dye cation absorption is centered at 780 nm. The recombination kinetics were measured for both dyes at this wavelength and the corresponding decay was fitted to a stretched exponential function as shown in equation 1:[48]

$$\Delta O.D. = A_1 \cdot e^{-\left(t/\tau\right)^{\beta}} \qquad (1)$$

where A_1 is a constant, τ is the electron recombination lifetime and β is the deviation from fully mono-exponential decay dynamics as a consequence of the electron trapping/detrapping processes in the nanocrystalline TiO_2 film. As can be seen in Figure 7, charge recombination is almost identical for both samples with similar lifetimes recorded 227 μs and 850 μs for **MP124** and **MP-I-50**, respectively. Furthermore, β was found to be the same for both decays (0.18) indicating that recombination is dominated by electron transport in the TiO_2 film. Thus, the interfacial dynamics between the electrons at the TiO_2 and the oxidized dyes cannot explain the difference in efficiency obtained for the DSSC devices. We would like to point out that that the measurements using dyes without taking care of the protonation degree lead different results as shown in supporting information S5.

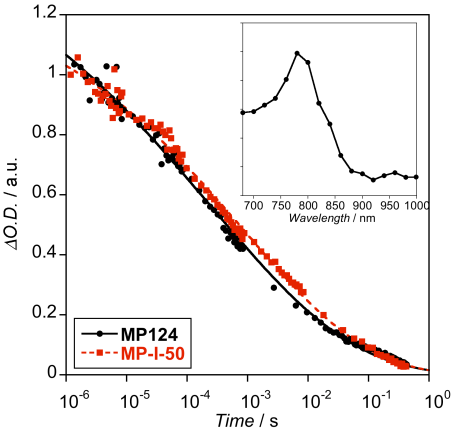

Figure 7. Charge recombination dynamics for a 4 μm think dye sensitized TiO_2 film (λ_{ex} = 0.5 a.u.) of **MP124** (black spheres) and **MP-I-50** (red squares). The films were excited with a 470 nm laser pulse and the decay kinetics were monitored at 780 nm. The inset shows the cation spectrum acquired at 1 μs following 470 nm laser excitation.

In order to evaluate the recombination of injected electrons with the oxidized redox electrolyte, transient photovoltage measurements (TPV) were employed.[50-52] These measurements are strongly dependent upon the accumulated charge at the tail of the density of states (DOS). This charge could be due to (a) the shift in the conduction band of TiO_2 (b) the different degree of surface blocking layer due to the dye packing and (c) the difference in the e^-_{TiO2}/electrolyte$^+$ recombination rate. Charge density as a function of cell voltage is shown in Figure 8 (left) indicating that the shift of conduction band is not significant so hypothesis (a) can be discarded. Hypothesis (b) can also be discarded due to the similar structure and size of both dyes, suggesting similar dye packing on the TiO_2 surface.[53] Therefore, we can assume that the differences in TPV measurements for devices based on **MP124** and **MP-I-50** are due to the differences in the e^-_{TiO2}/electrolyte$^+$ recombination rate in these cells, i.e. hypothesis (c). TPV transients were acquired at different charge densities and electron recombination lifetimes for each TPV are plotted together in Figure 8 (right). Slower recombination dynamics (i.e. longer electron lifetimes) were observed for **MP124**, which explains both the higher voltage for these devices compared with **MP-I-50** based devices. This difference in electron lifetime may be explained due to possible electrolyte/dye interactions. Several authors have reported that atoms such as oxygen and sulfur can bind I_3^- and/or I_2 species forming charge-transfer complexes.[54, 55] This can lead to a higher concentration of these species at the TiO_2 surface, catalyzing e^-_{TiO2}/electrolyte$^+$ recombination. Therefore, **MP-I-50**,

which contains two additional oxygen atoms in the π bridge compared to **MP124**, would be expected to better bind I_3^- and/or I_2 species leading to faster recombination pathways.

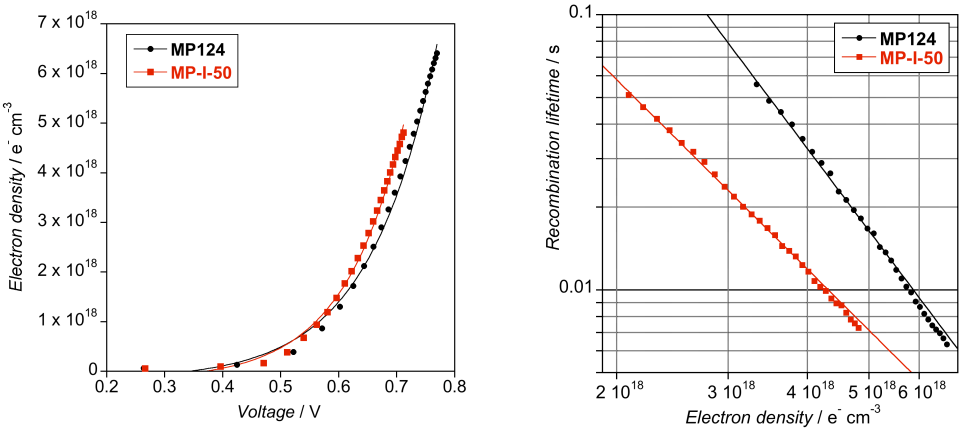

Figure 8. Charge extraction measurements showing electron density as a function of cell voltage (*left*) and Transient Photovoltage measurements (TPV) expressing electron recombination lifetime e^-_{TiO2}/electrolyte$^+$ as a function of cell electron density (*right*) for efficient **MP124** (black spheres) and **MP-I-50** (red squares) solar cells.

However, the higher photocurrent obtained for **MP124** cannot be explained by neither the electron injection nor recombination e^-_{TiO2}/dye$^+$ and e^-_{TiO2}/electrolyte$^+$. Therefore, we focused in the regeneration of oxidized dye by electrolyte process, which was measured in thin film solar cells was measured under 1 sun light irradiation, in a similar fashion to O'Regan and co-workers.[56] The resultant kinetics show a typical biphasic decay with the fast component due to loss of the dye cation signal due to regeneration of the oxidized dye while the slower long lived component is due to electrons in TiO_2 film.[57] As is shown in Figure 9, the regeneration is four times faster for **MP124** which can be explained because the HOMO energy level is lower for **MP124**, leading to higher driving force for the regeneration reaction. Thus, higher photocurrent for **MP124** can also be explained by more efficient regeneration kinetics.

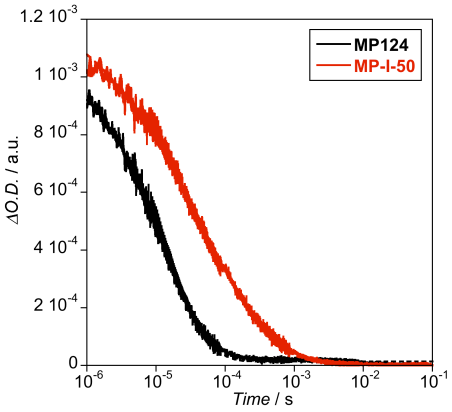

Figure 9. Transient absorption kinetics of thin film solar cells of **MP124** (black line) and **MP-I-50** (red line) recorded at 1 sun. After applying a pulse at 470 nm, the oxidized cation was monitored at 780 nm.

TAS measurements were also conducted monitoring at 980 nm (Figure 10). At this wavelength, the transient absorption intensity of the dye cation of both **MP124** and **MP-I-50** is lower and the contribution of the signal of the electrons in the TiO_2 conduction band is much bigger, as demonstrated previously.[56] The longer lived component of these transient absorption decays were compared with TPV decays at operational conditions of 1 sun. They can be seen to match quite well, indicating that the slower decay component of the transient absorption kinetics is due to the electrons in the conduction band of TiO_2 recombining with the red-ox electrolyte.

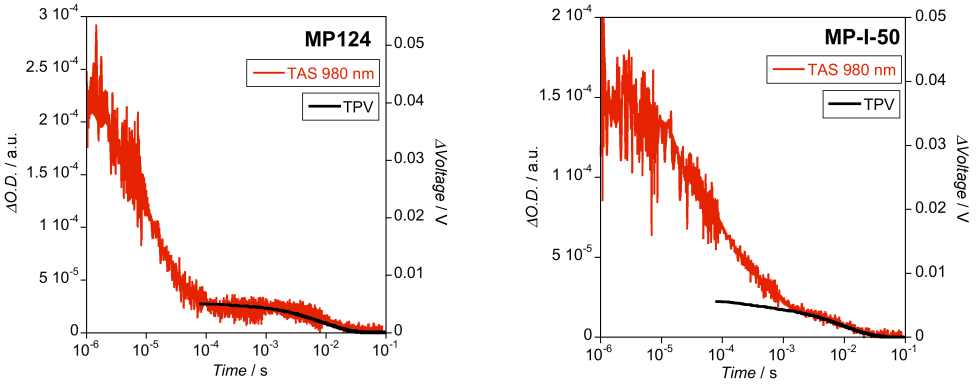

Figure 10. Comparison of transients of thin film cells of **MP124** (*left*) and **MP-I-50** (*right*) at 1 sun. After applying a laser pulse at 470 nm, TPV (black line) were recorded, followed by TAS (red line) at 980 nm.

5.2.4. Conclusions

In summary, we have designed and synthesized two push pull organic dyes featuring triphenylamine as donor and cyanoacrylic acid as acceptor. The π conjugated system was a binary spacer consisting of either two 3,4-ethylenedioxythiophene units, **MP-I-50**, or one 3,4-ethylenedioxythiophene and one thiophene unit, **MP124**. The DSSC performance gave, higher both photocurrent and voltage, for **MP124**, which was attributed to both higher regeneration dynamics and slower recombination e^-_{TiO2}/electrolyte$^+$ kinetics, respectively. The higher regeneration dynamics could be correlated with the molecular structure due to the lower HOMO position for **MP124**, which increased the regeneration driving force. The recombination of the electrons in the conduction band with oxidized electrolyte could be correlated due to the dye electrolyte interaction. **MP-I-50**, which contains several electronegative atoms, can interact with I_3^- and/or I_2 and increase their concentration close to the TiO_2 surface, increasing the recombination rate.

5.2.5. Acknowledgment

MP and JNC thank to the Spanish MICIIN for Ph.D. grant and Juan de la Cierva fellowship, respectively. NL thanks CTQ2009-07553BQU. We thank the BSC-RES for providing generous computational resources and the HPC2 that supported MCP visit to ICIQ. SRM thank the support from the Air Force Office of Scientific Research.

5.3. Supporting information

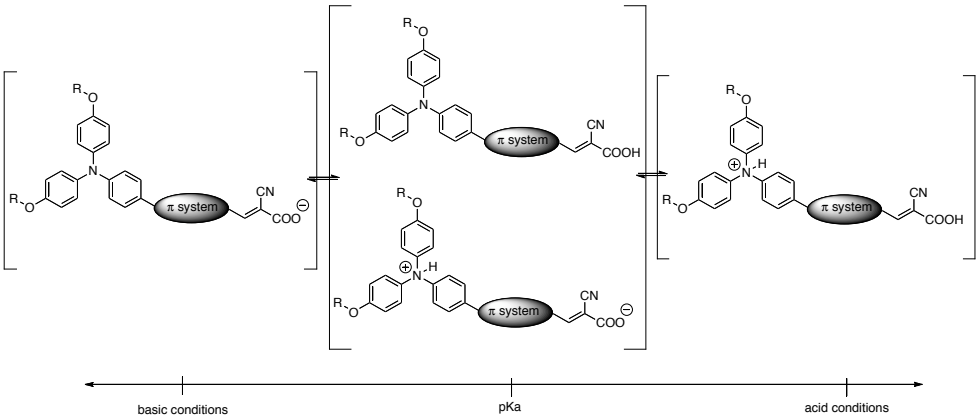

Figure S1. Schematic representation of the D - π - A dyes upon basic and acid conditions.

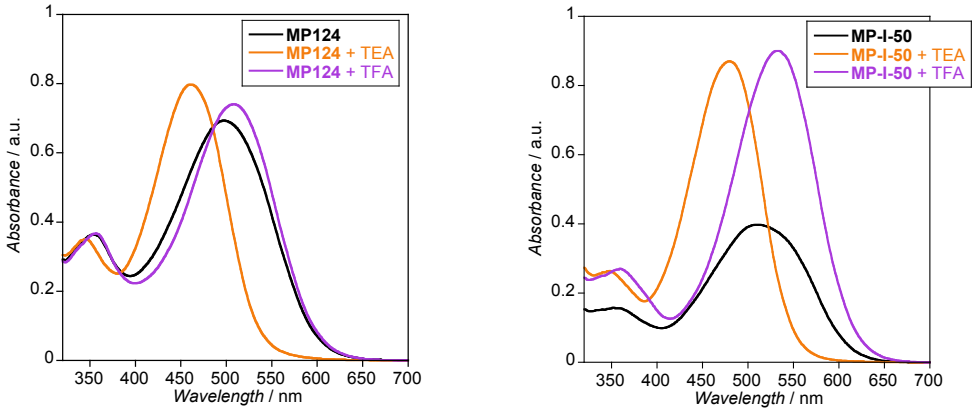

Figure S2. UV-Visible spectra in no modified (black line), basic (orange line) and acid (purple line) conditions for **MP124** (left) and **MP-I-50** (right) dyes in ACN/^{t}BuOH (1:1). Basic and acid conditions were obtained by adding 50 µL of triethylamine (TEA) and tryfluoroacetic acid (TFA), respectively.

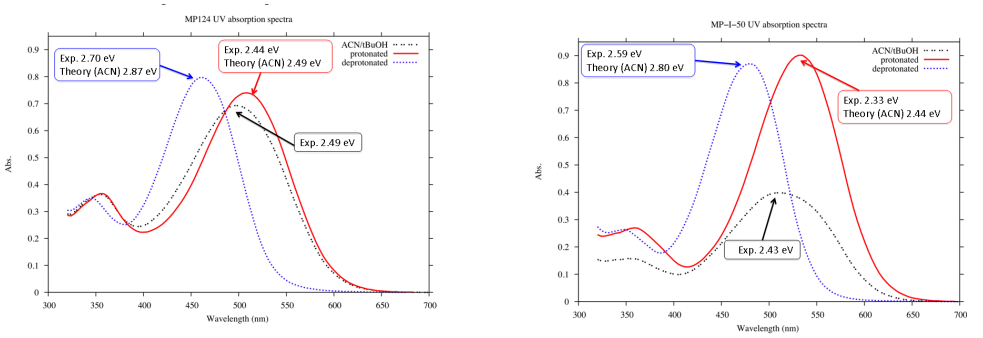

Figure S3. Experimental versus calculated normalized UV-Visible spectra of **MP124** and **MP-I-50** in ACN/^{t}BuOH together with the calculated values for the hydrogenated and dehydrogenated dyes.

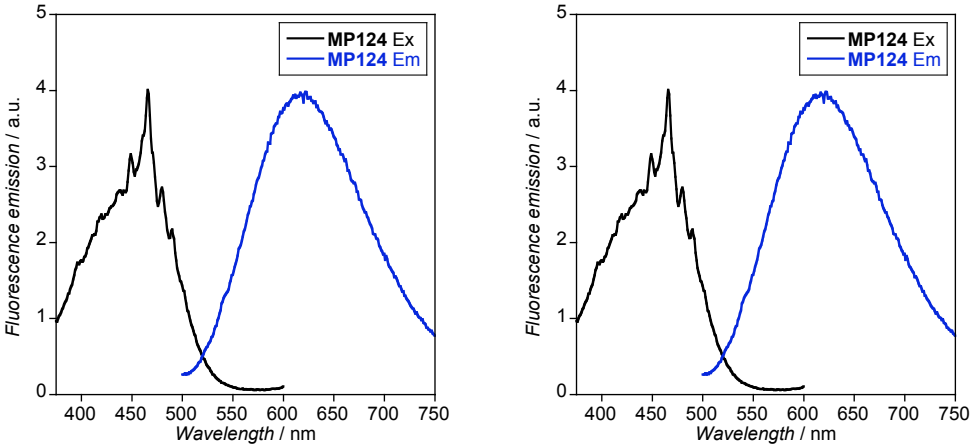

Figure S4. Excitation (black line) and fluorescence spectra (blue line) for **MP124** (left) and **MP-I-50** (right) dyes in ACN/^{t}BuOH (1:1). Both spectra were acquired under basic conditions described above.

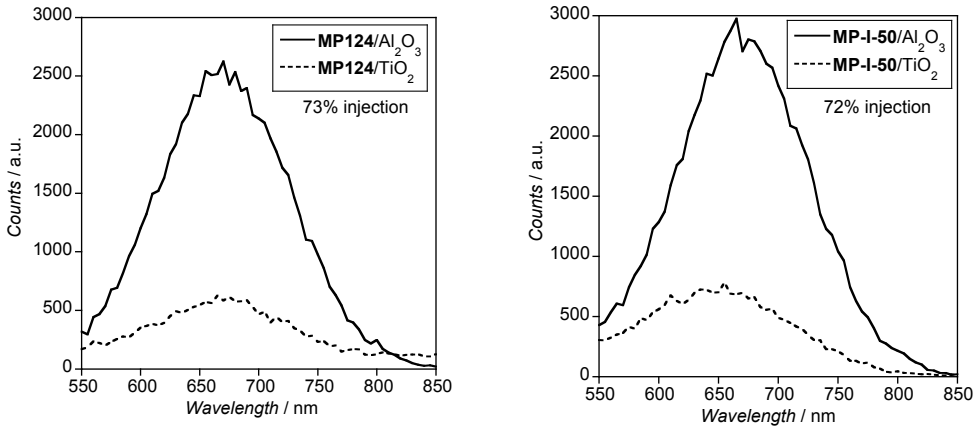

Figure S5. Emission spectra on Al_2O_3 (straight line) and TiO_2 (dash line) films for **MP124** (left) and **MP-I-50** (right) dyes. The emission spectra were measured using single photon counting apparatus under nanosecond laser irradiation at 405 nm for 15 minutes.

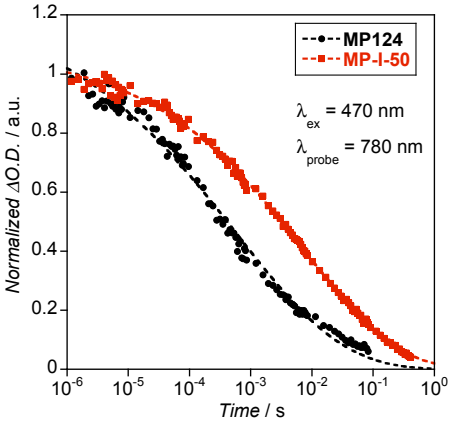

Figure S6. Transient absorption spectroscopy for sensitized 4 µm TiO_2 films sensitized **MP124** (black circles) and **MP-I-50** (red squares) with no triethylamine treatment. The data was fitted to eqn. 1. (dashed lines).

5.4. References

[1] R. Chen, X. Yang, H. Tian, X. Wang, A. Hagfeldt, L. Sun, *Chem. Mater.* **2007**, *19*, 4007.

[2] A. A. Kelkar, N. M. Patil, R. V. Chaudhari, *Tetrahedron Lett.* **2002**, *43*, 7143.

[3] K. Lancaster, S. A. Odom, S. C. Jones, S. Thayumanavan, S. R. Marder, J.-L. Bredas, V. Coropceanu, S. Barlow, *J. Am. Chem. Soc.* **2009**, *131*, 1717.

[4] N. Miyaura, A. Suzuki, *Chem. Rev.* **1995**, *95*, 2457.

[5] D. Milstein, J. K. Stille, *J. Am. Chem. Soc.* **1978**, *100*, 3636.

[6] N. Robertson, *Angew. Chem., Int. Ed.* **2006**, *45*, 2338.

[7] M. Gratzel, *Nature* **2001**, *414*, 338.

[8] B. O'Regan, M. Gratzel, *Nature* **1991**, *353*, 737.

[9] F. Gao, Y. Wang, D. Shi, J. Zhang, M. Wang, X. Jing, R. Humphry-Baker, P. Wang, S. M. Zakeeruddin, M. Gratzel, *J. Am. Chem. Soc.* **2008**, *130*, 10720.

[10] M. Grätzel, *Acc. Chem. Res.* **2009**, *42*, 1788.

[11] M. K. Nazeeruddin, P. Pechy, T. Renouard, S. M. Zakeeruddin, R. Humphry-Baker, P. Comte, P. Liska, L. Cevey, E. Costa, V. Shklover, L. Spiccia, G. B. Deacon, C. A. Bignozzi, M. Gratzel, *J. Am. Chem. Soc.* **2001**, *123*, 1613.

[12] A. Mishra, M. K. R. Fischer, P. Bauerle, *Angew. Chem., Int. Ed.* **2009**, *48*, 2474.

[13] S. Tatay, S. A. Haque, B. O'Regan, J. R. Durrant, W. J. H. Verhees, J. M. Kroon, A. Vidal-Ferran, P. Gavina, E. Palomares, *J. Mater. Chem.* **2007**, *17*, 3037.

[14] E. Palomares, M. V. Martinez-Diaz, S. A. Haque, T. Torres, J. R. Durrant, *Chem. Commun.* **2004**, 2112.

[15] D. Liu, R. W. Fessenden, G. L. Hug, P. V. Kamat, *J. Phys. Chem. B* **1997**, *101*, 2583.

[16] K. Hara, M. Kurashige, Y. Dan-oh, C. Kasada, A. Shinpo, S. Suga, K. Sayama, H. Arakawa, *New J. Chem.* **2003**, *27*, 783.

[17] Z.-S. Wang, Y. Cui, K. Hara, Y. Dan-oh, C. Kasada, A. Shinpo, *Adv. Mater.* **2007**, *19*, 1138.

[18] S. Ito, H. Miura, S. Uchida, M. Takata, K. Sumioka, P. Liska, P. Comte, P. Pechy, M. Gratzel, *Chem. Commun.* **2008**, 5194.

[19] S. Ito, S. M. Zakeeruddin, R. Humphry-Baker, P. Liska, R. Charvet, P. Comte, M. K. Nazeeruddin, P. PÈchy, M. Takata, H. Miura, S. Uchida, M. Gratzel, *Adv. Mater.* **2006**, *18*, 1202.

[20] M. Planells, F. J. Cespedes-Guirao, A. Forneli, A. Sastre-Santos, F. Fernandez-Lazaro, E. Palomares, *J. Mater. Chem.* **2008**, *18*, 5802.

[21] Y. Shibano, T. Umeyama, Y. Matano, H. Imahori, *Org. Lett.* **2007**, *9*, 1971.

[22] C. Li, J.-H. Yum, S.-J. Moon, A. Herrmann, F. Eickemeyer, N. G. Pschirer, P. Erk, J. Schoneboom, K. Mullen, M. Gratzel, M. K. Nazeeruddin, *ChemSusChem* **2008**, *1*, 615.

[23] M. Guo, P. Diao, Y.-J. Ren, F. Meng, H. Tian, S.-M. Cai, *Sol. Energy Mater. Sol. Cells* **2005**, *88*, 23.

[24] X. Ma, J. Hua, W. Wu, Y. Jin, F. Meng, W. Zhan, H. Tian, *Tetrahedron* **2008**, *64*, 345.

[25] Y. Chen, Z. Zeng, C. Li, W. Wang, X. Wang, B. Zhang, *New J. Chem.* **2005**, *29*, 773.

[26] W. M. Campbell, A. K. Burrell, D. L. Officer, K. W. Jolley, *Coord. Chem. Rev.* **2004**, *248*, 1363.

[27] W. M. Campbell, K. W. Jolley, P. Wagner, K. Wagner, P. J. Walsh, K. C. Gordon, L. Schmidt-Mende, M. K. Nazeeruddin, Q. Wang, M. Gratzel, D. L. Officer, *J. Phys. Chem. C* **2007**, *111*, 11760.

[28] K. Sayama, S. Tsukagoshi, T. Mori, K. Hara, Y. Ohga, A. Shinpou, Y. Abe, S. Suga, H. Arakawa, *Sol. Energy Mater. Sol. Cells* **2003**, *80*, 47.

[29] T. Geiger, S. Kuster, J.-H. Yum, S.-J. Moon, M. K. Nazeeruddin, M. Gratzel, F. Nueesch, *Adv. Funct. Mater.* **2009**, *19*, 2720.

[30] J.-J. Cid, M. Garcia-Iglesias, J.-H. Yum, A. Forneli, J. Albero, E. Martinez-Ferrero, P. Vazquez, M. Gratzel, M. K. Nazeeruddin, E. Palomares, T. Torres, *Chem.--Eur. J.* **2009**, *15*, 5130.

[31] W. Zeng, Y. Cao, Y. Bai, Y. Wang, Y. Shi, M. Zhang, F. Wang, C. Pan, P. Wang, *Chem. Mater.* **2010**, *22*, 1915.

[32] G. Zhang, H. Bala, Y. Cheng, D. Shi, X. Lv, Q. Yu, P. Wang, *Chem. Commun.* **2009**, 2198.

[33] H. Qin, S. Wenger, M. Xu, F. Gao, X. Jing, P. Wang, S. M. Zakeeruddin, M. Gratzel, *J. Am. Chem. Soc.* **2008**, *130*, 9202.

[34] M. K. R. Fischer, S. Wenger, M. Wang, A. Mishra, S. M. Zakeeruddin, M. Grätzel, P. Bäuerle, *Chem. Mater.* **2010**, *22*, 1836.

[35] J.-H. Yum, D. P. Hagberg, S.-J. Moon, K. M. Karlsson, T. Marinado, L. Sun, A. Hagfeldt, M. K. Nazeeruddin, M. Gratzel, *Angew. Chem., Int. Ed.* **2009**, *48*, 1576.

[36] H. Choi, C. Baik, S. O. Kang, J. Ko, M.-S. Kang, M. K. Nazeeruddin, M. Gratzel, *Angew. Chem., Int. Ed.* **2008**, *47*, 327.

[37] D. P. Hagberg, T. Marinado, K. M. Karlsson, K. Nonomura, P. Qin, G. Boschloo, T. Brinck, A. Hagfeldt, L. Sun, *J. Org. Chem.* **2007**, *72*, 9550.

[38] Y. Tachibana, J. E. Moser, M. Gratzel, D. R. Klug, J. R. Durrant, *J. Phys. Chem.* **1996**, *100*, 20056.

[39] S. A. Haque, Y. Tachibana, R. L. Willis, J. E. Moser, M. Gratzel, D. R. Klug, J. R. Durrant, *J. Phys. Chem. B* **2000**, *104*, 538.

[40] B. C. O'Regan, S. Scully, A. C. Mayer, E. Palomares, J. Durrant, *J. Phys. Chem. B* **2005**, *109*, 4616.

[41] B. C. O'Regan, K. Bakker, J. Kroeze, H. Smit, P. Sommeling, J. R. Durrant, *J. Phys. Chem. B* **2006**, *110*, 17155.

[42] Gaussian 09, Revision **A.1**; M. J. Frisch, G. W. Trucks, H. B. Schlegel, G. E. Scuseria, M. A. Robb, J. R. Cheeseman, G. Scalmani, V. Barone, B. Mennucci, G. A. Petersson, H. Nakatsuji, M. Caricato, X. Li, H. P. Hratchian, A. F. Izmaylov, J. Bloino, G. Zheng, J. L. Sonnenberg, M. Hada, M. Ehara, K. Toyota, R. Fukuda, J. Hasegawa, M. Ishida, T. Nakajima, Y. Honda, O. Kitao, H. Nakai, T. Vreven, J. A. Montgomery, J. E. Peralta, F. Ogliaro, M. Bearpark, J. J. Heyd, E. Brothers, K. N. Kudin, V. N. Staroverov, R. Kobayashi, J. Normand, K. Raghavachari, A. Rendell, J. C. Burant, S. S. Iyengar, J. Tomasi, M. Cossi, N. Rega, J. M. Millam, M. Klene, J. E. Knox, J. B. Cross, V. Bakken, C. Adamo, J. Jaramillo, R. Gomperts, R. E. Stratmann, O. Yazyev, A. J. Austin, R. Cammi, C. Pomelli, J. W. Ochterski, R. L. Martin, K. Morokuma, V. G. Zakrzewski, G. A. Voth, P. Salvador, J. J. Dannenberg, S. Dapprich, A. D. Daniel, O. Farkas, J. B. Foresman, J. V. Ortiz, J. Cioslowski, D. J. Fox; Gaussian, Inc.; Wallingford CT; **2009**

[43] P. J. Stephens, F. J. Devlin, C. F. Chabalowski, M. J. Frisch, *J. Phys. Chem.* **1994**, *98*, 11623.

[44] V. A. Rassolov, J. A. Pople, M. A. Ratner, T. L. Windus, *J. Chem. Phys.* **1998**, *109*, 1223.

[45] B. J. Lynch, P. L. Fast, M. Harris, D. G. Truhlar, *J. Phys. Chem. A* **2000**, *104*, 4811.

[46] M. Cossi, N. Rega, G. Scalmani, V. Barone, *J. Comput. Chem.* **2003**, *24*, 669.

[47] B. A. Jones, A. Facchetti, M. R. Wasielewski, T. J. Marks, *J. Am. Chem. Soc.* **2007**, *129*, 15259.

[48] J. N. Clifford, E. Palomares, M. K. Nazeeruddin, M. Gratzel, J. Nelson, X. Li, N. J. Long, J. R. Durrant, *J. Am. Chem. Soc.* **2004**, *126*, 5225.

[49] S. A. Haque, E. Palomares, B. M. Cho, A. N. M. Green, N. Hirata, D. R. Klug, J. R. Durrant, *J. Am. Chem. Soc.* **2005**, *127*, 3456.

[50] A. Reynal, A. Forneli, E. Martinez-Ferrero, A. Sanchez-Diaz, A. Vidal-Ferran, B. C. O'Regan, E. Palomares, *J. Am. Chem. Soc.* **2008**, *130*, 13558.

[51] M. Planells, A. Forneli, E. Martinez-Ferrero, A. Sanchez-Diaz, M. A. Sarmentero, P. Ballester, E. Palomares, B. C. O'Regan, *Appl. Phys. Lett.* **2008**, *92*, 153506/1.

[52] B. C. O'Regan, I. Lopez-Duarte, M. V. Martinez-Diaz, A. Forneli, J. Albero, A. Morandeira, E. Palomares, T. Torres, J. R. Durrant, *J. Am. Chem. Soc.* **2008**, *130*, 2906.

[53] T. Marinado, K. Nonomura, J. Nissfolk, M. K. Karlsson, D. P. Hagberg, L. Sun, S. Mori, A. Hagfeldt, *Langmuir* **2009**, *26*, 2592.

[54] B. C. O'Regan, K. Walley, M. Juozapavicius, A. Anderson, F. Matar, T. Ghaddar, S. M. Zakeeruddin, C. Klein, J. R. Durrant, *J. Am. Chem. Soc.* **2009**, *131*, 3541.

[55] M. Miyashita, K. Sunahara, T. Nishikawa, Y. Uemura, N. Koumura, K. Hara, A. Mori, T. Abe, E. Suzuki, S. Mori, *J. Am. Chem. Soc.* **2008**, *130*, 17874.

[56] A. Y. Anderson, P. R. F. Barnes, J. R. Durrant, B. C. O'Regan, *J. Phys. Chem. C* **2010**, *114*, 1953.

[57] I. Montanari, J. Nelson, J. R. Durrant, *J. Phys. Chem. B* **2002**, *106*, 12203.

UNIVERSITAT ROVIRA I VIRGILI
DESIGN AND SYNTHESIS OF ORGANIC SENSITIZERS FOR DYE SOLAR CELLS: MOLECULAR STRUCTURE VS DEVICE PERFORMANCE
Miquel Angels Planells Dillundé
ISBN:978-84-693-8861-7/DL:T.1946-2010

UNIVERSITAT ROVIRA I VIRGILI
DESIGN AND SYNTHESIS OF ORGANIC SENSITIZERS FOR DYE SOLAR CELLS: MOLECULAR STRUCTURE VS DEVICE PERFORMANCE
Miquel Angels Planells Dillundé
ISBN:978-84-693-8861-7/DL:T.1946-2010

6. Supramolecular Chemistry Applied to DSSC

TOC Figure

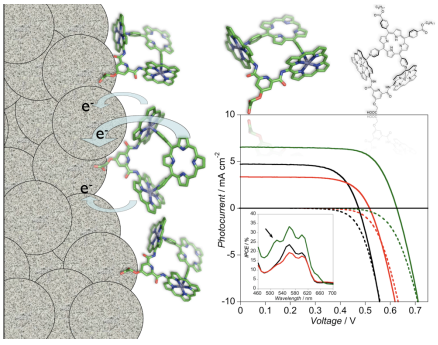

Submitted to *Energy Env. Sci.*

UNIVERSITAT ROVIRA I VIRGILI
DESIGN AND SYNTHESIS OF ORGANIC SENSITIZERS FOR DYE SOLAR CELLS: MOLECULAR STRUCTURE VS DEVICE PERFORMANCE
Miquel Angels Planells Dillundé
ISBN:978-84-693-8861-7/DL:T.1946-2010

6.1. General Introduction

Supramolecular chemistry is the area of chemistry which studies the assembly and properties of complexes which are composed of non-covalent interactions between their constituent atoms and/or molecules. These forces include interactions such as hydrogen bonding, π - π stacking, hydrophobic interactions, metal-ligand coordination bonds, van der Waals forces and electrostatic interactions.[1] In nature, supramolecular chemistry plays an important role in several well known systems. An obvious example is Photosystem II, which consists of a reaction center of donor-acceptor moieties which are connected through supramolecular interactions. Following absorption of a photon of energy, charge separation occurs at the reaction centre and the charge separated distance is increased through a series of antenna systems. In this way plants and certain bacteria are able to convert solar energy into chemical energy. Therefore, mimicking Photosystem II for light harvesting and energy generation proposes has attracted much attention from the scientific community.[2]

There are many examples of the self assembly of donor and acceptor macromolecules in solution, employing porphyrins, perylenes, fullerenes, etc.[3-8] In fact, their electron transfer processes have been extensively studied because they have an extraordinary resemblance to processes that take place in biological systems.[9] Several examples have been carried out in order to apply supramolecular chemistry to the photovoltaic area, mainly focused on OPVs.[10]

Supramolecular interactions involving photosensitizers anchored onto TiO_2 can be exploited in the DSSC field, providing further improvements to solar cell performance. In spite of this, only a few examples are reported in the literature which can be divided into the following categories: **1**) Supramolecular dye sensitizer encapsulation by cyclodextrines, **2**) host-guest receptors attached to photosensitizers and **3**) self assembly of dyes onto TiO_2 surface through supramolecular interactions.

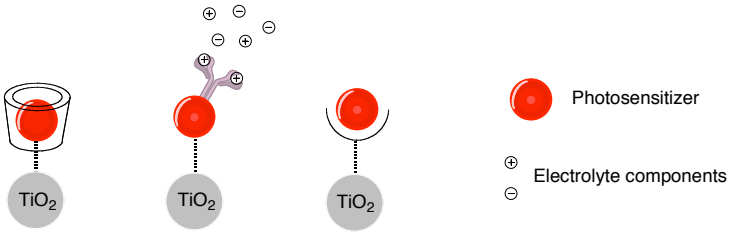

Figure 6.1 - Different approaches of supramolecular chemistry in the DSSC field: dye encapsulation (*left*), attached host guest receptor (*center*) and self-assembly on TiO_2 surface (*right*).

Large macromolecules can be used to encapsulate a dye sensitizer molecule. This approach results in the physical separation between the photosensitizer and the TiO_2 surface which can retard electron recombination between photo-injected electrons and dye cations on the TiO_2 surface. Furthermore, the macrocycle can act as a barrier avoiding dye degradation by the electrolyte components. As an illustrative example, Haque *et al.*[11] developed a rotaxane complex based on an azobenzene derivative dye as the thread and a *α*-cyclodextrine as the macrocycle (Figure 6.2). Transient absorption studies revealed that the supramolecular interaction retards electron recombination with the oxidized dye significantly when compared with the non complexed azobenzene based dye. Recently, Choi *et al.*[12] reported a donor - acceptor π conjugated dye encapsulated with a *β*-cyclodextrine. The rotaxane obtained reduced electron recombination with the oxidized electrolyte as well as improving dye stability (Figure 6.2). However, the two-step TiO_2 sensitization of firstly *β*-cyclodextrine, and subsequently the photosensitizer could not clarify the percentage of complexed and uncomplexed molecules present on the TiO_2 surface.

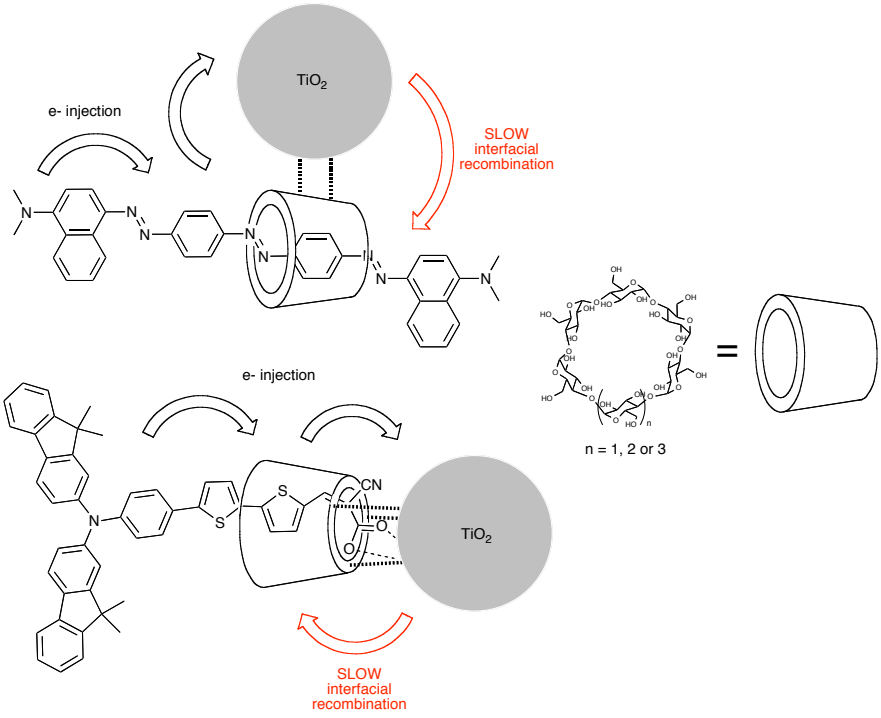

Figure 6.2 - Examples of rotaxanes, which consist in a supramolecular assembly of a cyclodextrine and an organic dye, applied to DSSC.

UNIVERSITAT ROVIRA I VIRGILI
DESIGN AND SYNTHESIS OF ORGANIC SENSITIZERS FOR DYE SOLAR CELLS: MOLECULAR STRUCTURE VS DEVICE PERFORMANCE
Miquel Angels Planells Dillundé
ISBN:978-84-693-8861-7/DL:T.1946-2010

Photosensitizers with attached supramolecular host-guest receptors have been mainly used for the recognition and for the control of electrolyte components in DSSC. It is well known that cations, anions and other additives present in the electrolyte can modify the conduction band edge of nanocrystalline TiO_2, as explained in Chapter 1.2. Snaith *et at*.[13, 14] designed a ruthenium complex with two tetraetyleneglycol derivative chains, **K51**, capable of complexing lithium cations (Figure 6.3). The presence of the lithium binding moieties positioned far from the TiO_2 surface resulted in an upward shift of the conduction band edge, since less lithium ions percolated onto the nanocrystalline film. **K51** photovoltaic devices achieved an impressive increase of 125 mV in V_{oc} compared to devices made with the reference **Z907** dye.

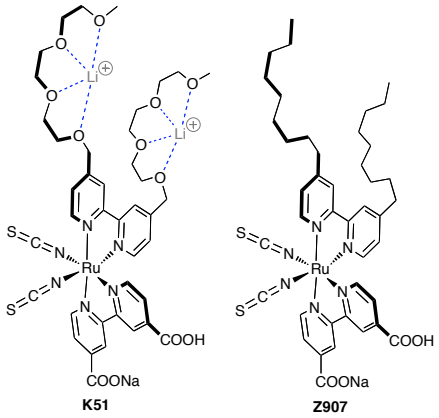

Figure 6.3 - Molecular structure of **K51**, a supramolecular sensitizer designed to complex Li^+ ions present in electrolyte in DSSC. **Z907** was the reference compound used in the study.

TiO_2 sensitization through supramolecular interactions was reported recently by D'Souza *et al*.[15] Their approach consisted of an imidazole derivative anchored onto TiO_2 nanoparticles and the subsequent self-assembly of a zinc porphyrin dye through a metal - ligand interaction (Figure 6.4). Although the zinc porphyrin was not anchored directly to the TiO_2, this system showed moderate efficiency. However, the stepwise sensitization of the TiO_2 films resulted in a mixture of complexed and non-complexed imidazole derivative ligands on the surface. In this sense, no control over the TiO_2 surface components was attained, thereby, the understanding of this system reminds limited.

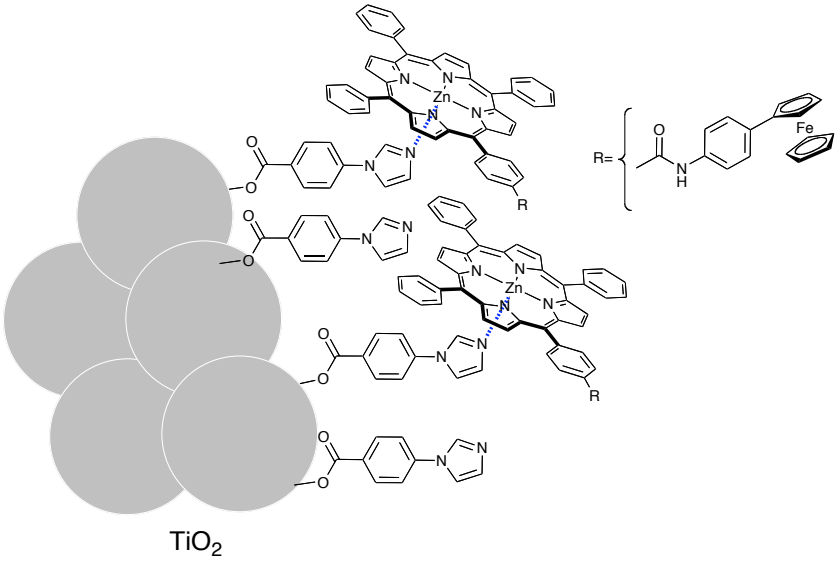

Figure 6.4 - Schematic representation of the supramolecular system described by D'Souza *et al*.

In this chapter, a bipyridyl free base porphyrin and a biszincporphyrin have been designed and synthesized with the aim of being able to self-assemble together on the TiO_2 surface. In this system, both units act as photoactive centers and, therefore an increase of the light harvesting through supramolecular interaction is expected. In addition, non-photoactive bipyridyl unit, developed by Prof. Ballester[5] was assembled with biszincporphyrin to act as the reference sample.

6.2. *Paper VI*: Heterosupramolecular Self-Assembly of a Functional Trisporphyrin Complex on Dye-Sensitised Solar Cells

Miquel Planells,[a] Laia Pellejà,[a] Pablo Ballester,[a,b,*] and Emilio Palomares [a,b,*]

[a] Institute of Chemical Research of Catalonia (ICIQ), Avda. Països Catalans,16, Tarragona, Spain. Fax: 34 977 920 224; Tel: 34 977 920 241;Corresponding Author E-mail: epalomares@iciq.es; pballester@iciq.es

[b] Catalan Institution for Research and Advanced Studies (ICREA). Spain.

Abstract: We describe the synthesis and the spectroscopic characterization of a supramolecular trisporphyrin complex on mesoporous TiO_2 films. The dye sensitised solar cell performance as well as the interfacial charge transfer kinetics have been evaluated. A large improvement has been achieved with the supramolecular assembly when compared with the individual molecular components when assembled on photovoltaic devices. The advantage of the supramolecular system is both: the improvement of the photocurrent and the retardation of the wasteful recombination dynamics between the photo-injected electrons at the TiO_2 and the oxidised electrolyte.

6.2.1. Introduction

The synthesis of multi-chromophores architectures using supramolecular self-assembly processes constitutes a promising alternative and integration to simply covalent systems. In this sense, many artificial multiporphyrin “non-covalent” assemblies have already been prepared in homogeneous conditions (in solution) through metal mediated interactions. Some of these systems have been idealized as bio-mimicking systems of one of the most superb biological complexes: the photo-system II (PSII).[6, 16-20] Furthermore, the electron and energy transfer processes that take place within these supramolecular assemblies have been also studied in great detail.[9, 21] The longstanding proposed application of supramolecular assemblies constituted by photo- and/or electro-active components have been the conversion of the energy stored in their excited or charge separated state into electrical (photovoltaic) or chemical (hydrogen) power. To achieve this goal, it is mandatory

that the supramolecular assemblies can be incorporated onto solid films of functional molecular devices, such as dye-sensitised solar cells (DSSC).

DSSC have attracted much interest to the scientific community since the breakthrough paper reported by O'Regan and Gratzel.[22] To date, ruthenium polypyridyl sensitisers have given the best light-to-energy conversion efficiencies.[23, 24] However, ruthenium is a costly element and their complexes show moderate absorption extinction coefficients ($\varepsilon \sim 18000\ cm^{-1}\ M^{-1}$), which would result in thicker and highly priced devices. Therefore, several efforts have been focused in developing new metal free sensitizers in order to reduce the solar cell cost, obtain thinner devices and improve the voltage.[25] A detailed description of the major organic sensitizers has been reviewed recently.[26] Those chromophores can be anchored onto metal oxide particles alone, or in a mixture of two (cocktail) but rarely employing supramolecular assemblies. This approach could provide further improvements of solar cell performance. Despite this, few examples are reported in the literature employing DSSC and supramolecular chemistry, which can be classified in: (*a*) the encapsulation of dye sensitizer by cyclodextrines forming rotaxanes,[11, 12] (*b*) the attachment of a host guest receptor to the dye, which is selective to electrolyte components,[13, 14, 27] and (*c*) the self-assembly of photoactive molecules onto TiO_2 surface.[15]

Herein, we describe the construction of a supramolecular trisporphyrin assembly on mesoporous nanocrystalline TiO_2 films by means of a step-wise self-assembly supramolecular process. The system titanium dioxide – zinc bisporphyrin – free base porphyrin (TiO_2 – ZnP – FbP) was reported previously by Koehorst *et al.*[28] using a covalently bounded porphyrin heterodimers. This approach was described as an unlikely system for DSSC due to a competition between electron injection and energy transfer process (Figure 1). In spite of this, we demonstrated that the above mentioned competition is not relevant when supramolecular assembly is used instead of covalently porphyrin architectures. Furthermore, DSSC performance and its interfacial charge transfer kinetics have been measured for plain zinc bisporphyrin, **MP216**, and its assembled trisporphyrin, **MP216**+**MP151**, as well as with reference supramolecular assembly involving a non-photoactive unit, **MP216**+**BP**. (Figure 2). We also would like to notice that our aim is to proof the principle and not to optimize the device efficiency that for obvious reasons is still higher when using ruthenium polypyridyl complexes.[29] The optimization of supramolecular systems for high efficiency DSSC is out of the scope of this work which is solely focussed on: (*i*) how to assemble individual molecular entities onto mesoporous nanocrystalline TiO_2 films

through supramolecular binding, (*ii*) the total characterization of the formation of the supramolecular complex, (*iii*) its application in DSSC and (*iv*) the complete characterization of the charge transfer processes in order to elucidate the reasons for the large improvement obtained with the supramolecular device.

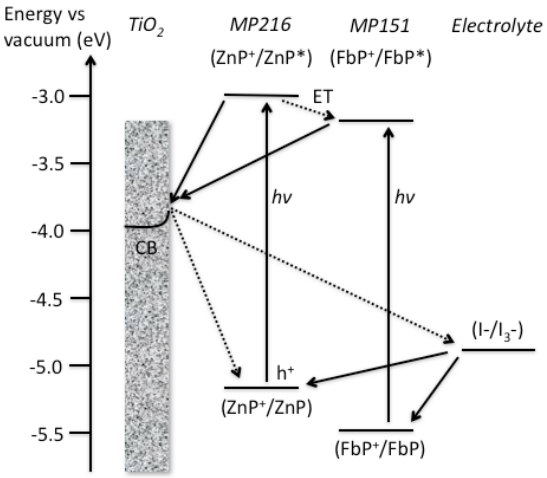

Fig. 1 Schematic representation of DSSC processes for the supramolecular assembly **MP216+MP151**. Straight and dashed lines denote the desired and undesired processes, respectively. ET denotes energy transfer and h+ the hole position after electron injection.

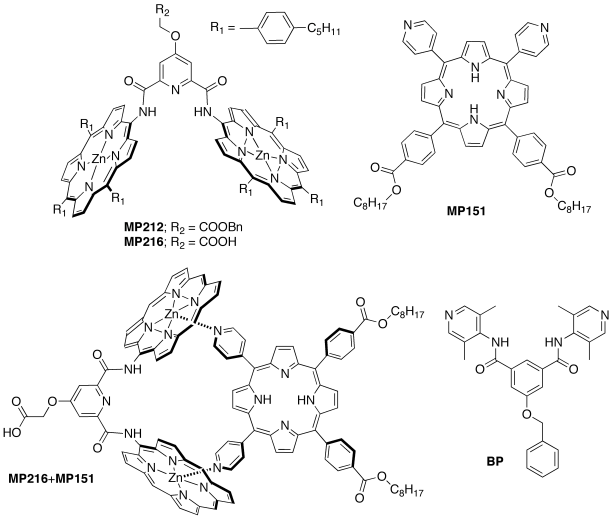

Fig. 2 Chemical structures of the molecules and its supramolecular assembly used in this study. The *meso* phenyl groups are omitted in assembly **MP216+MP151**.

6.2.2. Experimental section

Synthesis. The synthesis of zinc bisporphyrin **MP212** and **MP216** as well as bipyridyl free base porphyrin **MP151** were carried out using straightforward standard procedures (see supporting information).[5, 30, 31] Long alkyl chains were attached to **MP151** in order to increase the porphyrin solubility in common organic solvents and, thus, avoid possible purification issues. The synthesis of **BP** was described by Ballester *et al.* and can be found elsewhere.[5]

Optical and Spectroscopic Measurements. UV-Visible spectra were recorded using a 1 cm path length quartz cell on a Shimadzu© UV spectrophotometer 1700. The laser transient absorption spectroscopy (L-TAS) measurements were carried out by the same procedure as Durrant *et al.*[32] employing a PTI nitrogen dye laser as excitation source and a 150 W tungsten lamp is used as light probe. The charge extraction and transient photovoltage (TPV) decay were carried out with a system set-up as previously reported by O'Regan *et al.*[33]

Device preparation. In the present work two different types of devices are utilized depending on the measurements being conducted. Highly transparent thin film devices were utilized for TAS experiments. These devices were made using 9 µm thick films and sensitized with the porphyrin dyes until the absorbance reach 0.4 a.u. at the maximum absorption wavelength. On the other hand, for optimized cell efficiencies, devices were made using 13 µm thick films consisting of a layer of 9 µm of 20 nm TiO_2 nanoparticles (Dyesol© paste) and a layer of 4 µm of 400 nm TiO_2 particles (scatter layer). Prior to the deposition of the TiO_2 paste the conducting glass substrates were immersed in a solution of $TiCl_4$ (40 mM) for 30 minutes and then dried. The TiO_2 nanoparticle paste was deposited onto a conducting glass substrate (Hartford Glass inc. with 15 Ω cm^{-2} resistance) using the screen printing technique. The TiO_2 electrodes were gradually heated under an airflow at 325 ºC for 5 min, 375 ºC for 5 min, 450 ºC for 15 min and 500 ºC for 15 min. The heated TiO_2 electrodes were immersed again in a solution of $TiCl_4$ (40 mM) at 70 ºC for 30 min and then washed with ethanol. The electrodes were heated again at 500 ºC for 30 min and cooled before dye adsorption. For the thin film devices the area was 1 cm^2 while for the optimized thick film DSSC the active area was 0.16 cm^2. The counter electrode was made by spreading a 10 mM solution of H_2PtCl_6 in ethanol onto a conducting glass substrate with a small hole to allow the introduction of the liquid electrolyte using vacuum, followed by heating at 390 ºC for 15 minutes. A **MP216** dye solution of 300 µM in chlorobenzene was prepared and the film immersed at room temperature

for 24 hours. For the supramolecular assemblies **MP216**+**BP** and **MP216**+**MP151**, a 300 μM chlorobenzene solution that contain a mixture of zinc bisporphyrin **MP216** and its bipyridyl complementary moiety was prepared and the film immersed for 24 hours. It is worth to notice that the stepwise supramolecular assembly can also be attained by the subsequent film immersion into a **MP216** solution for 24 hours and into a **BP** or **MP151** solution for an additional 48 hours, attaining identical solar cell performance in both procedures. The sensitized electrodes were then washed with ethanol and dried under air. Finally, the working and counter electrodes were sandwiched together using a thin thermoplastic (Surlyn) frame that melts at 100 ºC. Electrolyte **LP2** consisted of 0.6 M butyl-methyl imidazolium iodide (BMII), 0.1 M lithium iodide and 0.05 M iodine in a mixture of acetonitrile/valeronitrile (1:1). In this case, well-known additive *tert*-butylpyridine was not used because it could compete with the bipyridyl ligand in the supramolecular assembly, affecting the solar cell performance.

Device Characterization. The photovoltaic measurements were carried out with a 150W solar simulator from ABET© Technologies with the appropriated set of filters for the correct simulation of the 1.5 AM G solar spectrum. The incident light power was measured at 1000 W/m^2 with a calibrated Silicon photodiode, which the spectral sensitivity was closed to the devices under test. The applied potential and cell current were measured with a Keithley model 2400 digital source meter. The current to voltage (I–V curve) was measured automatically with home-built Labview© software. Incident photon to current conversion efficiency (IPCE) measurements were carried out with a home made set up, consisting in a 150 W Oriel Xenon lamp, a motorized monochromator and a Keithley 2400. An integrating sphere was employed in order to provide homogeneous monochromatic light distribution over active area of the devices. In addition, photocurrent and irradiated light intensity were measured simultaneously.

6.2.3. Results and discussion

The homogeneous self-assembly of zinc bisporphyrin **MP212** induced by coordination with bipyridyl free base porphyrin **MP151** was first probed using UV-Visible titrations in chloroform solution. The incremental additions of **MP151** to a $CHCl_3$ solution of **MP212** (2×10^{-5} M) produce a small but detectable red shift of the zinc bisporphyrin Q bands. In addition, two new bands centered at 515 nm and 650 nm appeared due to free base porphyrin contribution (Figure 3). The fit of the titration

data, using SPECFIT© software,[34] to a 1:1 binding model allowed us to calculate the stability constant value $K_{1:1}$ = 9.8 ± 1.7 × 10^4 M^{-1} and the UV-Visible spectrum of the putative 1:1 complex.* The relative intensity of the bands for supramolecular assembly depicted in inset Figure 3 and corresponded to 0.53 (517 nm), 1 (560 nm), 0.60 (610 nm) and 0.06 (645 nm). Moreover, the highly value of the stability constant determined for the cyclic trisporphyrin **MP212**+**MP151** complex warrants its exclusive formation in the concentration range of the titration and is indicative of the existence of a ditopic axial coordination between bipyridyl porphyrin **MP151** and zinc bisporphyrin **MP212** (Figure 3).

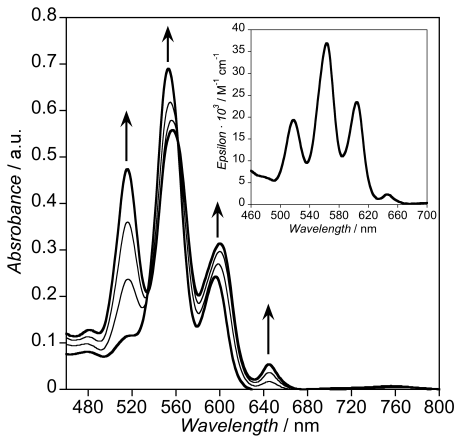

Fig. 3 Selected absorption spectra for the titration of zinc bisporphyrin **MP212** with bipyridyl free base porphyrin **MP151** in $CHCl_3$ corresponding to: 0, 0.5, 1 and 1.5 equivalents of **MP151** added. Inset: Calculated spectrum for the 1:1 complex **MP212**+**MP151**.

Having briefly investigated the solution behaviour and UV-Visible properties of trisporphyrin assembly, we decided to move into the study of tentative formation onto TiO_2 nanoparticles. Our approach involved the use of step-wise self-assembly process employing high surface area mesoporous 4 μm thick TiO_2 nanoparticles. Firstly, the TiO_2 film was immersed into a 250 μM zinc bisporphyrin **MP216** solution in $CHCl_3$ for different times, and the absorption kinetics was monitored by UV-Visible at the maxima absorption wavelength, 555 and 600 nm, until it reached a plateau (Figure S1 in supporting information). The adsorption kinetics can be fitted to Lagergren equation:[35]

* Only the value of the stability constant of the complex $K_{1:1}$ and the spectrum of **MP212**+**MP151** were used a variable fit.

$$Abs(t) = Abs_{\max}\left(1 - e^{-(K_{ads}\cdot t)}\right) \quad (1)$$

where Abs_{max} (a.u.) was the maximum absorption that the sample could reach on the film and K_{ads} (min-1) was the rate constant. The fitting resulted in a K_{ads} = 0.034 min^{-1} and indicated that fully loading 4 μm thick mesoporous TiO_2 films of **MP216** (Abs_{555} = 1 a.u., Abs_{600} = 0.412 a.u.) required 3 hours of sensitisation.

Having observed that the sensitisation time is a variable that controls the extent in which **MP216** is anchored onto the surface of nanocrystalline TiO_2, two films were prepared with different loadings of **MP216**, denoted as mid loading (Abs_{555} = 0.473 a.u.) and high loading (Abs_{555} = 1.006 a.u.). The next step was the heterogeneous self-assembly of previously anchored zinc bisporphyrin (**MP216**/TiO_2) with bipyridyl free base porphyrin **MP151**. The pre-sensitised film was immersed into a solution 250 μM of **MP151** in $CHCl_3$ for different times and the kinetics of the supramolecular assembly were monitored at 517 nm and 647 nm, where the free base porphyrin bands did not overlap with the zinc bisporphyrin absorption spectrum.

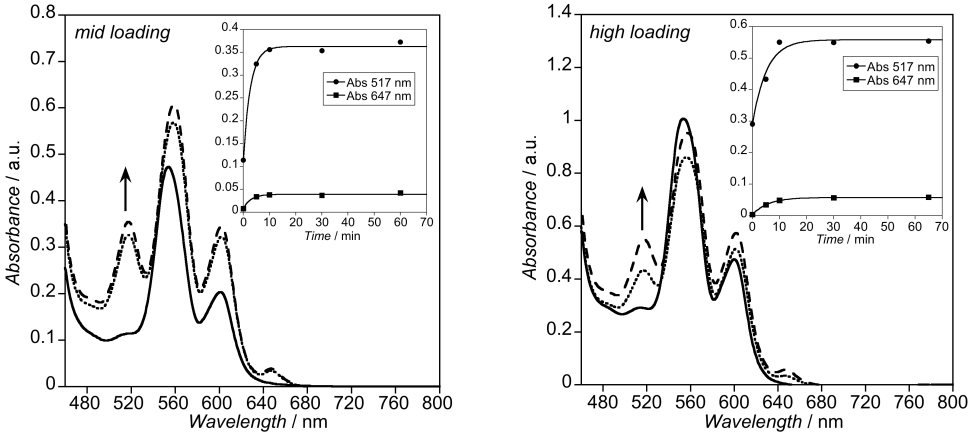

Fig. 4 Selected absorption spectra for *mid* and *high* loadings **MP216**/TiO_2 films after the immersion of **MP151** solution. Corresponding time: 0 (straight line), 5 (dotted line) and 30 minutes (dashed line). The insets show the supramolecular assembly kinetics, monitored at 517 and 647 nm, fitted to Lagergren equation.

The kinetic studies revealed that mid loading mesoporous TiO_2 films required 15 minutes (K_{ads} = 0.36 min^{-1}) soaking time for supramolecular assembly saturation whereas for the high loading films at least 40 minutes (K_{ads} = 0.19 min_{-1}) were required. These kinetic results indicated that lower zinc bisporphyrin **MP216**/TiO_2 loadings enabled easy penetration of bipyridyl **MP151** free base porphyrin into the

UNIVERSITAT ROVIRA I VIRGILI
DESIGN AND SYNTHESIS OF ORGANIC SENSITIZERS FOR DYE SOLAR CELLS: MOLECULAR STRUCTURE VS DEVICE PERFORMANCE
Miquel Angels Planells Dillundé
ISBN:978-84-693-8861-7/DL:T-1946-2010

TiO_2 porous. It is worth to point out that in both cases, the final UV-Visible spectra had a relative intensity of the bands of 0.58 (517 nm), 1 (560 nm), 0.58 (610 nm) and 0.06 (645 nm), which was in a good agreement with the UV-Visible spectrum of supramolecular assembly **MP212+MP151** obtained in solution. Therefore, we can conclude that supramolecular species on the film **MP216+MP151**/TiO_2 had the same geometry, a cyclic trisporphyrin via ditopic metal mediated interaction, which we found in $CHCl_3$ experiments. In addition, these experiments revealed that no free zinc bisporphyrin **MP216** reminded uncomplexed on the nanocrystalline TiO_2 films.

Once we confirmed that the supramolecular assembly supported on TiO_2 nanoparticles is identical to the solution experiments, we applied this methodology to DSSC as a step further. Solar cells were made with 9 µm of TiO_2 nanoparticles (20 nm diameter) plus a 4 µm scatter layer with an active area of 0.16 cm^2. As first step, solar cell containing only zinc bisporphyrin **MP216** was optimized by controlling the solvent, immersion time and additives. The best performance was obtained after 24 hours of sensitisation in chlorobenzene as solvent (Table 1). It is worth to notice that the addition of chenodeoxycholic acid as co-sensitiser, a well-known additive that avoids the formation of aggregates especially for organic dyes, did not have any significant effect on the device performance. This result suggested that zinc bisporphyrin **MP216** was bulky enough and it was able to break the possible aggregates formed by π - π stacking.

Table 1. Dye sensitised solar cell performance.[a]

Dye sample	J_{sc} / mA cm^{-2}	V_{oc} / V	FF / %	Eff. / %
MP216	4.69	0.47	67	1.50
MP216⊂BP[b]	3.36	0.52	67	1.18
MP216⊂MP151[b]	6.50	0.63	71	2.92

[a] Solar cell performance were measured at 1 sun 1.5 AM G without mask. The active area was 0.16 cm^2 and the electrolyte used was **LP2**. The solvent used for sensitisation was chlorobencene with a dye concetration of 0.3 mM. [b] DSSC with supramolecular assembly was attained by the immersion of net TiO_2 film into a solution mixture of **MP216** and its complementary moiety, **BP** or **MP151**.

Having optimised DSSC for **MP216**, we proceed to develop solar cells containing the trisporphyrin supramolecular assembly **MP216+MP151**. However, it is well known that supramolecular interactions induce a molecular reorganisation and, therefore, the molecular geometry on the TiO_2 film for assembled and non-assembled zinc

bisporphyrin **MP216** moiety could not be identical. It could outcome in a no reliable device performance results. Thus, no photoactive bipyridyl unit **BP** have been utilised in order to form an assembly with zinc bisporphyrin, **MP216**+**BP**, adopting the same geometry that trisporphyrin **MP216**+**MP151** onto TiO_2 surface. Solar cell performances are shown in Table 1. We would like to point out that the electrolyte could not contain *tert*-butyl pyridine, because pyridine derivatives could compete with bipyridyl free base porphyrin **MP151** in the supramolecular assembly.

Performance characteristics of DSSC are shown in Figure 5. Higher photocurrent was attained when trisporphyrin **MP216**+**MP151** was used, confirming that the photoactive unit supported via supramolecular interaction contributed effectively to the device performance. The band appeared at 517 nm on the IPCE spectrum supported clearly the effect of **MP151** moiety on the photocurrent generated and, therefore, it suggested electron injection from both zinc and free base porphyrin units in contrast to previous published results for TiO_2 – ZnP – FbP system.[28]

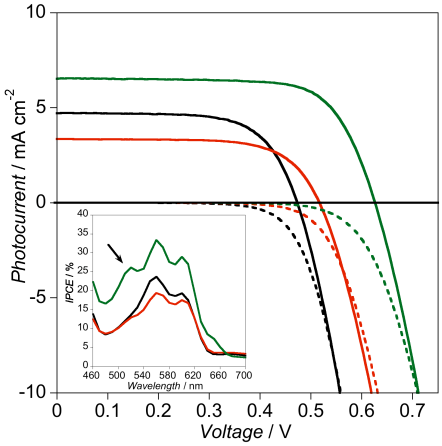

Fig. 5 Solar cell performances at 1 sun AM G (solid line) and under dark conditions (dash line) for **MP216** (dark line), **MP216**+**BP** (red line) and **MP216**+**MP151** (green line). The inset shows the IPCE spectra for the same samples. The arrow denotes the band corresponding to the free base porphyrin.

Laser transient absorption spectroscopy (L-TAS) have been used for several authors in order to monitoring the charge transfer processes upon light excitation in TiO_2 films.[32, 36] Thus, L-TAS technique was used for monitoring the e^-_{TiO2}/dye^+ recombination as well as the generated cation spectrum after a light pulse. In this study, we recorded the spectra of porphyrin cation for sensitized **MP216**, **MP216**+**BP** and **MP216**+**MP151** TiO_2 films upon excitation at 580 nm (maximum absorbance of zinc porphyrin) and fixing the acquired time at 100 μs. The resulting spectra had a

maximum at 660 nm and a shoulder at 860 nm (Inset Figure 6) and were identical for all samples (Figure S2 supporting information). The spectrum obtained corresponded to the zinc porphyrin cation, which was also in a good agreement with the literature precedent.[37] The photo-excitation of trisporphyrin **MP216**+**MP151** assembly onto the TiO_2 film resulted in an electron injection from both free base and zinc porphyrins, however, the hole generated was exclusively located onto the zinc porphyrin moiety. The charge recombination lifetimes between e^-_{TiO2}/dye^+ were measured for all samples exciting at 580 nm and acquiring at 660 nm (Figure 6). The data obtained can be fitted to the stretched exponential function:

$$\Delta O.D.(t) = A_1 \cdot e^{-\left(t/\tau\right)^{\beta}} \qquad (2)$$

where A_1 was the signal amplitude, τ was the cation lifetime and β is the stretched parameter. Recombination decays resulted in extremely long live charge separated states for **MP216**/TiO_2 (τ = 150 ms, β = 0.5), **MP216**+**BP**/TiO_2 (τ = 160 ms, β = 0.5) and **MP216**+**MP151**/TiO_2 (τ = 26 ms, β = 0.3), compared with other porphyrin dyes.[37, 38] Faster electron recombination lifetime for assembled **MP216**+**MP151** trisporphyrin on TiO_2 film was expected, because, the extra electrons injected from zinc and free base porphyrin accelerate this recombination.[36] However, in this case recombination e^-_{TiO2}/dye^+ did not limit the cell performance because the regeneration of oxidised dye resulted to be a very fast process, less than 10^{-6} s, which is on the limit of our system.

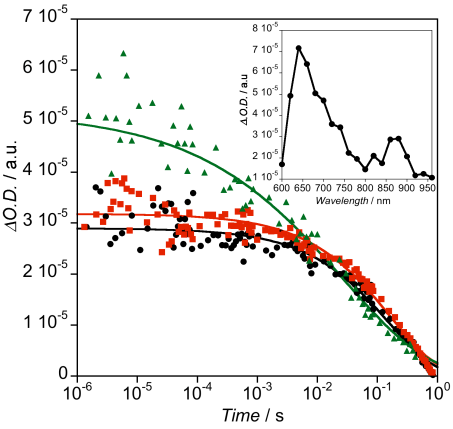

Fig. 6 L-TAS recombination decays dynamics for 4 µm TiO_2 sensitised films containing **MP216** (dark circles), **MP216**+**BP** (red squares) and **MP216**+**MP151** (green triangles) at λ_{probe} = 660 nm. Coloured solid lines represent their stretched exponential fittings. Laser excitation was set to 580 nm. Inset: Transient spectrum of **MP216**+**MP151**/TiO_2 acquired at fixed 100 µs.

Once confirmed that the e^-_{TiO2}/dye$^+$ recombination reaction had a negligible effect due to the larger lifetime attained, we focused on the e^-_{TiO2}/electrolyte$^+$ recombination reaction. Higher photovoltage (Figure 5) was obtained when supramolecular assemblies were present, either with **BP** and **MP151**. It could be due to (*a*) a shift in the conduction band of TiO_2 induced by the assembly and (*b*) a difference in the recombination kinetics between the electrons in the TiO_2 conduction band and the oxidised electrolyte. Charge extraction measurements were performed in order to elucidate the charge accumulated at the TiO_2 conduction band at different cell voltages.[39]

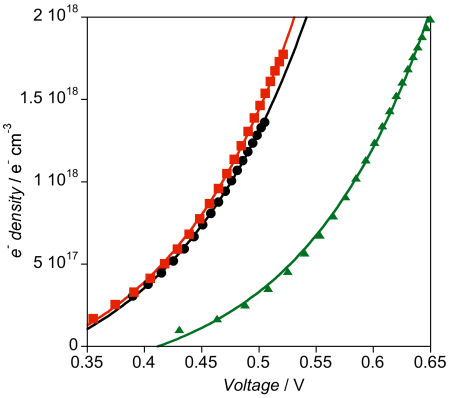

Fig. 7 Charge extraction measurements of solar cells containing **MP216** (dark circles), **MP216+BP** (red squares) and **MP216+MP151** (green triangles) expressing the electron density as function of the cell voltage.

As depicted in Figure 7, TiO_2 conduction band reminded invariable for **MP216** and **MP216+BP** cells, whose was expected, whereas for trisporphyrin assembly **MP216+MP151** resulted in an upward shift of 125 mV. This result is in good agreement with the increase in voltage observed for the supramolecular system as illustrated in Figure 5.

Transient photovoltage (TPV) decays have been used for several authors for the evaluation of the interfacial charge recombination e^-_{TiO2}/electrolyte$^+$.[40, 41] As can be seen in Figure 8, slower recombination e^-_{TiO2}/electrolyte$^+$ is obtained for trisporphyrin **MP216+MP151** supramolecular assemblies compared with the zinc bisporphyrin **MP216**. As mentioned above, additional molecules attached via supramolecular can induce a different geometry of zinc bisporphyrin moiety, which can act as an effective barrier preventing the contact between the oxidized electrolyte and the TiO_2 nanoparticles surface. Indeed the higher photovoltage for **MP216+BP** solar cell

supports our hypothesis and, as illustrated in Figure 8, the supramolecular system shows slower e^-_{TiO2}/electrolye$^+$ recombination dynamics. Thus, the higher V_{oc} attained for the trisporphyrin supramolecular assembly **MP216+MP151** can be rationalized in terms of an upward shift of the TiO_2 conduction band plus slower e^-_{TiO2}/electrolye$^+$ recombination dynamics.

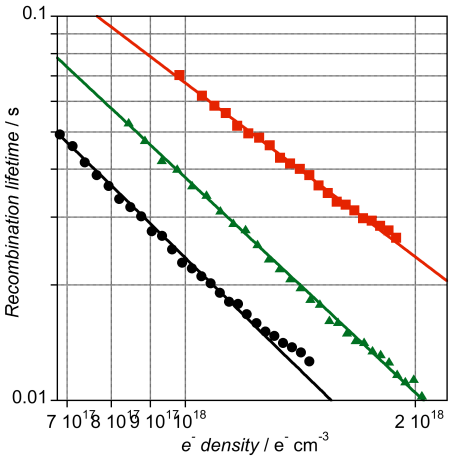

Fig. 8 Transient photovoltage of DSSC containing **MP216** (dark circles), **MP216+BP** (red squares) and **MP216+MP151** (green triangles) expressing the e^-_{TiO2}/electrolyte$^+$ recombination lifetime as function of the electron cell density.

6.2.4. Conclusions

As summary, novel zinc bisporphyrins **MP212** and **MP216** were designed and synthesised to interact through a supramolecular assembly with a bipyridyl free base porphyrin **MP151** onto mesoporous TiO_2 films. The resulting trisporphyrin supramolecular assembly was characterised previously in solution, where a ditopic metal mediated interaction zinc porphyrin – pyridyl moiety was assigned due to the high stability constant attained. Subsequently, the self-assembly process was characterised onto the nanoparticles surface by UV-Visible spectroscopy. The resulting supramolecular complex was assigned as a cyclic trisporphyrin with an identical geometry and ditopic interaction as the solution experiment. Furthermore, the adsorption results showed that the supramolecular assembly was not dependent of the dye loading, achieving full trisporphyrin either with middle and full dye loading onto the whole TiO_2 nanoparticles.

DSSC performance were evaluated, attaining two times better efficiency for the supramolecular trisporphyrin **MP216+MP151** assembly, compared with both plain zinc bisporphyrin, **MP216**, and its supramolecular assembly with no photoactive unit, **MP216+BP**. Higher photocurrent in trisporphyrin can be rationalised in terms of an extra photo-injection from zinc and free base porphyrin units, as is shown in the IPCE spectrum. Moreover, e^-_{TiO2}/dye^+ recombination reactions were slower. In addition, undesired energy transfer from zinc to free base porphyrin in our system TiO_2 – ZnP – FbP did not affect on the photo-injection process, in contrast to the literature precedent.[28] On the other hand, higher photovoltage were obtained for both supramolecular systems. It has been rationalised in terms of slower e^-_{TiO2}/$electrolyte^+$ recombination kinetics, due to the blocking layer effect when supramolecular assemblies are present. Furthermore, trisporphyrin assembly showed an upward shift of the TiO_2 conduction band, which is also in a good agreement with the higher photovoltage obtained. We would like to point out that inverted system TiO_2 – FbP – ZnP with a favourable energy transfer process, consisting in an hydrolysed free base porphyrin **MP151** and a **MP212** derivative, have been attempted on DSSC with extremely low performance. Further work to elucidate such low device performance is being carried out.

6.2.5. Acknowledgements

We thank DGI, Ministerio de Ciencia y Tecnología (CTQ2005-08989-C02/BQU, Consolider Ingenio 2010 Grant CSD2006-0003, Consolider-Hope 0007-2007), ICIQ Foundation and Generalitat de Catalunya DURSI (Grant 2005SGR00108) for generous financial support. M.P. thanks MICIIN Spain for a predoctoral fellowship.

6.3. Supporting information

6.3.1. Detailed synthetic procedure

General synthetic considerations. All reagents were purchased from either Sigma-Aldrich or Alfa Aesar and they were used as received without further purification unless otherwise stated. Common solvents were purchased from SdS and used without further purification. Dry solvents were purchased from Fluka with water content < 0.005%. 4-pentylbenzaldehyde was synthesised according the procedure described previously by our group.[38]

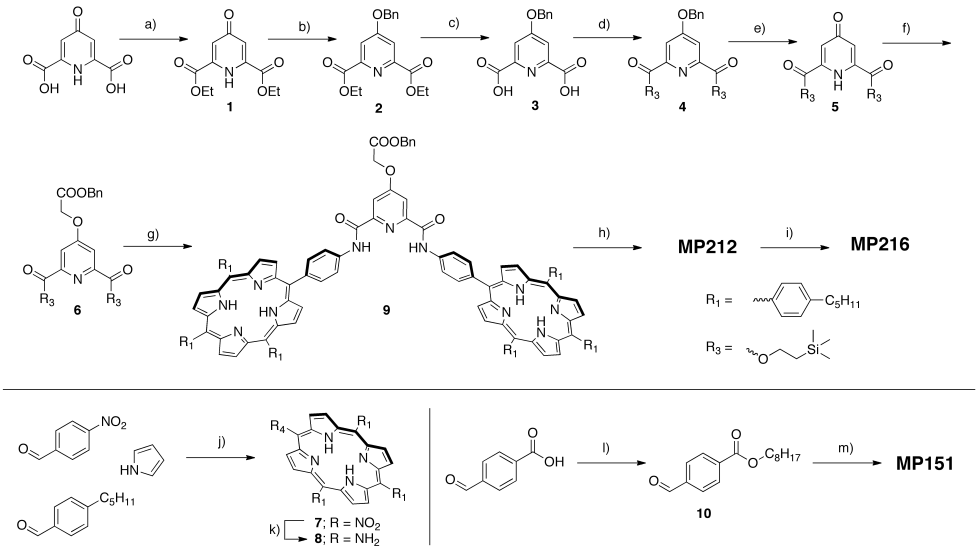

Scheme 1. Synthetic procedures for porphyrins **MP151**, **MP212** and **MP216**. Key: *a*) H_2SO_4, EtOH 16 h. 70 ºC (42%); *b*) benzyl bromide, K_2CO_3, 18-crown-6 ether, Acetone 16 h. 60 ºC (98%); *c*) NaOH 2M, THF/MeOH/H_2O (5:3:2) 16 h. 50 ºC. (46%); *d*) i) $SOCl_2$, 3 h. 80 ºC ii) trimethylsilylethanol, Et_3N, DMAP, CH_2Cl_2 16 h. 40 ºC (93%); *e*) Pd/C, H_2, EtOAc/EtOH (70:1) 16 h. r.t. (73 %); *f*) benzyl bromoacetate, K_2CO_3, 18-crown-6 ether, Acetone 16 h. 60 ºC (73%); *g*) i) TBAF 1M in THF 1 h. r.t., ii) $SOCl_2$, 3h. 75 ºC, iii) **8**, Et_3N, DMAP, CH_2Cl_2 16 h. 40 ºC (54%); *h*) $Zn(OAc)_2{\cdot}2H_2O$, $CHCl_3$/MeOH (5:1) 1.5 h. r.t. (73%); *i*) Pd/C, H_2, EtOAc/EtOH (60:1) 16 h. r.t (51%); *j*) i) $BF_3{\cdot}2Et_2O$, CH_2Cl_2 1 h. 40 ºC ii) DDQ, 1.5 h. r.t iii) Et_3N, 10 min, r.t (12%); *k*) i) $SnCl_2{\cdot}2H_2O$, HCl / dioxane (1:1) 2 h. 70 ºC, ii) NH_3 (95%); *l*) 1-octanol, DCC, DMAP, CH_2Cl_2 16 h. r.t. (91%); *m*) 4-pyridylcarbaldehyde, pyrrole, CH_3CH_2COOH 1 h. 110 ºC (3%).

Synthesis of diethyl 4-oxo-1,4-dihydropyridine-2,6-dicarboxylate (1). Chelidamic acid (1 g, 5.46 mmol) was added in a schlenk tube with 9.5 mL of EtOH. The mixture was stirred under N_2 at room temperature (r.t.) and then sulfuric acid (0.7 mL, 1.28 mmol) was added dropwise. The reaction was heated up to 70 ºC and stirred overnight under N_2. The reaction was quenched by the addition of 100 mL of satured $NaHCO_3$. The pH was adjusted to 4 by the addition of conc HCl and the aqueous layer was extracted with 100 mL of CH_2Cl_2. The organic layer was washed with brine, dried over Na_2SO_4 and the solvent removed. The crude was then purified by column chromatography (SiO_2, CH_2Cl_2 / EtOAc 6:1 up to 3:1) to afford a white solid as the final product (550 mg, 42% yield). ^{1}H-NMR (400 MHz, DMSO-d_6) δ_H: 7.57 (s, 2H); 4.35 (q, J = 7.1 Hz, 4H); 1.33 (t, J = 7.2 Hz, 6H). ^{13}C-NMR (100 MHz, DMSO-d_6) δ_C: 165.8; 164.2; 149.5; 115.1; 61.4; 14.1. MS-ESI (m/z): $[M+Na]^+$ calcd. for $C_{11}H_{13}NO_5Na$: 262.0691; found: 262.0698.

Synthesis of diethyl 4-(benzyloxy)pyridine-2,6-dicarboxylate (2). **1** (1.66 g, 7 mmol), K_2CO_3 (1.91 g, 14 mmol) and 18-crown-6 ether (183 mg, 0.7 mmol) were added to a round bottom flask with 20 mL of acetone. The mixture was stirred under N_2 at room temperature (r.t.) and then benzyl bromide (1.5 mL, 12.6 mmol) was added via syringe. The reaction was heated up to 60 ºC and stirred overnight under N_2. The crude was filtered off and washed with acetone and the solvent was removed. The residue was then purified by column chromatography (SiO_2, CH_2Cl_2 up to CH_2Cl_2/2% Acetone) to afford a white solid as the final product (2.25 g, 98% yield). ^{1}H-NMR (400 MHz, $CDCl_3$) δ_H: 7.86 (s, 2H); 7.43 (m, 5H); 5.22 (s, 2H); 4.47 (q, J = 7.1 Hz, 4H); 1.42 (t, J = 7.2 Hz, 6H). ^{13}C-NMR (100 MHz, $CDCl_3$) δ_C: 166.8; 164.9; 150.4; 134.9; 129.0; 128.9; 127.9; 114.8; 70.9; 62.6; 14.4. MS-ESI (m/z): $[M+Na]^+$ calcd. for $C_{18}H_{19}NO_5Na$: 352.1161; found: 352.1146.

Synthesis of 4-(benzyloxy)pyridine-2,6-dicarboxylic acid (3). **2** (384 mg, 1.16 mmol) was added to a round bottom flask with a solvent mixture of THF (5 mL), MeOH (3 mL). 2 mL of NaOH 2M aqueous solution was then added and white precipitate was precipitated straightforward. The reaction was stirred at 50 ºC under N_2 overnight. Organic solvents were removed and HCl 2M was added until pH was 4. EtOAc was added to the aqueous layer and a white precipitate appeared at the interface, which was filtered off to afford a white solid as the final product (146 mg, 46% yield). It is worth to notice that the product was insoluble with the most common organic solvents. ^{1}H-NMR (400 MHz, DMSO-d_6) δ_H: 7.72 (s, 2H); 7.44 (m, 5H); 5.42 (s, 2H).

Synthesis of bis(2-(trimethylsilyl)ethyl) 4-(benzyloxy)pyridine-2,6-dicarboxylate (4). **3** (1.45 g, 5.3 mmol) was added in a schlenk tube with 9 mL of $SOCl_2$. The mixture was stirred under N_2 for 3 hours at 80 ºC. After that, the suspension of the starting material disappeared. $SOCl_2$ was then removed carefully under vacuum by using a pre-trap of liquid N_2. The crude was then dried under high vacuum for 2 hours. A previous mixture of trimethylsilylethanol (2.2 mL, 15.9 mmol), triethylamine (5.9 mL, 42,4 mmol) and 4-dimethylaminopyridine, DMAP (129 mg, 0.2 mmol) dissolved in 10 mL of CH_2Cl_2, were added to the schlenk tube. The reaction was stirred overnight at 40 ºC under N_2. The crude was dissolved in 100 mL of CH_2Cl_2 and washed with 100 mL of satured aqueous $NaHCO_3$ solution. The organic layer was dried over Na_2SO_4 and the solvent removed. The crude was then purified by column chromatography (SiO_2, CH_2Cl_2) to afford a white solid as the final product (2.06 g, 93% yield). ^{1}H-NMR (400 MHz, $CDCl_3$) δ_H: 7.84 (s, 2H); 7.43 (m, 5H); 5.21 (s, 2H); 4.48 (m, 4H); 1.21 (m, 4H) 0.88 (s, 18H). ^{13}C-NMR (100 MHz, $CDCl_3$) δ_C: 166.7; 165.1; 150.6; 135.0; 129.1; 129.0; 128.0; 114.6; 70.9; 64.9; 17.6; 1.3. MS-ESI (m/z): $[M+Na]^+$ calcd. for $C_{24}H_{35}NO_5NaSi_2$: 496.1952; found: 496.1946.

Synthesis of bis(2-(trimethylsilyl)ethyl) 4-oxo-1,4-dihydropyridine-2,6-dicarboxylate (5). **4** (1.96 g, 4.7 mmol) and palladium on carbon (196 mg) were added to a round bottom flask and were dried under high vacuum for 1 hour. Then, 70 mL of EtOAc and 1 mL of EtOH were added and were also degassed by pump/freeze technique. The mixture was stirred overnight at r.t. under H_2 atmosphere. The crude was filtered off over celite and eluted with EtOAc. The solvent was removed and the residue was then purified by column chromatography (SiO_2, CH_2Cl_2/EtOAc 10:1 up to 10:2) to afford a white solid as the final product (1.31 g, 73% yield). ^{1}H-NMR (400 MHz, $CDCl_3$) δ_H: 7.24 (s, 2H); 4.50 (m, 4H); 1.15 (m, 4H) 0.90 (s, 18H).

Synthesis of bis(2-(trimethylsilyl)ethyl) 4-(2-(benzyloxy)-2-oxoethoxy)pyridine-2,6-dicarboxylate (6). **5** (1.31 g, 3.4 mmol), K_2CO_3 (940 mg, 6.8 mmol) and 18-crown-6 ether (90 mg, 0.34 mmol) were added to a round bottom flask with 68 mL of acetone. The mixture was stirred under N_2 at room temperature (r.t.) and then benzyl bromoacetate (646 µL, 4.1 mmol) was added via syringe. The reaction was heated up to 60 ºC and stirred overnight under N_2. The crude was filtered off and washed with acetone and the solvent was removed. The residue was then purified by column chromatography (SiO_2, CH_2Cl_2) to afford colourless oil as the final product (1.31 g, 73% yield). ^{1}H-NMR (400 MHz, $CDCl_3$) δ_H: 7.75 (s, 2H); 7.35 (m, 5H); 5.25 (s, 2H); 4.81 (s, 2H); 4.84 (m, 4H); 1.20 (m, 4H); 0.88 (s, 18H). ^{13}C-NMR (100 MHz, $CDCl_3$) δ_C: 167.2; 165.9; 164.8; 150.8; 134.8; 129.0; 128.9; 128.8;

114.2; 67.8; 65.2; 64.9; 17.6; 1.2. MS-ESI (m/z): $[M+H]^+$ calcd. for $C_{26}H_{38}NO_7Si_2$: 532.2187; found: 532.2182.

Synthesis of 5-(4-nitrophenyl)-10,15,20-(4-pentylphenyl)porphyrin (7). freshly distilled pyrrole (1.15 mL, 16.5 mmol), 4-nitrobenzaldehyde (1 g, 6.6 mmol) and 4-pentylbenzaldehyde (1.7 g, 10 mmol) were added to a round bottom flask with 600 mL of CH_2Cl_2 and 5 mL of EtOH. The mixture was stirred under N_2 in the dark and degassed for 10 minutes. Then, $BF_3{\cdot}2Et_2O$ (836 µL, 6.6 mmol) was added and the reaction was stirred for 1 hour at 40 ºC. The reaction changed the colour to black. After that, 2,3-dichloro-5,6-dicyanobenzoquinone (3.7 g, 16.5 mmol) was added and the reaction was stirred for another 1.5 hours. Finally, triethylamine (7.4 mL, 52.8 mmol) was added in order to quench the reaction. The crude was then purified by column chromatography (SiO_2, CH_2Cl_2/Hexane 3:2 up gradually to pure CH_2Cl_2) to afford a purple solid as the final product (425 mg, 12% yield). ^{1}H-NMR (400 MHz, $CDCl_3$) δ_H: 8.91 (d, *J* = 4.8 Hz, 2H); 8.87 (s, 4H); 8.72 (d, *J* = 5.2 Hz, 2H); 8.63 (d, *J* = 8.0 Hz, 2H); 8.40 (d, *J* = 8.3 Hz, 2H); 8.11 (d, *J* = 7.6 Hz, 6H); 7.56 (d, *J* = 7.6 Hz, 6H); 2.95 (t, *J* = 7.7 Hz, 6H); 1.92 (m, 6H); 1.51 (m, 12H); 1.02 (t, *J* = 7.0 Hz, 9H); -2.77 (s, 2H). MS-ESI (m/z): $[M+H]^+$ calcd. for $C_{59}H_{60}N_5O_2$: 870.4747; found: 870.4755.

Synthesis of 5-(4-aminophenyl)-10,15,20-(4-pentylphenyl)porphyrin (8). **7** (425 mg, 0.49 mmol) was added to a preheated mixture at 70 ºC of 50 mL of conc. HCl and 50 mL of dioxane. $SnCl_2{\cdot}2H_2O$ (1.3 g, 5.88 mmol) was added and the reaction was stirred at 70 ºC for 2 hours under N_2. The heater was shotted down and with the reaction still hot, 100 mL of NH_3 was added dropwise in order to quench the reaction. The crude was extracted with 100 mL of EtOAc. The organic layer was washed with brine, dried over Na_2SO_4 and the solvent removed. The crude was then purified by column chromatography (SiO_2, CH_2Cl_2/Hexane 2:1 up to 4:1) to afford a purple solid as the final product (390 mg, 95% yield). ^{1}H-NMR (400 MHz, $CDCl_3$) δ_H: 8.92 (d, *J* = 4.8 Hz, 2H); 8.8 (m, 6H); 8.11 (d, *J* = 7.9 Hz, 6H); 8.00 (d, *J* = 8.1 Hz, 2H); 7.55 (d, *J* = 7.6 Hz, 6H); 7.07 (d, *J* = 8.3 Hz, 2H); 4.03 (br s, 2H); 2.95 (t, *J* = 7.9 Hz, 6H); 1.93 (m, 6H); 1.53 (m, 12H); 1.03 (t, *J* = 6.9 Hz, 9H); -2.73 (s, 2H). MS-ESI (m/z): $[M+H]^+$ calcd. for $C_{59}H_{62}N_5$: 840.5005; found: 840.4973.

Synthesis of free base bisporphyrin 9. **6** (98 mg, 0.185 mmol) was added to a schlenk tube with 3.7 mL of CH_2Cl_2. The mixture was stirred at r.t. under N_2 for 5 minutes and then tetrabutylamonium fluoride 1M solution in THF (460 µL, 0.46 mmol) was added. The reaction was stirred for 1 hour and then the solvent was removed. $SOCl_2$ (670 µL, 9.25 mmol) and the mixture was heated up to 75 ºC and stirred for 3

hours under N_2. After that, $SOCl_2$ was removed carefully under vacuum by using a pre-trap of liquid N_2. The crude was then dried under high vacuum for 2 hours. A previous mixture of **8** (390 mg, 0.46 mmol), triethylamine (206 µL, 1.48 mmol) and DMAP (4.5 mg, 0.037 mmol) dissolved in 4 mL of dry CH_2Cl_2, were added to the schlenk tube. The reaction was stirred overnight at 40 ºC under N_2. The crude was dissolved in 30 mL of CH_2Cl_2 and washed with 50 mL of satured aqueous $NaHCO_3$ solution. The organic layer was dried over Na_2SO_4 and the solvent removed. The crude was then purified by column chromatography (SiO_2, CH_2Cl_2/Hexane 4:1 up to pure CH_2Cl_2) to afford a purple solid as the final product (197 mg, 54% yield). ^{1}H-NMR (400 MHz, $CDCl_3$ + 5% TFA) δ_H: 10.41 (s, 2H); 8.77 (m, 22H); 8.47 (m, 16H); 8.32 (s, 2H); 7.85 (m, 12H); 7.42 (m, 5H); 5.42 (s, 2H); 5.19 (s, 2H); 3.02 (m, 12H); 1.94 (m, 12H); 1.55 (m, 24H); 1.01 (m, 18H); -7.2 (m, 6H). MS-MALDI (m/z): $[M]^+$ calcd for $C_{134}H_{131}N_{11}O_5$: 1974.0329; found: 1974.0221.

Synthesis of zinc bisporphyrin MP212. **9** (93 mg, 0.047 mmol) and $Zn(OAc)_2{\cdot}2H_2O$ (165 mg, 0.75 mmol) were added in a round bottom flask with a mixture of 15 mL of $CHCl_3$ and 3 mL of MeOH. The reaction was stirred under N_2 in the dark for 1.5 hours. The solvent was removed and the crude was then purified by column chromatography (SiO_2, CH_2Cl_2 up to CH_2Cl_2/EtOAc 2%) to afford a purple solid as the final product (73 mg, 73% yield). ^{1}H-NMR (400 MHz, $CDCl_3$ + 5% pyridine-d_5) δ_H: 10.27 (s, 2H); 8.86 (s, 8H); 8.83 (s, 8H); 8.21 (d, J = 8.4 Hz, 4H); 8.19 (s, 2H); 8.10 (d, J = 8.4 Hz, 4H); 8.04 (d, J = 7.6 Hz, 12H); 7.46 (d, J = 8.0 Hz, 12H); 7.39 (m, 5H); 5.24 (s, 2H); 4.99 (s, 2H); 2.88 (m, 12H); 1.84 (s, 12H); 1.46 (m, 24H); 0.96 (m, 18H). MS-MALDI (m/z): $[M]^+$ calcd for $C_{134}H_{127}N_{11}O_5Zn_2$: 2097.8599; found: 2097.8660. Anal. Calcd for $C_{134}H_{127}N_{11}O_5Zn_2$: C, 76.56; H, 6.09; N, 7.33; Found: C, 75.63; H, 6.02; N, 6.86.

Synthesis of zinc bisporphyrin MP216. **MP212** (165 mg, 0.082 mmol) and palladium on carbon (25 mg) were added to a round bottom flask and were dried under high vacuum for 1 hour. Then, 20 mL of EtOAc and 0.4 mL of EtOH were added and were also degassed by pump/freeze technique. The mixture was stirred overnight at r.t. under H_2 atmosphere. The crude was filtered off over celite and eluted with EtOAc/MeOH 5%. The solvent was removed and the residue was then purified by column chromatography (SiO_2, CH_2Cl_2 up gradually to CH_2Cl_2/MeOH 10%) to afford a purple solid as the final product (84 mg, 51% yield). ^{1}H-NMR (400 MHz, DMSO-d_6) δ_H: 11.51 (s, 2H); 8.87 (d, J = 4.5 Hz, 4H); 8.78 (d, J = 4.8 Hz, 4H); 8.76 (m, 8H); 8.41 (d, J = 8.1 Hz, 4H); 8.26 (d, J = 8.5 Hz, 4H); 8.06 (d, J = 7.6 Hz, 12 H); 7.93 (s, 2H); 7.58 (m, 12H); 4.58 (br s, 2H); 2.91 (m, 12H); 1.97 (m, 12H); 1.48

(m, 24 H); 0.99 (m, 18H). MS-MALDI (m/z): $[M]^+$ calcd. for $C_{127}H_{121}N_{11}O_5Zn_2$: 2007.8135; found: 2007.8267. Anal. Calcd for $C_{127}H_{121}N_{11}O_5Zn_2 \cdot 5H_2O$: C, 72.56; H, 6.28; N, 7.33; Found: C, 72.63; H, 5.95; N, 7.11.

Synthesis of octyl 4-formylbenzoate (10). 4-formylbenzoic acid (2.3 g, 15.8 mmol) and 1-octanol were added in a round bottom flask with 60 mL of CH_2Cl_2. The mixture was cooled at 0 ºC and was stirred for 10 minutes. Then, a previous solution of *N,N'*-dicyclohexylcarbodiimide, DCC (3.6 g, 17.4 mmol) and DMAP (2.1 g, 17.4 mmol) in 20 mL of CH_2Cl_2 was added. The reaction was stirred 10 minutes at 0 ºC and after that overnight at r.t. The reaction was then filtered off and the solvent removed. The crude was dissolved in 100 mL of Et_2O and washed with 100 mL satured $NaHCO_3$ aqueous solution. The organic layer was dried over Na_2SO_4 and solvent removed. The residue was then purified by column chromatography (SiO_2, CH_2Cl_2) to afford colourless oil as the final product (3.7 g, 91% yield). ^{1}H-NMR (400 MHz, $CDCl_3$) δ_H: 10.10 (s, 1H); 8.20 (d, J = 8.2 Hz, 2H); 7.95 (d, J = 8.2 Hz, 2H); 4.36 (t, J = 6.7 Hz, 2H); 1.78 (m, 2H); 1.47 (m, 2H); 1.29 (m, 8H); 0.88 (t, J = 6.8 Hz, 3H). ^{13}C-NMR (100 MHz, $CDCl_3$) δ_C: 191.8; 165.8; 139.2; 135.7; 130.4; 129.7; 66.0; 31.9; 29.4; 29.3; 28.8; 26.2; 22.8; 14.3.

Synthesis of 5,10-(4-pyridyl)-15,20-(4-carboxyoctylphenyl)porphyrin (MP151). **10** (3.7 g, 14.3 mmol) and 4-pyridylcarbaldehyde (1.3 mL, 14.3 mmol) were added to a round bottom flask with 100 mL of propanoic acid. The mixture was stirred 10 minutes under N_2 and then was heated up to 110 ºC. When the mixture reached that temperature, freshly distilled pyrrole (2 mL, 28 mmol) was added slowly. The colour of the reaction changed to black and was stirred for 1 hour at 110 ºC. The reaction was cooled down to r.t. and propanoic acid was removed carefully under vacuum. The crude was then purified by column chromatography (CH_2Cl_2 - CH_2Cl_2/pyridine 1% up gradually to CH_2Cl_2/THF 8%/pyridine 1%). The desired product was on the 4th red fluorescent spot.[42] Several columns on SiO_2 and size exclusion chromatography (Bio-Beads S-X1 in CH_2Cl_2) were required in order to obtain the final product as purple solid (208 mg, 3.1% yield). ^{1}H-NMR (400 MHz, $CDCl_3$) δ_H: 9.06 (d, J = 5.9 Hz, 4H); 8.85 (m, 8H); 8.46 (d, J = 8.2 Hz, 4H); 8.29 (d, J = 8.2 Hz, 4H); 8.16 (d, J = 5.9 Hz, 4H); 4.52 (t, J = 6.7 Hz, 4H); 1.92 (m, 4H); 1.52 (m, 4H); 1.33 (m, 16H); 0.91 (t, J = 7.0 Hz, 6H). MS-ESI (m/z): $[M+H]^+$ calcd. for $C_{60}H_{61}N_6O_4$: 929.4754; found: 929.4760. Anal. Calcd for $C_{60}H_{60}N_6O_4$: C, 77.56; H, 6.51; N, 9.04; Found: C, 77.66; H, 6.43; N, 8.83.

Characterization techniques: ^{1}H and ^{13}C NMR spectra were recorded on Bruker Avance 400 (400 MHz for ^{1}H and 100 MHz for ^{13}C) spectrometer. The deuterated

solvents used are indicated; chemical shifts, δ, are given in ppm, referenced to the solvent residual signal (^{1}H, ^{13}C). Coupling constants, *J*, are given in Hz. MS spectra were recorded on Waters LCT Premier, using electrospray ionization (ESI) and matrix-assisted laser desorption/ionization (MALDI) modes depending on the sample. Elemental analyses were carried out by elemental analysis services from Santiago de Compostela University using a LECO 932 CHNS elemental analyzer.

6.3.2. Supporting information figures

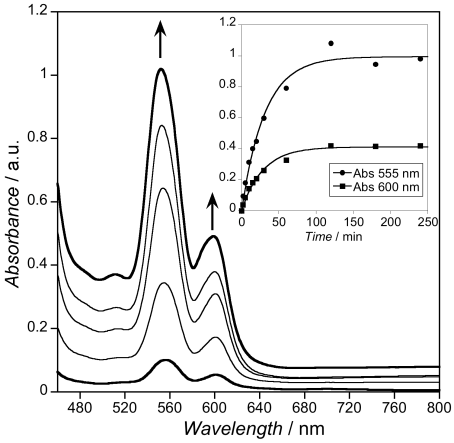

Figure S1. Selected absorption spectra for 4 µm mesoporous TiO_2 films after the immersion into **MP216** $CHCl_3$ solution. Corresponding immersion time: 2, 10, 30, 60 and 180 minutes. The insets shows the kinetics fitted to Lagergren equation.

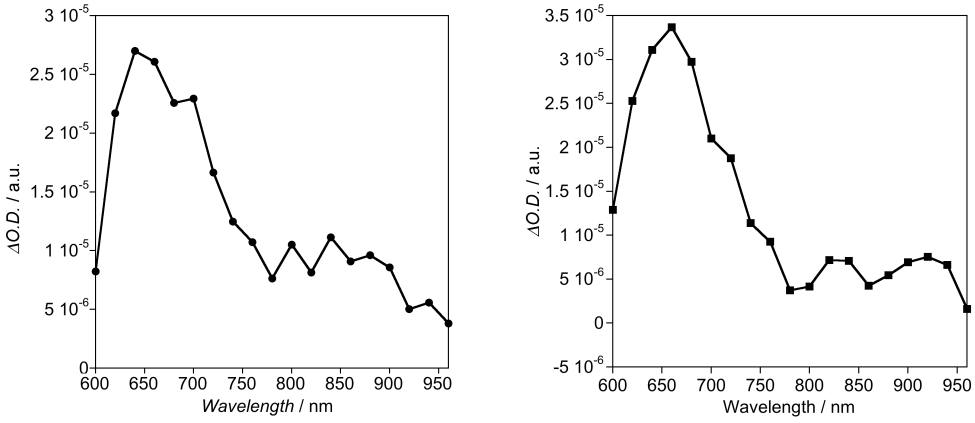

Figure S2. L-TAS spectra for **MP216**/TiO_2 (left) and **MP216**+**BP**/TiO_2 (right) after laser excitation at 580 nm. Acquisition time was fixed at 100 µs.

6.4. References

[1] J. M. Lehn, *Supramolecular Chemistry: Concepts and Perspectives*, **1995**.

[2] T. Hasobe, *Phys. Chem. Chem. Phys.* **2010**, *12*, 44.

[3] M. Capo, P. Ballester, *Tetrahedron Lett.* **2004**, *45*, 1055.

[4] P. Ballester, A. I. Oliva, A. Costa, P. M. Deya, A. Frontera, R. M. Gomila, C. A. Hunter, *J. Am. Chem. Soc.* **2006**, *128*, 5560.

[5] P. Ballester, A. Costa, P. M. Deya, A. Frontera, R. M. Gomila, A. I. Oliva, J. K. M. Sanders, C. A. Hunter, *J. Org. Chem.* **2005**, *70*, 6616.

[6] R. A. Haycock, A. Yartsev, U. Michelsen, V. Sundstrom, C. A. Hunter, *Angew. Chem., Int. Ed.* **2000**, *39*, 3616.

[7] C. A. Hunter, R. K. Hyde, *Angew. Chem., Int. Ed.* **1996**, *35*, 1936.

[8] H. L. Anderson, C. A. Hunter, J. K. M. Sanders, *J. Chem. Soc., Chem. Commun.* **1989**, 226.

[9] F. D'Souza, O. Ito, *Coord. Chem. Rev.* **2005**, *249*, 1410.

[10] H. Imahori, S. Fukuzumi, *Adv. Funct. Mater.* **2004**, *14*, 525.

[11] S. A. Haque, J. S. Park, M. Srinivasarao, J. R. Durrant, *Adv. Mater.* **2004**, *16*, 1177.

[12] H. Choi, S. O. Kang, J. Ko, G. Gao, H. S. Kang, M.-S. Kang, M. K. Nazeeruddin, M. Gratzel, *Angew. Chem., Int. Ed.* **2009**, *48*, 5938.

[13] H. J. Snaith, S. M. Zakeeruddin, L. Schmidt-Mende, C. Klein, M. Gratzel, *Angew. Chem., Int. Ed.* **2005**, *44*, 6413.

[14] D. Kuang, C. Klein, H. J. Snaith, R. Humphry-Baker, S. M. Zakeeruddin, M. Gratzel, *Inorg. Chim. Acta* **2008**, *361*, 699.

[15] N. K. Subbaiyan, C. A. Wijesinghe, F. D'Souza, *J. Am. Chem. Soc.* **2009**, *131*, 14646.

[16] J. R. Durrant, S. A. Haque, E. Palomares, *Chem. Commun.* **2006**, 3279.

[17] T. Hayashi, H. Ogoshi, *Chem. Soc. Rev.* **1997**, *26*, 355.

[18] Y. Kuroda, K. Sugou, K. Sasaki, *J. Am. Chem. Soc.* **2000**, *122*, 7833.

[19] O. Shoji, S. Okada, A. Satake, Y. Kobuke, *J. Am. Chem. Soc.* **2005**, *127*, 2201.

[20] R. Takahashi, Y. Kobuke, *J. Am. Chem. Soc.* **2003**, *125*, 2372.

[21] A. K. Burrell, D. L. Officer, P. G. Plieger, D. C. W. Reid, *Chem. Rev.* **2001**, *101*, 2751.

[22] B. O'Regan, M. Gratzel, *Nature* **1991**, *353*, 737.

[23] C.-Y. Chen, M. Wang, J.-Y. Li, N. Pootrakulchote, L. Alibabaei, C.-H. Ngoc-Le, J.-D. Decoppet, J.-H. Tsai, C. Gratzel, C.-G. Wu, S. M. Zakeeruddin, M. Gratzel, *ACS Nano* **2009**, *3*, 3103.

[24] F. Gao, Y. Wang, D. Shi, J. Zhang, M. Wang, X. Jing, R. Humphry-Baker, P. Wang, S. M. Zakeeruddin, M. Gratzel, *J. Am. Chem. Soc.* **2008**, *130*, 10720.

[25] J. M. Kroon, N. J. Bakker, H. J. P. Smit, P. Liska, K. R. Thampi, P. Wang, S. M. Zakeeruddin, M. Gratzel, A. Hinsch, S. Hore, U. Wuerfel, R. Sastrawan, J. R. Durrant, E. Palomares, H. Pettersson, T. Gruszecki, J. Walter, K. Skupien, G. E. Tulloch, *Prog. Photovolt. Res. Appl.* **2007**, *15*, 1.

[26] A. Mishra, M. K. R. Fischer, P. Bauerle, *Angew. Chem., Int. Ed.* **2009**, *48*, 2474.

[27] M. Planells, F. J. Cespedes-Guirao, L. Goncalves, A. Sastre-Santos, F. Fernandez-Lazaro, E. Palomares, *J. Mater. Chem.* **2009**, *19*, 5818.

[28] R. B. M. Koehorst, G. K. Boschloo, T. J. Savenije, A. Goossens, T. J. Schaafsma, *J. Phys. Chem. B* **2000**, *104*, 2371.

[29] A. Reynal, A. Forneli, E. Palomares, *Energy Environ. Sci.* **2010**, *3*, 805.

[30] I. Kim, B. H. Han, C.-S. Ha, J.-K. Kim, H. Suh, *Macromolecules* **2003**, *36*, 6689.

[31] A. D. Adler, F. R. Longo, J. D. Finarelli, J. Goldmacher, J. Assour, L. Korsakoff, *J. Org. Chem.* **1967**, *32*, 476.

[32] Y. Tachibana, J. E. Moser, M. Gratzel, D. R. Klug, J. R. Durrant, *J. Phys. Chem.* **1996**, *100*, 20056.

[33] B. C. O'Regan, S. Scully, A. C. Mayer, E. Palomares, J. Durrant, *J. Phys. Chem. B* **2005**, *109*, 4616.

[34] SPECFIT v3.0; Spectra Software Associates;

[35] G. Annadurai, M. Chellapandian, M. R. V. Krishnan, *Environ. Monit. Assess.* **1999**, *59*, 111.

[36] S. A. Haque, Y. Tachibana, R. L. Willis, J. E. Moser, M. Gratzel, D. R. Klug, J. R. Durrant, *J. Phys. Chem. B* **2000**, *104*, 538.

[37] Y. Tachibana, S. A. Haque, I. P. Mercer, J. R. Durrant, D. R. Klug, *J. Phys. Chem. B* **2000**, *104*, 1198.

[38] A. Forneli, M. Planells, M. A. Sarmentero, E. Martinez-Ferrero, B. C. O'Regan, P. Ballester, E. Palomares, *J. Mater. Chem.* **2008**, *18*, 1652.

[39] N. W. Duffy, L. M. Peter, R. M. G. Rajapakse, K. G. U. Wijayantha, *Electrochem. Commun.* **2000**, *2*, 658.

[40] B. C. O'Regan, K. Bakker, J. Kroeze, H. Smit, P. Sommeling, J. R. Durrant, *J. Phys. Chem. B* **2006**, *110*, 17155.

[41] B. C. O'Regan, K. Walley, M. Juozapavicius, A. Anderson, F. Matar, T. Ghaddar, S. M. Zakeeruddin, C. Klein, J. R. Durrant, *J. Am. Chem. Soc.* **2009**, *131*, 3541.

[42] T. Gianferrara, D. Giust, I. Bratsos, E. Alessio, *Tetrahedron* **2007**, *63*, 5006.

7. Concluding Remarks

In this thesis, the synthesis of novel organic chromophores was described and their application in DSSC discussed. The device efficiency was rationalized in terms of interfacial charge transfer kinetics which, in turn was correlated with molecular structure. The understanding of these relationships will provide a better and more rational design of organic dyes for DSSC in the future.

The main findings can be summarized as follows:

1. The effect of adding alkyl chains to porphyrin dye structures was described in *Paper I* and *Paper II*. In these studies it was observed that the presence of the alkyl chains can retard the e^-_{TiO2}/electrolyte$^+$ recombination reaction, resulting in an improvement in cell voltage. In addition, the alkyl chains can reduce aggregation formation resulting in improved cell photocurrent.
2. The effect of sensitization time upon interfacial electron transfer processes at the TiO_2/dye/electrolyte interface and cell efficiency was investigated for a bulky perylene sensitizer in *Paper III*. It was shown that the sensitization time can be a crucial parameter which needs to be considered for the fabrication of efficient DSSC using these sensitizers. In addition the effect of supramolecular binding of lithium cations by a sensitizer on solar cell efficiency was investigated in *Paper IV*, where a lithium selective crown ether is attached to a perylene dye. The results indicate that keeping lithium cations far from the nanoparticle surface can result in an upward shift of the TiO_2 conduction band.
3. The effect of the π conjugated spacer on DSSC efficiency in push-pull organic dyes was examined in *Paper V*. It was found that the sensitizer which contained additional oxygen atoms in its π bridge showed increased e^-_{TiO2}/electrolyte$^+$ recombination, lower V_{oc} and therefore lower cell efficiency. This was explained by the greater tendency of this sensitizer to form charge-transfer complexes with I_3^- and/or I_2 species in the electrolyte due to the presence of the additional oxygen atoms in its structure. This work highlights the effect that small changes to sensitizer structure can have on device function and ultimately on device efficiency.
4. Finally, in *Paper VI*, the supramolecular self-assembly of porphyrins on the TiO_2 surface was investigated. The results indicate that not only can the photocurrent be improved, but also the photovoltage becomes favorable by the

UNIVERSITAT ROVIRA I VIRGILI
DESIGN AND SYNTHESIS OF ORGANIC SENSITIZERS FOR DYE SOLAR CELLS: MOLECULAR STRUCTURE VS DEVICE PERFORMANCE
Miquel Angels Planells Dillundé
ISBN:978-84-693-8861-7/DL:T.1946-2010

addition of extra chromophores through supramolecular interactions. The photocurrent increase is attained due to the increased electron injection whereas the photovoltage improvement can be explained by the slower e^-_{TiO2}/electrolyte$^+$ recombination reaction obtained as well as an upward shift to the TiO_2 conduction band.

UNIVERSITAT ROVIRA I VIRGILI
DESIGN AND SYNTHESIS OF ORGANIC SENSITIZERS FOR DYE SOLAR CELLS: MOLECULAR STRUCTURE VS DEVICE PERFORMANCE
Miquel Angels Planells Dillundé
ISBN:978-84-693-8861-7/DL:T.1946-2010

Annexes

UNIVERSITAT ROVIRA I VIRGILI
DESIGN AND SYNTHESIS OF ORGANIC SENSITIZERS FOR DYE SOLAR CELLS: MOLECULAR STRUCTURE VS DEVICE PERFORMANCE
Miquel Angels Planells Dillundé
ISBN:978-84-693-8861-7/DL:T.1946-2010

Annex I: Contributions to the Scientific Community

Publications presented in this thesis:

• *Paper I*: **The role of para-alkyl substituents on *meso*-phenyl porphyrin sensitised TiO_2 solar cells: control of the e^-_{TiO2}/electrolyte$^+$ recombination reaction**. Amparo Forneli, Miquel Planells, Maria A. Sarmentero, Eugenia Martínez-Ferrero, Brian C. O'Regan, Pablo Ballester and Emilio Palomares.

Journal of Materials Chemistry, **2008**, *18*, 1652-1658.

• *Paper II*: **The effect of molecular aggregates over the interfacial charge transfer processes on dye sensitized solar cells**. Miquel Planells, Amparo Forneli, Eugenia Martínez-Ferrero, Antonio Sánchez-Díaz, Maria Ángeles Sarmentero, Pablo Ballester, Emilio Palomares and Brian C. O'Regan.

Applied Physics Letters, **2008**, *92*, 153506/1-153506/3.

• *Paper III*: **Interfacial photo-induced charge transfer reactions in perylene imide dye sensitised solar cells**. Miquel Planells, Francisco Javier Céspedes-Guirao, Amparo Forneli, Ángela Sastre-Santos, Fernando Fernández-Lázaro and Emilio Palomares.

Journal of Materials Chemistry, **2008**, *18*, 5802-5808.

• *Paper IV*: **Supramolecular interactions in dye-sensitised solar cells**. Miquel Planells, Francisco Javier Céspedes-Guirao, Luis Gonçalves, Ángela Sastre-Santos, Fernando. Fernández-Lázaro and Emilio Palomares.

Journal of Materials Chemistry, **2009**, *19*, 5818-5825.

• *Paper V*: **Energy levels, charge injection, charge recombination and dye regeneration dynamics for donor - acceptor π conjugated organic dyes in mesoscopic TiO_2 sensitized solar cells**. Miquel Planells, Laia Pellejà, John N. Clifford, Núria López, Mariachiara Pastore, Filippo DeAngelis, Seth R. Marder and Emilio Palomares.

Ready to be submitted to *Chemistry of Materials*.

• *Paper VI*: **Heterosupramolecular self-assembly of a functional trisporphyrin complex on dye-sensitised solar cells**. Miquel Planells, Laia Pellejà, Emilio Palomares and Pablo Ballester.

Submitted to *Energy and Environmental Science*.

Publications not included in this thesis:

• *Paper VII*: **A colorimetric molecular probe for Cu(II) ions based on the redox properties of Ru(II) phthalocyanines.** Maria Salomé Rodriguez-Morgade, Miquel Planells, Tomás Torres, Pablo Ballester and Emilio Palomares.

Journal of Materials Chemistry, **2008**, *18*, 176-181.

Annex II: Abbreviations

a-Si	Amorphous silicon
a.u.	Arbitrary units
ACN	Acetonitrile
BMII	3-butyl-1-methylimidazolium iodide
c-Si	Monocrystalline silicon
CB	Conduction band
CDCA	Chenodeoxycolic acid
CE	Charge extraction
CV	Cyclic voltammetry
DCM	Dichlorometthane
DMF	dimethylformamide
DMPII	1,2-dimethyl-3-propylimidazolium iodide
DMSO	dimethylsulfoxide
DSSC	Dye-sensitized solar cell
EA	Elemental analysis
E_F	Fermi energy level
ESI	Electrospray ionization
FF	Fill factor
FT-IR	Fourier transform infrared
FTO	Fluorinated tin oxide
GaAs	Gallium arsenide
GuSCN	Guanidinium thiocyanate
HOMO	Highest occupied molecular orbital
HTM	Hole transport material
IPCE	Incident photon-to-current conversion efficiency

J_{sc}	Current at short circuit
LED	Light emiting diode
LUMO	Lowest unoccupied molecular orbital
MALDI	Matrix assisted laser desorption/ionization
MLCT	Metal-to-ligand charge transfer
MS	Mass spectroscopy
NIR	Near infrared
NMR	Nuclear magnetic ressonance
O.D.	Optical density
OPV	Organic photovoltaic
p-Si	Polycristallyne silicon
PV	Photovoltaic
SWV	Square wave voltammetry
TAS	Transient absorbance spectroscopy
TBA	tetrabutylammonium
TBP	Tert-butylpyridine
TC-SPC	Time correlated single photon counting
TEA	Triethylamine
TFA	Trifluoroacetic acid
THF	Tetrahydrofurane
TPV	Transient photovoltage
UV	Ultraviolet
VB	Valence band
V_{oc}	Voltage at open circuit
ε	Molar extinction coeficient
η	Power conversion efficieny
λ	Wavelength
τ	Lifetime